ECMWF COPERNICUS REPORT

Copernicus Atmosphere Monitoring Service

Upgrade verification note for the CAMS real-time global atmospheric composition service

Evaluation of the e-suite for the CAMS upgrade of July 2019; e-suite experiments h4x1, h4xd (2017); e-suite run January-May 2019

Issued by: KNMI

Date: 04-07-2019

Ref: CAMS84_2018SC1_D3.2.1-201907_esuite_v1

IMPLEMENTED BY ECMWF

Upgrade verification note for the CAMS real-time global atmospheric composition service

Evaluation of the e-suite for the CAMS upgrade of July 2019; e-suite experiments h4x1, h4xd (2017); e-suite run January-May 2019

AUTHORS:
S. Basart (BSC), A. Benedictow (MetNo), Y. Bennouna (CNRS-LA), A.-M. Blechschmidt (IUP-UB), S. Chabrillat (BIRA-IASB), Y. Christophe (BIRA-IASB), E. Cuevas (AEMET), H. J. Eskes (KNMI), K. M. Hansen (AU),O. Jorba (BSC), J. Kapsomenakis (AA), B. Langerock (BIRA-IASB), T. Pay (BSC), A. Richter (IUP-UB), N. Sudarchikova (MPG), M. Schulz (METNO), A. Wagner (MPG), C. Zerefos (AA)

REPORT OF THE COPERNICUS ATMOSPHERE MONITORING SERVICE, VALIDATION SUBPROJECT.

CITATION:
Basart, S, A. Benedictow, Y. Bennouna, A.-M. Blechschmidt, S. Chabrillat, Y. Christophe, E. Cuevas, H. J. Eskes, K. M. Hansen, O. Jorba, J. Kapsomenakis, B. Langerock, T. Pay, A. Richter, N. Sudarchikova, M. Schulz, A. Wagner, C. Zerefos, Upgrade verification note for the CAMS real-time global atmospheric composition service: Evaluation of the e-suite for the CAMS upgrade of July 2019, Copernicus Atmosphere Monitoring Service (CAMS) report, CAMS84_2018SC1_D3.2.1-201907_esuite_v1.pdf, July 2019, doi:10.24380/fcwq-yp50.

STATUS:
Version 1, final

DATE:
4 July 2019

Executive Summary

The Copernicus Atmosphere Monitoring Service (CAMS, http://atmosphere.copernicus.eu) is a component of the European Earth Observation programme Copernicus. The CAMS global near-real time (NRT) service provides daily analyses and forecasts of reactive trace gases, greenhouse gases and aerosol concentrations.

The CAMS service includes an activity (CAMS-84) dedicated to the validation of the service products. The latest validation results for the CAMS-global real-time service (the o-suite) products can be found in Schulz et al. (2019) and the activity is described in Eskes et al. (2015). The observational datasets used for this validation are described in Eskes et al. (2018a). These validation reports and the verification websites can be found at http://atmosphere.copernicus.eu/user-support/validation/verification-global-services.

Before each upgrade, the new model and assimilation configuration is operated in parallel (the e-suite) to the operational NRT service (the o-suite) for about half a year. For the July 2019 upgrade the e-suite run has experiment id "0073", with class=mc, and is available from January 2019 onwards. Furthermore, a separate run was conducted for 2017, with experiment identifiers “h4x1” and “h4xd”. This is referred to as the “pre-e-suite” in the text below.

Below a set of quick-look validation results are presented from a comparison of the performance of the forecasts with the e-suite and pre-e-suite runs, the operational run (o-suite) and independent observations. The main conclusions are listed below, and the evidence for these findings is presented in section 2 in the form of a series of plots comparing e-suite, o-suite and independent observations. The o-suite and e-suite system changes are discussed in section 1.

Main conclusions on the performance of the e-suite

The upgrade of the CAMS global system of July 2019 involves major changes, including modelling aspects, updated emissions and the move from 60 to 137 vertical model levels. These changes are reflected in the validation results presented. Overall, the quality of the e-suite is comparable to the o-suite, with many examples where the performance is slightly improved and examples where the performance is slightly degraded. In the lower and middle stratosphere (25-32 km altitude) the e-suite experiments in 2017 and 2019 show significantly larger positive biases than the 60-layer o-suite. The conclusions drawn for the e-suite in 2019 are generally consistent with the results obtained for the pre-e-suite runs in 2017 (when the aerosol model changes in the 2018 o-suite upgrade are taken into account).

Global Aerosol

The 2019 e-suite shows a similar performance as the corresponding pre-e-suite in March-May 2019 as in March-May or June-August 2017. Comparison with Aeronet daily AOD, globally, shows that the e-suite (both 2017 and 2019 runs) has a slightly higher bias compared to the o-suite. RMS error is similar in e-suite and o-suite. The pre-e-suite in the second half of 2017 has the highest temporal

correlation. The spatial correlation of the 2017 pre-e-suite and 2019 e-suite are similar to the o-suite.

Comparison with the Angstrøm exponent reveals that the pre-e-suite has a smaller bias and similar correlation compared with the current o-suite. The pre-e-suite and current o-suite have both smaller bias and higher correlation than the 2017 o-suite. The e-suite exhibits a smaller RMS error, due to less fine particles.

The recent improvements related to the inclusion of nitrate and the more realistic simulation of several other anthropogenic aerosol related emission and formation processes are visible in the improved performance for the Angstrøm Exponent, an indicator of aerosol composition. This is visible in particular over North America (March-May 2019: RMS 0.29 -> 0.20; Correlation 0.48 -> 0.66; MNMB 18% -> 9%, for o-suite -> e-suite). North America is less influenced by dust aerosol and any improvement in anthropogenic aerosol composition, related to nitrate, organics and sulphate, become apparent here. Particulate matter (PM) simulation performance is likely to follow the Angstrøm exponent improvement.

The changes in composition create a small increase or no increase in the (pre-)e-suite total AOD depending on the season. An increase of the e-suite sulphate is seen in particular at high latitudes, northern hemisphere, but less in highly polluted areas in East Asia. There is less organic aerosol in the e-suite, especially at high latitudes. Globally there is less sea salt AOD in the e-suite than in the o-suite. Mean dust AOD is slightly increased in the e-suite, and there is in particular more dust in North Africa and less in East Asia.

Dust and aerosol evaluation over North Africa, the Middle East and Europe

The comparison with AERONET Level 1.5 3-hourly and MODIS Collection 6.1 Level 3 Daily measurements shows a clear increase of mineral dust in the aerosol budget in comparison with the 2017 and 2019 o-suite experiments, leading to overestimations in the Eastern Sahara and Mauritania-Mali border. This change in the activity of the desert dust sources (now more active in the Eastern Sahara than Western Sahara) are associated to the new desert dust source mask considered in the e-suite.

For surface concentrations, a clear increase is observed in the PM10 for the main desert dust sources in the Sahara (showing the highest PM10 seasonal averages in the Eastern part of the Sahara) and the Middle East, in comparison with the current o-suite, achieving seasonal averages over 700 $\mu g/m^3$ over sources (in the case of o-suite the values are up to 300 $\mu g/m^3$). In some hot spots in Southern Europe the seasonal PM10 reaches values up to 150μg/m3. In contrast, PM2.5 levels are strongly reduced in comparison with the o-suite. This is related to the changes in the dust size distribution considered in the new dust emission scheme that shifts emissions towards larger particle sizes.

Tropospheric ozone (O_3)

Model profiles of the CAMS runs were compared to balloon sonde measurement data. Validation results for the pre-e-suite and o-suite are very similar in most regions for the UTLS and free troposphere. Differences show up for the Tropics in the UTLS (larger positive biases for the e-suite).

For the free troposphere larger deviations between pre-e-suite and o-suite are noticeable over the Arctic, where the e-suite shows a larger positive bias.

Ozone in-situ surface concentrations have been compared with WMO Global Atmosphere Watch observations, ESRL station and European Airbase observations. For GAW, the performance of the pre-e-suite, e-suite and o-suite are very similar, the pre-e-suite showing slightly larger biases for Europe and lower biases for stations in Asia. The pre-e-suite and e-suite show improved correlation coefficients.

In the USA (Table Mountain ESRL station) the pre-e-suite shows higher correlation (positive) but also higher ozone values (in most cases this results in higher biases). An almost equal performance compared to the o-suite is found in the Tropics for the pre-e-suite. The 2019 e-suite performs a bit better in the tropics and a bit worse for Lauder, New Zealand. Over Antarctica and especially at the South Pole station during mid-April and May the e-suite shows lower values than the o-suite and the observations, resulting in a negative offset and lower correlations.

The pre-e-suite and e-suite experiments have been compared with IAGOS aircraft observations and the different o-suite experiments for both analysis and 1-day forecast. In general, for ozone at Frankfurt the results of both pre-e-suite and e-suite are very similar to those of the o-suite. Meanwhile, the e-suite presents a smaller seasonal bias than the o-suite or the ozone in the upper troposphere and UTLS especially in spring. Correlation results for ozone in the lower troposphere are slightly better than those of the o-suite while the results are more similar higher up.

Ozone total columns from the o-suite, pre-e-suite and e-suite have been compared to IASI Metop-A version v20151001 daytime only satellite observations. Model configurations are in good agreement with the observations. The e-suite shows improvements compared to o-suite over the high latitudes, which is reflected in the regional and temporal bias reduction. Note that the IASI sensitivity is the lowest over the cold surfaces of Antarctica and Greenland (especially during March-April-May season) where IASI O3 values are positively biased up to 20%. The highest IASI sensitivity is in the northern mid-latitudes during summer (Boynard et al., 2018). Overall, the IASI ozone total column global mean bias is within 2 %.

Tropospheric ozone (O_3) in the Mediterranean

In the Mediterranean (Airbase) and the USA (Table Mountain ESRL) stations the pre-e-suite shows higher correlations compared to the o-suite almost everywhere (positive effect) but also higher ozone values. In most cases this results in higher biases, in particular over the Mediterranean shore of Spain.

Tropospheric ozone (O_3) in the Arctic

Surface ozone mixing ratios predicted with the pre-e-suite was evaluated against measurements from four sites within the Arctic: Alert (Canada), Eureka (Canada), Tiksi (Russia) and the Villum Research Station (Greenland) from March – December 2017. There is a shift in bias from positive to negative in summer and from negative to positive in autumn/winter at all sites. Overall there is an improved agreement with observations for the pre-e-suite with slightly improved correlations and a better description of the seasonal pattern with changes in levels from summer to autumn/winter.

The 2017 pre-e-suite (October-December) and 2019 e-suite (January-March) show higher surface ozone mixing ratios in winter and spring, with improved bias in some stations, but large bias in others. This finding is confirmed by the comparison with the Arctic ESRL stations. From mid-March and onwards the measurements are dominated by ozone depletion events that arise due to halogen chemistry that is not represented by the model. The correlation is improved at all sites.

Tropospheric Carbon Monoxide (CO)

Carbon monoxide surface concentrations have been compared with WMO Global Atmosphere Watch observations. The results of the MNMB are similar for the pre-e-suite, e-suite and o-suite. The o-suite partly shows better correlation coefficients.

The pre-e-suite and e-suite experiments have been compared with IAGOS aircraft observations and the different o-suite experiments for both analysis and 1-day forecast. Although in general the behavior of both pre-e-suite and e-suite are very similar to those of the o-suite, the results for CO comparisons are different over Europe (Frankfurt, Paris) and Asia (Taipei). Over Europe, the model versions with 137 levels present smaller values of the seasonal biases than the o-suite in the mid-troposphere and UTLS. Over Asia, the model versions with 137 levels present larger biases than the o-suite in the lowest layers especially in summer. Correlation results from all models are very similar in all layers and for all locations.

CO total columns from the o-suite, pre-e-suite and e-suite have been compared to MOPITT v8 (thermal infrared radiances) and IASI Metop-A version v20151001 daytime satellite retrievals. Verification with the satellite observations shows that the pre-e-suite, e-suite and o-suite experiments are in very good agreement with observations and almost similar to each other. Some discrepancies between two model runs have a regional and/or temporal character. Time series over the selected regions show that the e-suite is in slightly better agreement with the MOPITT data compared to o-suite over East and South Asia. Overall, 2019 e-suite shows improvements compared to the o-suite with a smaller positive bias over the tropics especially for forecast day 4. The pre-e-suite run 2017 also shows significant bias reduction compared to the o-suite.

Comparisons with NDACC and TCCON FTIR indicate that CO is significantly different between the pre-e-suite and o-suite. From the comparison with the NDACC data, both the pre-e-suite and e-suite perform significantly better in stratosphere. The tropospheric columns (NDACC) and total columns (TCCON) are slightly underestimated by the 2017 pre-e-suite and 2019 e-suite runs. In particular at the high latitude stations at Eureka, Thule and Kiruna the tropospheric columns are strongly underestimated in the pre-e-suite. The pre-e-suite weekly mean bias decreases towards the end of 2017 (overestimation in spring 2017 towards underestimation at end of 2017). Correlations and the standard deviation of the differences are comparable between the o-suite and e-suite(s).

Tropospheric Nitrogen dioxide (NO_2)

Tropospheric columns of NO_2 have been compared with GOME-2 satellite observations. Similar issues as reported in the regular o-suite validation reports are in general found for the e-suites, but the magnitude and details of the mismatches compared to GOME-2 partly differ. Time series comparisons show a positive offset compared to o-suite and GOME-2 over East-Asia, the seasonal cycle over South Africa is underestimated compared to GOME-2 (the o-suite overestimated the

seasonal cycle here). Monthly mean maps show an overestimation to the south of lake Balkhash in Kazakhstan which does not show up for the o-suite and is most pronounced during autumn and winter. A possible explanation could be the overestimation of fire emissions. Emissions also appear overestimated for boreal forest fires over Siberia and Northern America during summer (August 2017) which do not show up in the satellite observations (both o-suite and e-suite overestimate values here, the magnitude of the overestimation differs between both runs and shows variability).

Comparisons against NDACC MAXDOAS data confirm that there is little difference between the o- and e-suite performance.

Formaldehyde (HCHO)

Total columns of HCHO have been compared with GOME-2 satellite observations. Similar issues as reported in the regular o-suite validation reports are in general found for the e-suites, but the magnitude and details of the mismatches compared to GOME-2 partly differ. Map-based comparisons show differences over Central/Northern Africa possibly related to changes in fire emissions with respect to the o-suite, the e-suite is closer to GOME-2 for some months and shows larger differences for others. HCHO columns decreased over Mecca and Teheran compared to the o-suite. Values over Northern Australia are overestimated less by the e-suite than by the o-suite in November 2017 possibly related to changes in fire emissions.

The comparisons against NDACC MAXDOAS instruments show that the smoothed e-suite column values are higher. In particular the comparison at Uccle shows that the e-suite (AN and FC) captures more high pollution events.

Stratospheric ozone

Model profiles of the CAMS runs were compared to balloon sonde measurements. Results for the integrated profiles (10-70 hPa in the tropics and 10-90 hPa elsewhere) for pre-e-suite and o-suite are similar in most regions for the stratosphere. Differences show up for the Tropics (lower biases for the pre-e-suite).

Ozone columns and profiles from the 2019 e-suite (mc.0073) and the pre-e-suite experiments h4x1/h4xd (in year 2017) have been compared with the o-suite at the same period, and an experiment configured as the current o-suite but for the period up to May 2017 (h30x), using satellite observations by MLS and ACE-FTS as reference. The 2017 o-suite or h30x (2018-2019 o-suite configuration run for 2017) L60 results have nearly the same biases.

The biases in the L137 (h4x1) analyses are better in the upper stratosphere (z>40km) but this does not hold with the 4-day forecasts which reach the same biases as the L60 experiments. In the mid-upper stratosphere (30-40km) above the winter hemisphere, a significant underestimation appears with L137 while it was not present in the L60 experiments. This underestimation with L137 is even worse in the 4-day forecasts. In the mid-lower stratosphere (25-30km) a significant overestimation appears with L137, especially above the Tropics where it is present all year long (the severity above the mid-latitudes and Poles depends on the considered season). In the lower stratosphere (z<25km), we had to look at the normalized mean bias, but no clear "winner" emerged between L60 and L137 (figures not included). Overall the outcome of the pre-e-suite against ACE-FTS is negative:

the L137 experiment h4x1-h4xd delivers larger biases than the L60 o-suite in the lower and middle stratosphere. For most CAMS users, this is more important than the improvement seen in the analyses of the upper stratosphere.

These conclusions are confirmed for the e-suite experiment mc.0073 in the period January to May 2019. The shape of the bias profile is more distorted in the e-suite forecasts in the altitude range 25-50km, resulting in more marked biases in the analyses (negative in the 30-40km region, positive in the 25-30km region)

The stratospheric partial column comparison against FTIR, LIDAR and MWR shows an overall reduced bias in the pre-e-suite AN compared to the o-suite AN. The mean relative bias averaged over all available sites decreases from -1.5% to -1%. From the MWR and LIDAR comparison we observe that the CAMS stratospheric ozone profile shape has changed significantly in the pre-e-suite and e-suite, including the appearance of a positive bias around 25-32 km altitude, and confirm the results from the ACE-FTS comparison.

Ozone sonde profiles also confirm the larger biases around 20hPa in the e-suite. However, this effect does not show up constantly. It seems to be more obvious during the northern summer season. For Antarctica, there is a larger underestimation around 20hPa. Generally, for the high latitudes, the increased biases are less obvious than in the Tropics or northern hemisphere.

Table of Contents

1. Description of the o-suite and e-suite

Below a short model description is given on both the CAMS o-suite operational data-assimilation and forecast run and the new e-suite.

1.1 o-suite: model and data assimilation aspects

This section provides information on the CAMS global data-assimilation and forecast operational configuration (the CAMS o-suite). The dates of past upgrades are listed in Table 1.1. Table 1.2 provides information on the satellite data used in the o-suite. Further details on the model runs and their data usage can be found at http://atmosphere.copernicus.eu/documentation-global-systems.

The o-suite consists of the IFS-CB05 chemistry combined with the CAMS bulk aerosol model. The chemistry is described in Flemming et al. (2015) and Flemming et al. (2017), aerosol is described in Morcrette et al. (2009). The forecast length is 120 h. The o-suite data is stored under **expver '0001'** of **class 'MC'**. On 21 June 2016 the model resolution has seen an upgrade from T255 to T511, and forecasts are produced twice per day. The latest upgrade of the system is based on IFS version cy45r1_CAMS (https://confluence.ecmwf.int/display/COPSRV/Current+global+production+suites) and took place on 26 June 2018. The validation for this upgrade is described in Eskes et al., 2018b/2018c.

A short summary of the main specifications:

- The modified CB05 tropospheric chemistry is used (Williams et al., 2013), originally taken from the TM5 chemistry transport model (Huijnen et al., 2010)
- Stratospheric ozone during the forecast is computed from the Cariolle scheme (Cariolle and Teyssèdre, 2007) as already available in IFS, while stratospheric NOx is constrained through a climatological ratio of HNO_3/O_3 at 10 hPa.
- Monthly mean dry deposition velocities are based on the SUMO model provided by the MOCAGE team.
- Data assimilation is described in Inness et al. (2015) and Benedetti et al. (2009) for chemical trace gases and aerosol, respectively. Satellite data assimilated is listed in Table 1.2 and Fig. 1.1.
- Anthropogenic and biogenic emissions are based on MACCity (Granier et al., 2011) and a climatology of the MEGAN-MACC emission inventories (Sindelarova et al., 2014)
- NRT fire emissions are taken from GFASv1.2 (Kaiser et al. 2012).

Table 1.1: Overview of o-suite upgrades.

CAMS system	Exp. ID	Brief description	Upgrade dates of the o-suite
o-suite	0001	Operational CAMS DA/FC run	20190709 (planned date) 20180626 20170926 20170124 20160621 20150903 20140918

Table 1.2: Satellite retrievals of reactive gases and aerosol optical depth that are assimilated in the o-suite.

Instrument	Satellite	Provider	Version	Type	Status
MLS	AURA	NASA	V4	O3 Profiles	20130107 -
OMI	AURA	NASA	V883	O3 Total column	20090901 -
GOME-2A	Metop-A	Eumetsat	GDP 4.8	O3 Total column	20131007 - 20181231
GOME-2B	Metop-B	Eumetsat	GDP 4.8	O3 Total column	20140512 -
SBUV-2	NOAA-19	NOAA	V8	O3 21-layer profiles	20121007 -
OMPS	Suomi-NPP	NOAA / EUMETSAT		O3 Profiles	20170124 -
IASI	MetOp-A	LATMOS/ULB Eumetsat	-	CO Total column	20090901 - 20180621 20180622 -
IASI	MetOp-B	LATMOS/ULB Eumetsat	-	CO Total column	20140918 - 20180621 20180622 -
MOPITT	TERRA	NCAR	V5-TIR V7-TIR V7-TIR Lance	CO Total column	20130129 - 20160124 - 20180626 20180626
OMI	AURA	KNMI	DOMINO V2.0	NO2 Tropospheric column	20120705 -
GOME-2A/2B	METOP A/B	Eumetsat	GDP 4.8	NO2 Tropospheric column	20180626 -
OMI	AURA	NASA	v003	SO2 Tropospheric column	20120705-20150901
GOME-2A/2B	METOP A/B	Eumetsat	GDP 4.8	SO2 Tropospheric column	20150902 -
MODIS	AQUA / TERRA	NASA	Col. 5 Deep Blue Col. 6, 6.1	Aerosol total optical depth, fire radiative power	20090901 - 20150902 - 20170124 -
PMAp	METOP-A METOP-B	EUMETSAT		AOD	20170124 - 20170926 -

The aerosol model includes 12 prognostic variables, which are 3 bins for sea salt and desert dust, hydrophobic and hydrophilic organic matter and black carbon, sulphate aerosols and its precursor trace gas SO_2 (Morcrette et al., 2009). Aerosol total mass is constrained by the assimilation of MODIS AOD (Benedetti et al. 2009). A variational bias correction for the MODIS AOD is in place based on the approach used also elsewhere in the IFS (Dee and Uppala, 2009).

The CAMS o-suite system is upgraded regularly (Table 1.1), following updates to the ECMWF meteorological model as well as CAMS-specific updates such as changes in chemical data assimilation. These changes are documented in e-suite validation reports. A validation report for this previous upgrade of 26 June 2018, cy45r1 (Eskes et al., 2018b) is available as https://atmosphere.copernicus.eu/sites/default/files/2018-06/CAMS84_2015SC2_D84.3.1.5_201802_esuite_v1_0.pdf The addendum to this document is called CAMS84_2015SC3_D84.3.1.5_201802_esuite_addendum.pdf (Eskes et al., 2018c).

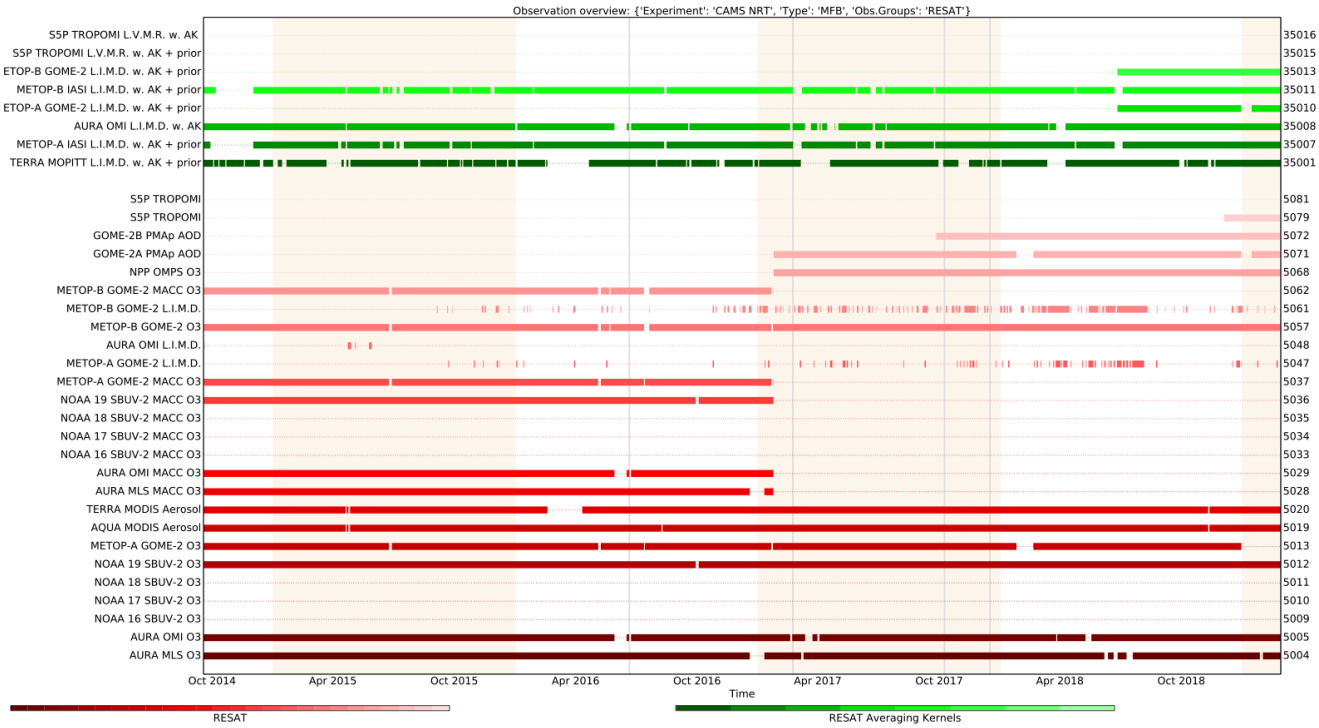

Figure 1.1: Satellite observation usage in the real-time analysis, for ozone, CO, aerosol AOD, from October 2014 onwards. Top eight rows: products assimilated using averaging kernels. New assimilated products since the 24 January 2017 upgrade are the PMaP AOD including GOME-2B and OMPS ozone profile observations. Sentinel-5P TROPOMI ozone is assimilated since Dec. 2018 (5079=O_3) and other products are monitored (35016=NO_2, 35015=CO, 5081=SO_2). Note that the lines mentioning "MACC O3" should be discarded.

1.2 e-suite

A major change to be implemented on 6 July 2019 is the transition from 60 layers to 137 layers, which is a major change for the modelling, the assimilation and operations aspects. The main changes in the upgrade are listed in the following CAMS webpage https://confluence.ecmwf.int/display/COPSRV/Implementation+of+IFS+cycle+46r1.
Technical details on grib encoding and changes in model output parameters can also be found on this page.

The e-suite data is available from ECMWF MARS under **class=mc**, **expver=0073**, and is evaluated from 10 January 2019 until the end of May 2019, and compared with the 2019 o-suite.

A pre-e-suite test run was conducted covering a large part of 2017. The experiments are:

- **h4x1** : 20170301-20170630
- **h4xd** : 20170701-20171231

These two 2017 pre-e-suite runs are evaluated in this report. The results are compared with the 2017 o-suite, as well as with an experiment **h30x** (available for March-May 2017) corresponding to the 2019 o-suite configuration.

1.2.1 Meteorological content of the new cycle

The meteorological changes can be found on the ECMWF-IFS CY46R1 page, https://confluence.ecmwf.int/display/FCST/Implementation+of+IFS+cycle+46R1.

1.2.2 Atmospheric composition content of the new cycle

Assimilation:

- New model-error covariance matrices for aerosol and chemistry at 137 levels.

Observations:

- No new atmospheric composition observations compared to Cycle 45r1.

Emissions:

- New emissions inventories: CAMS_GLOB_ANT v2.1 (anthropogenic) and CAMS_GLOB_BIO v1.1 (biogenic), in place of previous MACCity and MEGAN_MACC inventories.
- Biomass-burning injection heights from GFAS and updated diurnal cycle. In particular, this reduces the overestimation of near-surface PM2.5 during fire events.
- Anthropogenic SOA production was updated with a diurnal cycle and regionally-varying ratio to CO emissions. This has a small impact on AOD, but significantly reduces night-time near-surface PM2.5 in polluted regions.
- New online dust emission scheme (Nabat et al., 2012). This increases total dust emissions and shifts them towards larger particle sizes, in line with recent literature. An updated dust source function improves the selection of source regions, reducing "gaps" in dust emissions.
- Sea-salt production over freshwater lakes eliminated. This corrects an issue that was particularly noticeable over the Great Lakes.

Other model changes:

- Vertical resolution increased from 60 levels to 137 levels, matching that used at ECMWF for NWP. This includes moving the model top from 0.1 hPa to 0.01 hPa.
- New nitrate and ammonium aerosol species, coupled to the gas-phase nitrogen chemistry. See new model parameters below. This is a major expansion of the aerosol species represented in the model, giving a more complete representation of the species which contribute to e.g. PM2.5 over Europe.
- Sulphur species (SO2 and SO4) coupled between chemistry and aerosol schemes. See discontinued parameters below. This brings a greater consistency between the chemistry and aerosol products related to the sulphur cycle.
- Online calculation of dry deposition velocities for trace gases. This was already in place for aerosols in 45r1 and allows the deposition scheme to better account for variations in surface properties.

- Updates to wet deposition parameterisations. This brings improvements in the distinction between scavenging by liquid and ice and harmonises the treatment for aerosols and trace gases.
- Updates to chemical reaction rates following latest recommendations by JPL/IUPAC.

Impact of the new cycle:

- The new cycle is being validated by the CAMS Validation team and the results are presented in this report.

2. Upgrade evaluation results: e-suite versus o-suite

2.1 Global aerosol evaluation

Table 2.1.1: Mean global total and speciated AOD in o-suite, H4XD (pre-e-suite A) and H4X1 (pre-e-suite B) for spring and summer 2017. More total AOD in the pre-e-suite is mainly due to overall more sea salt. Noteworthy is the larger relative contribution from sea salt to total AOD and the change of organic AOD in the e-suite compared to o-suite in spring and summer 2017.

JJA2017

AOD	o-suite	H4XD	H4X1
Total aerosol	0.166	0.177	0.168
Black Carbon	0.011	0.005	0.005
Dust	0.026	0.031	0.031
Organic Matter	0.059	0.044	0.042
Sulphate	0.046	0.035	0.034
Sea salt	0.025	0.056	0.049

MAM2017

AOD	o-suite	H30X	H4X1
Total aerosol	0.160	0.169	0.167
Black Carbon	0.011	0.005	0.005
Dust	0.023	0.024	0.027
Organic Matter	0.054	0.046	0.038
Sulphate	0.048	0.039	0.042
Sea salt	0.024	0.055	0.048

Table 2.1.2: Mean global total and speciated AOD in o-suite and 0073 (e-suite) for spring (March, April, May) 2019. Compared to spring 2017 (table 2.1.1) a little less total AOD is present in the e-suite than in the o-suite mainly due to overall less sea salt and organic matter compensated by relatively more dust and sulphate.

MAM2019

AOD	o-suite	e-suite
Total aerosol	0.168	0.164
Black Carbon	0.006	0.005
Dust	0.022	0.026
Organic Matter	0.049	0.039
Sulphate	0.037	0.040
Sea salt	0.053	0.047

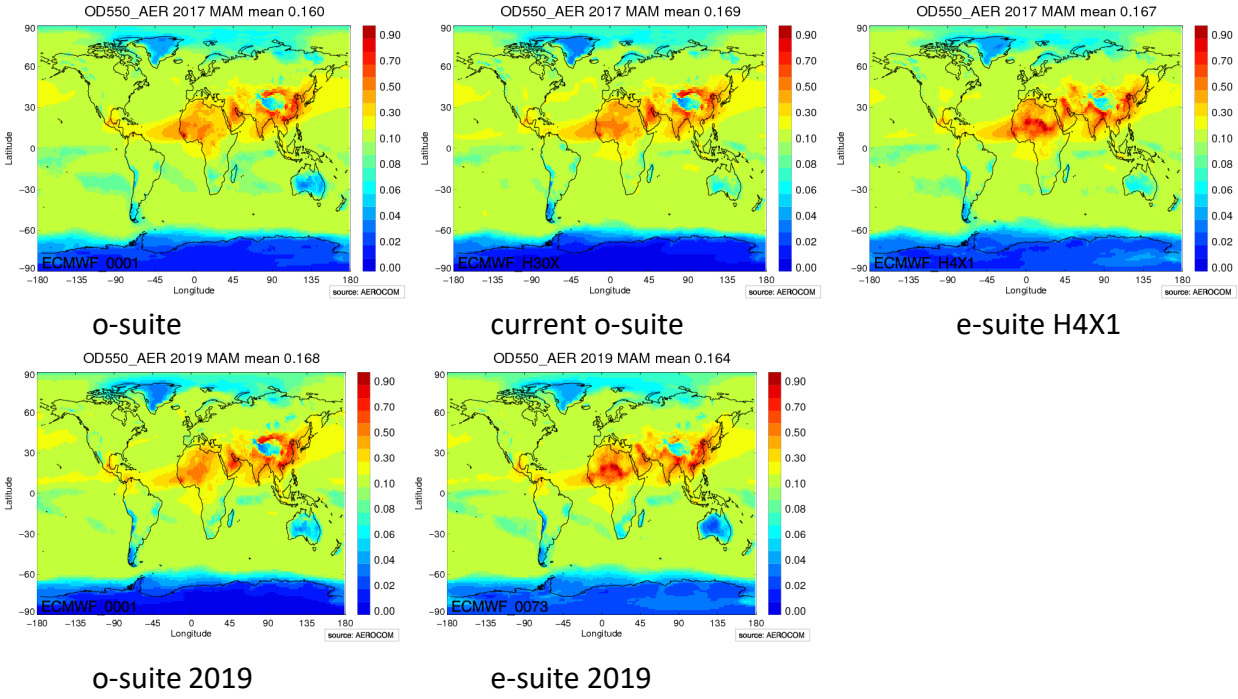

Fig. 2.1.1. Averaged aerosol optical depth (AOD) from the old o-suite (left), current o-suite H30X (middle) and e-suite H4X1 (right) IFS model for March-April-May 2017 (top row) and 2019 (bottom row). Mean AOD in the e-suite is about the same as in the o-suite, but in e-suite an increase is seen in North Africa and a decrease in East Asia.

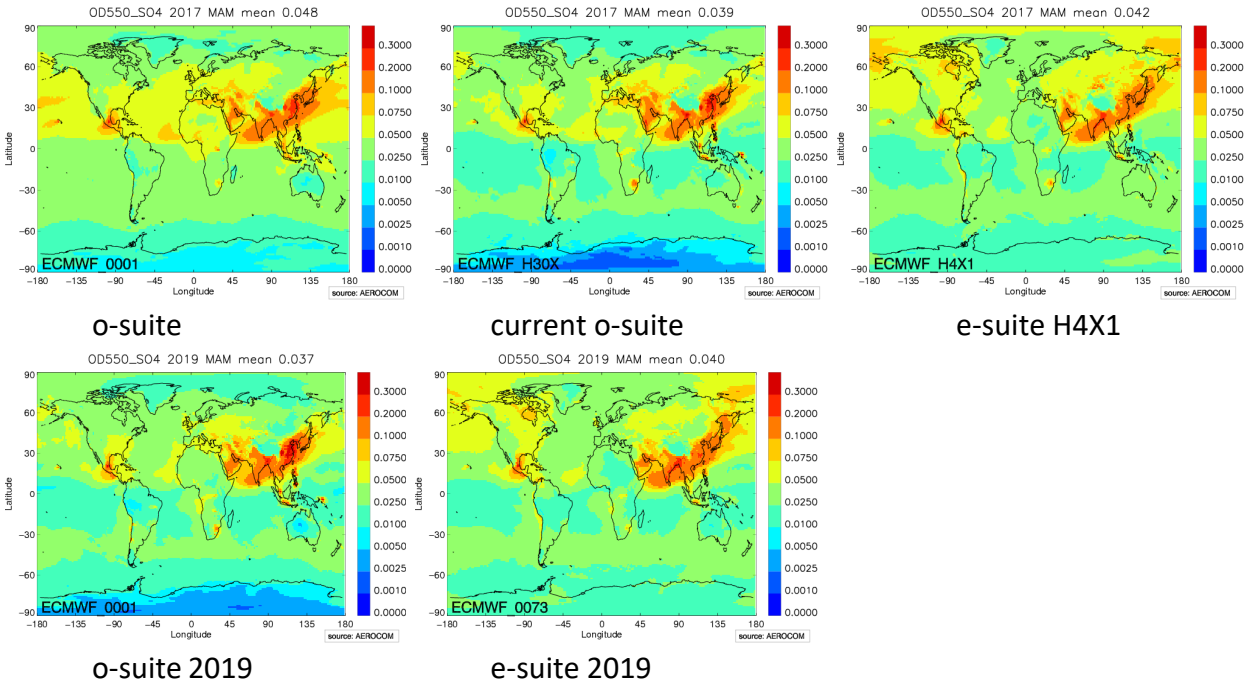

Fig. 2.1.2. Top row: Averaged sulphate optical depth from o-suite (left), current o-suite H30X (middle) and e-suite H4X1 (right) IFS model for March-April-May 2017 (top row). Bottom row: Averaged sulphate optical depth from the 2019 o-suite (left) and e-suite (right). In the e-suite an increase is seen in particular in high latitudes, northern hemisphere, with less sulphate in sea areas and in East Asia.

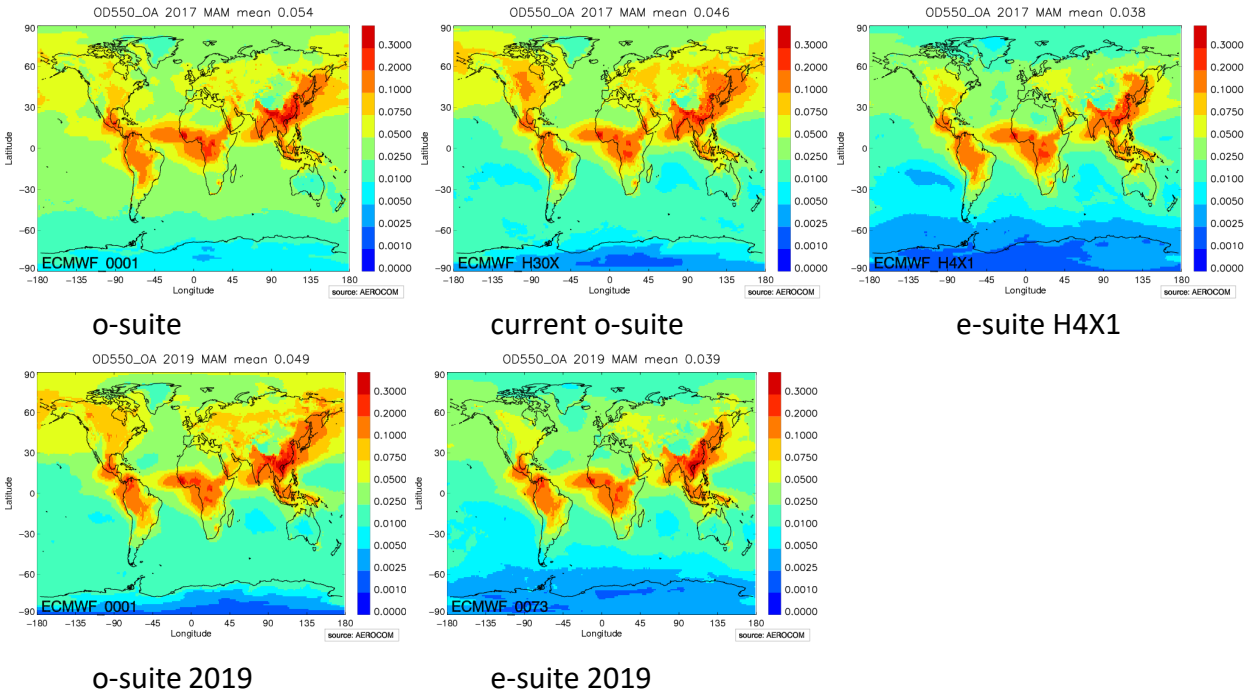

o-suite | current o-suite | e-suite H4X1

o-suite 2019 | e-suite 2019

Fig. 2.1.3. Top: Averaged organic aerosol optical depth from o-suite (left), current o-suite H30X (middle) and e-suite H4X1 (right) IFS model for March-April-May 2017. Bottom: same for the 2019 o-suite and e-suite. There is less organics in the e-suite especially in high latitudes.

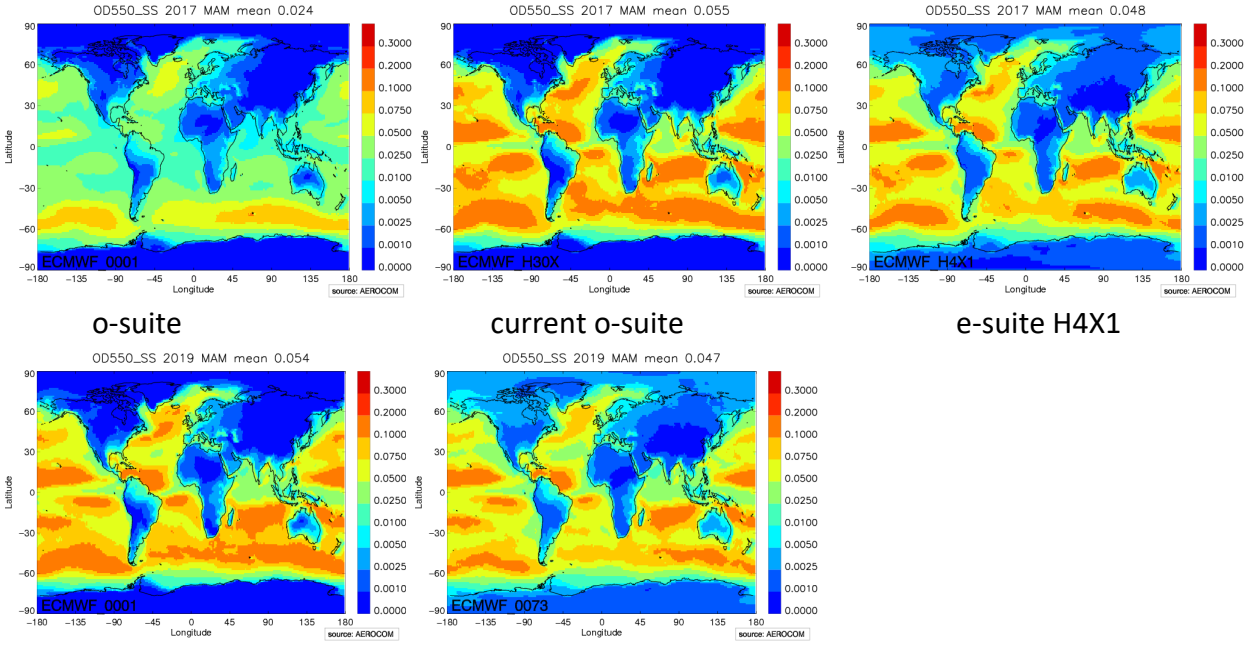

o-suite | current o-suite | e-suite H4X1

o-suite 2019 | e-suite 2019

Fig. 2.1.4. Top: Averaged sea salt aerosol optical depth from o-suite (left), current o-suite H30X (middle) and e-suite H4X1 (right) IFS model for March-April-May 2017. Bottom: same for the 2019 o-suite and e-suite. Mean sea salt AOD in e-suite is at 0.048, which is 50% more than what was in the o-suite in 2017.

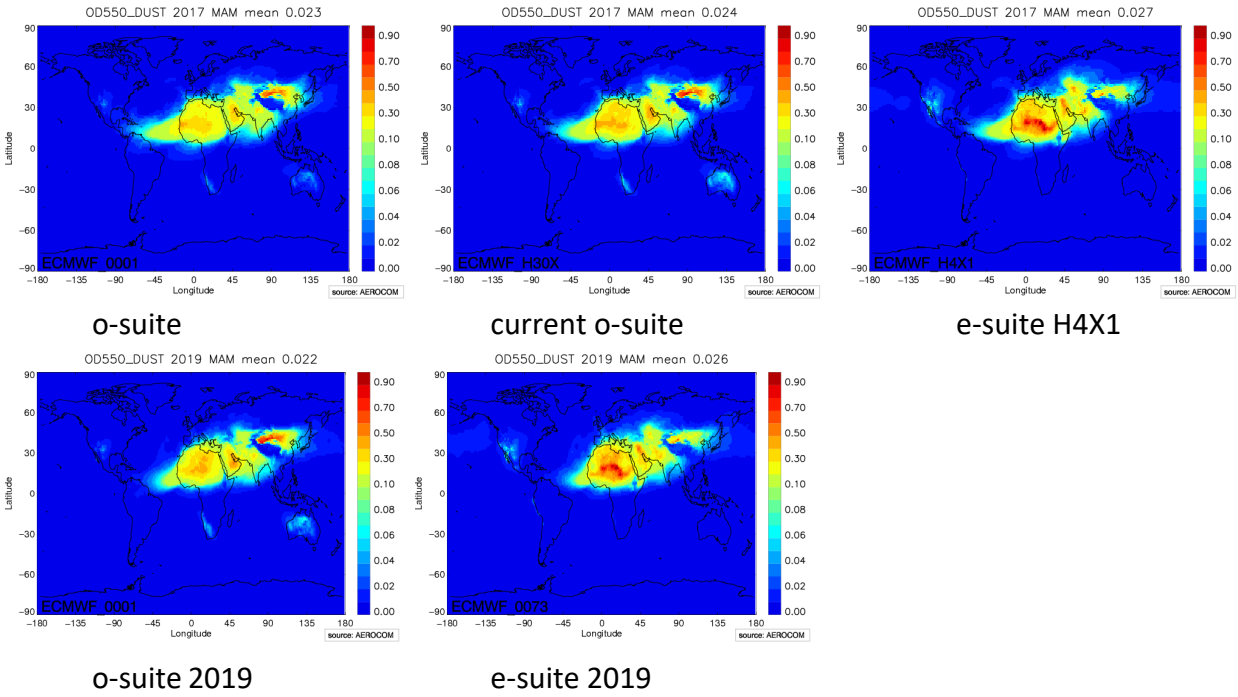

o-suite | current o-suite | e-suite H4X1

o-suite 2019 | e-suite 2019

Fig. 2.1.5. Top: Averaged dust aerosol optical depth (AOD) from o-suite (left), current o-suite H30X (middle) and e-suite H4X1 (right) IFS model for March-April-May 2017. Bottom: same for the 2019 o-suite and e-suite. Globally, mean dust AOD in e-suite has increased by 20%, while there is in particular more dust in North Africa and less in East Asia.

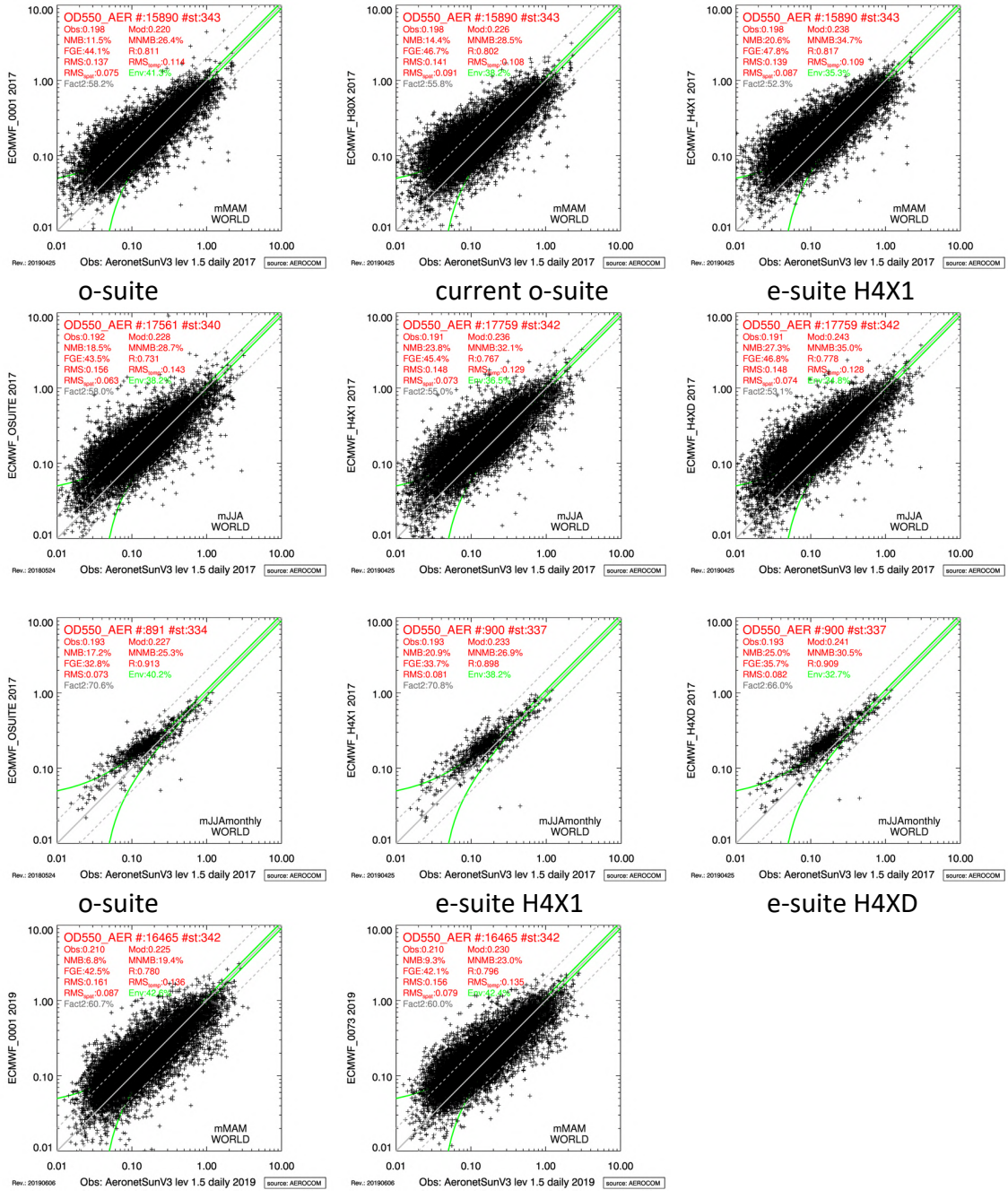

o-suite | current o-suite | e-suite H4X1

o-suite | e-suite H4X1 | e-suite H4XD

o-suite 2019 | e-suite 2019

Fig. 2.1.6. Evaluation of IFS simulated AOD against Aeronet NRT version 3, level 1.5 photometer measurements at circa 340 stations for the period MAM-2017 (top row), JJJA-2017 (two middle rows) and MAM-2019 (bottom row). In the third row monthly consistent averages are shown, while the other rows contain daily data. The new sea salt source (and changes in composition) creates an increase in AOD, globally +10%. This makes FGE, MNMB, NMB against Aeronet increase relative to the o-suite. RMS increased, mainly due to a spatial error, both in the current o-suite and e-suite. Temporal RMS (RMStemp) decreased. Bias is highest in H4XD as visible in MNMB, NMB, FGE, and factor 2 statistics. Correlation R is highest for daily H4XD, while spatial R is equal to o-suite visible in monthly average scatter plots.

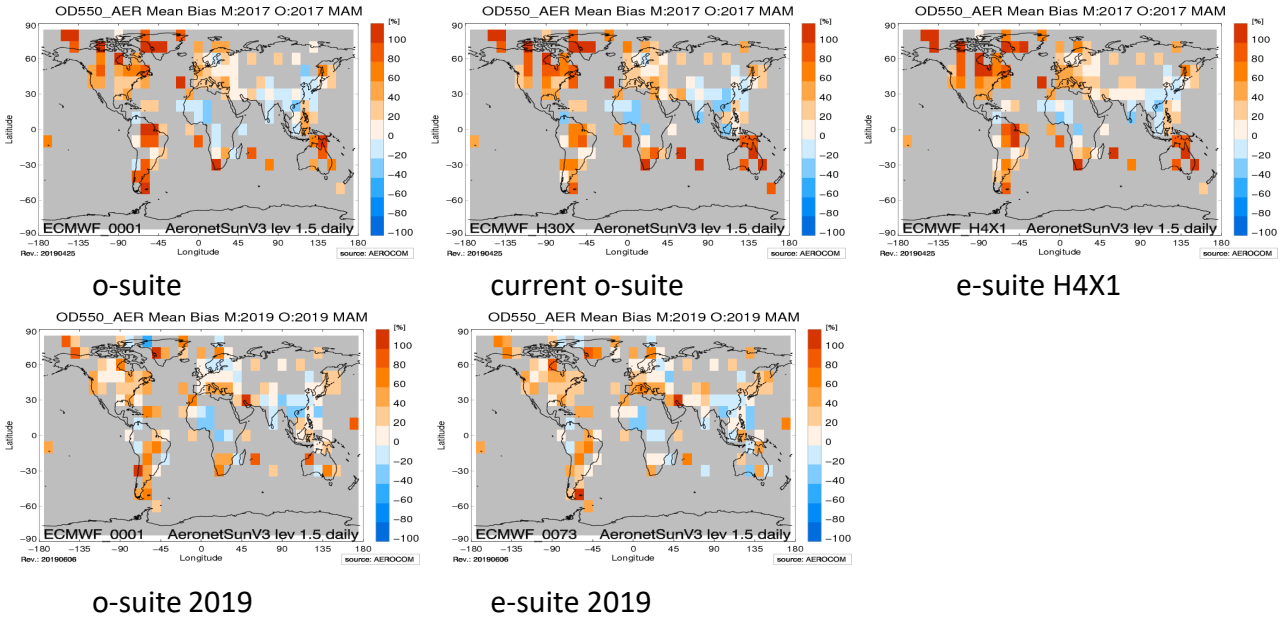

Fig. 2.1.7. Regional relative mean bias of simulated daily AOD against NRT level 1.5 Aeronet SunV3 photometer measurements for the period March-April-May 2017 (top) and 2019 (bottom).

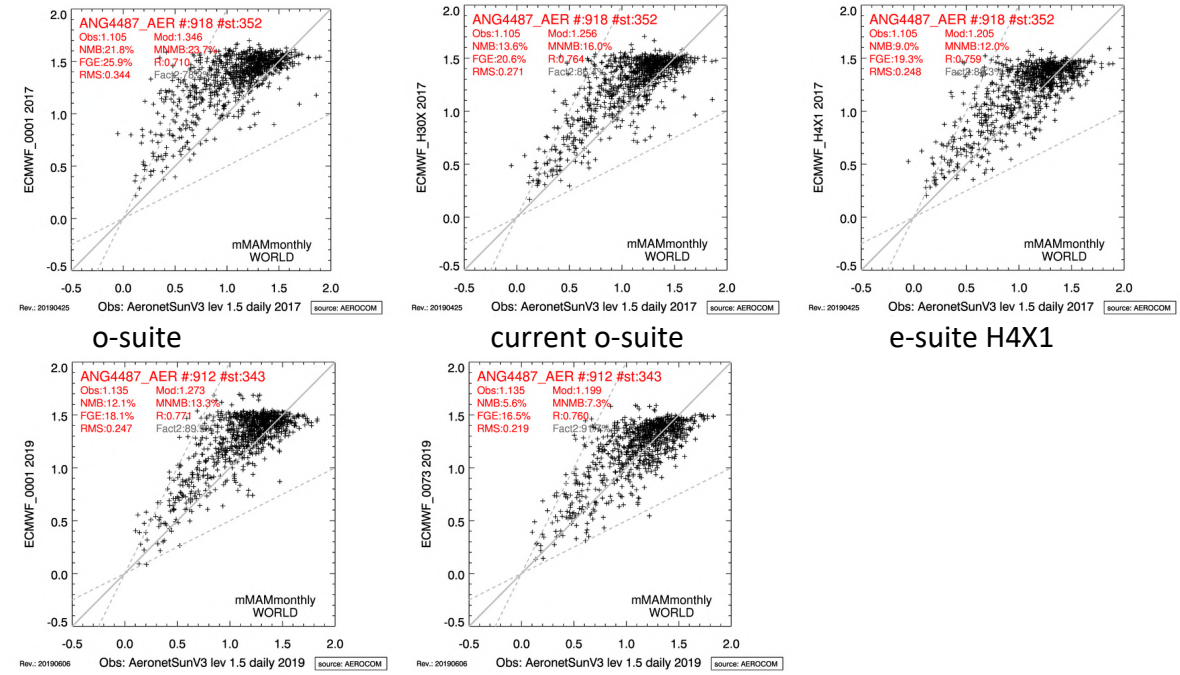

Fig 2.1.8. Angström Exponent scatterplots (o-suite upper left, current o-suite H30X (upper middle), pre-e-suite upper right). The e-suite bias and RMS is lower. The statistics reflect less fine particles and better RMS score in e-suite in 2017 and 2019.

2.2 Dust and aerosol evaluation over North Africa, the Middle East and Europe

Analysis for the year 2017

Table 2.2.1. Skill scores (MB, FGE, RMSE and r) of the 24h forecasts for the o-suite (expid 0001), current o-suite (expid h30x), e-suite (expid h4xd) and SDS-WAS Multi-model Median for March-April-May 2017, and the number of data (NDATA) used. Dust AOD (DOD) from AERONET is the reference.
In spring and summer 2017, e-suite presents higher AOD values associated with sea-salt in the Atlantic, Arabian and the Mediterranean in comparison with o-suite. In terms of correlation, the e-suite shows lower values for spring and summer 2017 (0.79 and 0.82 respectively for spring and summer) in comparison with the o-suite (0.86 and 0.87 respectively for spring and summer).
In the Sahara and Sahel regions the e-suite shows lower correlation values (0.77 and 0.64 respectively for Sahara and Sahel) in comparison with the o-suite (0.80 and 0.68 respectively for Sahara and Sahel) and the SDS-WAS multi-model product (0.84 and 0.66 respectively for Sahara and Sahel).
During spring 2017, the e-suite overestimates the maximum DOD peaks in the Sahara (see Tamanrasset_INM AERONET site below) and Northwester Magrebh (see Tizi Ouzou AERONET sites below).

		o-suite				current o-suite				e-suite				SDS-WAS				
	NDATA	MB	MFB	RMSE	COR	MB	MFB	RMSE	COR	MB	MFB	RMSE	COR	NDATA	MB	MFB	RMSE	COR
Sahara	340	-0.07	-0.13	0.21	0.80	-0.05	0.00	0.21	0.77	0.03	0.24	0.23	0.63	337	-0.09	-0.22	0.21	0.84
Sahel	716	-0.29	-0.66	0.36	0.68	-0.27	-0.63	0.36	0.64	-0.24	-0.52	0.34	0.60	710	-0.25	-0.53	0.34	0.66
Tropical N. Atl.	111	-0.24	-0.52	0.31	0.84	-0.23	-0.48	0.30	0.82	-0.25	-0.54	0.33	0.78	111	-0.30	-0.64	0.37	0.81
Sub-trop. N. Atl.	399	-0.04	-0.07	0.09	0.61	-0.02	-0.01	0.09	0.60	-0.01	0.07	0.11	0.55	396	-0.02	-0.05	0.10	0.54
NW Maghreb	176	-0.16	-0.90	0.22	0.92	-0.15	-0.82	0.22	0.87	-0.02	0.12	0.20	0.72	172	-0.12	-0.68	0.18	0.86
W. Iberian Peninsula	499	-0.07	-0.27	0.11	0.78	-0.07	-0.26	0.11	0.75	-0.05	-0.04	0.09	0.74	489	-0.06	-0.17	0.10	0.78
Iberian Peninsula	754	-0.03	0.95	0.07	0.79	-0.03	0.95	0.07	0.77	-0.01	1.09	0.07	0.73	746	-0.02	1.01	0.07	0.78
Western Mediterranean	2434	-0.01	1.27	0.06	0.79	-0.01	1.28	0.06	0.78	0.02	1.42	0.08	0.73	2414	-0.01	1.31	0.05	0.82
Central Mediterranean	2145	-0.03	1.11	0.09	0.90	-0.02	1.13	0.09	0.87	0.01	1.30	0.09	0.85	2110	-0.02	1.14	0.08	0.90
Eastern Mediterranean	1639	-0.05	0.84	0.12	0.86	-0.04	0.89	0.11	0.84	-0.01	1.00	0.10	0.84	1616	-0.04	0.91	0.12	0.84
Eastern Sahara	132	-0.06	-0.05	0.15	0.85	-0.01	0.15	0.14	0.86	0.00	0.23	0.19	0.71	129	-0.04	0.09	0.15	0.85
Middle East	1007	-0.14	-0.31	0.25	0.68	-0.12	-0.26	0.23	0.67	-0.12	-0.20	0.26	0.53	986	-0.14	-0.25	0.26	0.62
All sites	**10352**	**-0.07**	**0.61**	**0.16**	**0.86**	**-0.06**	**0.65**	**0.15**	**0.84**	**-0.03**	**0.79**	**0.16**	**0.79**	**10216**	**-0.06**	**0.67**	**0.15**	**0.86**

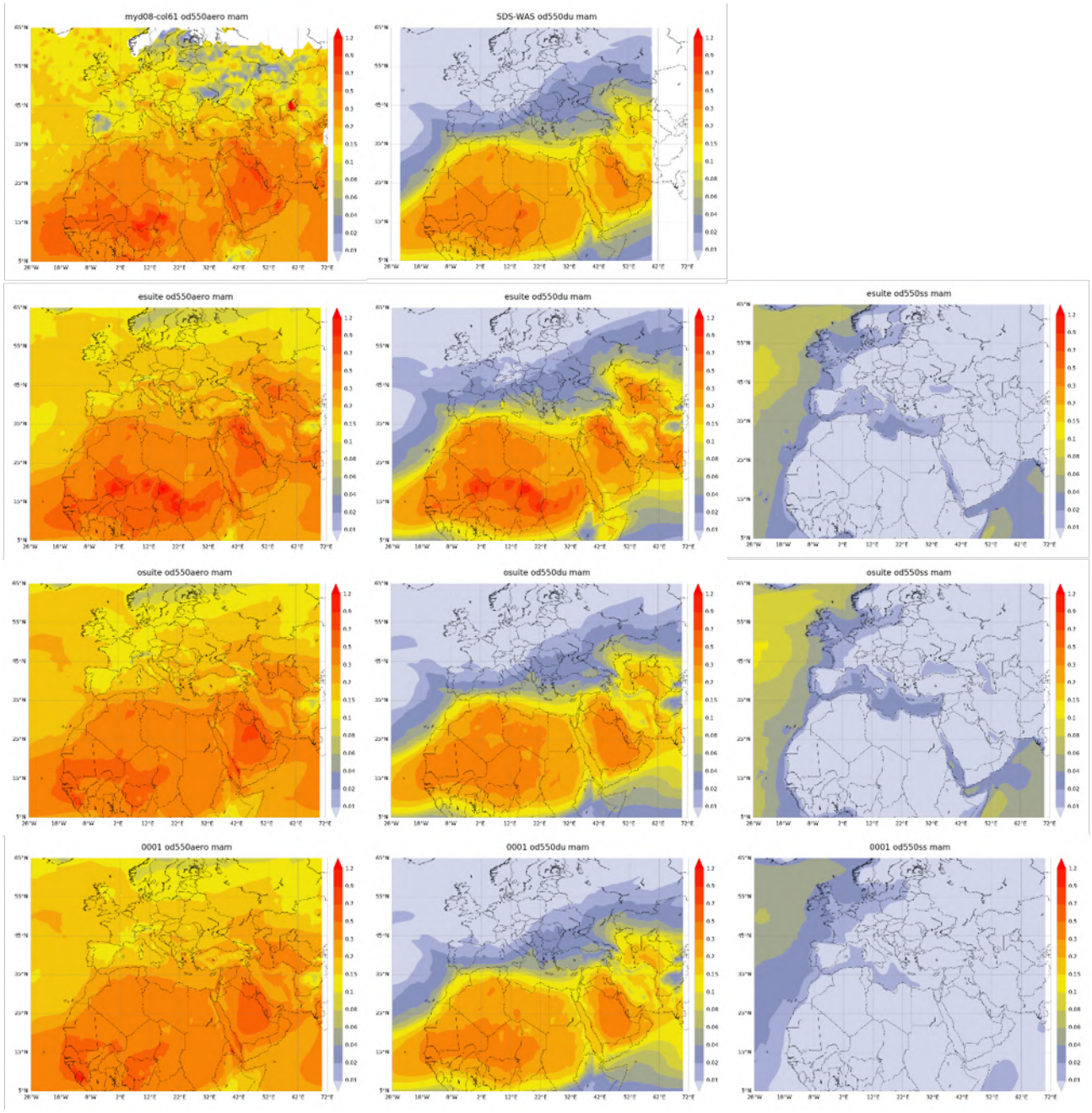

Figure 2.2.1. Seasonal averaged aerosol optical depth (od550aero), dust optical depth (od550aero) and sea-salt (od550ss) from the pre-e-suite (expid h4x1, second row), current o-suite (expid h30x, third row) and o-suite (expid 0001, four row) for March-April-May 2017. CAMS outputs are compared with MODIS Collection 6.1 Level 3 aerosol optical depth and the SDS-WAS Multi-model dust optical depth.

Table 2.2.2. Skill scores (MB, FGE, RMSE and r) of 24h forecasts for o-suite (expid 0001), pre-e-suite (expid h4xd and h4x1) and SDS-WAS Multi-model Median for June-July-August 2017, and the number of data (NDATA) used. Dust AOD (DOD) from AERONET is the reference.

		o-suite				e-suite				SDS-WAS				
	NDATA	MB	MFB	RMSE	COR	MB	MFB	RMSE	COR	NDATA	MB	MFB	RMSE	COR
Sahara	26	-0.40	-0.67	0.51	0.30	-0.15	-0.21	0.33	0.51	26	-0.40	-0.63	0.51	0.33
Sahel	723	-0.20	-0.40	0.30	0.70	-0.10	-0.18	0.25	0.68	723	-0.20	-0.39	0.31	0.71
Tropical North Atlantic	12	-0.09	-0.22	0.13	0.88	-0.10	-0.27	0.13	0.96	12	-0.12	-0.35	0.16	0.90
Subtropical North Atlantic	598	-0.06	-0.11	0.18	0.82	-0.04	-0.03	0.16	0.86	598	-0.10	-0.31	0.21	0.83
North Western Maghreb	76	-0.14	-0.68	0.18	0.87	0.00	0.02	0.14	0.80	76	-0.14	-0.60	0.18	0.88
Western Iberian Peninsula	707	-0.04	0.62	0.08	0.77	-0.02	0.71	0.07	0.79	707	-0.04	0.57	0.09	0.76
Iberian Peninsula	1191	-0.02	1.16	0.07	0.81	0.01	1.27	0.07	0.78	1191	-0.02	1.14	0.07	0.82
Western Mediterranean	3403	-0.03	0.91	0.09	0.82	0.03	1.12	0.09	0.82	3403	-0.03	0.93	0.09	0.82
Central Mediterranean	2923	-0.02	1.14	0.07	0.88	0.04	1.33	0.09	0.87	2923	-0.02	1.14	0.08	0.88
Eastern Mediterranean	2062	0.00	1.59	0.08	0.90	0.04	1.65	0.09	0.80	2062	0.00	1.59	0.08	0.87
Eastern Sahara	119	0.04	0.98	0.07	0.86	0.10	1.16	0.12	0.81	119	0.03	0.96	0.08	0.80
Middle East	1060	-0.14	-0.24	0.23	0.80	-0.09	-0.05	0.26	0.54	1060	-0.13	-0.14	0.24	0.71
All sites	**12900**	**-0.04**	**0.85**	**0.13**	**0.87**	**0.01**	**1.01**	**0.13**	**0.82**	**12900**	**-0.04**	**0.85**	**0.14**	**0.87**

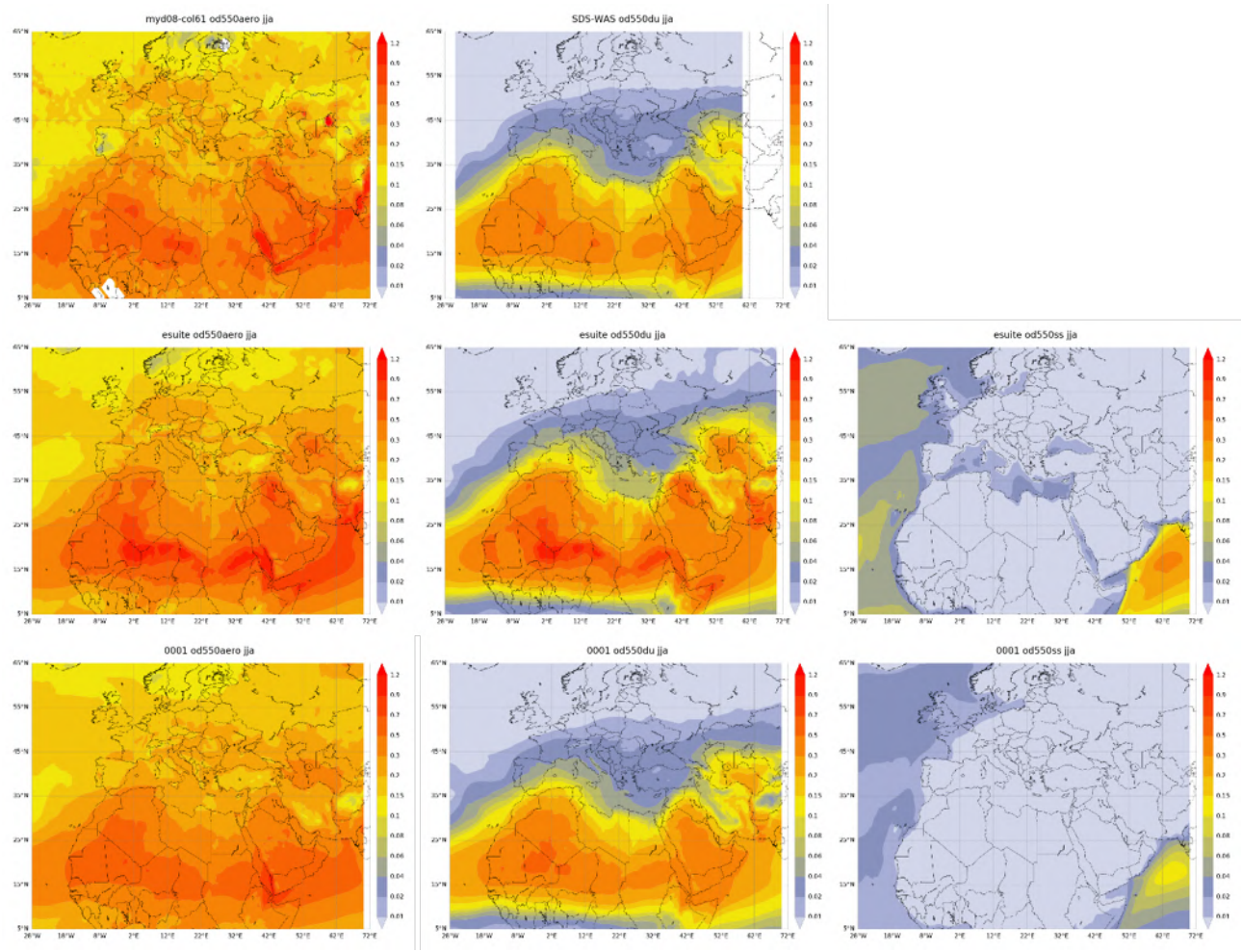

Figure 2.2.2. Seasonal averaged aerosol optical depth (od550aero), dust optical depth (od550du) and sea-salt (od550ss) from e-suite (expid h4xd, second row), current o-suite (expid h30x, third row) and o-suite (expid 0001, four row) for June-July-August 2017. CAMS outputs are compared with MODIS Collection 6.1 Level 3 aerosol optical depth and the SDS-WAS Multi-model dust optical depth.

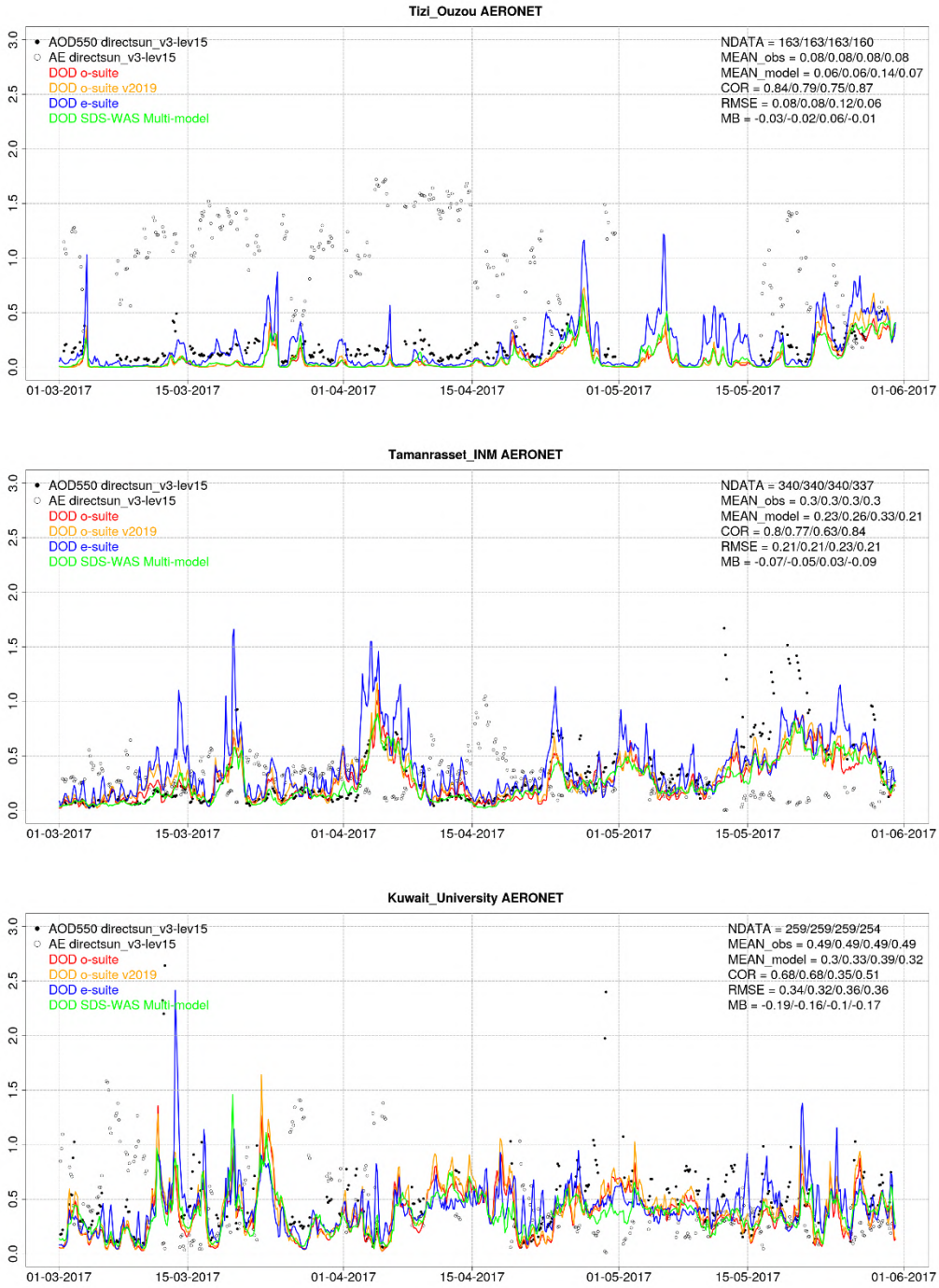

Figure 2.2.3. AOD and Angstrom Exponent from AERONET (black dots), DOD o-suite (red line, expid 0001), DOD current o-suite (expid h30x, orange line), DOD e-suite (expid h4x1, blue line) and DOD Multimodel SDS-WAS Median (green line) for Spring 2017 over Tizi Ouuzou (North Western Magrebh), Tamanrasset_INM (Sahara) and Kuwait University (Middle East)). Skill scores per each individual site and model (o—suite/control/SDS-WAS Multi-model) are shown in the upper right corner (NDATA: available 3-hourly values used for the calculations, MEAN observations, MEAN_model, COR, RMSE, MB).

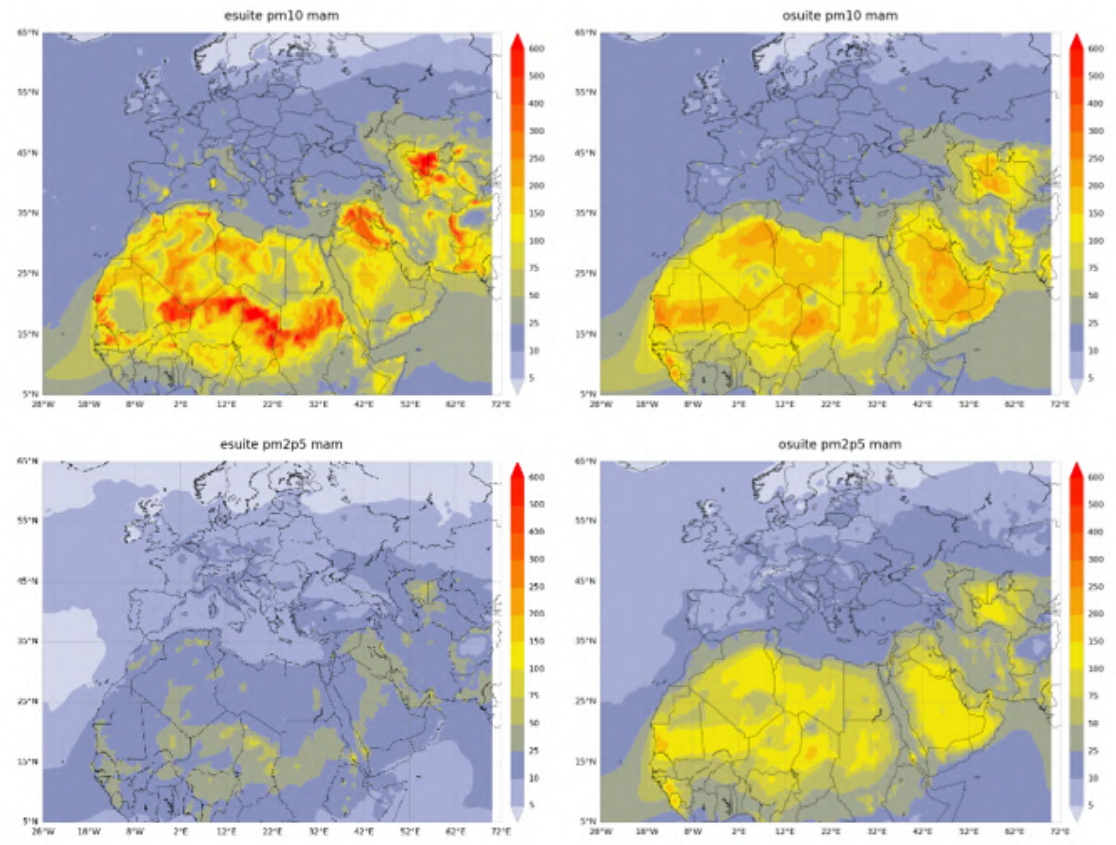

Figure 2.2.4. Seasonal averaged PM10 (top panels) and PM2.5 (bottom panels) in µg/m^3 from e-suite (expid h4x1, left panels) and current o-suite (expid h30x, right panels) for March-April-May 2017.

Analysis for the year 2019

Table 2.2.3. Skill scores (MB, FGE, RMSE and r) of 24h forecasts for the o-suite (expid 0001), the e-suite (expid 0073) and the SDS-WAS Multi-model Median for March-April-May 2019. Also shown is the number of observations (NDATA) used. Dust AOD (DOD) from AERONET is the reference.
In spring 2019, the same skills is observed as for spring 2017. The e-suite shows higher AOD values associated with sea-salt in the Atlantic, Arabian and the Mediterranean in comparison with the o-suite. In terms of correlation, the e-suite shows lower values for spring 2019 (0.77) in comparison with the o-suite (0.80). As in the case of spring 2017, it is in the Sahara and the Sahel regions where the e-suite shows lower correlation values (0.74 and 0.48, respectively for Sahara and Sahel) in comparison with the o-suite (0.82 and 0.58, respectively for Sahara and Sahel) and the SDS-WAS multi-model product (0.80 and 0.62, respectively for Sahara and Sahel). As in 2017, during spring 2019 the e-suite overestimates the maximum DOD peaks in Sahara (Tamanrasset_INM AERONET site) and Northwester Magrebh (Tunis_Carthage AERONET site).

		o-suite				e-suite				SDS-WAS				
	NDATA	MB	MFB	RMSE	COR	MB	MFB	RMSE	COR	NDATA	MB	MFB	RMSE	COR
Sahara	334	-0.02	0.01	0.13	0.82	0.10	0.40	0.20	0.74	303	-0.05	-0.08	0.16	0.80
Sahel	872	-0.33	-0.72	0.46	0.58	-0.28	-0.58	0.43	0.48	779	-0.31	-0.61	0.44	0.62
Tropical North Atlantic	196	-0.13	-1.05	0.15	0.93	-0.14	-1.07	0.18	0.91	175	-0.15	-1.15	0.19	0.89
Subtropical North Atlantic	462	-0.04	0.01	0.07	0.46	-0.02	0.19	0.06	0.43	404	-0.03	0.08	0.06	0.52
North Western Maghreb	219	-0.10	-0.93	0.14	0.71	0.03	0.13	0.11	0.68	185	-0.09	-0.73	0.13	0.74
Western Iberian Peninsula	511	-0.03	0.42	0.07	0.44	-0.02	0.55	0.06	0.49	469	-0.04	0.38	0.07	0.55
Iberian Peninsula	907	-0.01	1.39	0.05	0.77	0.00	1.46	0.04	0.71	827	-0.01	1.38	0.04	0.83
Western Mediterranean	1813	-0.01	1.48	0.06	0.71	0.01	1.59	0.06	0.72	1662	-0.01	1.46	0.06	0.70
Central Mediterranean	1561	-0.03	0.73	0.10	0.88	0.01	0.97	0.10	0.88	1450	-0.03	0.70	0.10	0.90
Eastern Mediterranean	958	-0.06	0.31	0.16	0.75	-0.03	0.49	0.14	0.77	859	-0.04	0.44	0.13	0.82
Eastern Sahara	-	-	-	-	-	-	-	-	-	-	-	-	-	-
Middle East	220	-0.02	0.22	0.12	0.85	-0.06	0.09	0.16	0.75	220	-0.03	0.24	0.12	0.86
All sites	**8053**	**-0.06**	**0.57**	**0.18**	**0.80**	**-0.03**	**0.75**	**0.17**	**0.77**	**7333**	**-0.06**	**0.60**	**0.17**	**0.83**

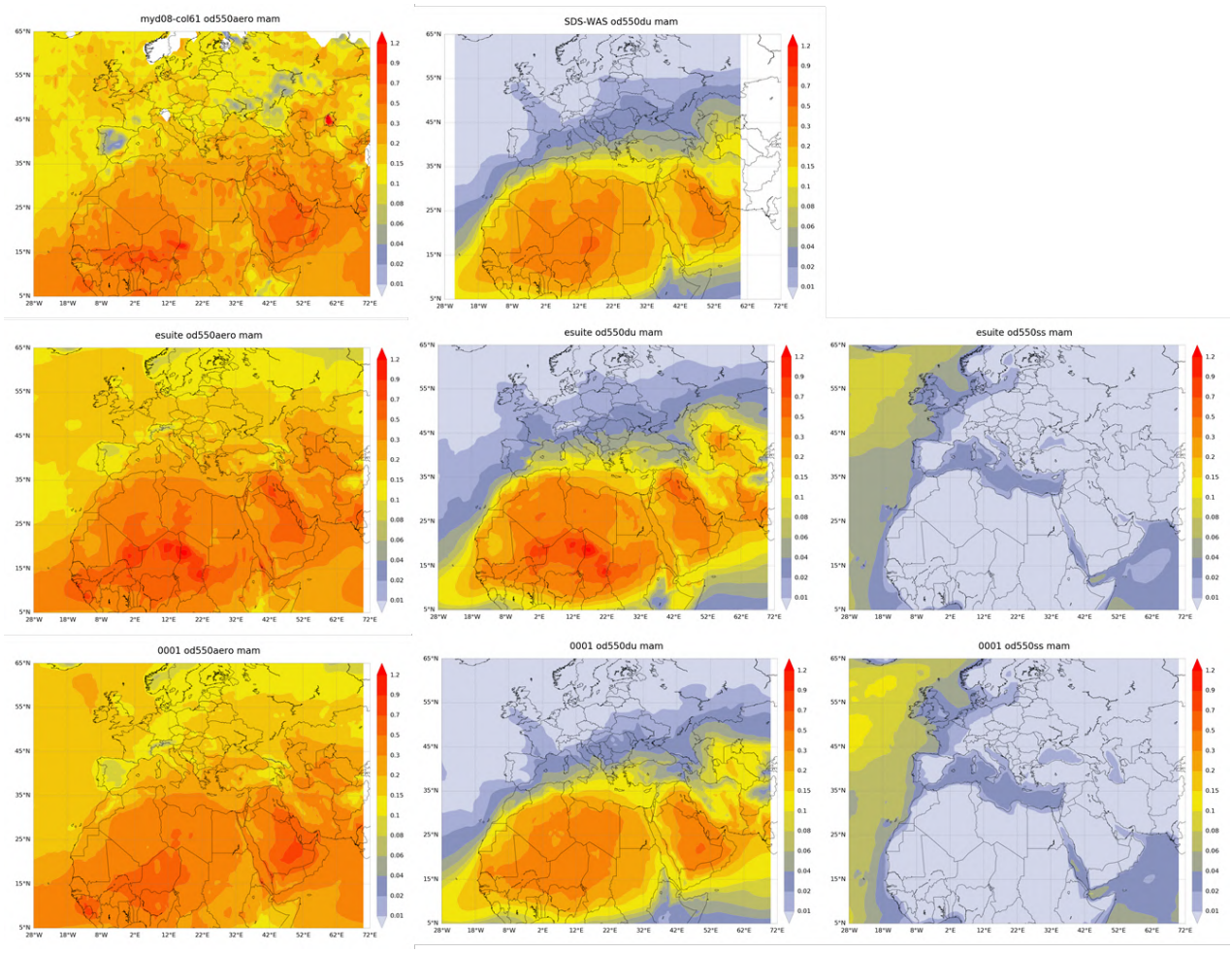

Figure 2.2.5. Seasonal averaged aerosol optical depth (od550aero), dust optical depth (od550du) and sea-salt (od550ss) from e-suite (expid 0073, second row) and o-suite (expid 0001, third row) for March-April-May 2019. CAMS outputs are compared with MODIS Collection 6.1 Level 3 aerosol optical depth and the SDS-WAS Multi-model dust optical depth.

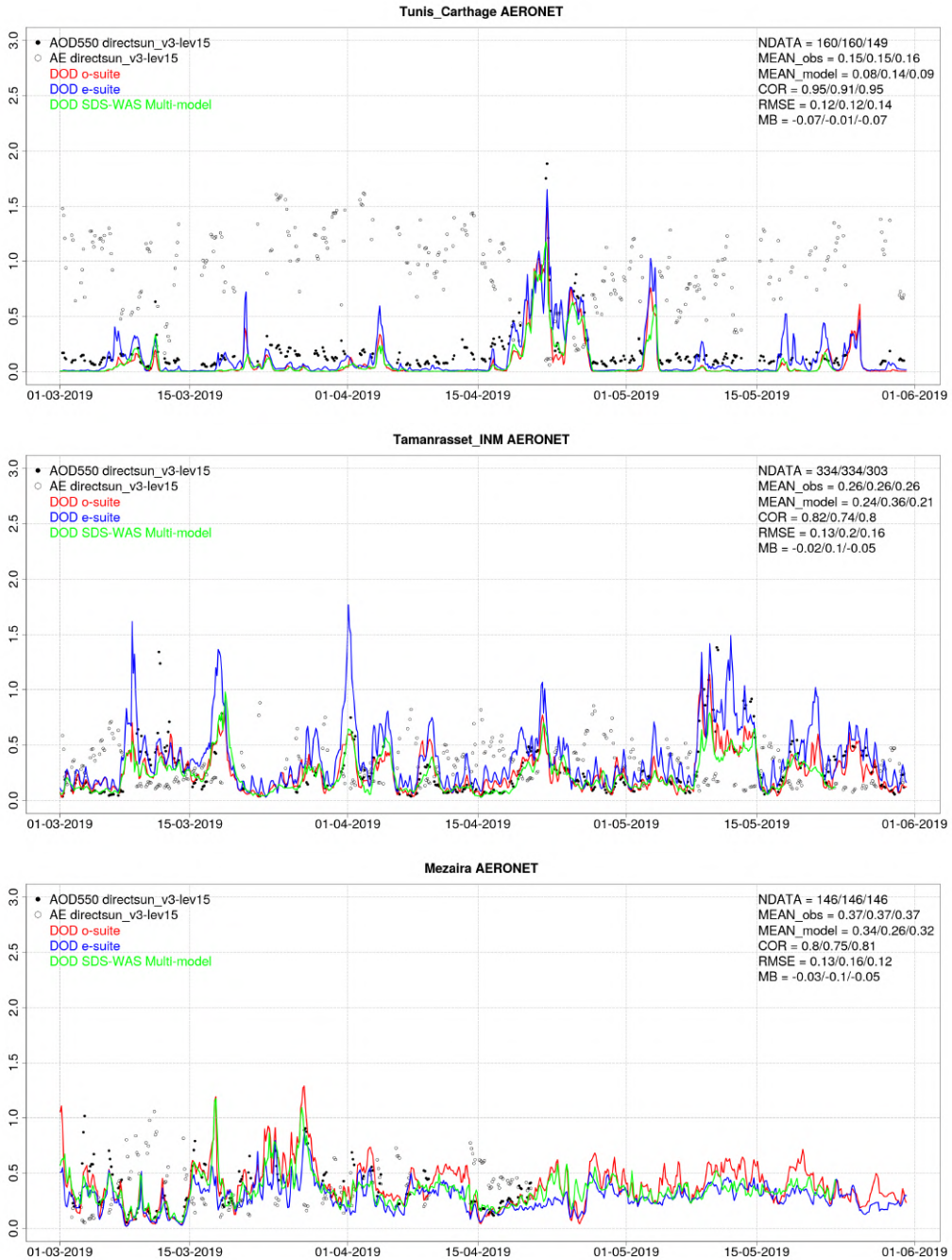

Figure 2.2.6. AOD and Angstrom Exponent from AERONET (black dots), DOD o-suite (red line, expid 0001), DOD e-suite (expid 0073, blue line) and DOD Multimodel SDS-WAS Median (green line) for Spring 2019 over Tunis_Carthage (North Western Magrebh), Tamanrasset_INM (Sahara) and Kuwait University (Middle East)). Skill scores per each individual site and model (o—suite/control/SDS-WAS Multi-model) are shown in the upper right corner (NDATA: available 3-hourly values used for the calculations, MEAN observations, MEAN_model, COR, RMSE, MB).

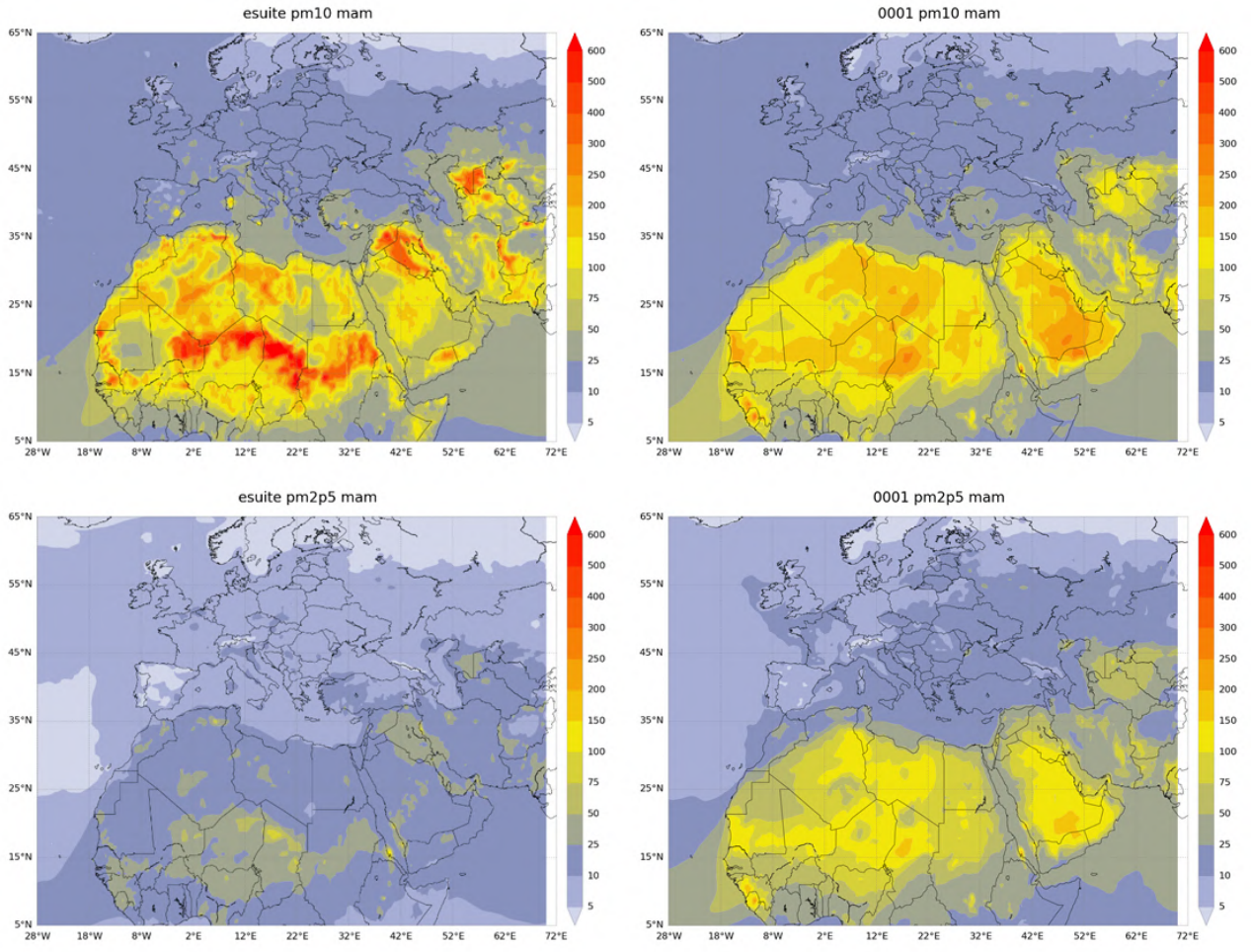

Figure 2.2.7. Seasonal averaged PM10 (top panels) and PM2.5 (bottom panels) in µg/m^3 from e-suite (expid 0073, left panels) and current o-suite (expid 0001, right panels) for March-April-May 2019.

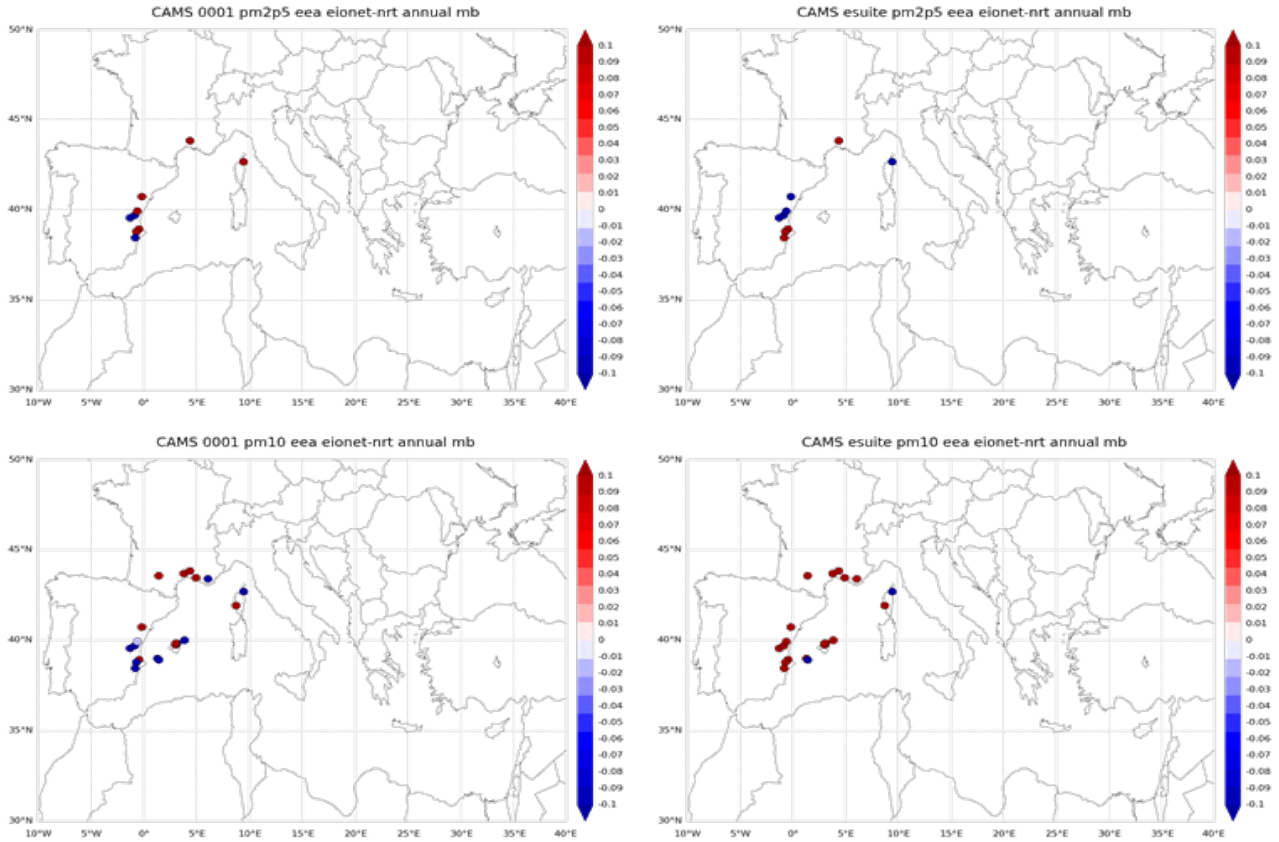

Figure 2.2.8: Mean bias for 24-hour forecasts of CAMS o-suite and e-suite for the study period. PM10 and PM2.5 from EIONET-Airbase is the reference.

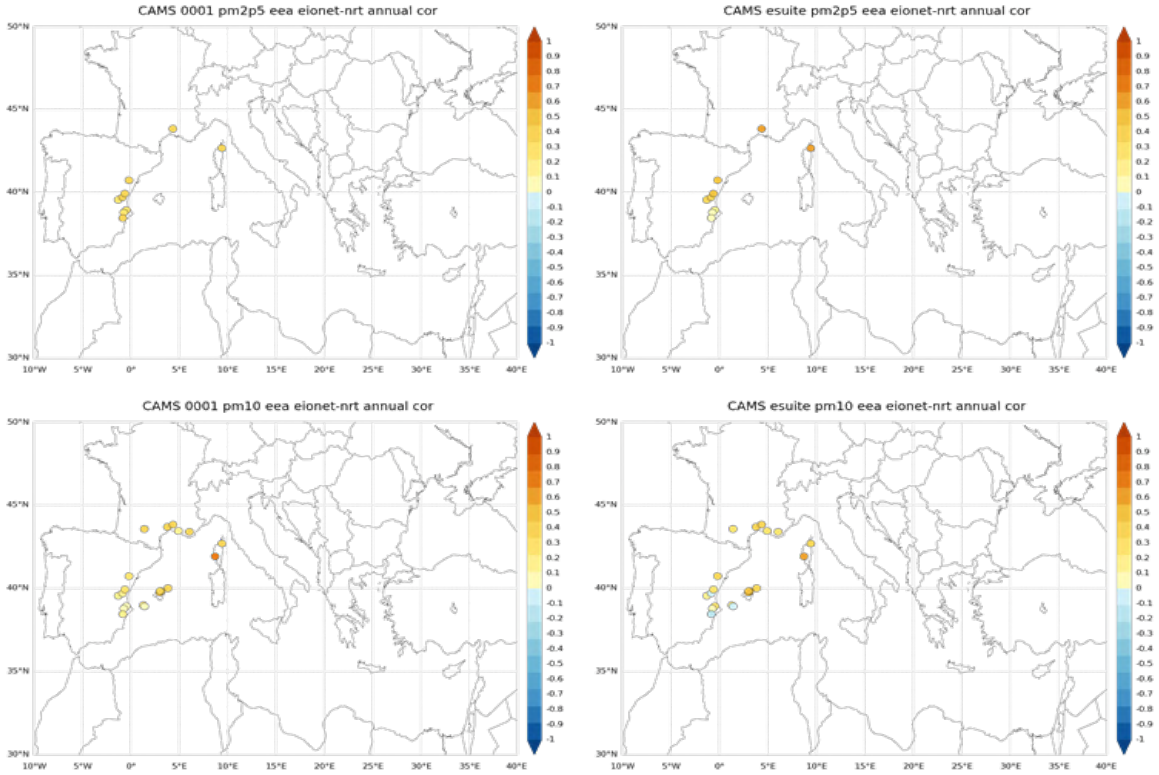

Figure 2.2.9: Correlation for 24-hour forecasts of PM2.5 and PM10 of CAMS o-suite and e-suite for the study period. PM10 and PM2.5 from EIONET-Airbase is the reference.

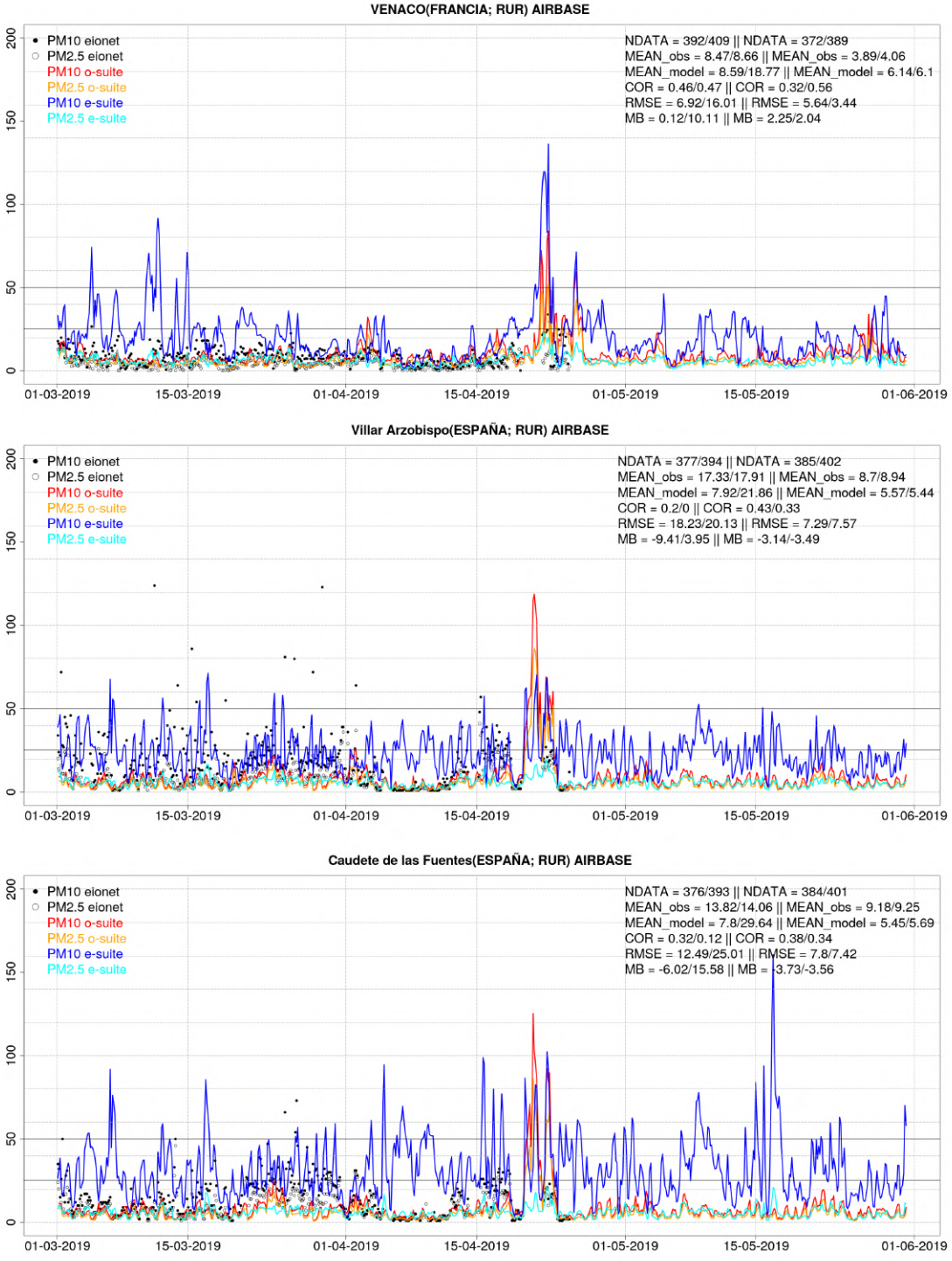

Figure 2.2.10: PM10 and PM2.5 Airbase observations (black and grey dots, respectively), PM10 and PM2.5 o-suite (expid 0001, red and orange lines, respectively) and PM10 and PM2.5 e-suite (expid 0073, blue and cyan lines, respectively) for the study period over Venaco (Corsica, France), Sa Pobla (Balearic Islands, Spain) and Caudete de las Fuentes (Spain). Skill scores per each individual site and model (o—suite/e-suite) are shown in the upper right corner (NDATA: available 3-hourly values used for the calculations, MEAN observations, MEAN_model, COR, RMSE, MB for PM10 and PM2.5, respectively).

2.3 Verification with ozone sonde data in the free troposphere and UT-LS

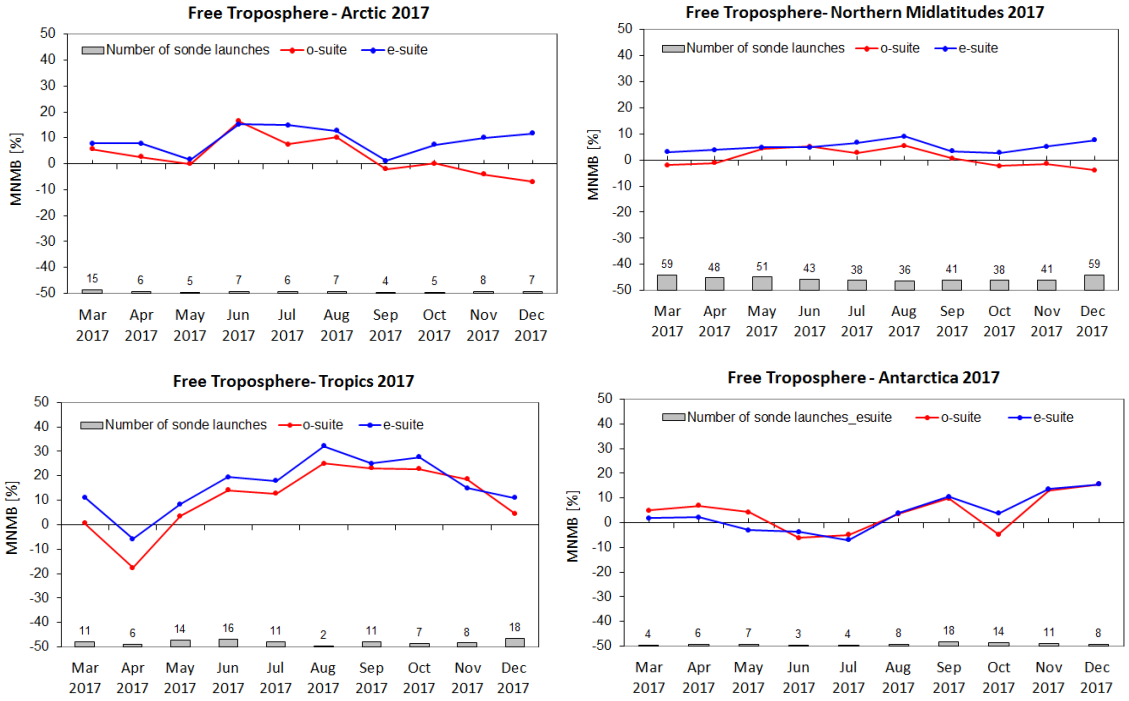

Fig. 2.3.1: Modified normalised mean bias (MNMB) for the o-suite (red) and pre-e-suite (blue) in 2017, averaged in height over the free troposphere (750-350 hPa; Tropics 750-200 hPa), for the Arctic, Northern midlatitudes, Antarctica and Tropics. The e-suite shows slightly larger positive MNMBs for the Arctic, the Northern Midlatitudes, and the Tropics.

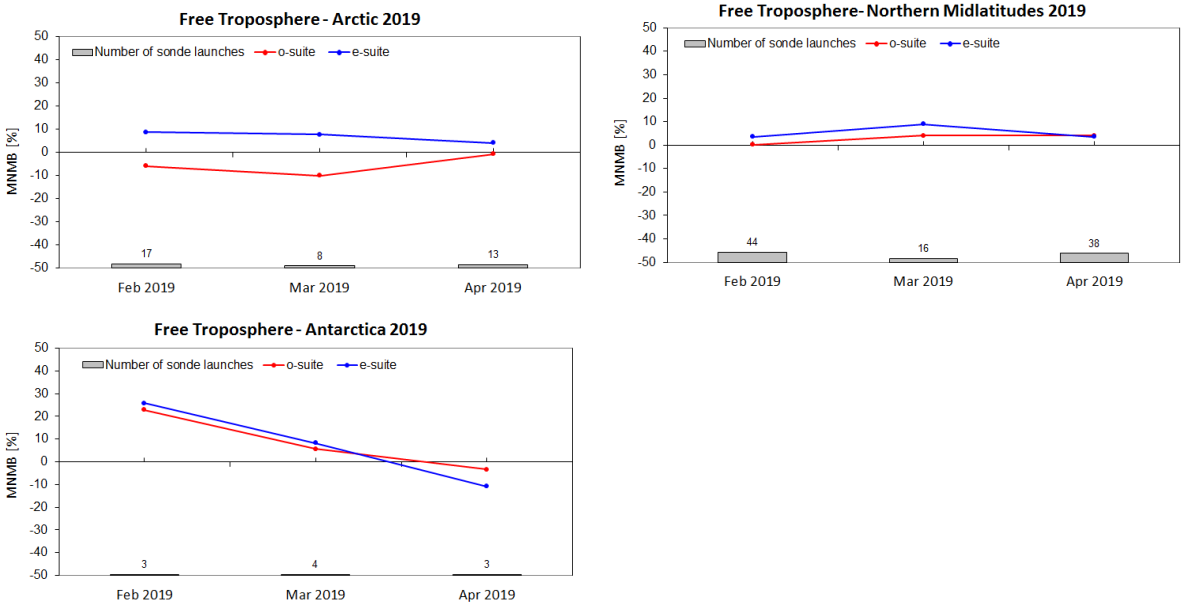

Fig. 2.3.2: MNMBs for the o-suite (red) and e-suite (blue) in February, March and April 2019, averaged over the free troposphere (750-350 hPa; Tropics 750-200 hPa). Plots are provided for the Arctic, Northern midlatitudes and Antarctica. Observational data for the Tropics was not yet available for this period in 2019. Again, the e-suite shows generally slightly larger positive MNMBs.

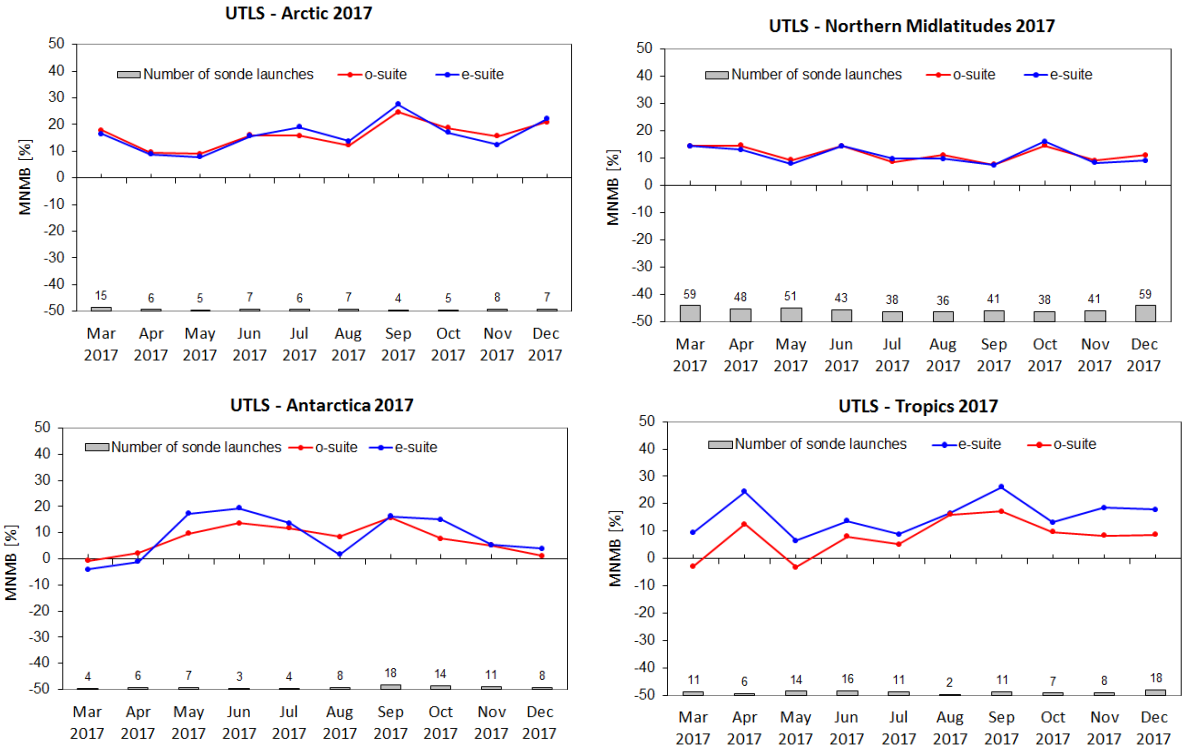

Fig. 2.3.3. MNMBs for the o-suite (red) and pre-e-suite (blue) in 2017 over the UTLS (300-100 hPa; Tropics 100-60 hPa) of the Arctic, Northern midlatitudes, Tropics and Antarctica. For Antarctica and the Tropics, the pre-e-suite shows slightly larger positive MNMBs compared to the o-suite.

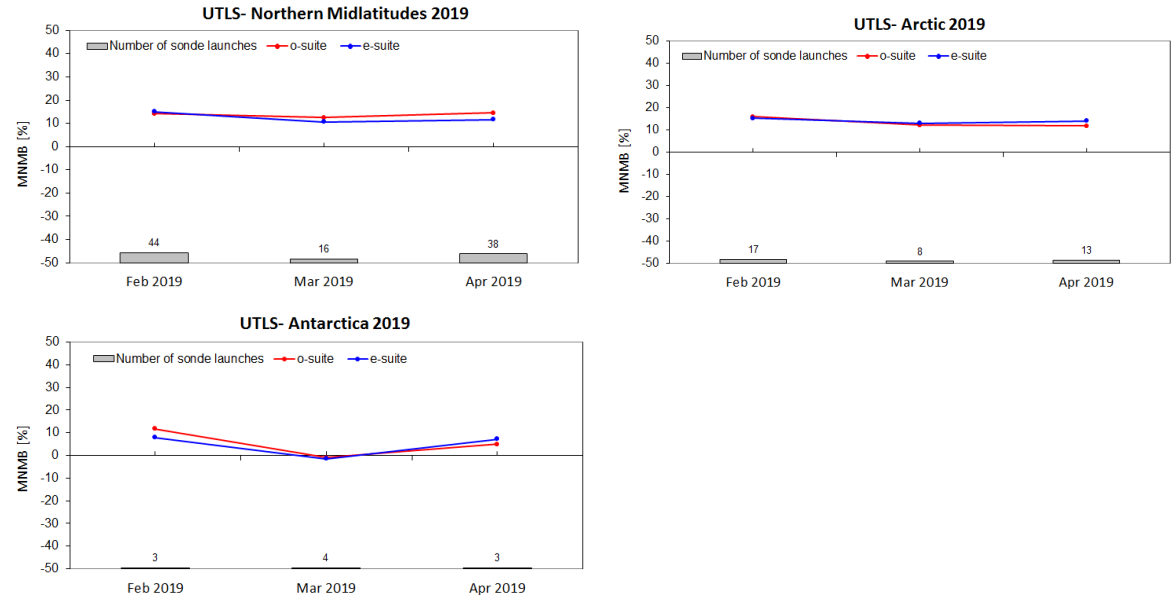

Fig. 2.3.4. MNMBs for the o-suite (red) and e-suite (blue) in 2019 over the UTLS (300-100 hPa; Tropics 100-60 hPa) of the Northern midlatitudes, Arctic, and Antarctica. Observational data for the Tropics was not yet available. Differences between the o-suite and e-suite are small.

2.4 Verification with GAW and ESRL-GMD surface ozone observations

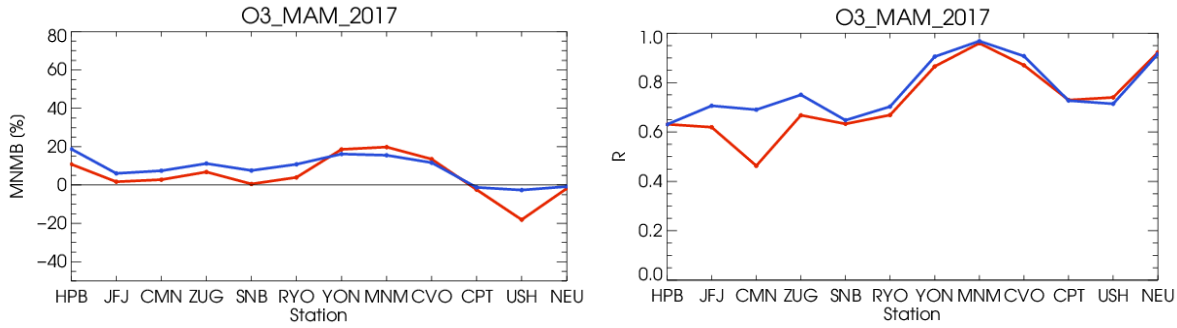

Fig. 2.4.1: MNMBs (left) and R (right) for the o-suite (red) and pre-e-suite (blue) over the period March-May 2017 for ozone. For the quarter MAM, the pre e-suite shows slightly larger MNMBs for Europe, but lower MNMBs for the Southern Hemisphere. The correlation is better for the e-suite.

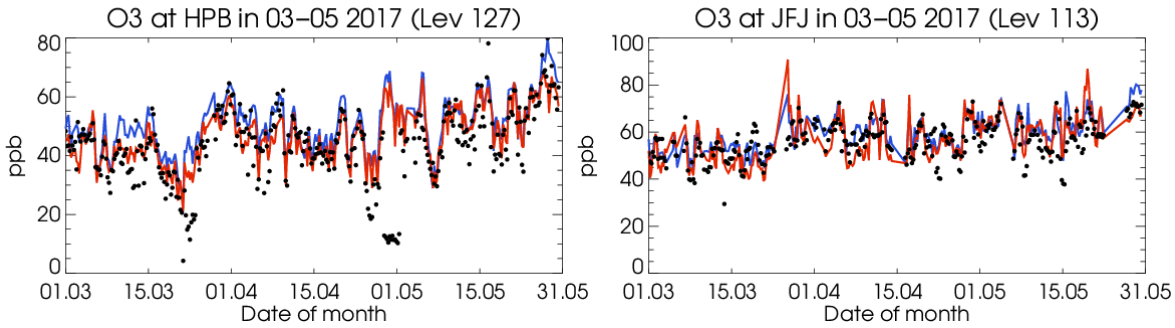

Fig. 2.4.2: Timeseries for the o-suite (red) and pre-e-suite (blue) over the period March-May 2017 for ozone for Hohenpeissenberg (left) and Jungfraujoch (right).

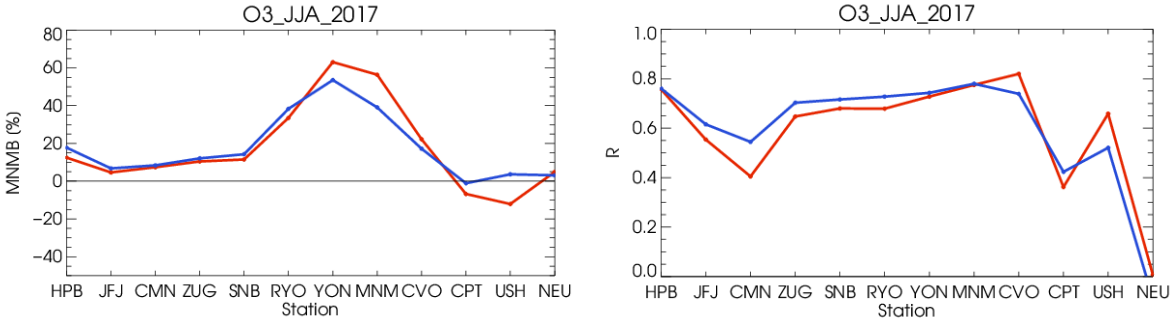

Fig. 2.4.3: MNMBs (left) and R (right) for the o-suite (red) and pre-e-suite (blue) over the period June-August 2017 for ozone. The e-suite shows lover MNMBs for stations in Asia. Correlation is mostly better for the e-suite.

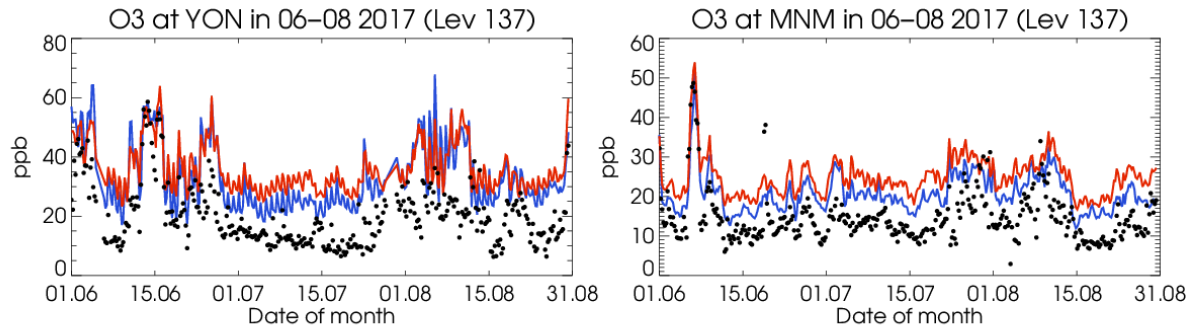

Fig. 2.4.4: Timeseries for the o-suite (red) and pre-e-suite (blue) over the period June-August 2017 for ozone for Yonagunijima (left) and Minamitroshima (right). The bias is reduced in the pre-e-suite over Japan.

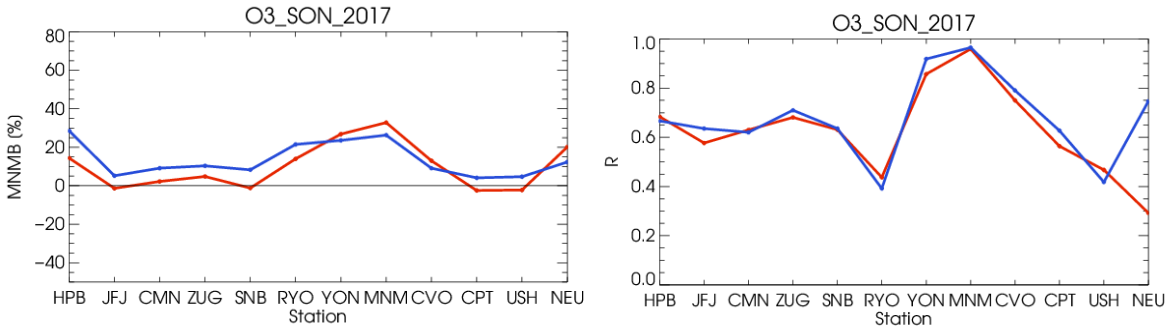

Fig. 2.4.5: MNMBs (left) and R (right) for the o-suite (red) and pre-e-suite (blue) over the period September-November 2017 for ozone. The e-suite shows slightly larger MNMBs for Europe.

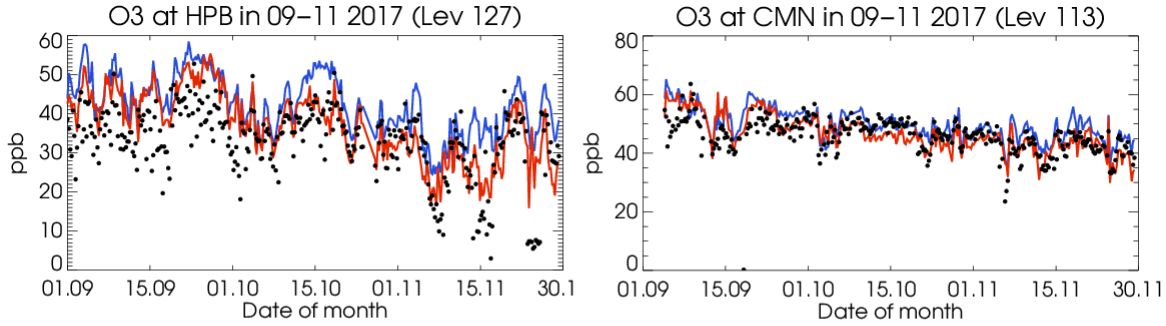

Fig. 2.4.6: Timeseries for the o-suite (red) and pre-e-suite (blue) over the period March-May 2017 for ozone for Hohenpeissenberg (left) and Monte Cimone (right).

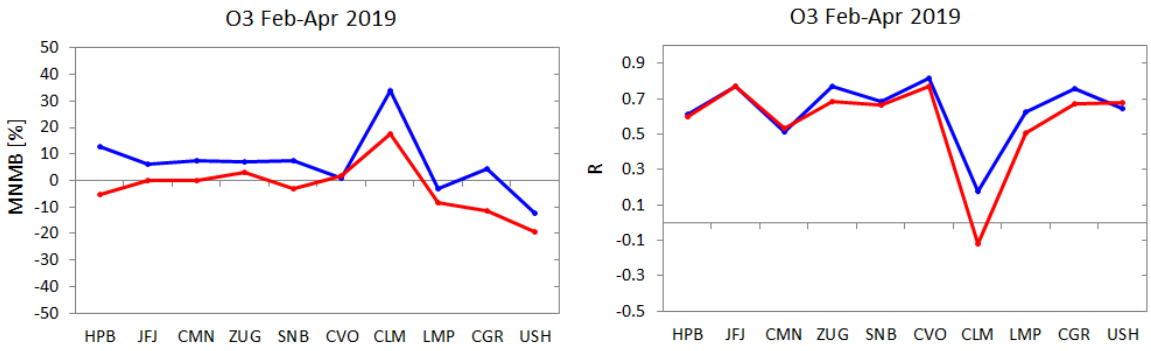

Fig. 2.4.7: MNMBs (left) and R (right) for the o-suite (red) and e-suite (blue) over the period February- April 2019 for ozone. The e-suite shows larger positive MNMBs for European stations.

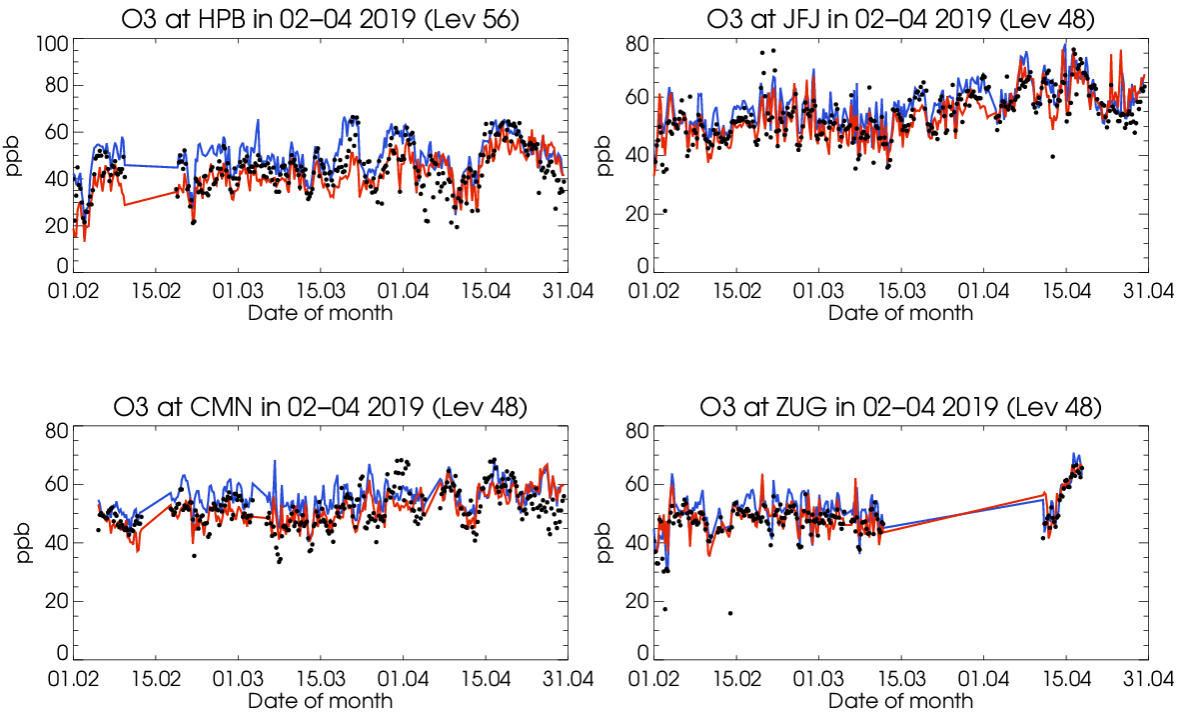

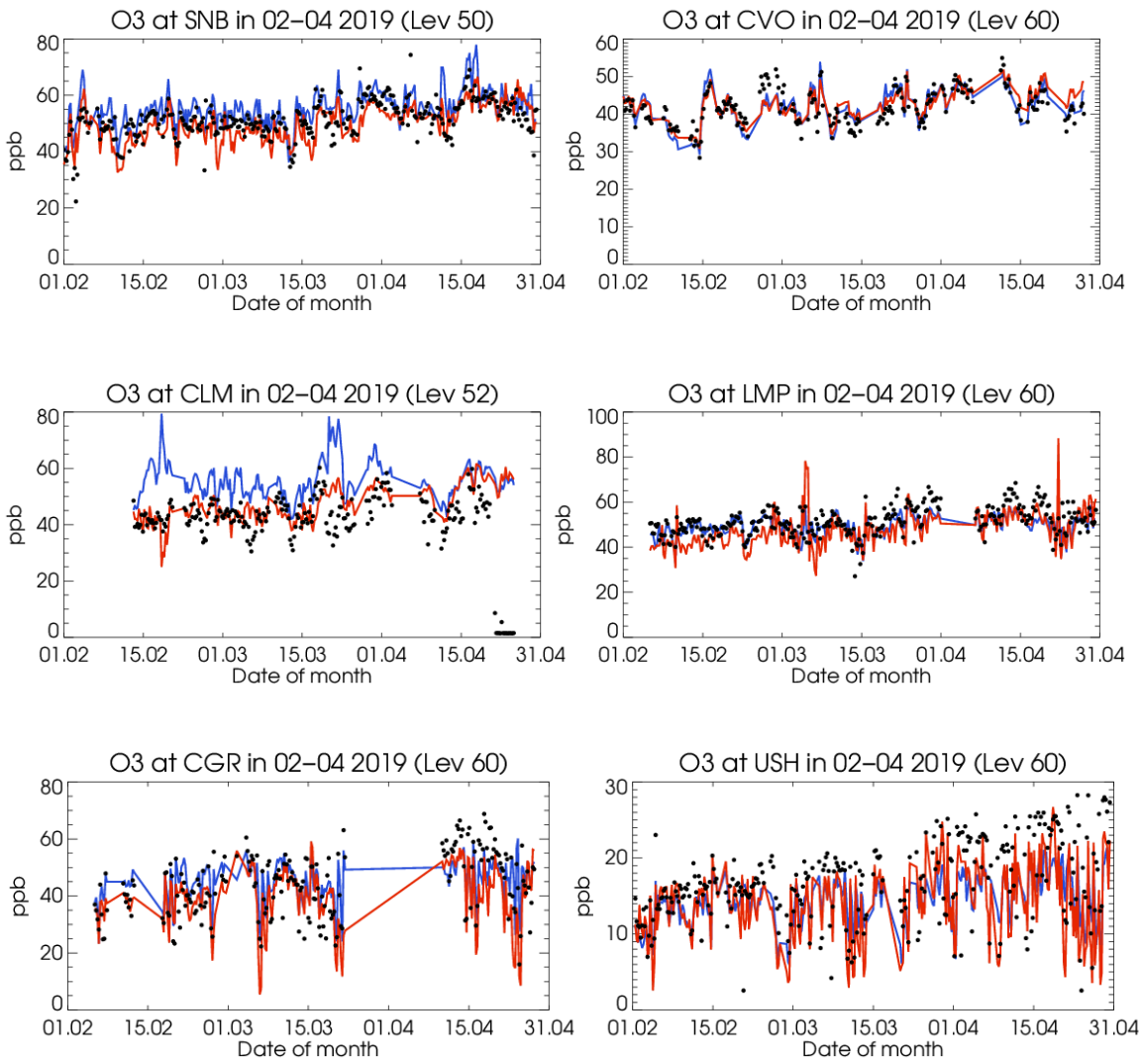

Fig. 2.4.8: Timeseries for the o-suite (red) and e-suite (blue) over the period February-April 2019 for ozone for different GAW stations. Larger positive deviations show up for the e-suite for Col Margherita in Italy.

Arctic ESRL Stations:

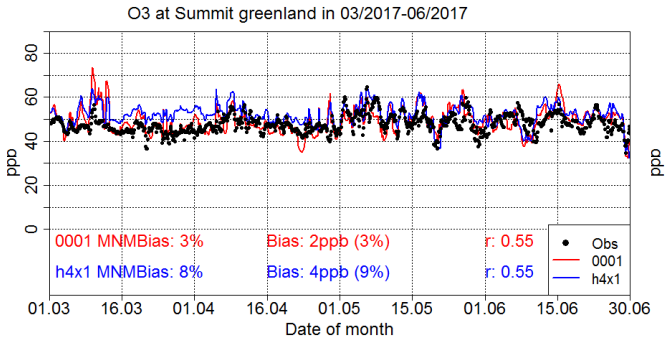

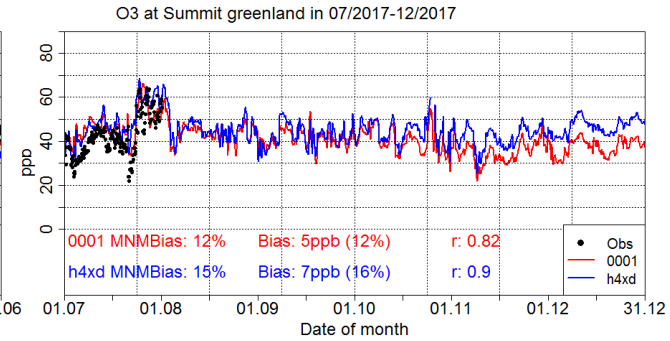

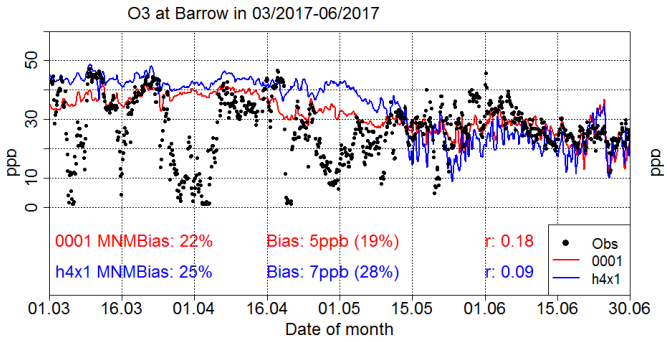

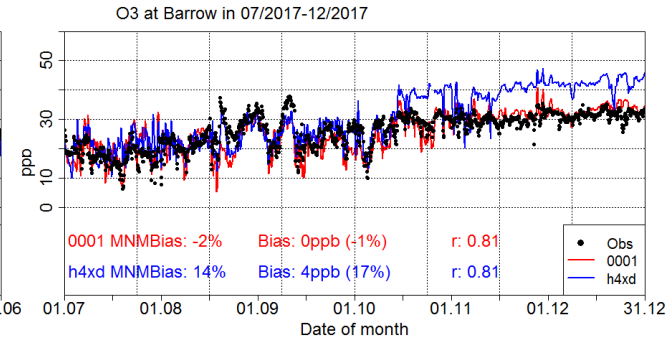

USA ESRL station:

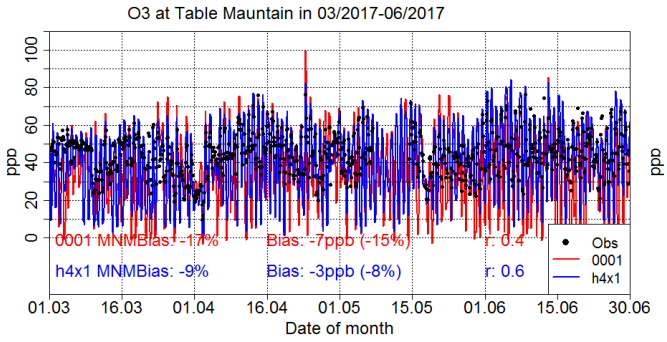

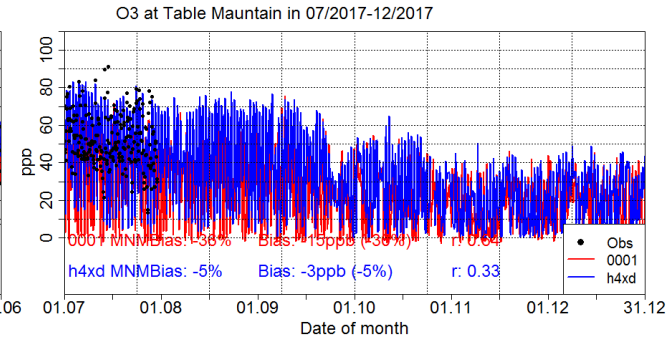

Tropical ESRL stations:

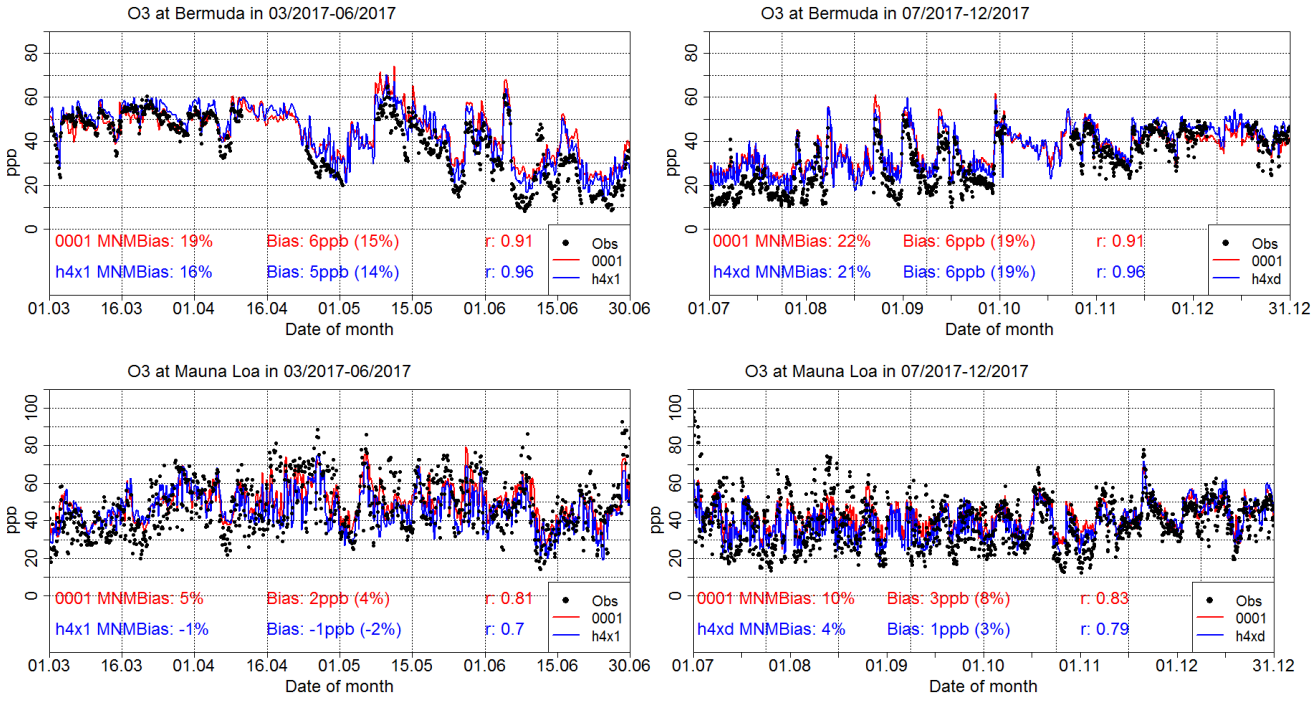

Antarctica ESRL stations

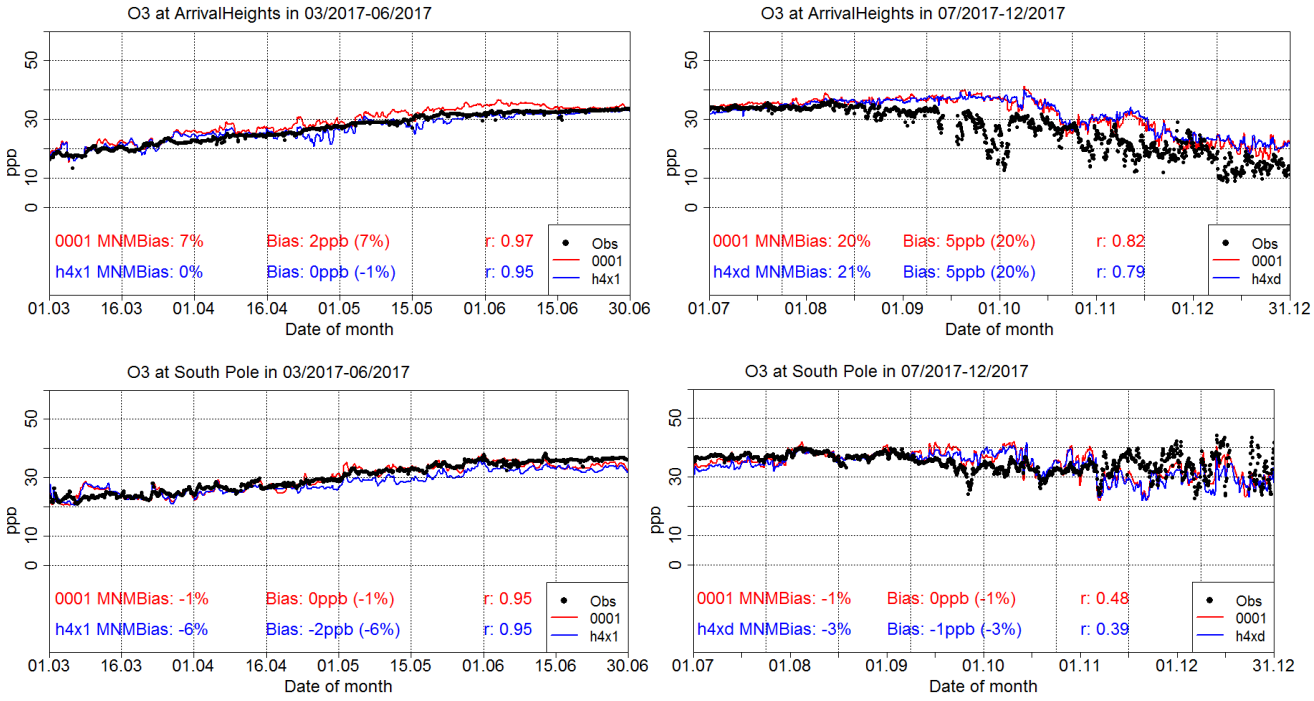

Fig. 2.4.9: Comparisons with ESRL surface ozone measurements for 1 March to 31 December 2017. Timeseries are shown for the o-suite (red) and pre-e-suite (blue). Stations are ordered from north to south.

Arctic ESRL Stations:

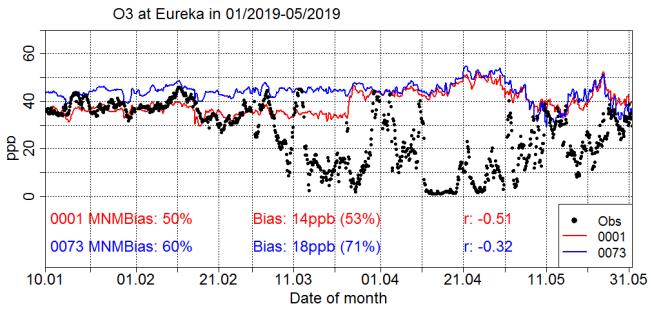

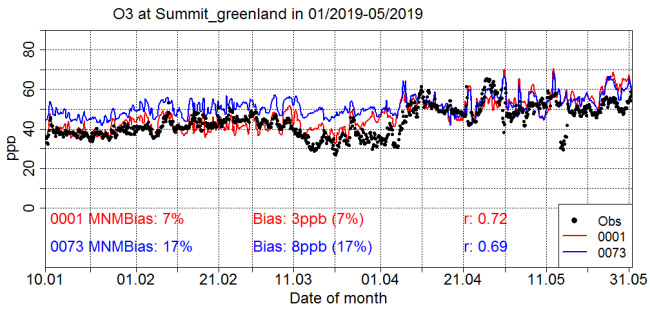

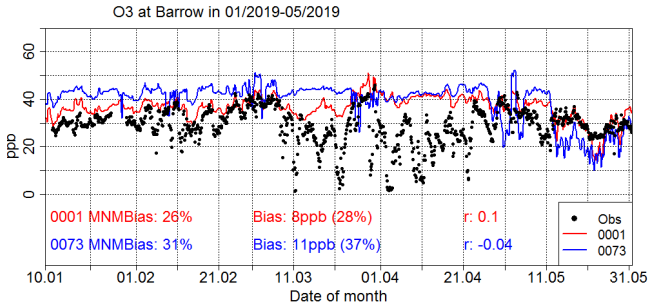

Table Mountain USA ESRL station:

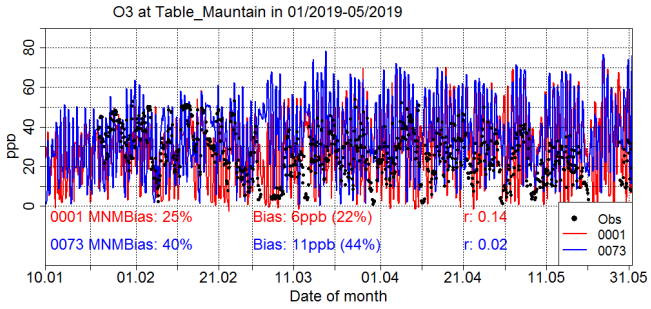

Tropical ESRL stations:

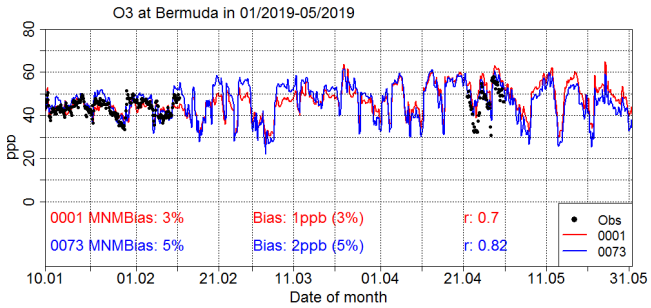

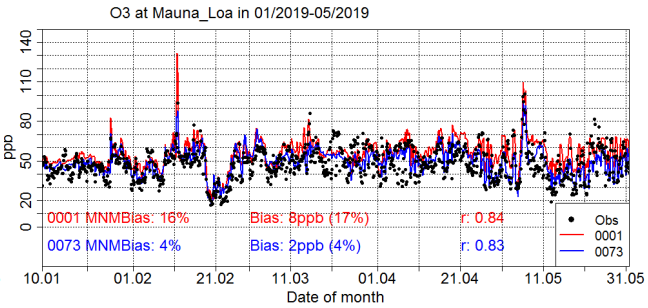

Lauder New Zealand ESRL station:

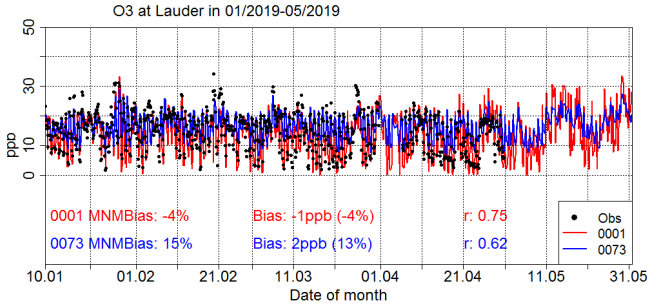

Antarctica ESRL stations:

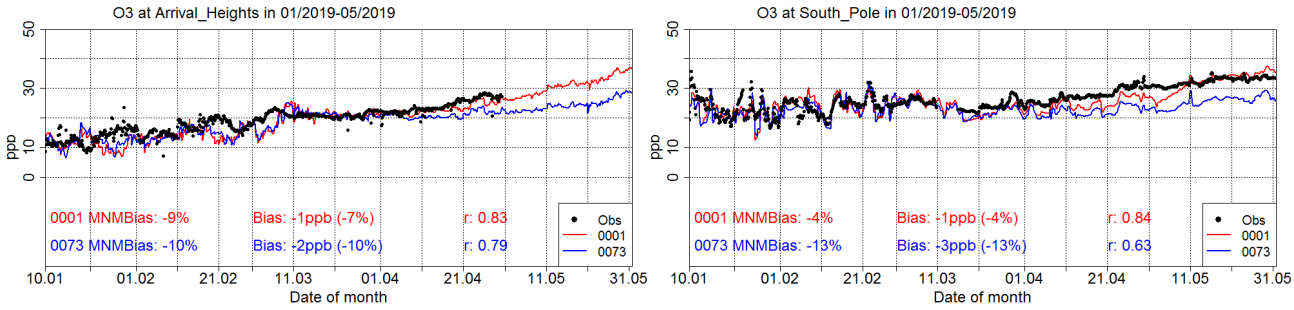

Fig. 2.4.10: Comparisons with ESRL surface ozone measurements for 10 January to 31 May 2019. Timeseries are shown for the o-suite (red) and e-suite (blue). Stations are ordered from north to south.

2.5 Verification with IAGOS ozone and CO observations

For the verifications with IAGOS, Level-1 data was used for comparisons in 2019 and level-2 data for comparisons in 2017. For the considered periods, continuous observations are available at Frankfurt, Paris (only CO) and Taipei (only CO) between March and December 2017, and only at Frankfurt in spring of 2019.

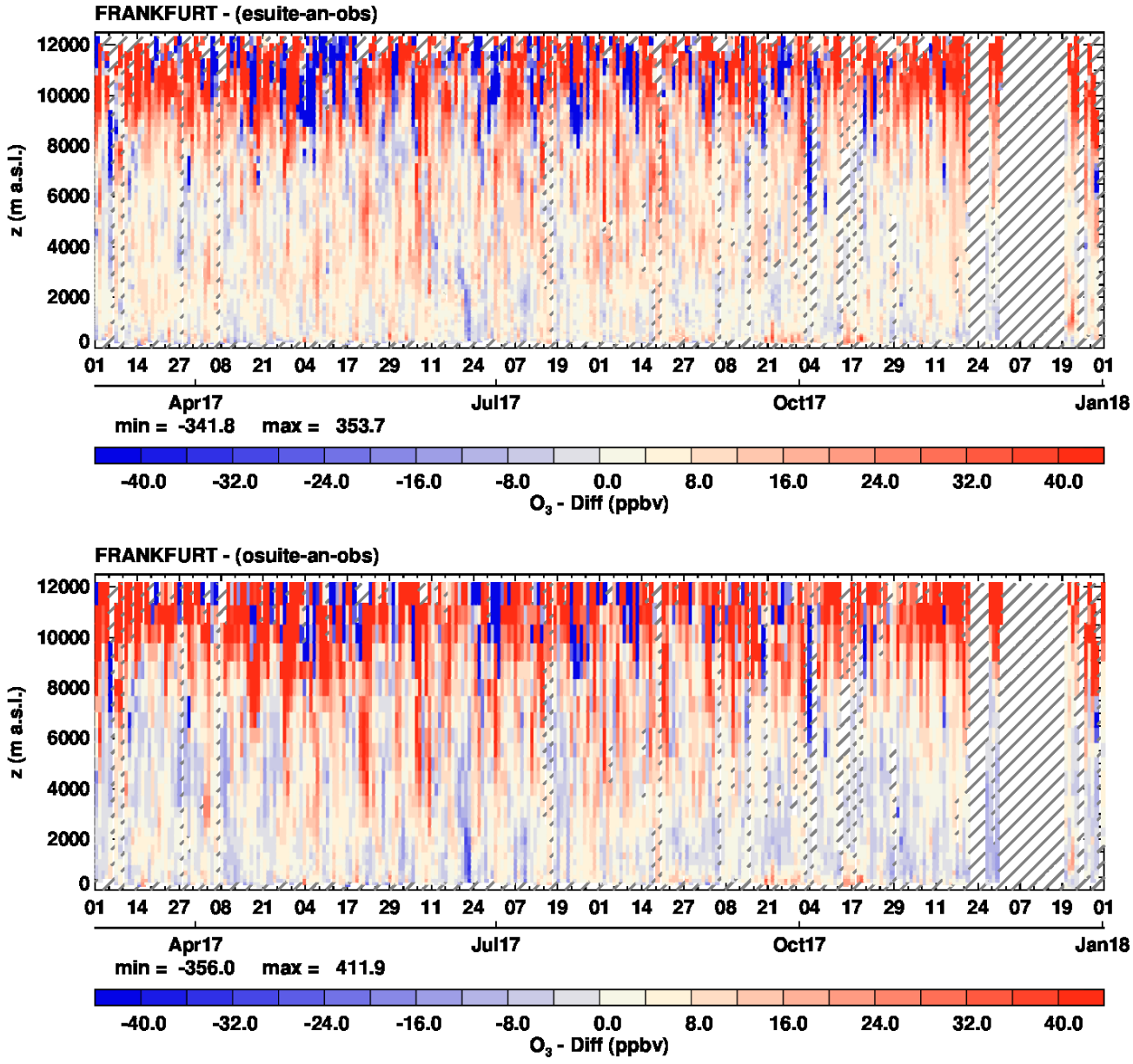

Fig. 2.5.1: Time series of the differences (model analysis minus IAGOS) in the daily profiles for ozone at Frankfurt during March-December 2017 for the pre-e-suite (h4x1-h4xd) on the top panel and o-suite (0001) on the bottom panel. The e-suite behaviour is very similar to that of the o-suite, and the bias from the pre-e-suite appears in general smaller than that of the o-suite.

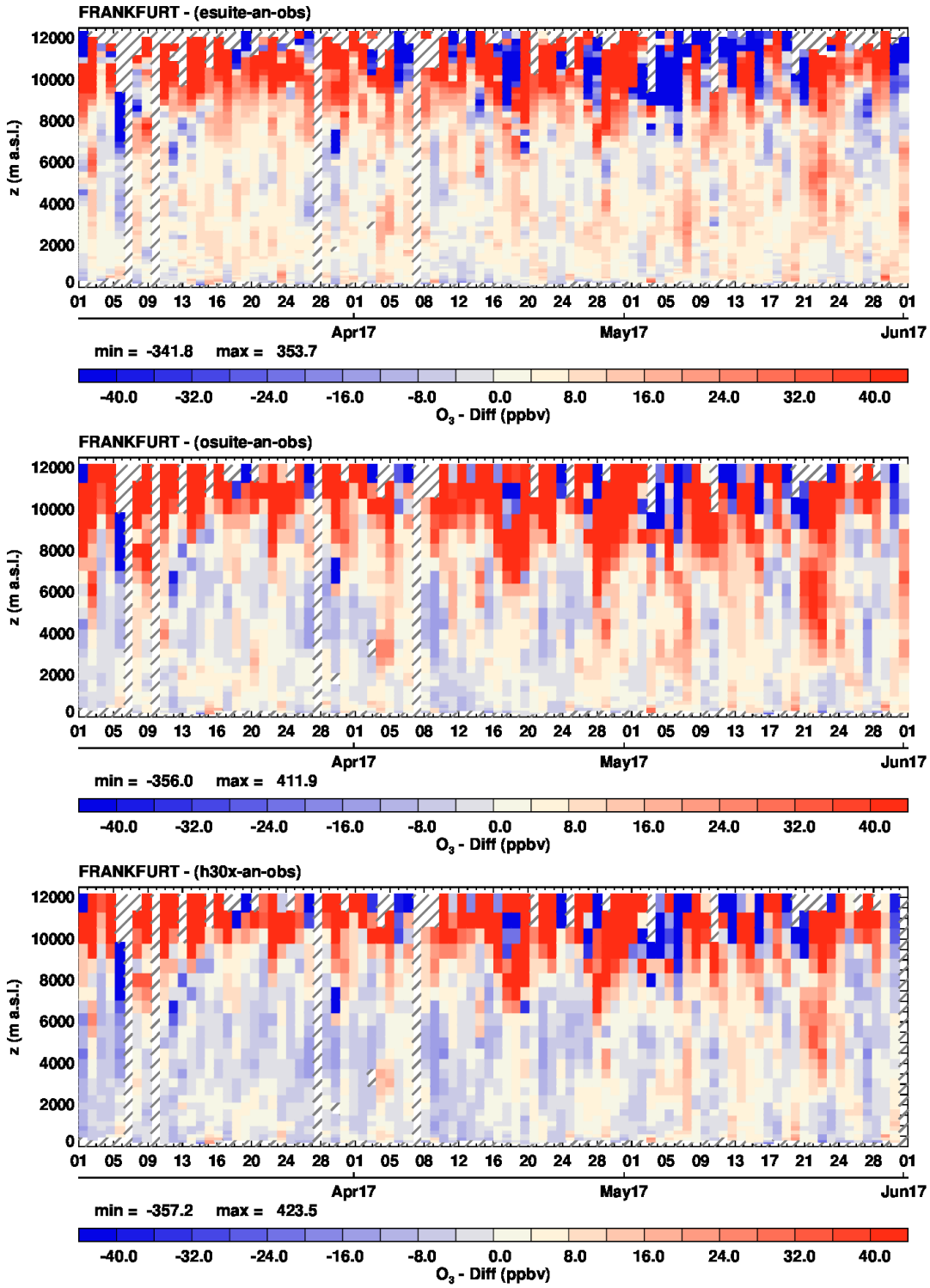

Fig. 2.5.2: Time series of the differences (model analysis minus IAGOS) in the daily profiles for ozone at Frankfurt during March-May 2017 for the pre-e-suite (h4x1) on the top panel, the former o-suite (0001) on the middle panel and the current o-suite (h30x) on the bottom panel. The bias from the e-suite is in general smaller than that of both o-suite configurations.

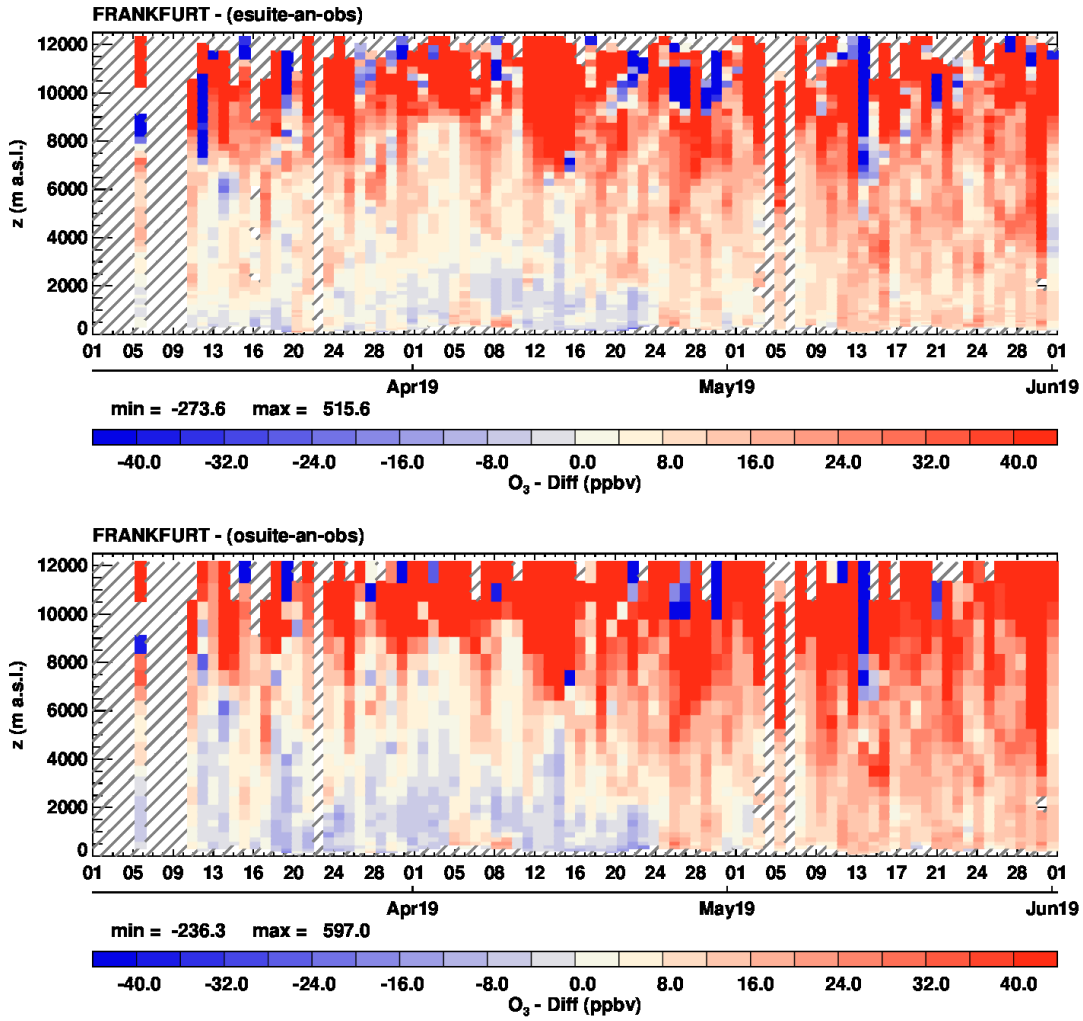

Fig. 2.5.3: Time series of the differences (model analysis minus IAGOS) in the daily profiles for ozone at Frankfurt during March-May 2019 for the e-suite (0073) on the top panel and o-suite (0001) on the bottom panel. The evolution of the bias toward positive values starting from the end of May present in both o-suite and e-suite is likely due to a problem with the IAGOS data (L1) due to instrument issues with an ozone sensor (which still has to be confirmed). Apart from this period, both models present very similar.

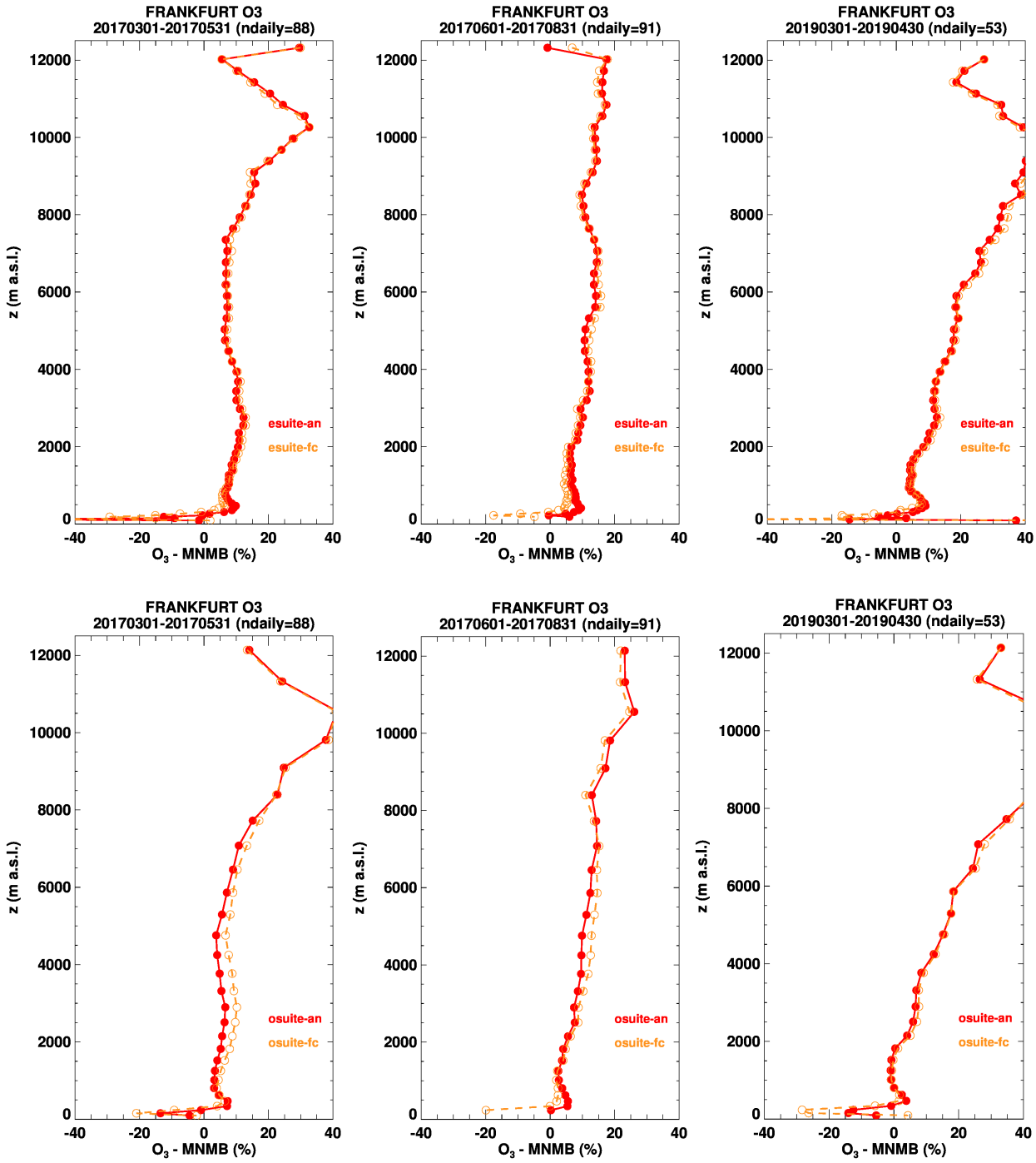

Fig. 2.5.4: Seasonal profiles of MNMB (model analysis/1 day-forecast) for ozone at Frankfurt. Results are presented for three periods: March-May 2017, June-August 2017 and March-April 2019. Upper panels correspond to the pre-e-suite (h4x1-h4xd, left and middle) and lower panels to the o-suite (0001, right). The bias from the e-suite is slightly smaller than that of the o-suite in the upper troposphere and UTLS, the results are rather similar in the lowest layers.

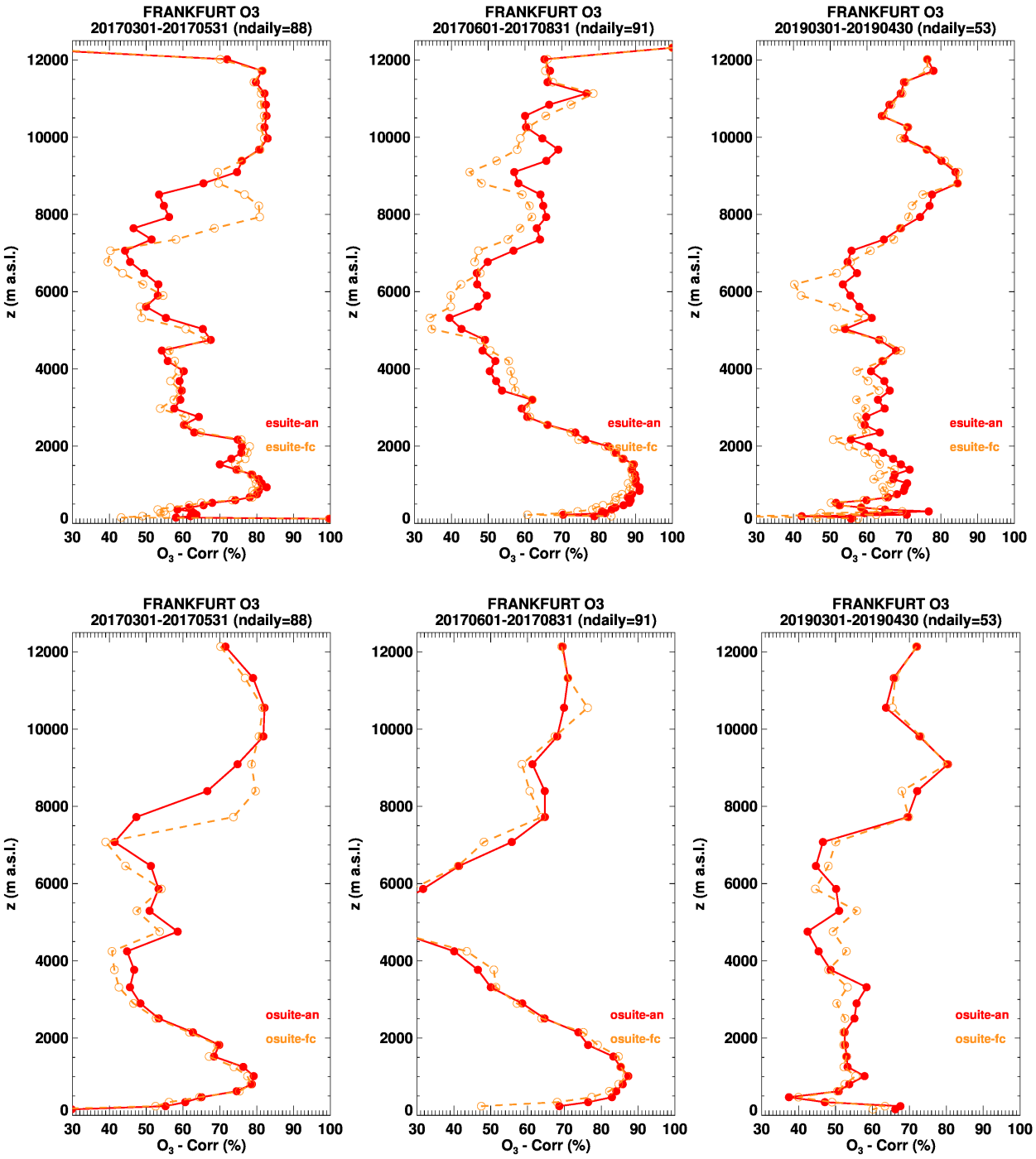

Fig. 2.5.5: Seasonal profiles of correlation coefficient for ozone at Frankfurt. It is presented for three periods: March-May 2017, June-July 2017 and March-April 2019. Upper panels correspond to pre-e-suite (h4x1-h4xd, left and middle) and lower panels to the o-suite (0001, right). Correlation coefficient are higher for the e-suite than for the o-suite in the lowest layers and mid-troposphere, in the upper layers the results are more similar.

2.6 Verification of ozone in the Mediterranean

Table 2.6.1: Coordinates, elevation, corresponding model level, as well as validation scores (MNMBs and correlations for the periods 03/2017-06-2017 and 07/2017-12/2017) obtained with the 2 forecast runs (o-suite and pre-e-suite), for each one of the selected Mediterranean stations. MNMBs and correlations with blue denote stations where pre e-suite run performs better while with red are denoted stations where o-suite performs better.

								03/2017-06/2017				07/2017-12/2017			
								MNMB		Cor. Coef		MNMB		Cor. Coef	
Station Name	Stat_ID	Lon	Lat	Alt (m)	Level o-suite	Level pre e-suite	Distance from the shore	o-suite	x4x1	o-suite	x4x1	o-suite	x4xd	o-suite	x4xd
Al Cornocales	ES1648A	-5.66	36.23	189	57	136	16	20.4	10.5	0.56	0.72	19.5	13.0	0.59	0.67
Caravaka	ES1882A	-1.87	38.12	1	60	137	73	-15.1	4.9	0.54	0.71	-19.6	8.9	0.73	0.85
Zarra	ES0012R	-1.10	39.08	885	56	130	70	1.9	3.1	0.74	0.80	-1.7	4.2	0.84	0.90
VIillar Del Arzobispo	ES1671A	-0.83	39.71	430	60	137	48	-4.8	5.2	0.57	0.70	-2.3	14.1	0.78	0.87
Cirat	ES1689A	-0.47	40.05	466	60	137	37	7.5	15.6	0.65	0.73	10.9	27.0	0.75	0.80
Bujaraloz	ES1400A	-0.15	41.51	327	60	136	60	-13.6	13.9	0.53	0.68	-19.6	22.2	0.80	0.85
Morella	ES1441A	-0.09	40.64	1150	53	123	51	5.0	5.0	0.77	0.85	1.0	5.8	0.79	0.85
Bc-La Senia	ES1754A	0.29	40.64	428	59	133	21	1.0	12.7	0.45	0.60	-8.9	9.9	0.67	0.74
Ay-Gandesa	ES1379A	0.44	41.06	368	58	135	15	12.6	12.5	0.71	0.78	15.8	21.0	0.80	0.81
Ak-Pardines	ES1310A	2.21	42.31	1226	57	130	81	26.1	28.5	0.51	0.60	20.9	27.9	0.67	0.73
Al-Agullana	ES1201A	2.84	42.39	214	60	137	25	-1.9	9.6	0.47	0.44	-12.8	12.2	0.64	0.65
Av-Begur	ES1311A	3.21	41.96	200	56	131	9	14.0	15.8	0.57	0.61	10.4	17.9	0.71	0.78
Plan Aups/Ste Baume	FR03027	5.73	43.34	675	54	123	21	12.9	17.1	0.75	0.79	6.8	17.5	0.86	0.84
Gharb	MT00007	14.20	36.07	114	57	133	31	7.4	5.8	0.45	0.66	-1.8	-1.0	0.71	0.79
Finokalia	GR0002R	25.67	35.32	250	57	134	4	-2.3	0.9	0.57	0.73	-10.8	-1.6	0.86	0.92
Agia Marina	CY0002R	33.06	35.04	532	55	129	14	12.4	12.4	0.46	0.59	1.0	2.6	0.77	0.76

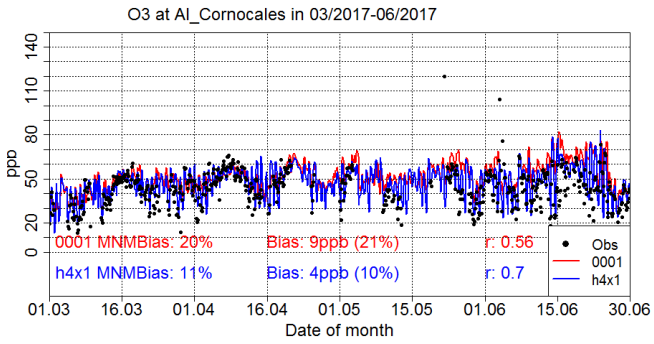

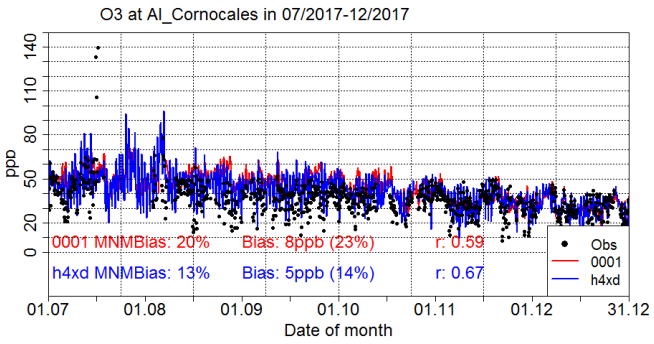

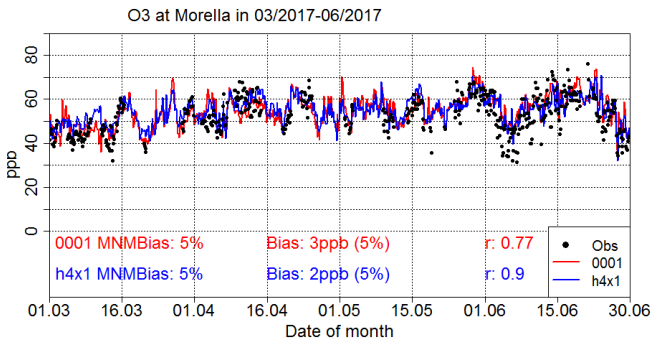

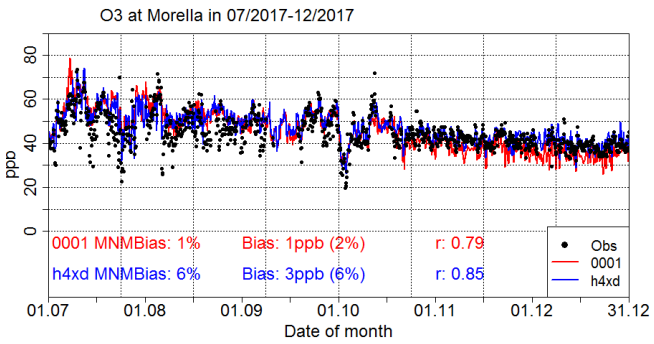

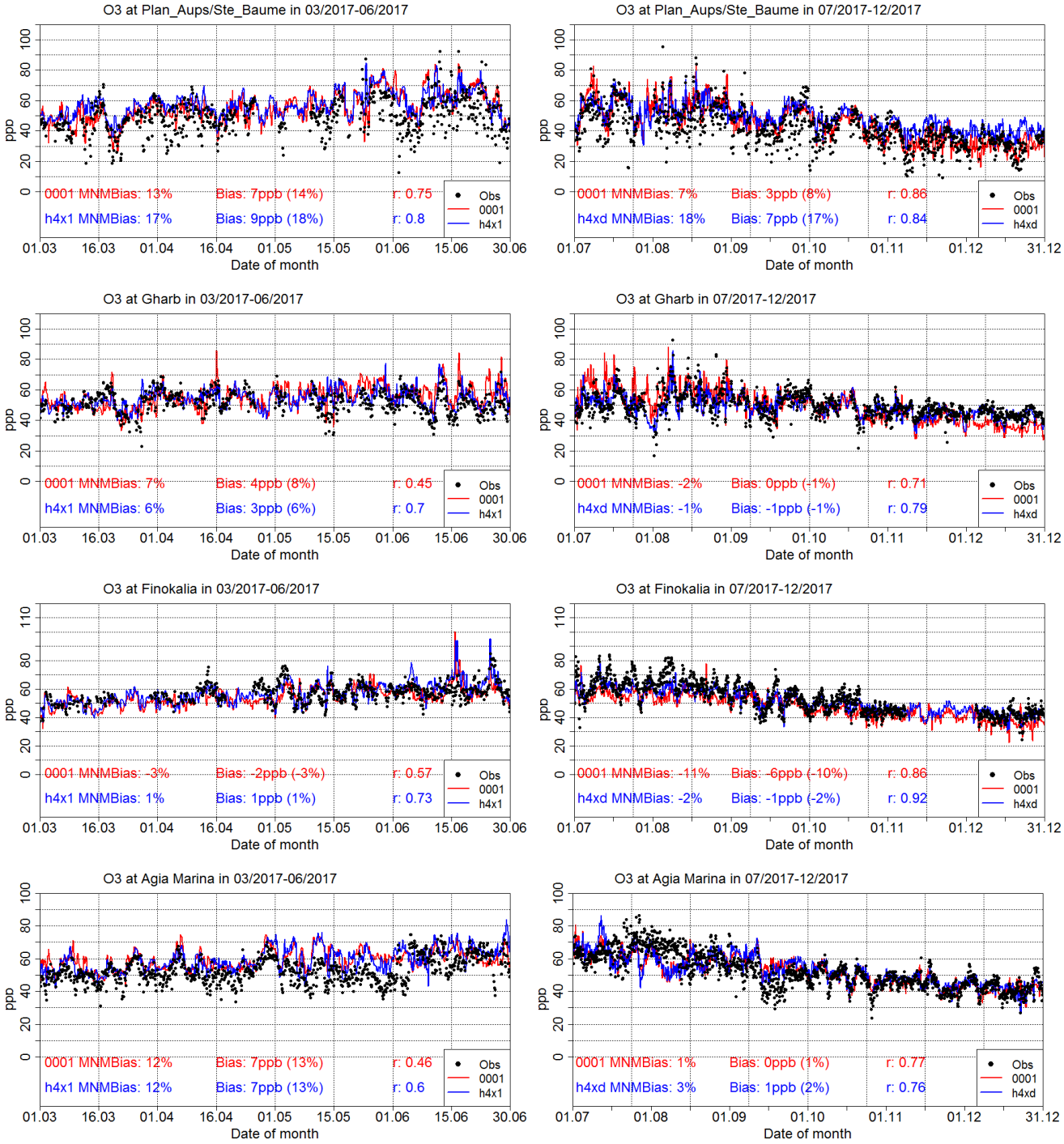

Fig. 2.6.1. Time series for the o-suite (red) and the pre-e-suite runs (blue) h4x1 (period 03/2017-06/2017; left) and h4hd period 07/2017-12/2017; right) compared to Airbase observations at: Al Cornocales, Spain station (36.23°N, 5.66 °W, 1st row), at Morrela, Spain station (40.64°N, 0.09°W, 2nd row), at Plan Aups/Ste Baume, France station (43.34°N, 5.73°E, 3rd row), at Gharb, Malta station (36.07°N, 14.20°E, 4th row), at Finokalia, Crete Greece station (35.32°N, 25.67°E, 5th row) and compared to observations provided by the Department of Labour Inspection - Ministry of Labour and Social Insurance of Cyprus) at Agia Marina, Cyprus station (35.04°N, 33.06 °E, 6th row).

Table 2.6.2: Coordinates, elevation, corresponding model level, as well as validation scores (MNMBs and correlations for the periods 10/01/2019-31/05/2019) obtained with the 2 forecast runs (o-suite and e-suite), for each one of the selected Mediterranean stations. MNMBs and correlations with blue denote stations where e-suite run performs better while with red are denoted stations where o-suite performs better.

								01/2019-05/2019			
							Distance from	MNMB		Cor. Coef	
Station Name	Stat_ID	Lon	Lat	Alt (m)	Level o-suite	Level pre e-suite	the shore	o-suite	0073	o-suite	0073
Al Cornocales	ES1648A	-5.66	36.23	189	57	136	16	17.9	12.2	0.72	0.87
Caravaka	ES1882A	-1.87	38.12	1	60	137	73	7.0	32.9	0.60	0.75
Zarra	ES0012R	-1.10	39.08	885	56	130	70	-2.9	3.8	0.78	0.90
VIillar Del Arzobispo	ES1671A	-0.83	39.71	430	60	137	48	0.3	12.1	0.55	0.76
Cirat	ES1689A	-0.47	40.05	466	60	137	37	-9.3	0.5	0.59	0.73
Bujaraloz	ES1400A	-0.15	41.51	327	60	136	60	-8.6	13.6	0.72	0.86
Morella	ES1441A	-0.09	40.64	1150	53	123	51	7.0	15.7	0.79	0.85
Bc-La Senia	ES1754A	0.29	40.64	428	59	133	21	-12.3	4.3	0.65	0.81
Ay-Gandesa	ES1379A	0.44	41.06	368	58	135	15	10.4	15.3	0.70	0.81
Ak-Pardines	ES1310A	2.21	42.31	1226	57	130	81	11.1	17.1	0.45	0.61
Al-Agullana	ES1201A	2.84	42.39	214	60	137	25	-27.1	1.1	0.69	0.70
Av-Begur	ES1311A	3.21	41.96	200	56	131	9	0.8	10.5	0.66	0.81
Plan Aups/Ste Baume	FR03027	5.73	43.34	675	54	123	21	6.2	17.5	0.75	0.78
Gharb	MT00007	14.20	36.07	114	57	133	31	-5.4	0.0	0.25	0.41
Finokalia	GR0002R	25.67	35.32	250	57	134	4	-3.1	0.5	0.74	0.84
Agia Marina	CY0002R	33.06	35.04	532	55	129	14	10.1	8.7	0.80	0.83

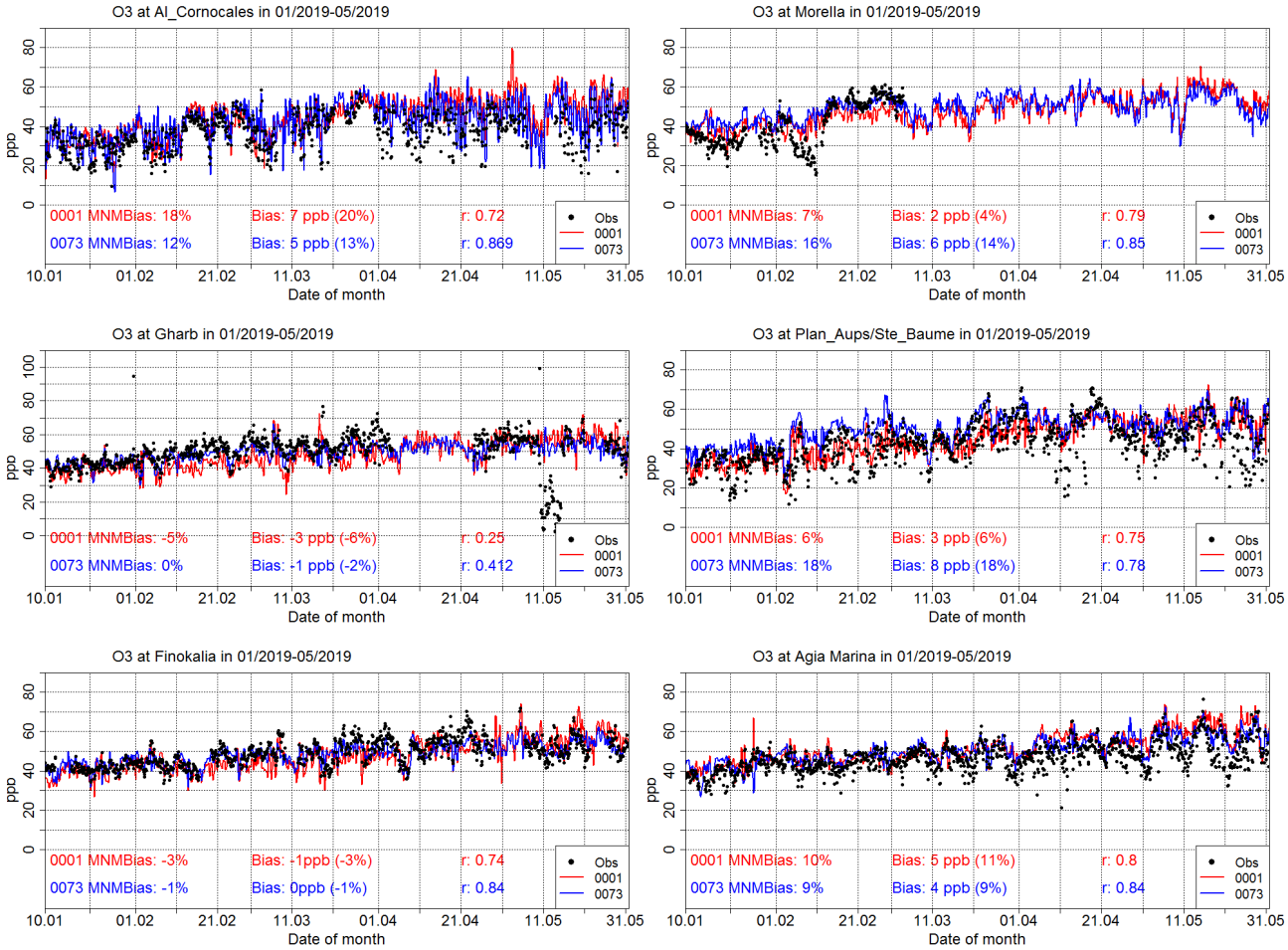

Fig. 2.6.2. Time series for the o-suite (red) and the e-suite (blue) compared to Airbase observations at Al Cornocales, Spain station (36.23°N, 5.66 °W, top left), at Zarra, Spain station (39.08°N, 1.10°W, top right), at Plan Aups/Ste Baume, France station (43.34°N, 5.73°E, center left), at Gharb, Malta station (36.07°N, 14.20°E, center right), at Finokalia, Crete Greece station (35.32°N, 25.67°E, low right) and compared to observations provided by the Department of Labour Inspection - Ministry of Labour and Social Insurance of Cyprus at Agia Marina, Cyprus station (35.04°N, 33.06 °E, low right). Time Period: 10/01/2019-31/05/2019

2.7 Verification with ozone surface data in the Arctic

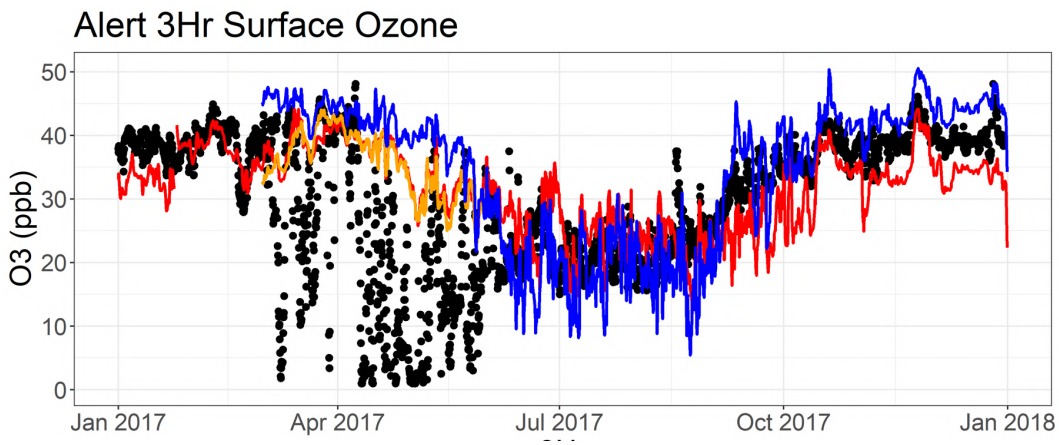

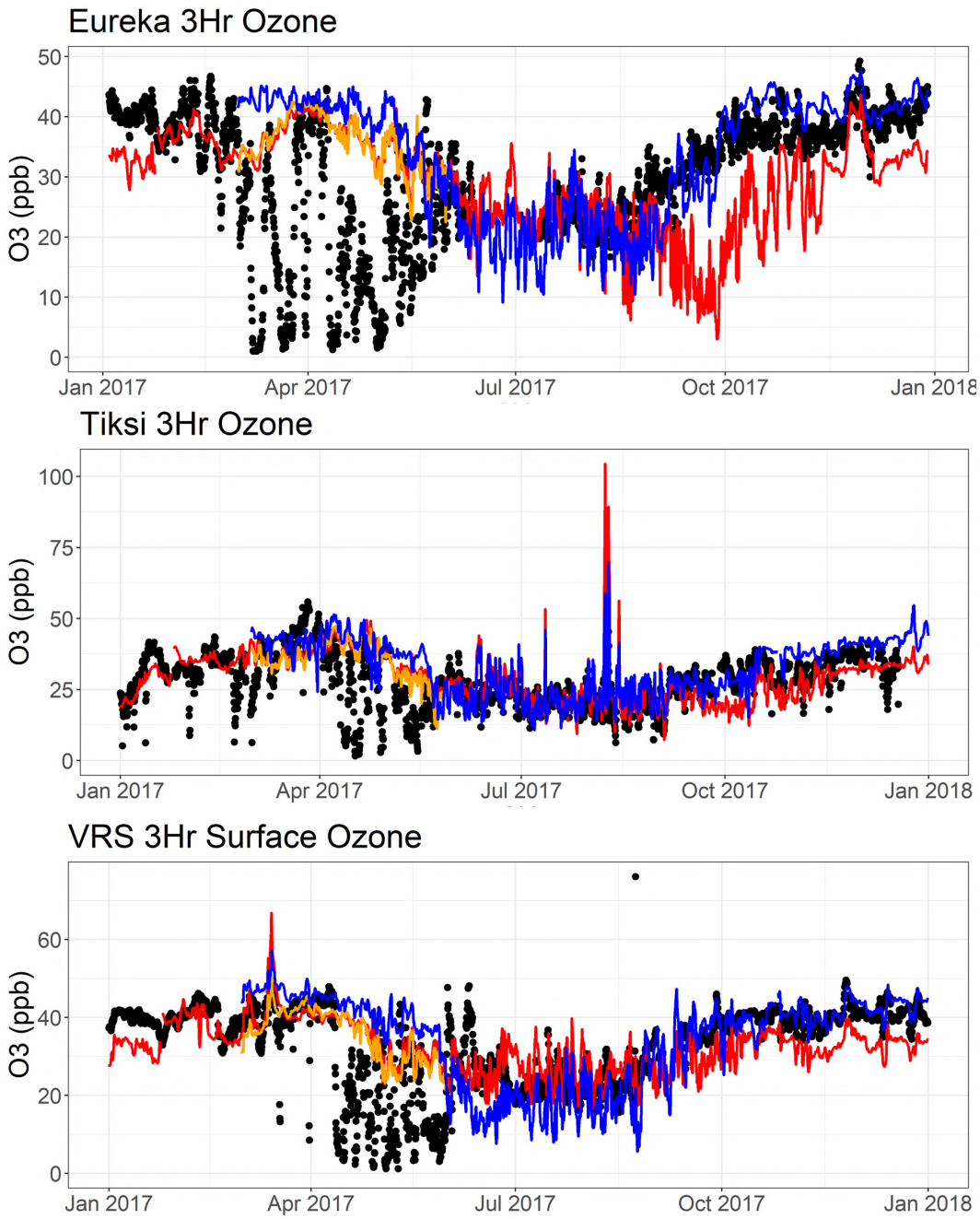

Fig. 2.7.1: Surface ozone mixing ratios at Alert (Canada), Eureka (Canada), Tiksi (Russia) and the Villum Research Station (Greenland) from January - December 2017 for the 2017 o-suite (red), for the 2018 o-suite configuration (h30x, orange) and for the 2017 pre-e-suite (blue). Overall there is an improved agreement with observations for the pre-e-suite with slightly improved correlations and a better description of the seasonal pattern with changes in levels from summer to autumn/winter.

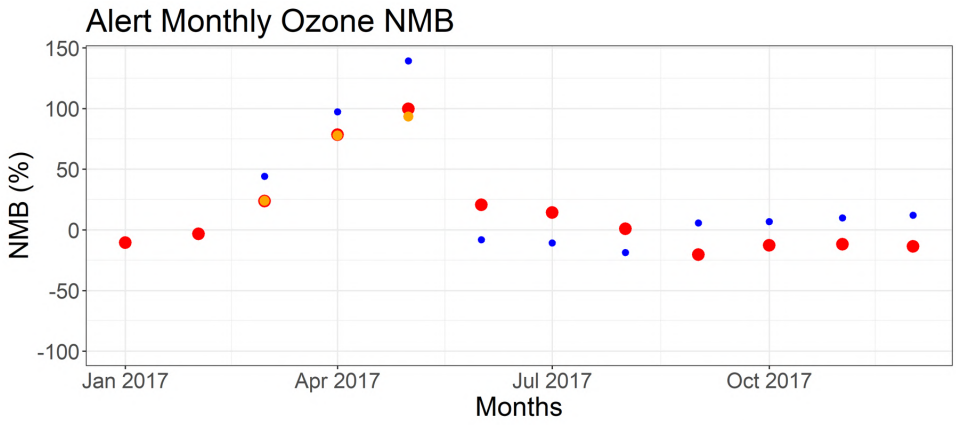

Fig. 2.7.2: Monthly mean normalised mean bias for Alert (Canada) for the 2017 o-suite (red), the new o-suite configuration applied to 2017 (h30x, orange) and the pre-e-suite (blue). High bias in spring is due to ozone depletion events caused by halogen reactions that are not represented in the model. From the old o-suite to the pre-e-suite there is a shift in bias from positive to negative in summer and from negative to positive in autumn/winter. Similar results are seen at the other four Arctic sites.

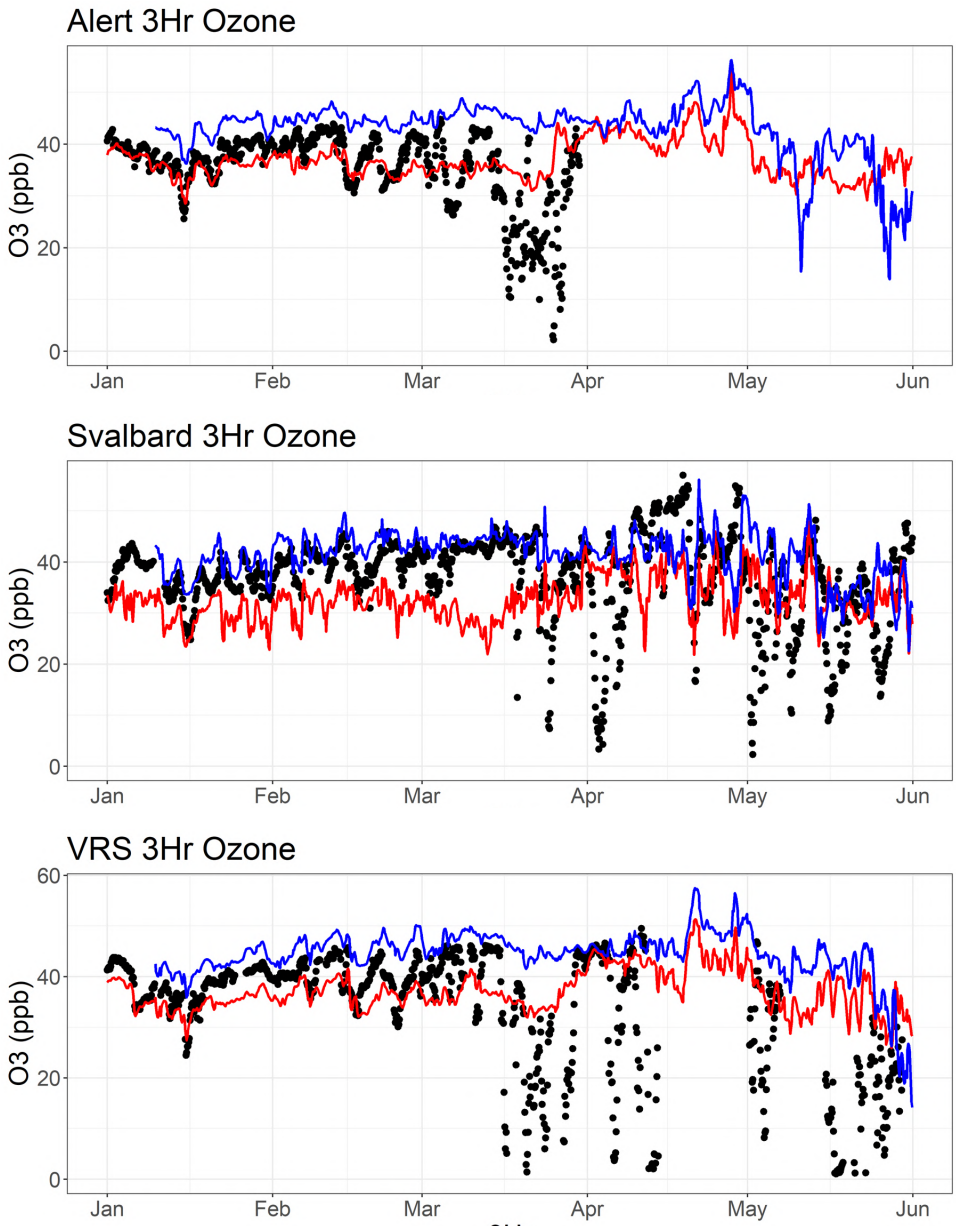

Fig. 2.7.3: Surface ozone mixing ratios at Alert (Canada), Zeppelin Mountain (Svalbard) and the Villum Research Station (Greenland) from January – May 2019 for the o-suite (red), and the e-suite (blue). Overall there is an improved agreement with observations for the e-suite with slightly improved correlations and a better description of the seasonal pattern, apart from the spring ozone depletion events.

2.8 O3 validation with IASI satellite observations

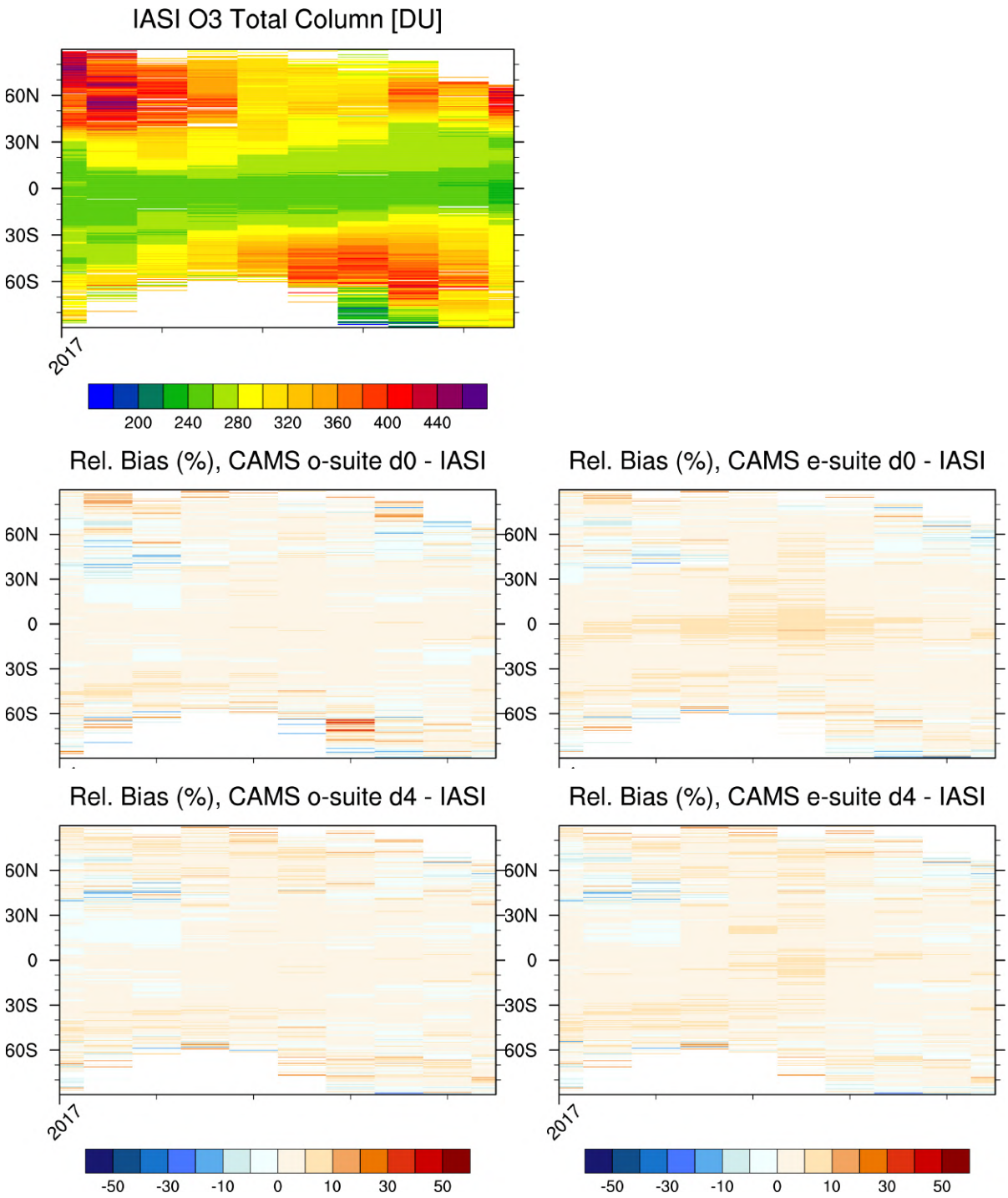

Fig. 2.8.1: IASI Metop-A total column (daytime), in Dobson units (DU), as a function of latitude and time (top) from March till December 2017. Relative difference (in %) with CAMS o-suite d0 and d4 (left column) and CAMS pre-e-suite d0 and d4 (right column). Model configurations are in good agreement with the observations. The e-suite shows improvements compared to o-suite over the high latitudes, which is reflected in the regional and temporal bias reduction.

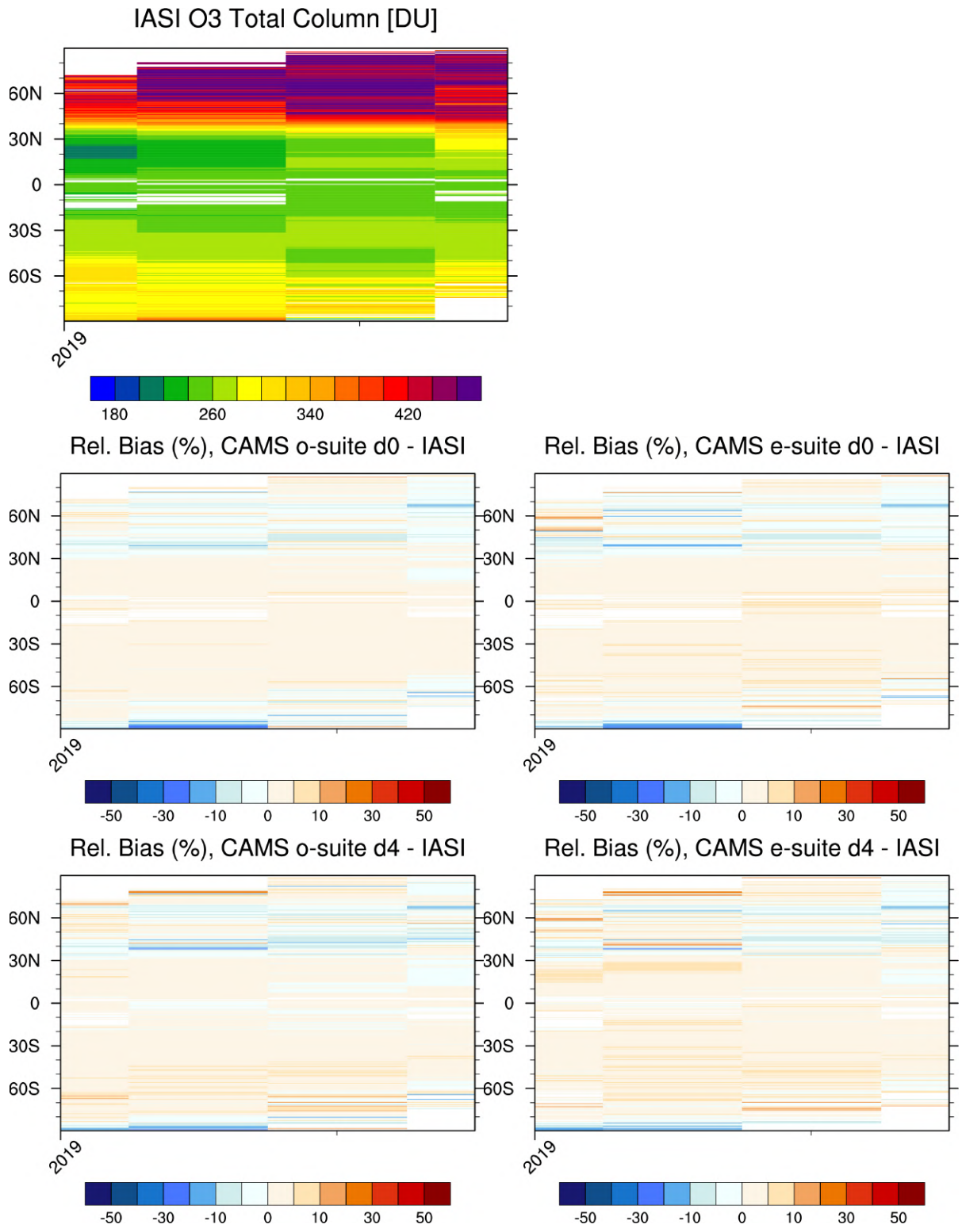

Fig. 2.8.2: IASI Metop-A total column (daytime) as a function of latitude and time (top) from January till April 2019. Relative difference with CAMS o-suite d0 and d4 (left column) and CAMS e-suite d0 and d4 (right column). Model configurations are in good agreement with the observations. The 2019 e-suite is very similar to the o-suite.

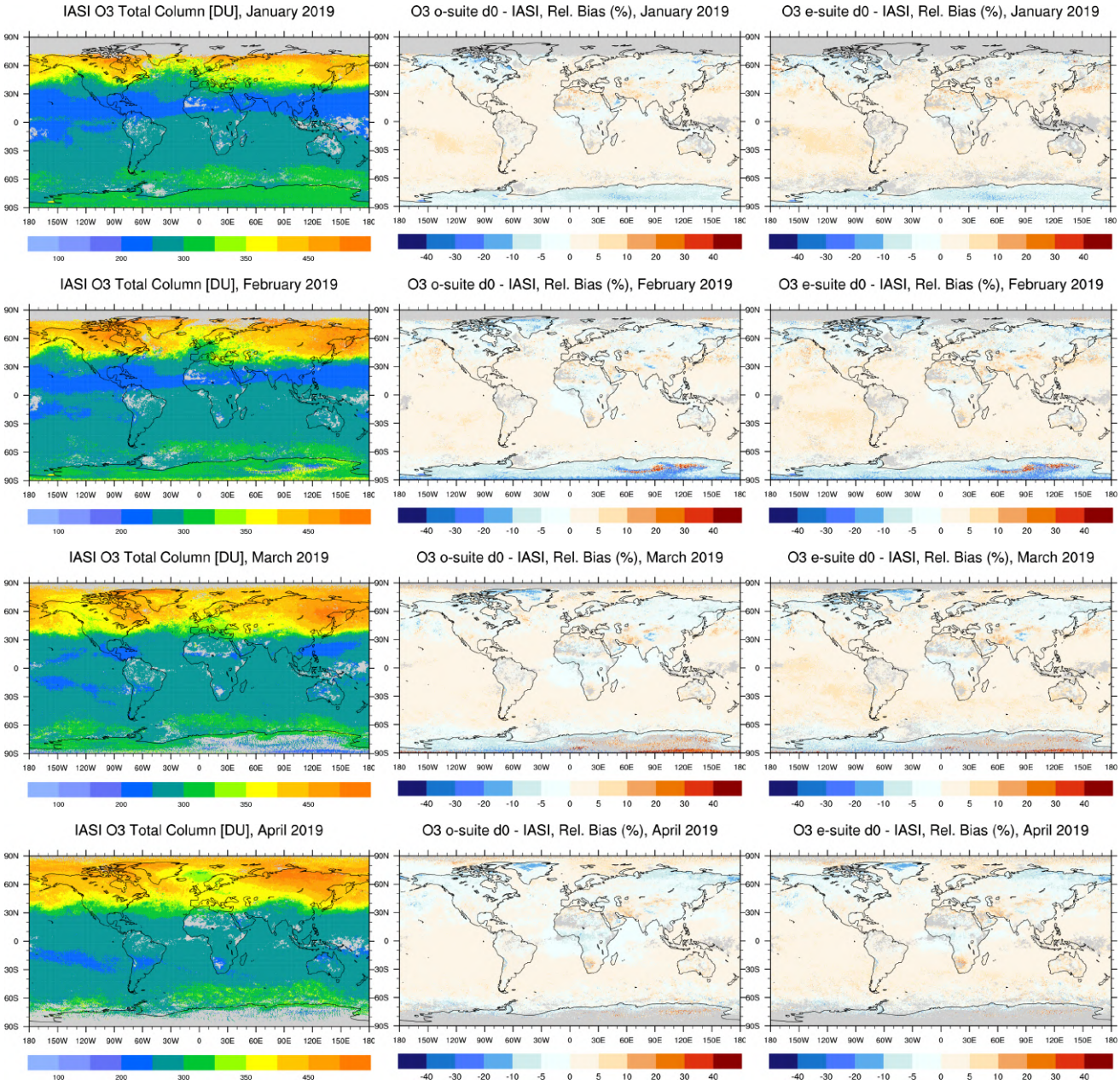

Fig. 2.8.3: O3 total column for IASI Metop-A daytime satellite observations (left column) and relative difference with CAMS o-suite d0 (middle) and e-suite d0 (right column) for January-April 2019 (from top to bottom). Model configurations are in good agreement with the observations. The 2019 e-suite is very similar to the o-suite.

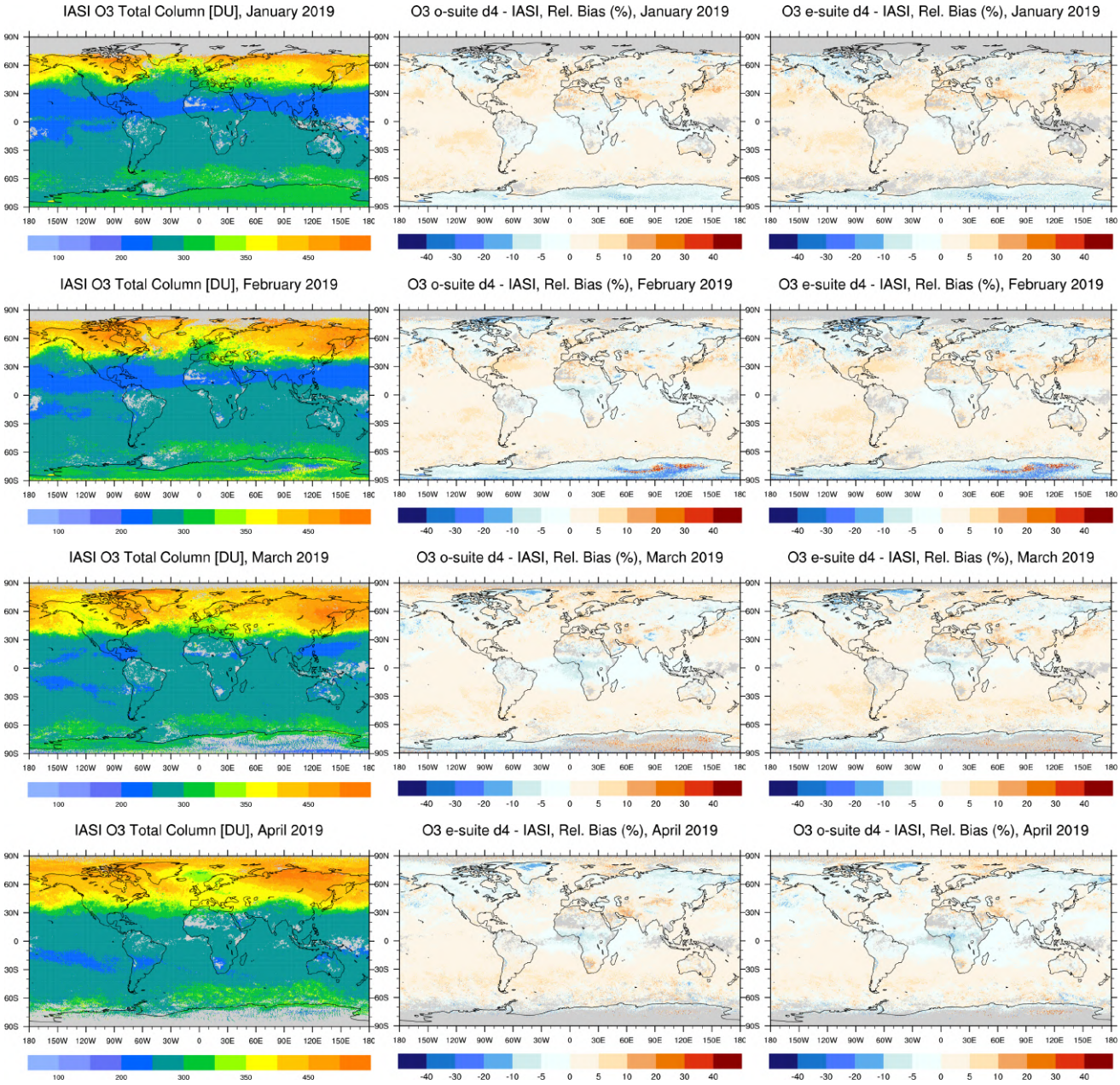

Fig. 2.8.4: O3 total column for IASI Metop-A daytime satellite observations (left column) and relative difference with CAMS o-suite d4 (middle) and e-suite d4 (right column) for January-April 2019 (from top to bottom). Model configurations are in good agreement with the observations. The 2019 e-suite is very similar to the o-suite.

2.9 CO validation with Global Atmosphere Watch (GAW) Surface Observations

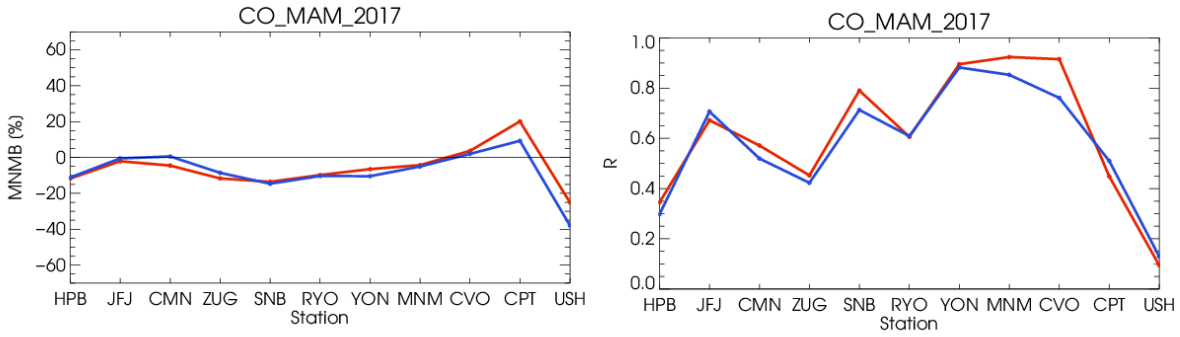

Fig 2.9.1: MNMBs (left) and R (right) for the o-suite (red) and pre-e-suite (blue) over the period March-May 2017 for CO. Results for the pre-e-suite and o-suite are almost the same.

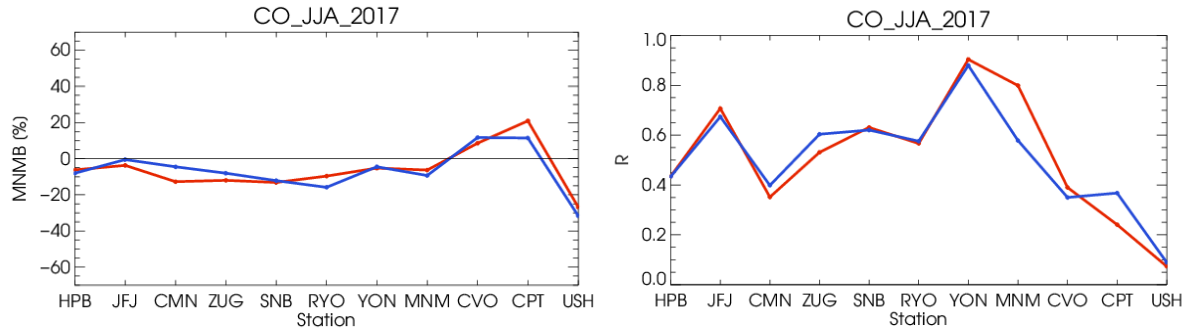

Fig 2.9.2: MNMBs (left) and R (right) for the o-suite (red) and pre-esuite (blue) over the period June-August 2017 for CO. Results for e-suite and o-suite are almost the same.

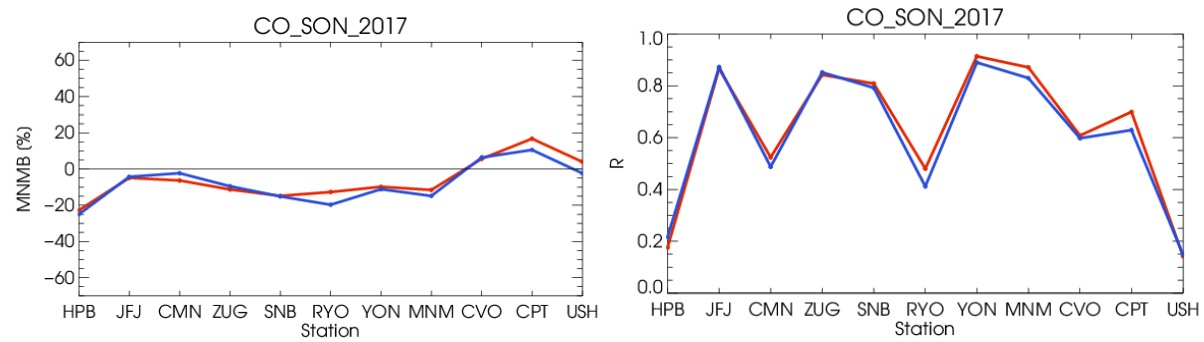

Fig 2.9.3: MNMBs (left) and R (right) for the o-suite (red) and pre-e-suite (blue) over the period September-November 2017 for CO. Results for pre-e-suite and o-suite are almost the same.

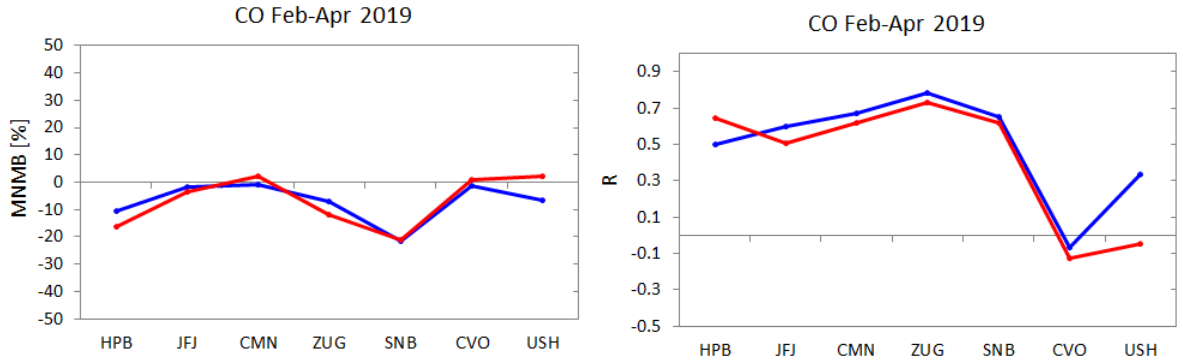

Fig 2.9.4: MNMBs (left) and correlation R (right) for the o-suite (red) and e-suite (blue) over the period February-April 2019 for CO. Results for e-suite and o-suite are almost the same. The correlation is slightly better for the e-suite.

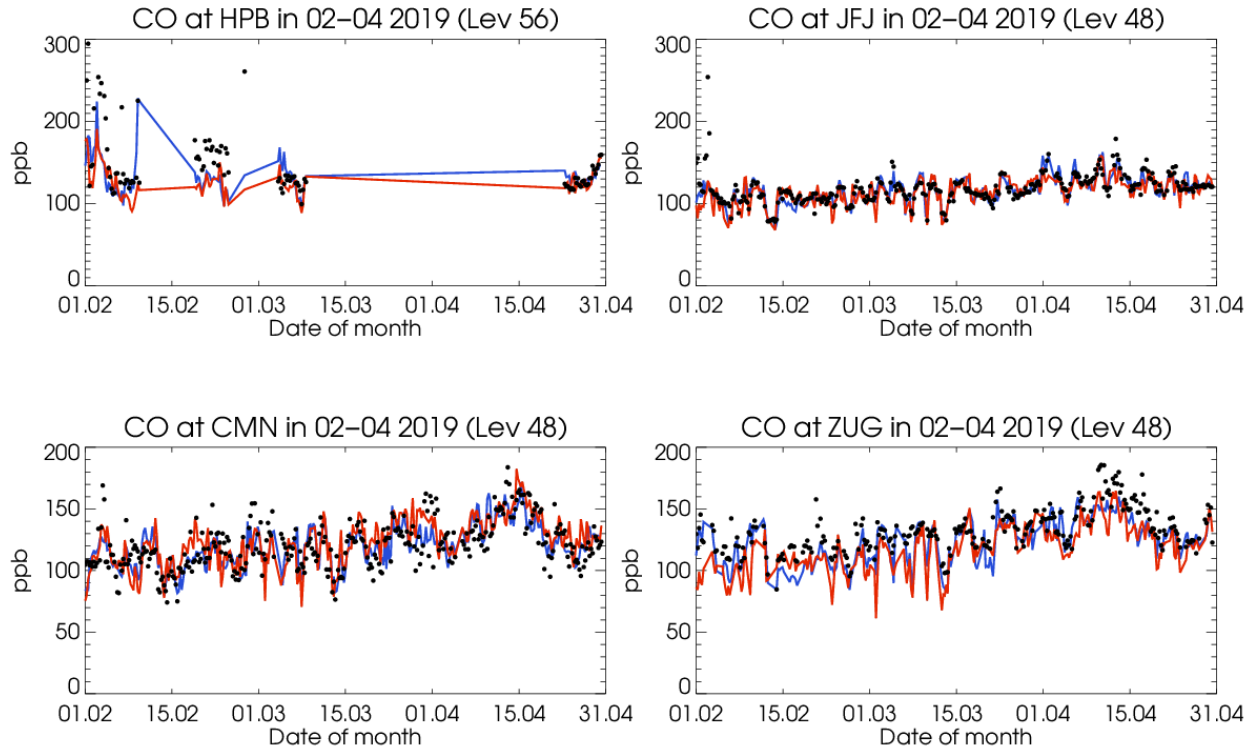

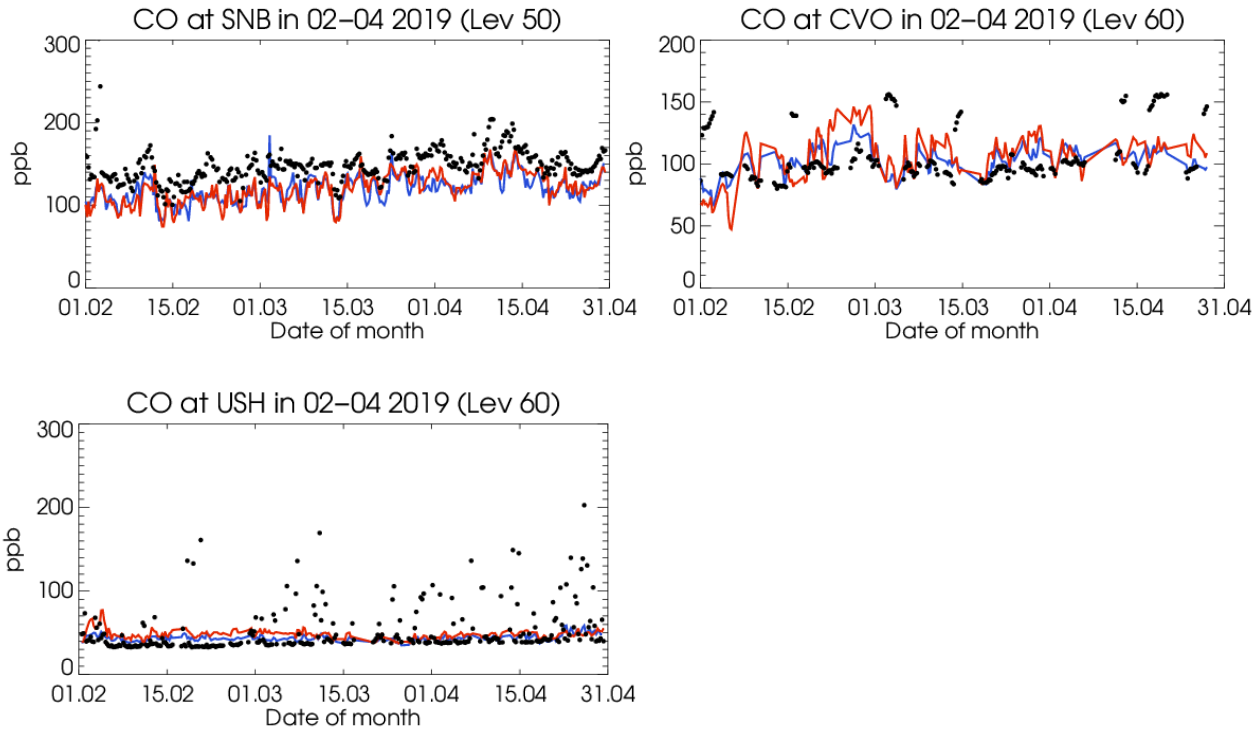

Fig. 2.9.5: Timeseries for the o-suite (red) and e-suite (blue) for CO over the period February-April 2019 over different GAW stations.

2.10 CO validation with IAGOS Aircraft observations

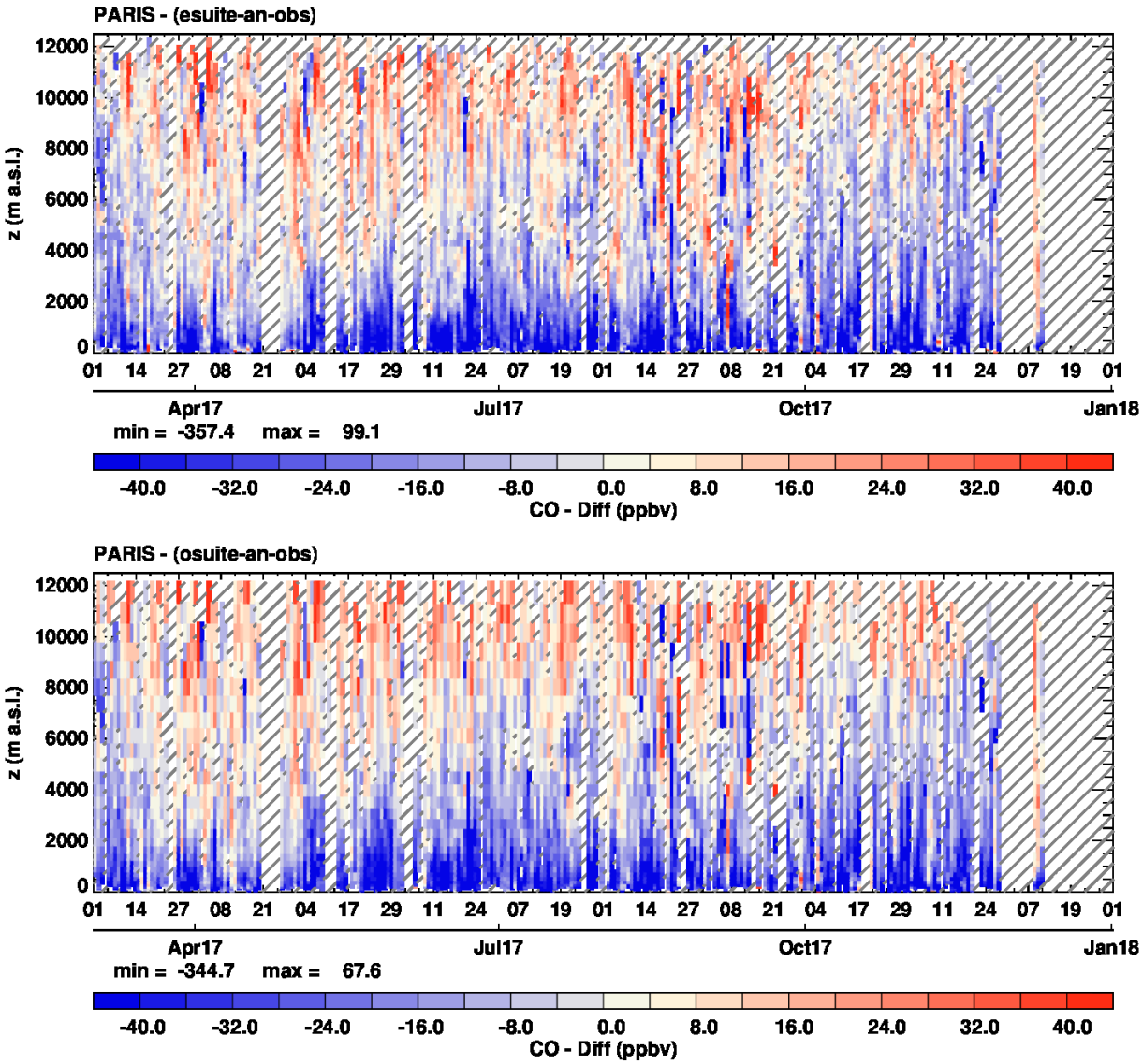

Fig. 2.10.1: Time series of the differences (model analysis minus IAGOS) in the daily profiles for CO at Paris during March-December 2017 for the pre-e-suite (h4x1-h4xd) on the top panel and o-suite (0001) on the bottom panel. IAGOS level-2 data is used. No notable difference is found in the comparison between the e-suite and the o-suite at Paris. The differences are more obvious on the seasonal profiles of the bias (see Fig. 2.10.3).

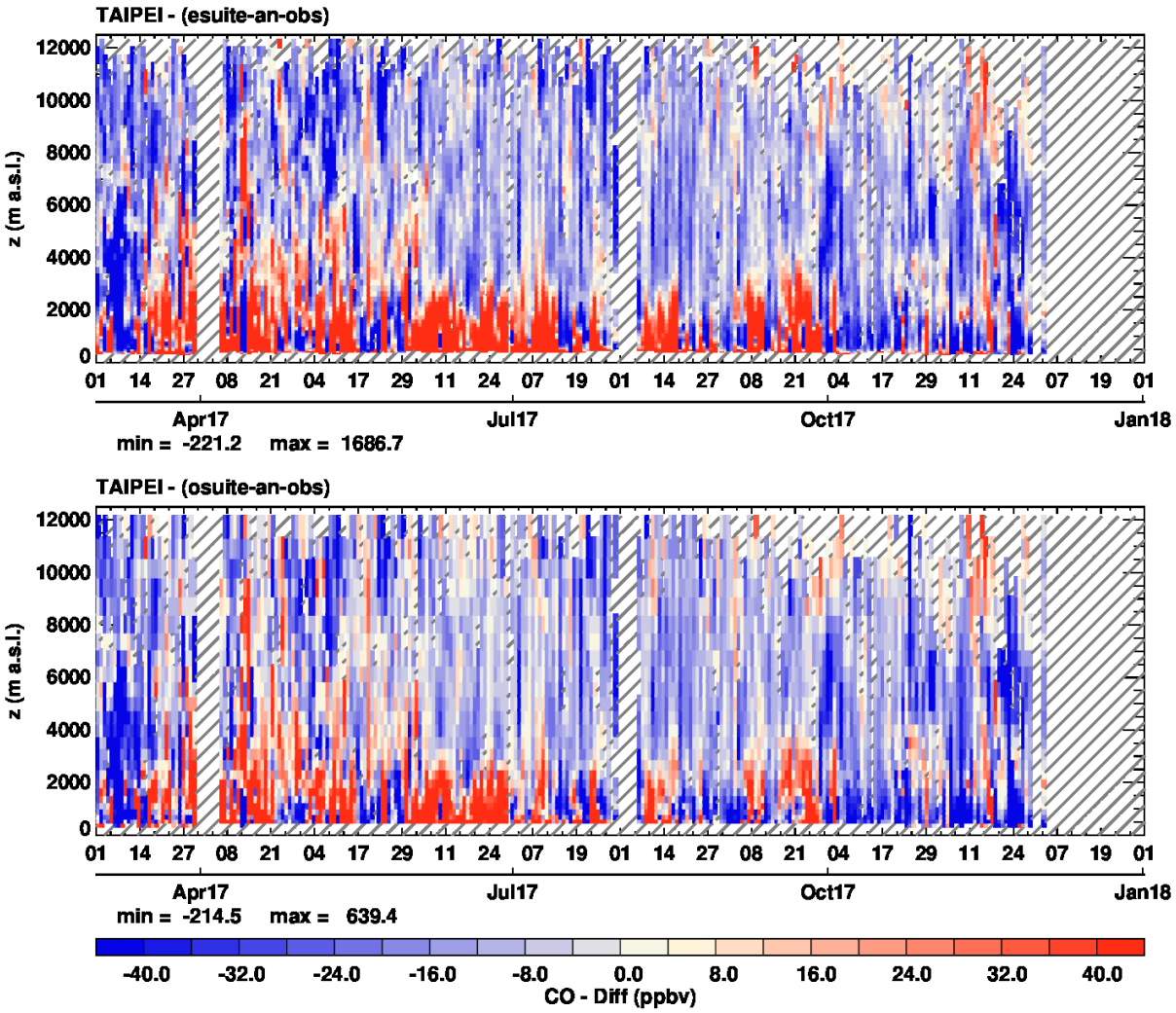

Fig. 2.10.2: Time series of the differences (model minus IAGOS) in the daily profiles for CO at Paris during March-December 2017 for the pre-e-suite (h4x1-h4xd) on the top panel and o-suite (0001) on the bottom panel. Unlike Paris, some differences can be noted between e-suite and o-suite: in the low troposphere the bias is often larger for the e-suite as shown clearly in the months and July and August 2017. The differences are more obvious on the seasonal profiles of the bias (see Fig. 2.10.4).

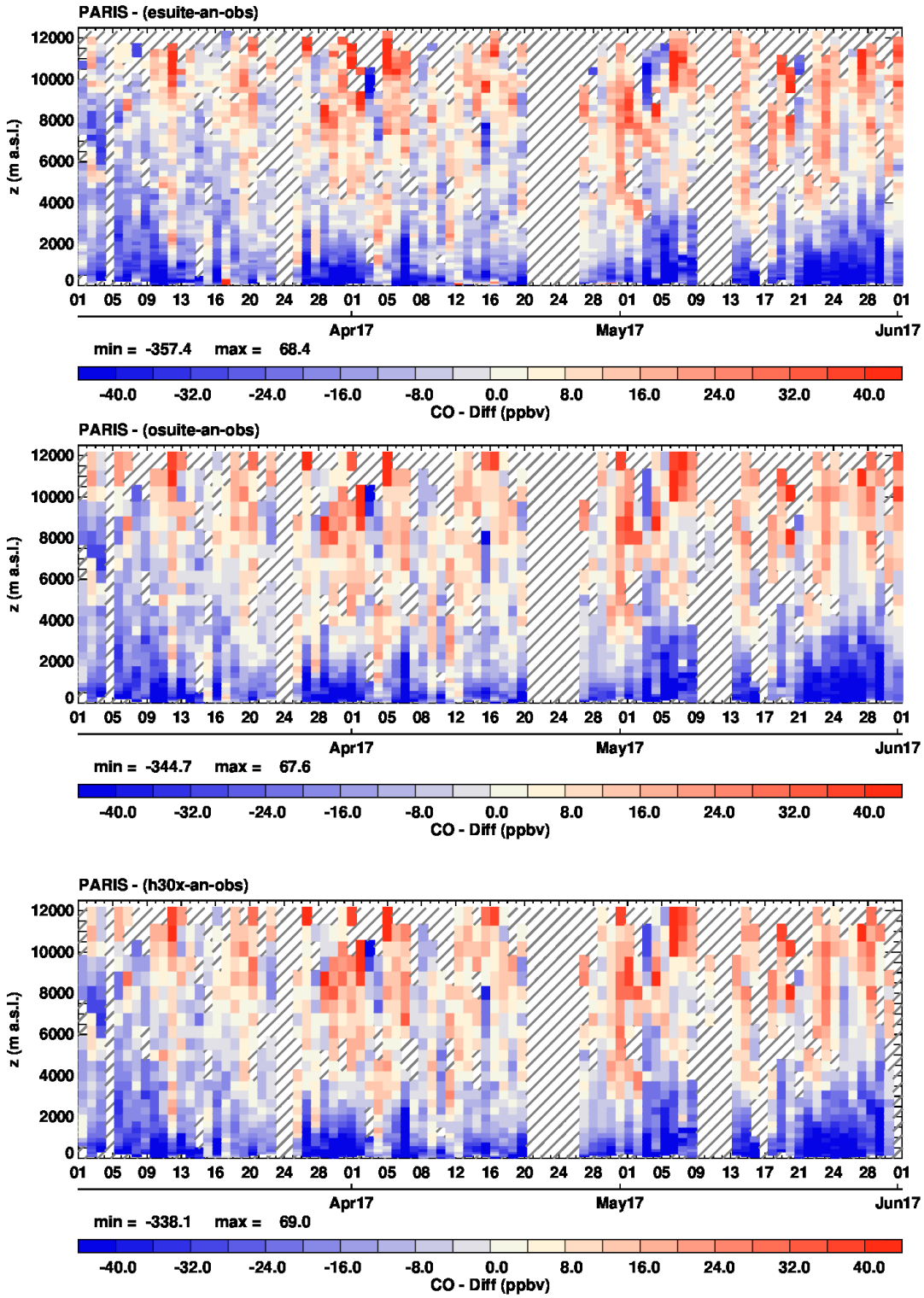

Fig. 2.10.3: Time series of the differences (model minus IAGOS) in the daily profiles for CO at Paris during March-May 2017 for the pre-e-suite (h4x1, analysis) on the top panel, the former o-suite (0001, analysis) on the middle panel and the current o-suite (h30x, analysis) on the bottom panel. The behaviour and magnitude of the bias appears very similar for all runs. More details can be seen on Fig. 2.10.5.

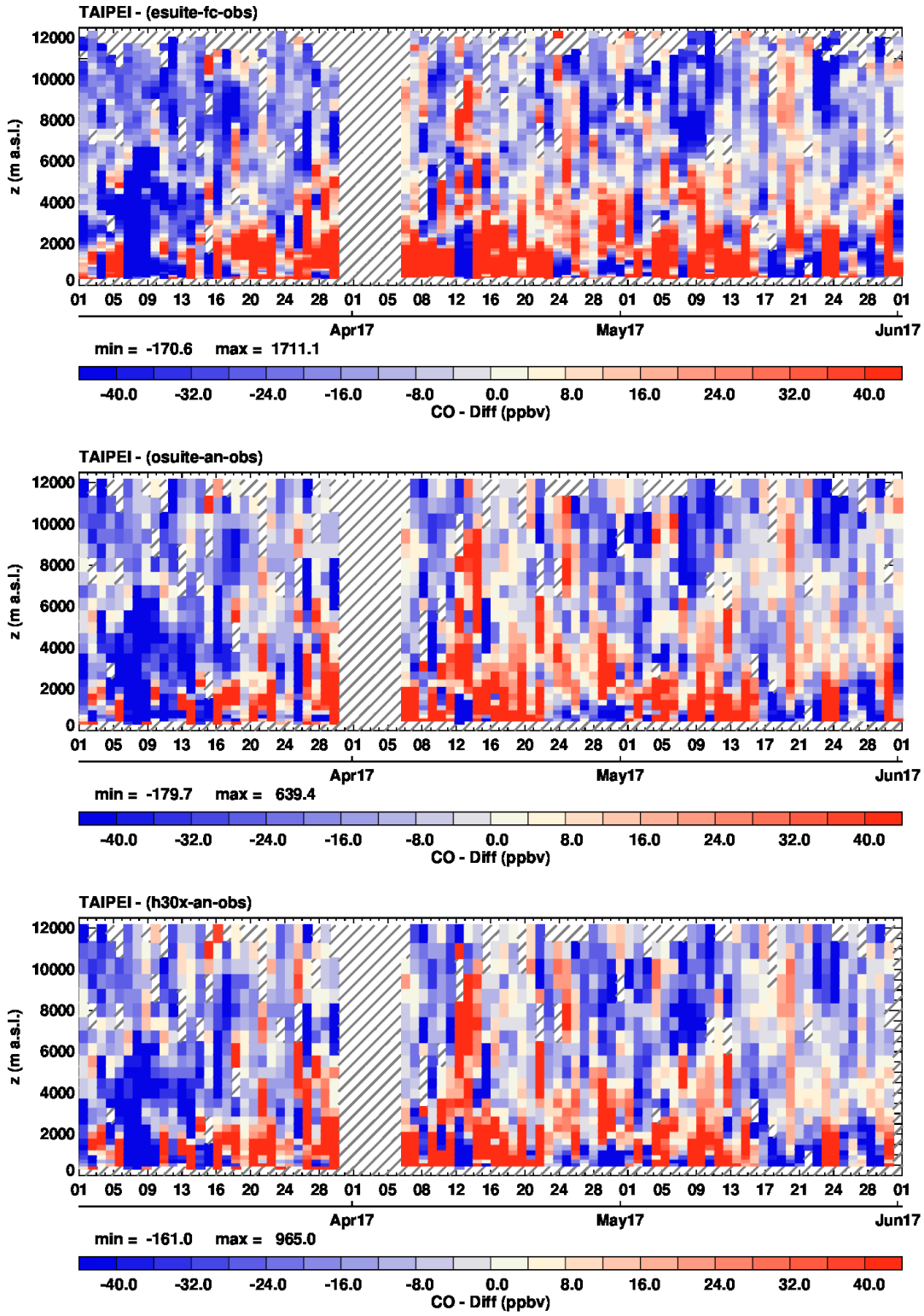

Fig. 2.10.4: Time series of the differences (model minus IAGOS) in the daily profiles for CO at Taipei during March-May 2017 for the pre-e-suite (h4x1, analysis) on the top panel and o-suite (h30x, analysis) on the bottom panel. Although the behaviour of the bias is very similar for all runs, the bias from the e-suite in the lowest layers appears sometimes larger than that of the two o-suites. More details can be seen on Fig. 2.10.6.

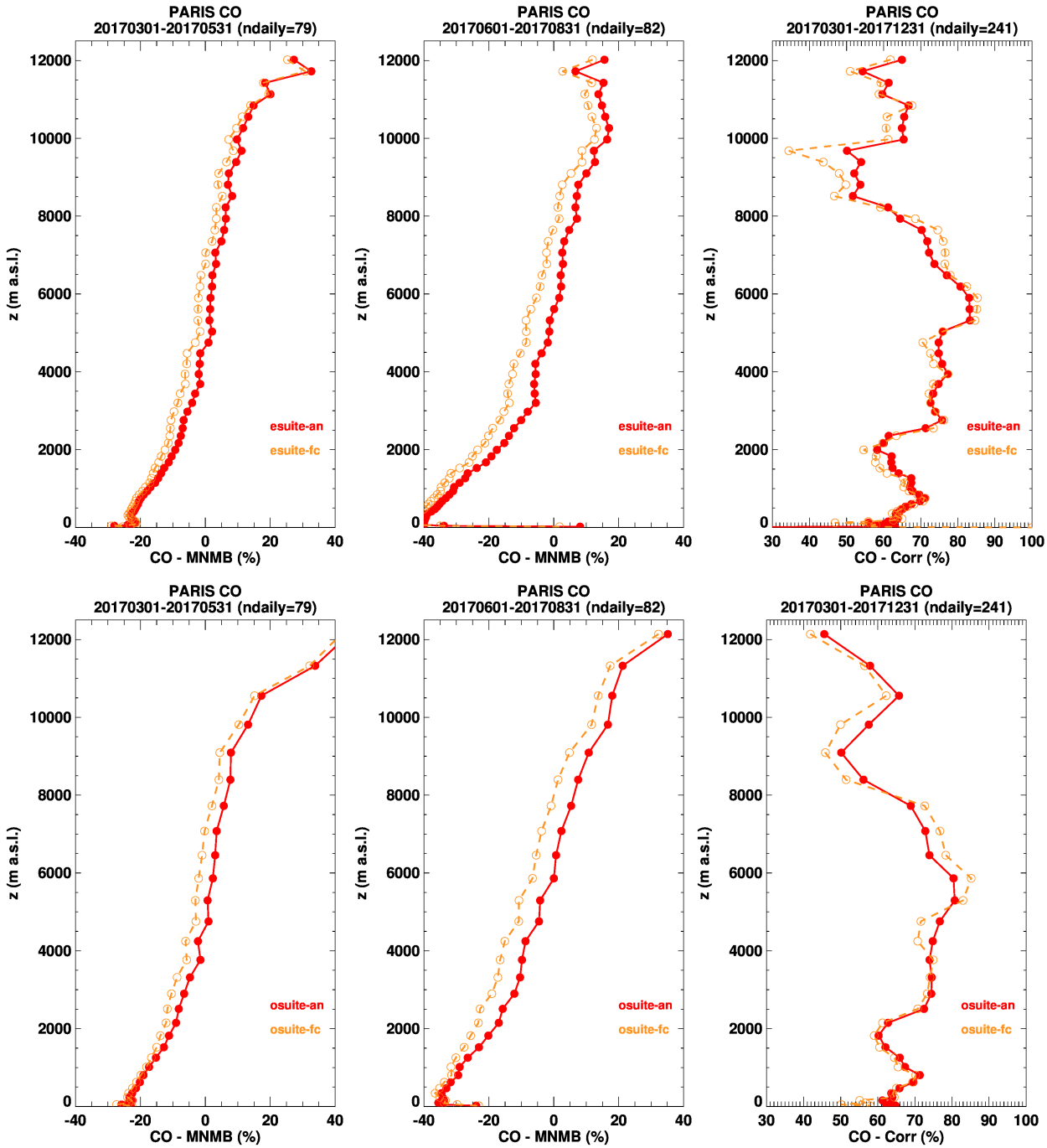

Fig. 2.10.5: Seasonal profiles of modified normalised mean bias (MNMB) (model analysis/1 day-forecast) and correlation coefficient for CO at Paris. The MNMB (left, middle) is presented for two periods: March-May 2017 and June-July 2017, and correlation (right) for the full period March-December 2017. Upper panels correspond to pre-e-suite (h4x1-h4xd) and lower panels to the o-suite (0001). The e-suite shows smaller biases than the o-suite in the UTLS. Correlation results are very similar for both models.

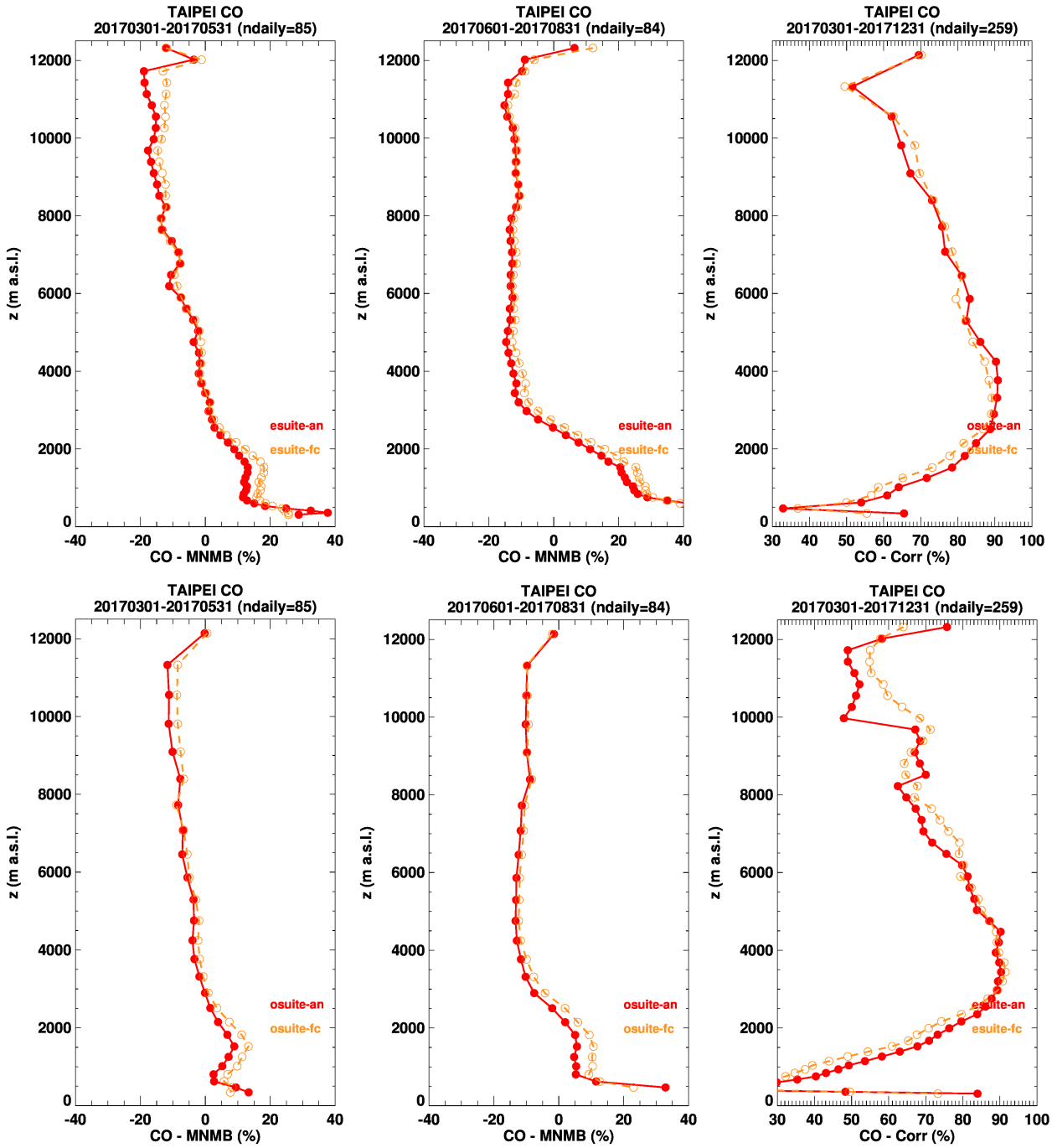

Fig. 2.10.6: Seasonal profiles of MNMB (model analysis and 1-day forecast) and correlation coefficient for CO at Taipei. MNMB (left, middle) is presented for two periods: March-May 2017 and June-July 2017, and correlation (right) for the full period March-December 2017. Upper panels correspond to pre-e-suite (h4x1-h4xd) and lower panels to the o-suite (0001). The e-suite presents larger biases than the o-suite in the low-troposphere. Correlation results are very similar for both models.

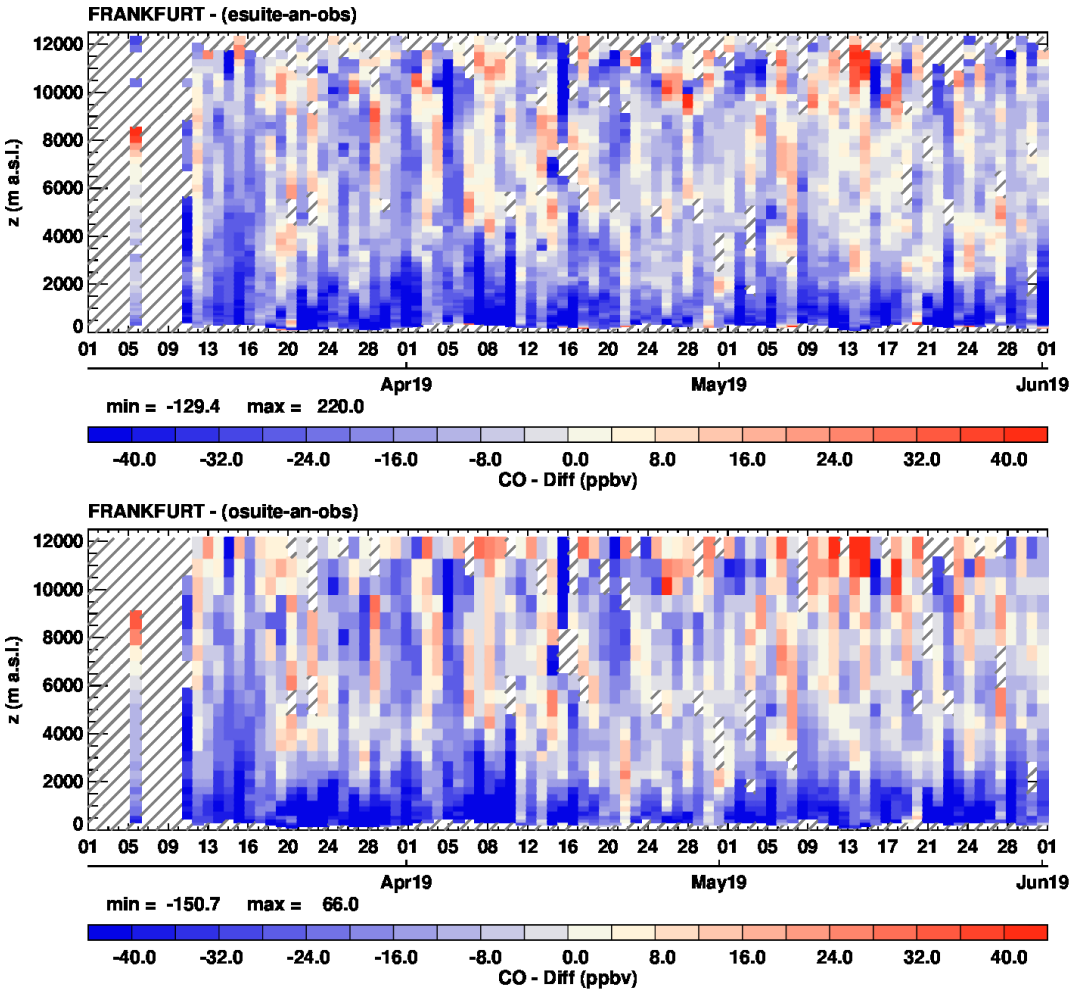

Fig. 2.10.7: Time series of differences (model analysis minus IAGOS) in the daily profiles for CO at Frankfurt during March-May 2019 for the e-suite (0073) on the top panel and o-suite (0001) on the bottom panel. The results from the e-suite and o-suite appear very similar. More details can be seen on Fig. 2.10.8.

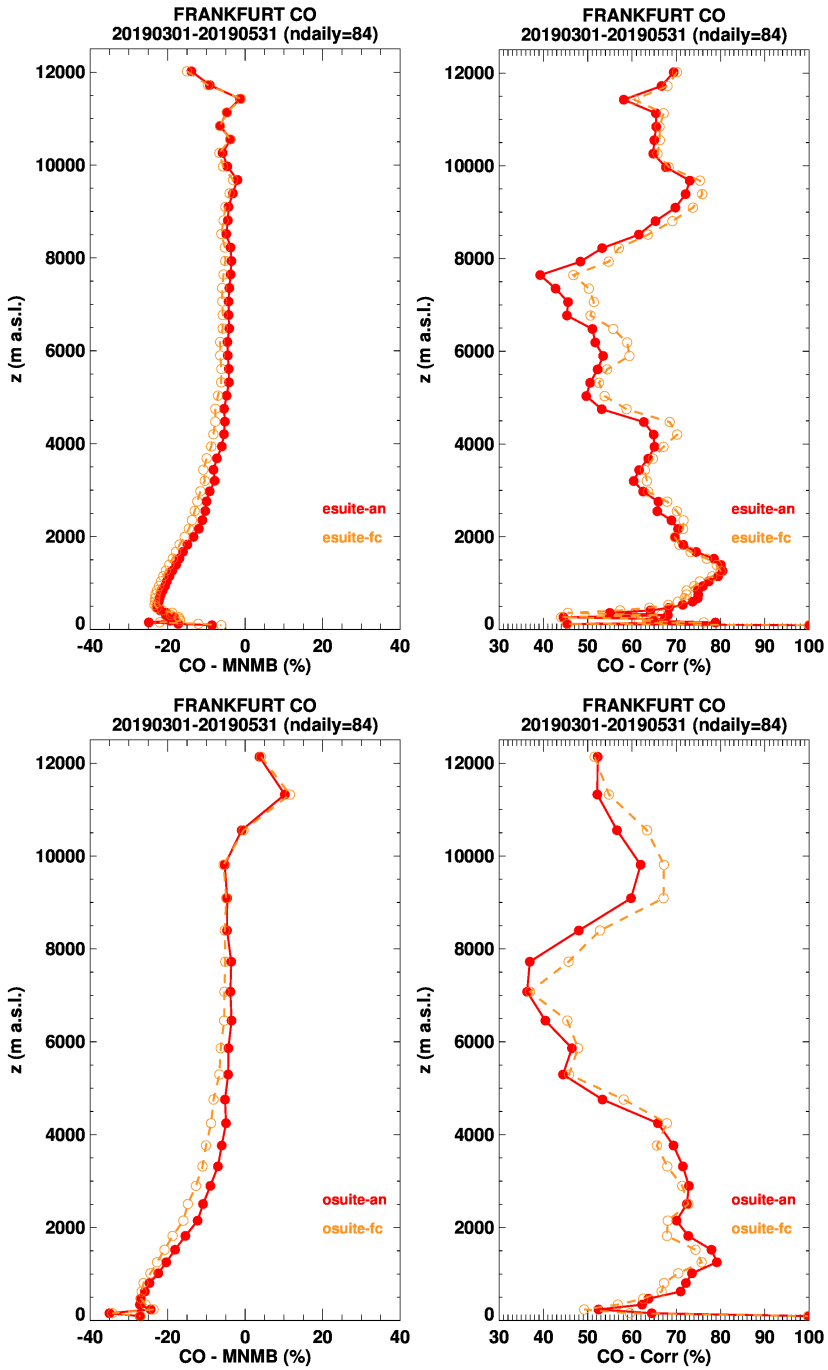

Fig. 2.10.8: Seasonal profiles of MNMB (model analysis/1 day-forecast) and correlation coefficient for CO at Frankfurt. Both MNMB (left) and correlation coefficient (right) are presented for the period of March-May 2019. Upper panels correspond to the e-suite (0073), and lower panels to the o-suite (0001). The results of the e-suite are slightly better than the o-suite in the UTLS. Correlation results are very similar for e-suite and o-suite.

2.11 Comparisons with MOPITTv6 and IASI CO data

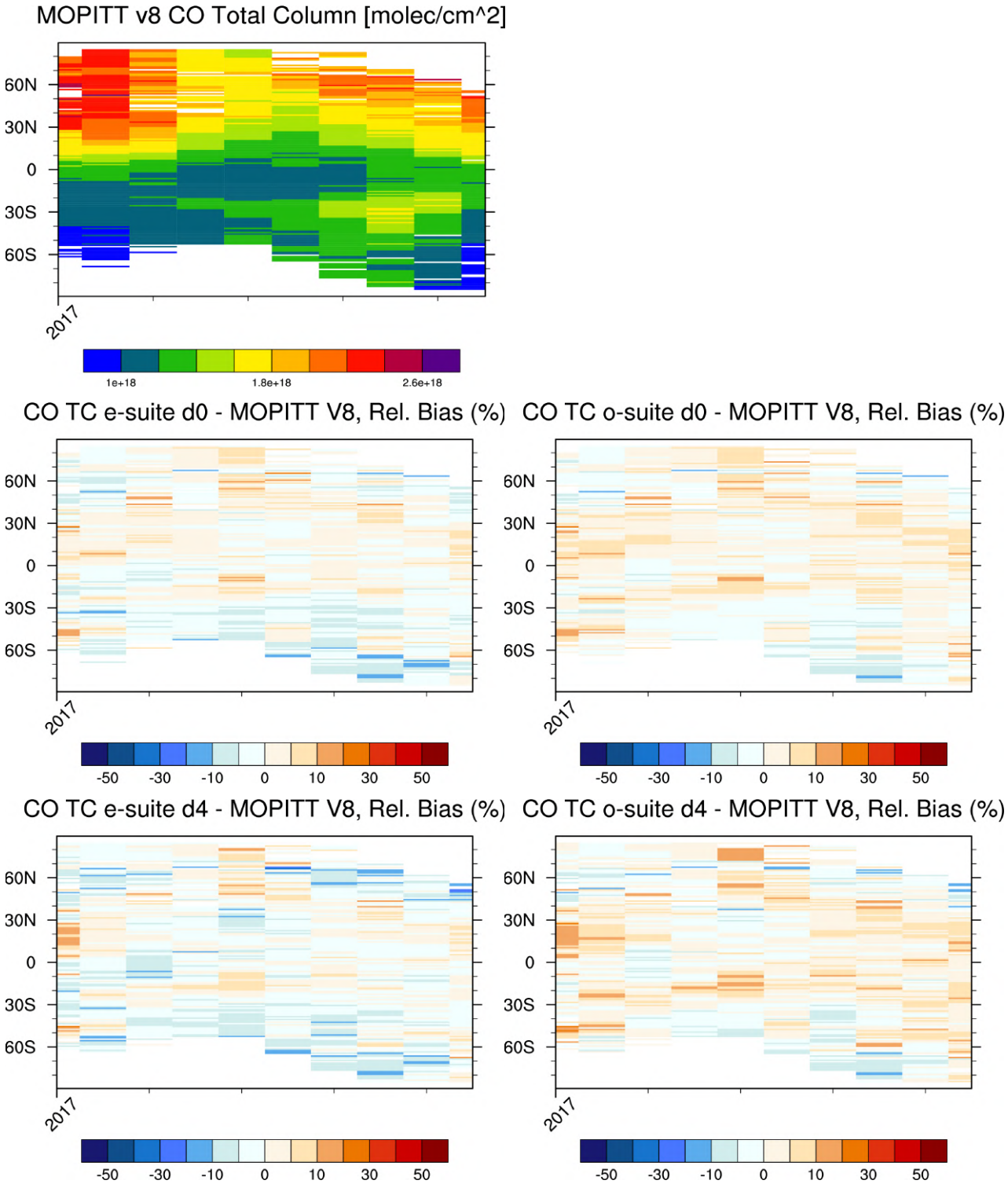

Fig. 2.11.1: MOPITT V8 CO total column as a function of latitude and time (top), from March 2017 till December 2017. Relative difference with CAMS o-suite d0 and d4 (left column) and CAMS pre-e-suite d0 and d4 (right column). The pre-e-suite run 2017 shows significant bias reduction compared to o-suite, especially for the forecast day 4.

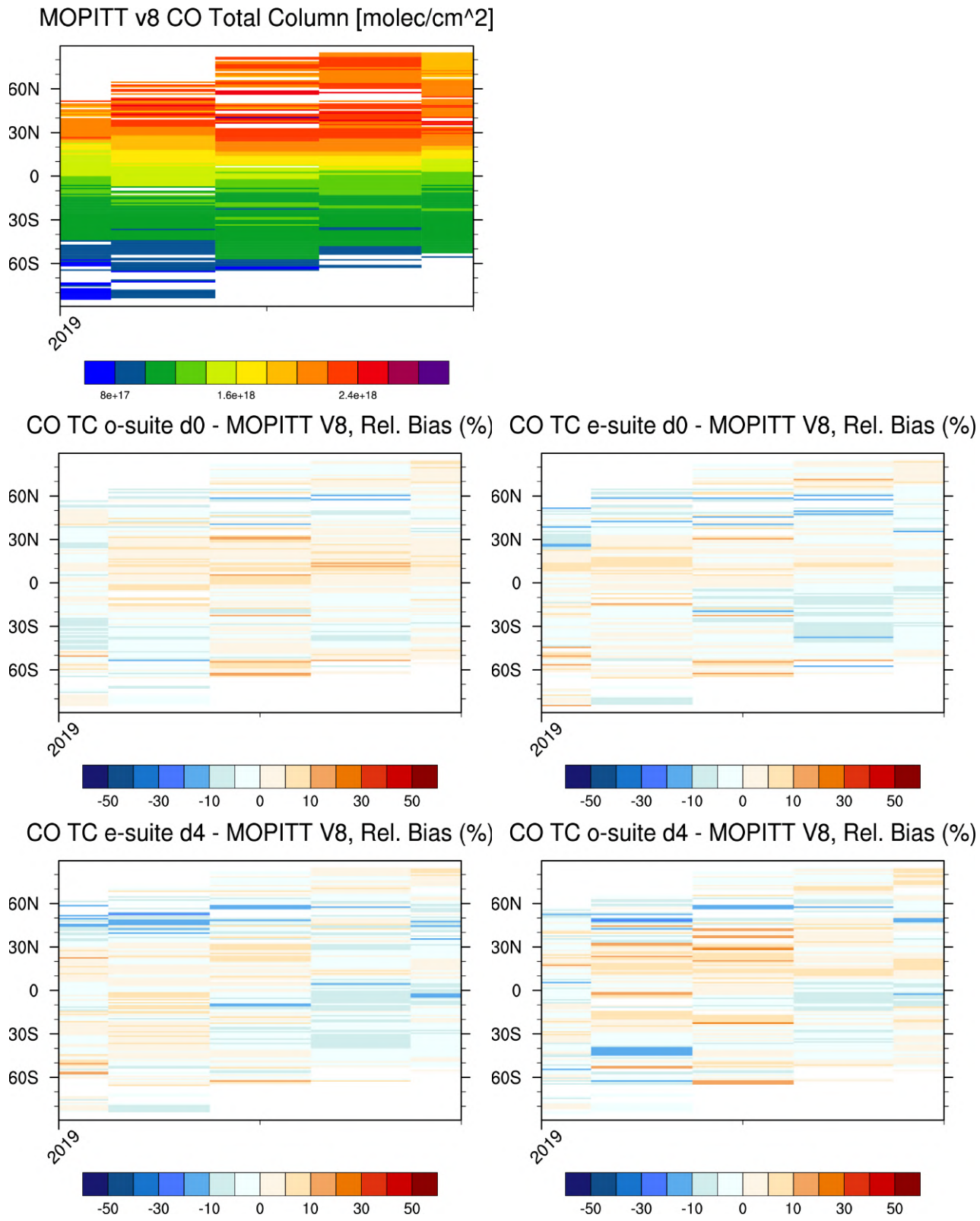

Fig. 2.11.2: MOPITT V8 CO total column as a function of latitude and time (top), from January 2019 till May 2019. Relative difference with CAMS o-suite d0 and d4 (left column) and CAMS e-suite d0 and d4 (right column). 2019 e-suite shows improvements compared to o-suite reflecting in the smaller positive bias over the tropics especially for the forecast day 4.

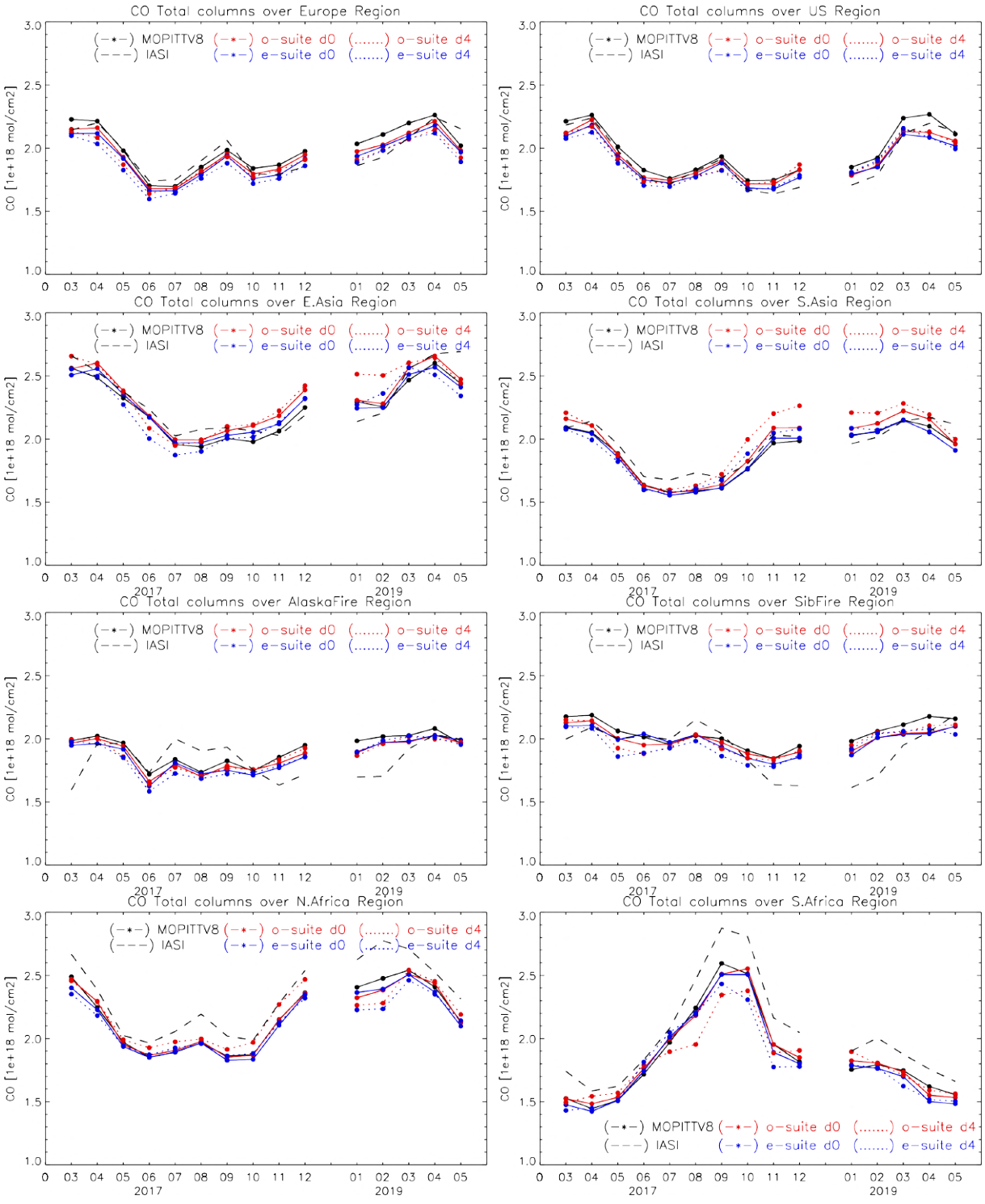

Fig. 2.11.3: Time series of CO total columns for MOPITT V8, IASI and the model runs over the selected regions: o-suite (red, solid), 2017 pre-e-suite (blue, solid), 2019 e-suite (blue, solid), o-suite 4th forecast day (red, dotted), 2017 pre-e-suite 4th forecast day (blue, dotted) and 2019 e-suite 4th forecast day (blue, dotted). Period: March-December 2017, January-May 2019. The pre-e-suite, e-suite and o-suite experiments are in very good agreement with observations and almost similar to each other. Some discrepancies between two model runs have a regional and/or temporal character. The e-suite is in slightly better agreement with the MOPITT data compared to o-suite over East and South Asia.

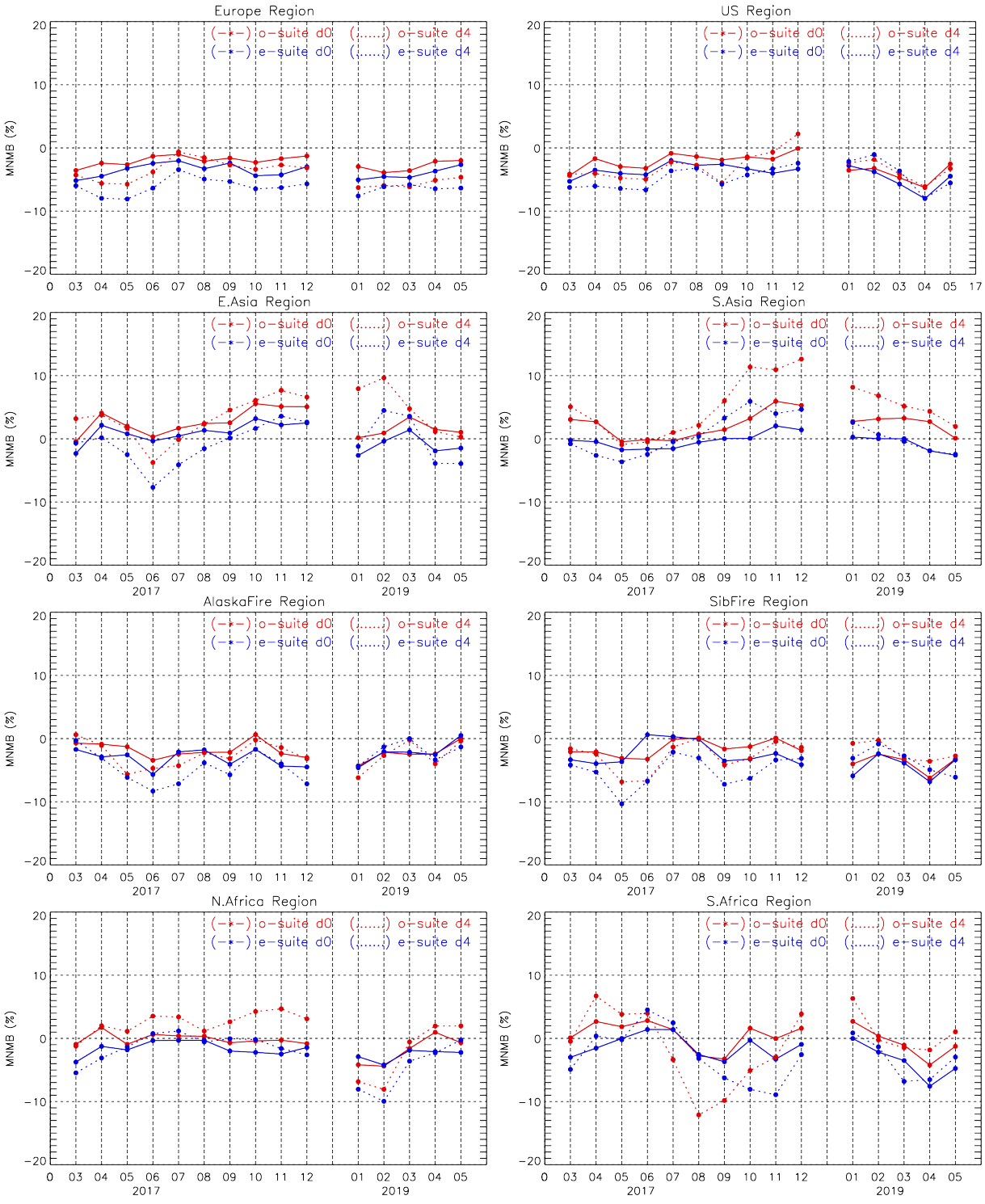

Fig. 2.11.4: Time series of modified normalized mean bias (%) for CO total columns from the model simulation vs MOPITT V8 over the selected regions: o-suite (red, solid), 2017 pre-e-suite (blue, solid), 2019 e-suite (blue, solid), o-suite 4th forecast day (red, dotted), 2017 pre-e-suite 4th forecast day (blue, dotted) and 2019 e-suite 4th forecast day (blue, dotted). Period: March-December 2017, January-May 2019. The e-suite is in slightly better agreement with the MOPITT data compared to o-suite over East and South Asia.

2.12 CO validation with NDACC and TCCON surface remote-sensing observations

Note on NDACC and TCCON CO observations: It is important to mention that there is an overall bias between NDACC and TCCON of approximately 6%, where TCCON is biased low compared to NDACC.

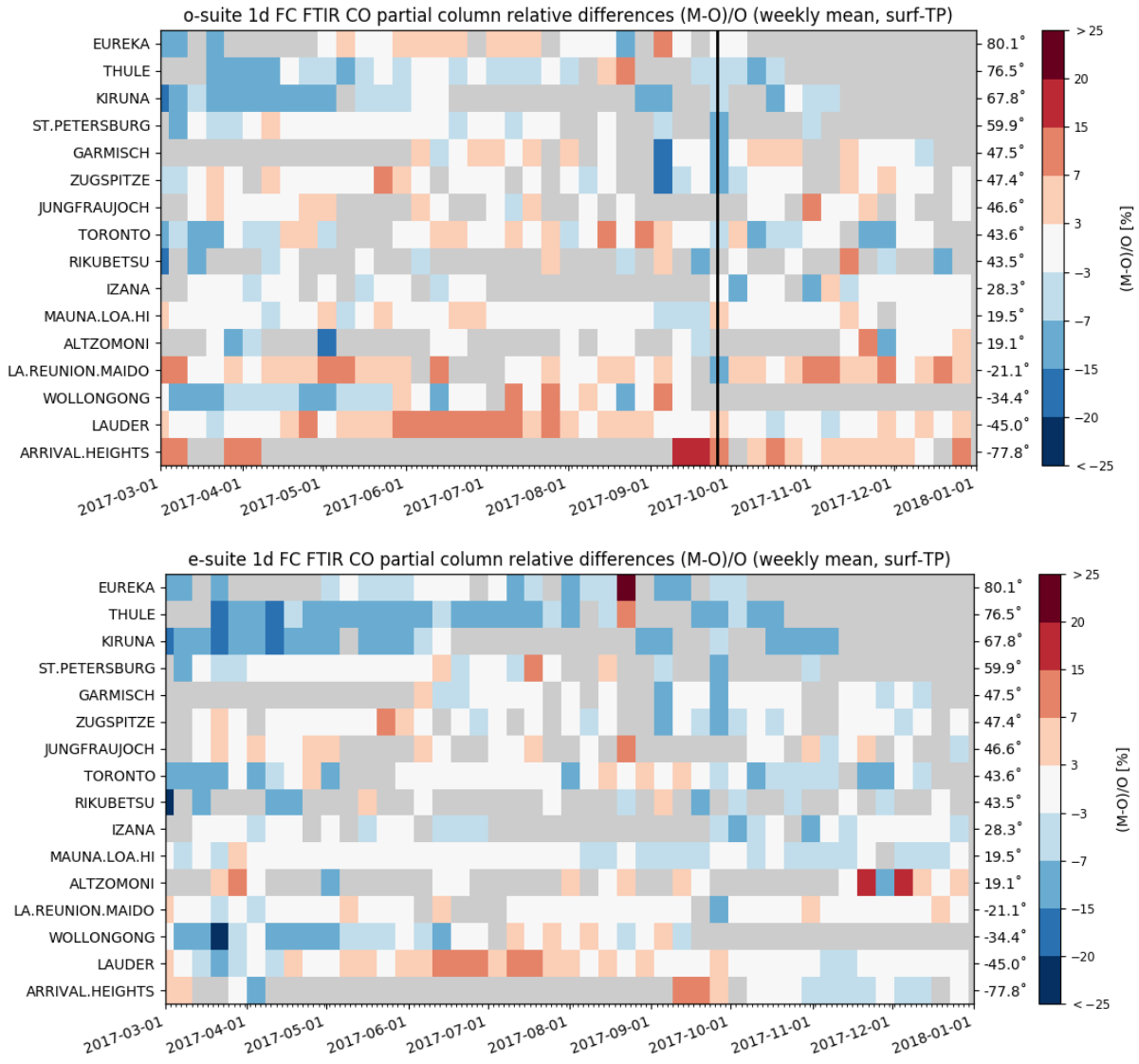

Fig. 2.12.1.: Relative weekly-mean bias for tropospheric NDACC CO columns (MB, %) for the period March-December 2017 for the o-suite (top) and pre-e-suite (bottom). The relative bias is computed as (forecast-observation)/observation for the 1-day forecasts (0:00h start time, steps 3-24h) in both cases. The CAMS o-suite system upgrade is indicated with the black vertical line. The overall uncertainty for the CO measurements is approximately 3%. Stations are sorted with decreasing latitude (northern to southern hemisphere). For the northern high latitude stations a stronger underestimation (<-10%) is observed in the pre-e-suite compared to the o-suite.

	o-suite AN					Pre-e-suite AN					
NDACC troposphere	#	rel. std	correlation	rel diff bias(%)	rel diff std(%)	#	rel. std	correlation	rel diff bias(%)	rel diff std(%)	lat
EUREKA	56	1.4	0.94	-0.42	6.97	43	0.7	0.96	-6.56	8.5	80.1
THULE	102	0.9	0.93	-4.05	6.45	90	0.8	0.94	-9.33	6.76	76.5
KIRUNA	60	1.3	0.89	-7.58	4.51	52	1.2	0.88	-11.86	3.93	67.8
ST.PETERSBURG	52	1	0.95	-0.89	3.59	43	1	0.91	0.74	4.54	59.9
GARMISCH	54	1.1	0.96	2.16	3.84	48	1	0.96	-1.11	3.72	47.5
ZUGSPITZE	80	0.9	0.96	-1.16	4.48	76	0.9	0.97	-3.42	4.18	47.4
JUNGFRAUJOCH	52	0.9	0.92	-0.65	4.79	47	1	0.9	-4.31	4.87	46.6
TORONTO	112	1	0.88	-0.41	6.17	100	0.9	0.89	-1.18	6.07	43.6
RIKUBETSU	16	1.3	0.87	-4.38	6.58	14	1.5	0.86	-6.32	6.91	43.5
IZANA	54	0.9	0.96	-3.17	3.5	44	0.9	0.96	-5.04	3.58	28.3
MAUNA.LOA.HI	210	0.9	0.98	0.81	3.47	185	0.9	0.98	-2.35	3.49	19.5
ALTZOMONI	53	1.2	0.87	-2.38	5.66	45	1	0.85	-1.85	7.1	19.1
LA.REUNION.MAIDO	153	1	0.99	1.19	3.71	151	1	0.99	-1	3.04	-21.1
WOLLONGONG	116	1.2	0.73	-2.29	9.31	99	1.2	0.73	-3.45	9.21	-34.4
LAUDER	146	1	0.97	3.16	4.42	135	1	0.97	0.57	4.15	-45
ARRIVAL.HEIGHTS	34	0.9	0.97	8.26	5.17	34	0.9	0.97	-0.37	5.35	-77.8
		1.1	0.92	-0.74	5.16		1	0.92	-3.55	5.34	

Table 2.12.1 Overview of the 2017 o-suite/pre-e-suite analysis performance against the NDACC FTIR tropospheric CO column. Although the pre-e-suite has a lower global bias its performance in the southern hemisphere is significantly improved (Lauder and ALH). Correlations and the standard deviation on the relative difference similar. Red: the o-suite absolute relative bias is smaller; blue: the pre-e-suite absolute relative bias is smaller

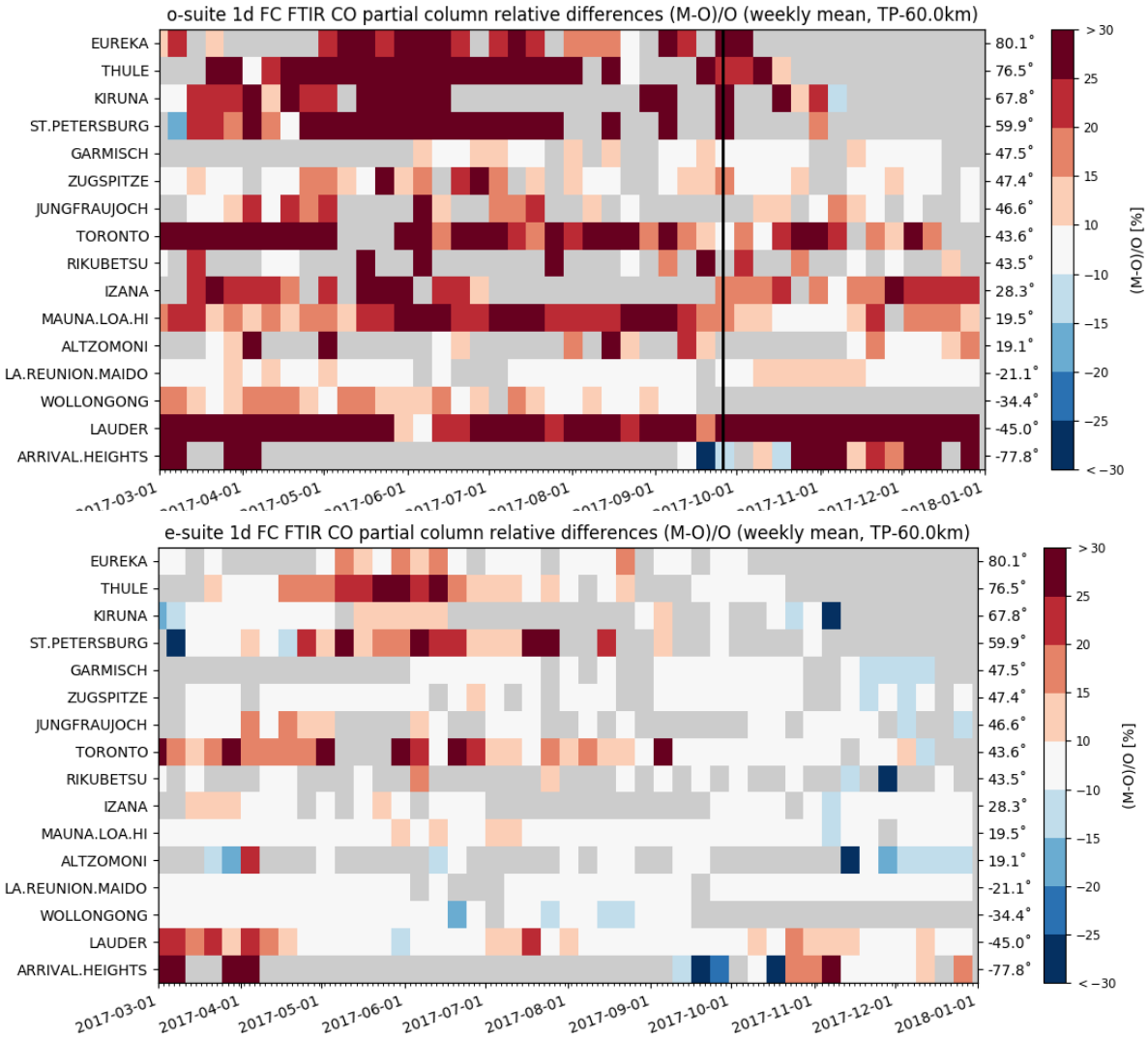

Fig. 2.12.2.: Relative mean bias for stratospheric NDACC FTIR CO columns (MB, %) for the considered period in 2017 (top, o-suite 1d FC and bottom pre-e-suite 1d FC) (the o-suite model upgrade is indicated with the black vertical line). The overall uncertainty for the CO measurements is approximately 10%. Stations are sorted with decreasing latitude (northern to southern hemisphere). The o-suite shows significant positive biases in the stratosphere, largely removed in the pre-e-suite run. The pre-e-suite bias evolves from an overestimation in the spring/early summer months to an underestimation in December 2017.

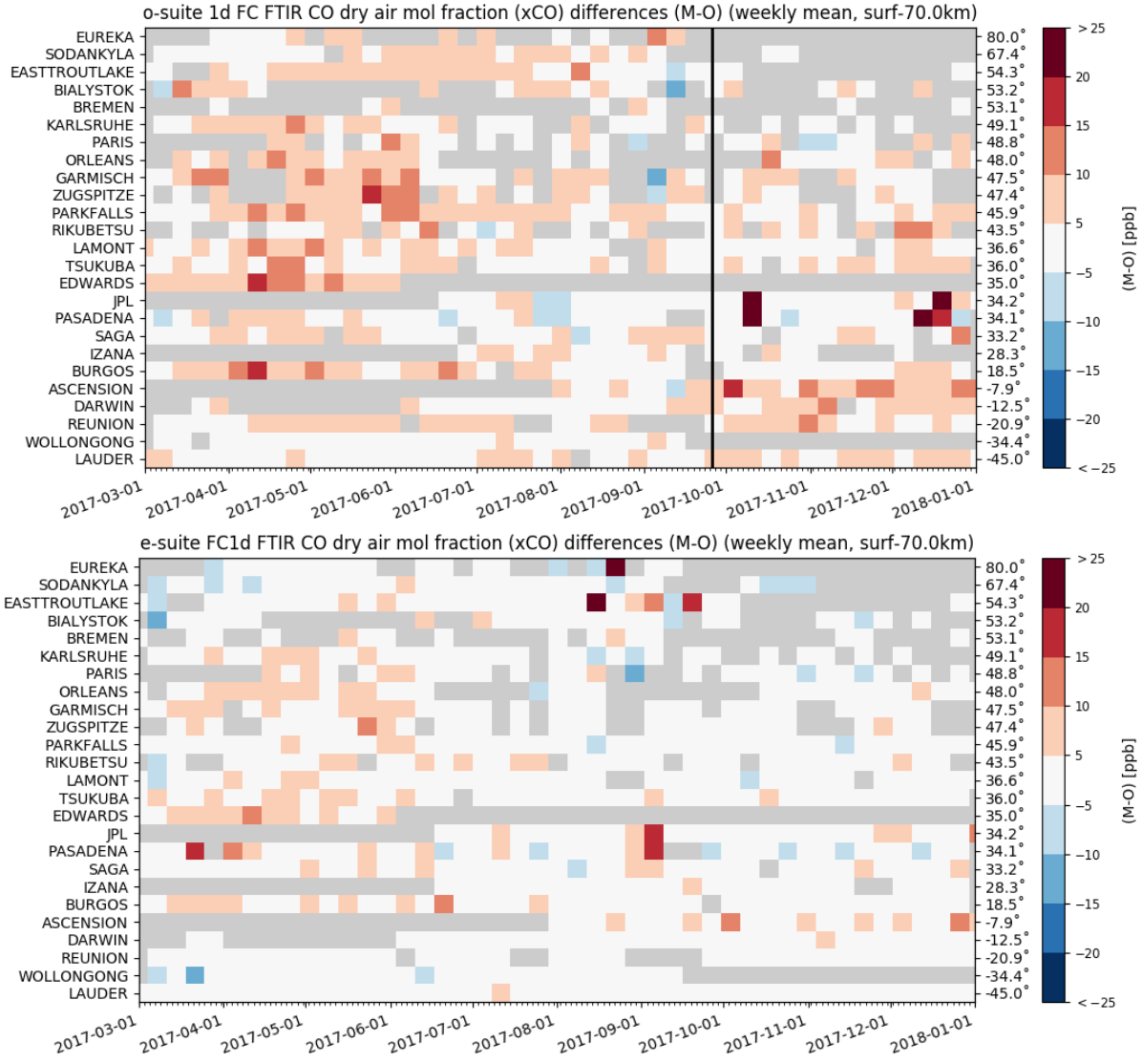

Fig. 2.12.3.: Mean bias for stratospheric TCCON FTIR CO columns (MB, unit ppbv) for the period March-December 2017 (top: o-suite 1d FC; bottom: pre-e-suite 1d FC). The o-suite model upgrade is indicated with the black vertical line. The overall uncertainty for the CO measurements is approximately 5ppb. Stations are sorted with decreasing latitude (northern to southern hemisphere). The positive bias of the o-suite has almost disappeared for the pre-e-suite. The pre-e-suite bias evolves from a slight overestimation in the spring months to near zero bias in December 2017. This is in agreement with the NDACC comparison given the offset between TCCON and NDACC CO observations.

	o-suite AN					Pre e-suite AN					
TCCON xCO	#	rel. std	correlation	diff bias(ppb)	diff std(ppb)	#	rel. std	correlation	diff bias(ppb)	diff std(ppb)	lat
EUREKA	26	1.1	0.91	4.49	4.11	26	1.1	0.92	-2.56	3.74	80
SODANKYLA	88	1.3	0.95	4.59	4.53	85	1.3	0.92	-0.7	4.9	67.4
EASTTROUTLAKE	151	1.2	0.87	5.57	7.05	148	0.8	0.58	2.76	15.24	54.3
BIALYSTOK	56	1.1	0.94	7.43	4.23	54	1.1	0.96	4.01	3.46	53.2
BREMEN	11	1	0.77	7.37	4.77	11	1	0.82	4.92	4.18	53.1
KARLSRUHE	76	0.9	0.94	6.83	4.12	76	0.8	0.94	4.54	4.4	49.1
PARIS	47	0.9	0.86	5.53	5.48	47	0.8	0.89	3.35	5.32	48.8
ORLEANS	64	0.8	0.94	9.4	4.25	63	0.8	0.94	6.44	4.16	48
GARMISCH	64	0.9	0.96	6.28	3.74	64	0.8	0.97	2.41	3.94	47.5
ZUGSPITZE	50	0.8	0.94	5.47	4.96	50	0.7	0.95	1.17	5.41	47.4
PARKFALLS	157	1	0.91	5.98	4.65	154	0.9	0.91	2.84	4.65	45.9
RIKUBETSU	40	1.2	0.93	4.51	5.13	39	1.1	0.94	1.66	4.79	43.5
LAMONT	178	0.9	0.94	5.2	4.62	177	0.9	0.95	2.4	4.19	36.6
TSUKUBA	104	1.1	0.91	4.41	5.34	104	1	0.93	2.87	4.83	36
EDWARDS	67	1	0.96	7.52	2.92	67	1	0.96	4.47	3.02	35
JPL	165	0.5	0.63	2.6	12.53	164	0.6	0.76	1.46	7.47	34.2
PASADENA	193	0.7	0.77	0.72	12.06	193	0.7	0.81	1	10.73	34.1
SAGA	106	1	0.91	3.18	5.61	104	1	0.93	1.35	5	33.2
IZANA	39	0.7	0.68	2.98	3.09	39	0.7	0.67	-0.32	3.07	28.3
BURGOS	124	0.9	0.95	5.67	4.88	124	0.9	0.96	3.16	4.56	18.5
ASCENSION	76	0.9	0.94	7.53	4.48	74	0.9	0.96	4.64	3.6	-7.9
DARWIN	164	0.8	0.85	3.38	5.71	163	0.8	0.88	0.26	4.74	-12.5
REUNION	158	0.9	0.98	4.56	2.71	156	0.9	0.99	0.76	2.06	-20.9
WOLLONGONG	83	1.1	0.83	1.58	3.68	83	1.1	0.84	-0.88	3.62	-34.4
LAUDER	140	1	0.98	4.62	1.85	139	1	0.98	1.58	1.6	-45
		0.9	0.89	5.1	5.06		0.9	0.89	2.14	4.91	

Table 2.12.2 Overview of o-suite/pre-e-suite analysis performance against the TCCON FTIR dry air averaged CO column. Red: the o-suite absolute relative bias is smaller; blue: the pre-e-suite absolute relative bias is smaller. The positive bias of the o-suite has significantly reduced for the pre-e-suite. Similar to the NDACC results, the network wide difference of the pre-e-suite has decreased. Correlations and the standard deviation on the relative difference are similar between the two CAMS products.

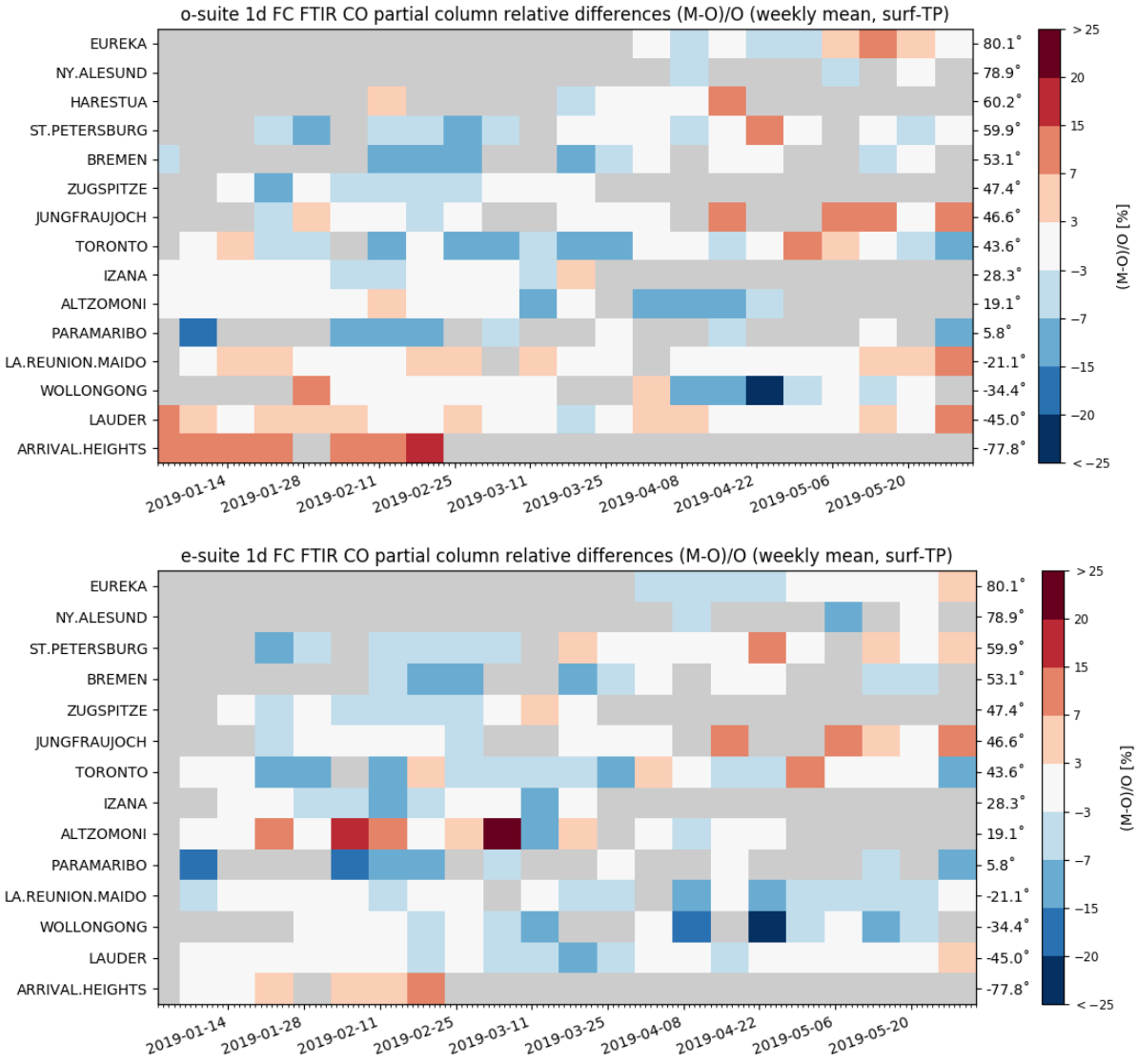

Fig. 2.12.4.: Relative weekly-mean bias for tropospheric NDACC CO columns (MB, %) for the period January-May 2019 for the o-suite (top) and e-suite (bottom). Similar to the pre-e-suite, the e-suite has lower overall bias. The Arctic stations in the e-suite do not show the strong underestimation observed in the pre-e-suite.

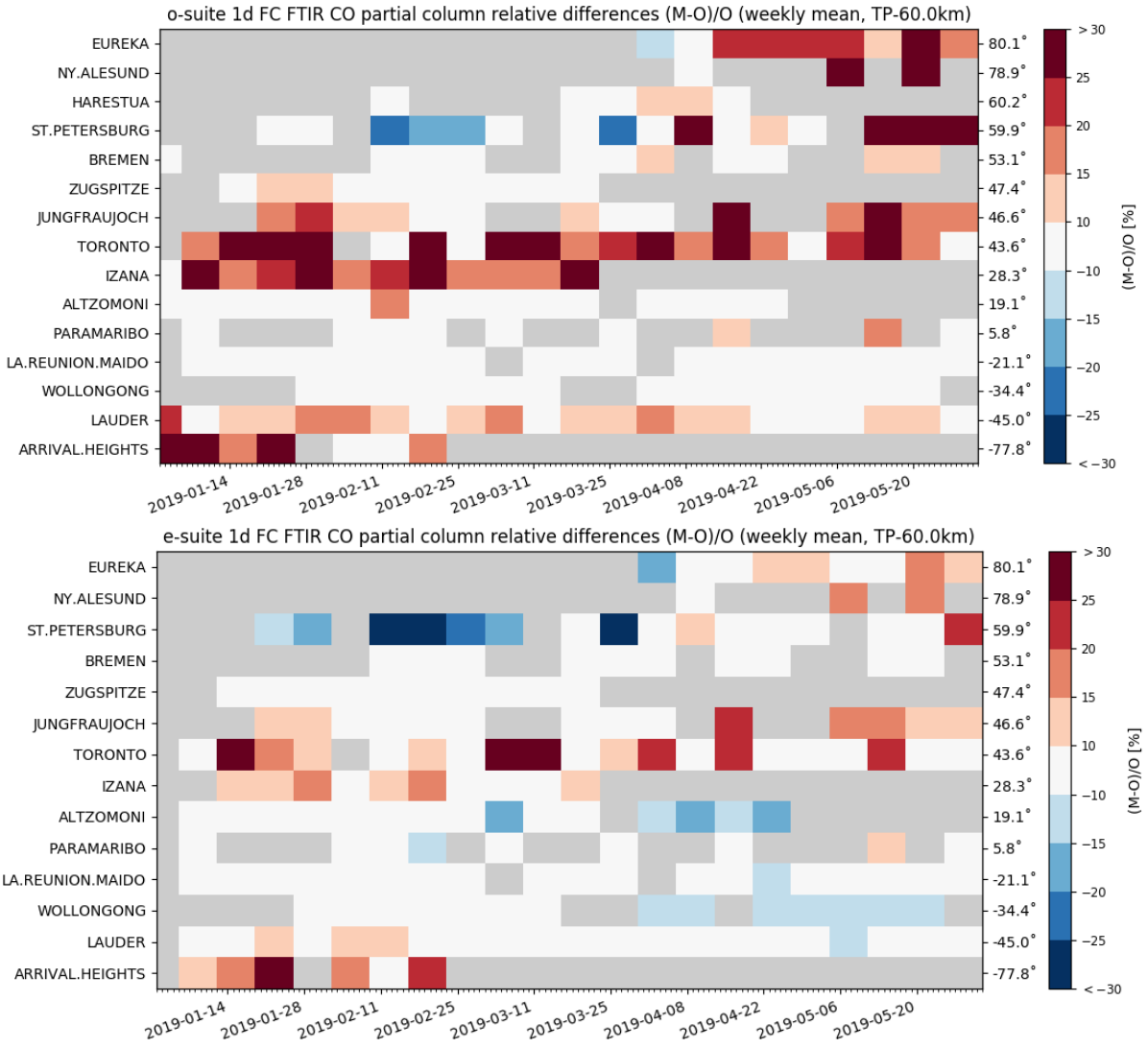

Fig. 2.12.5.: Relative mean bias for stratospheric NDACC FTIR CO columns (MB, %) for the period January-May 2019 (top, o-suite 1d forecast and bottom e-suite 1d forecast). The overall uncertainty for the CO measurements is approximately 10%. Similar to the pre-e-suite, the e-suite has an overall lower bias than the o-suite.

2.13 Tropospheric nitrogen dioxide comparisons with GOME-2

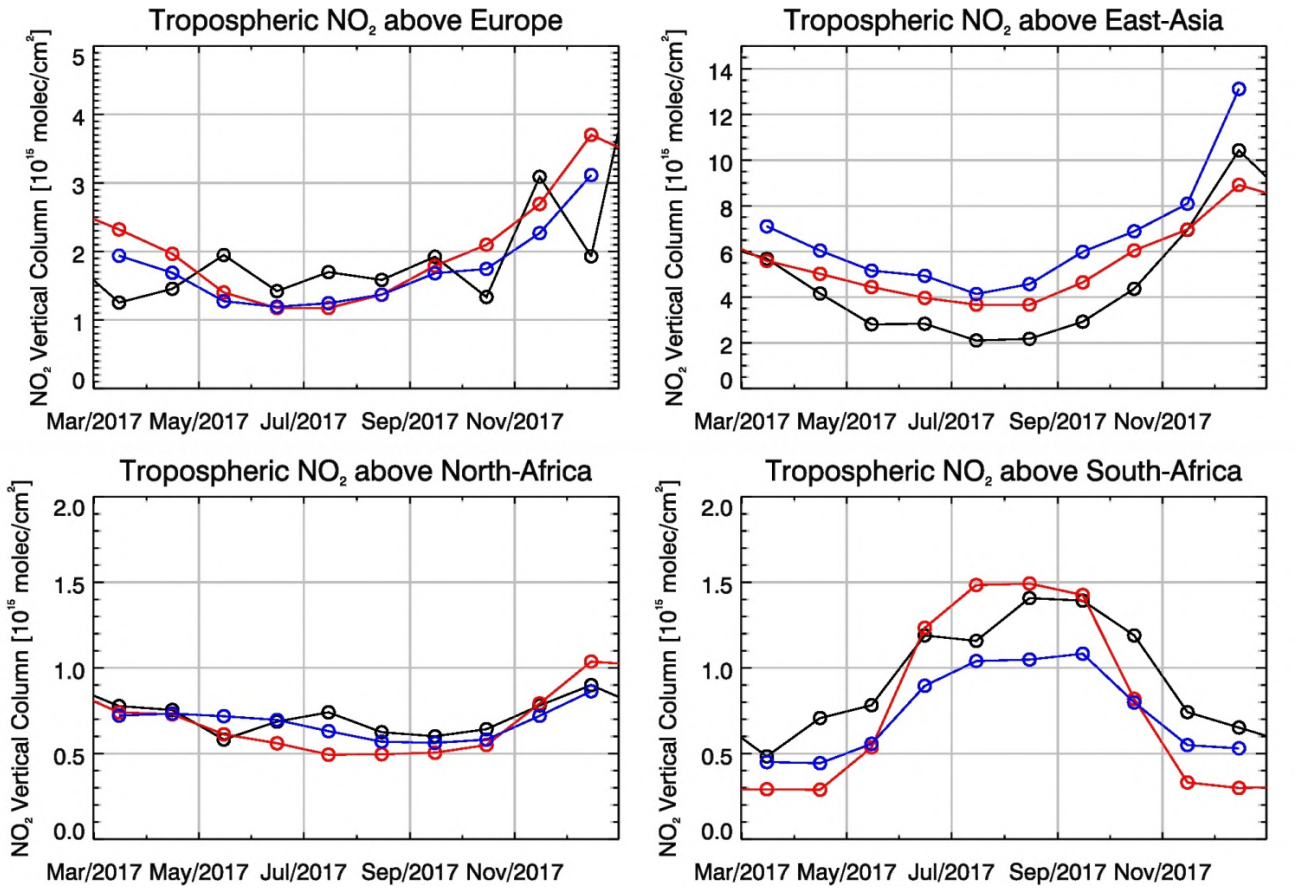

Figure 2.13.1: Time series of average tropospheric NO_2 columns [10^{15} molec cm^{-2}] from (black) GOME-2 compared to the (red) o-suite and (blue) pre-e-suite for different regions. Upper panels represent regions dominated by anthropogenic emissions; lower panels represent those dominated by biomass burning. The pre-e-suite shows a positive offset compared to GOME-2 over East-Asia, a negative offset is found for South Africa.

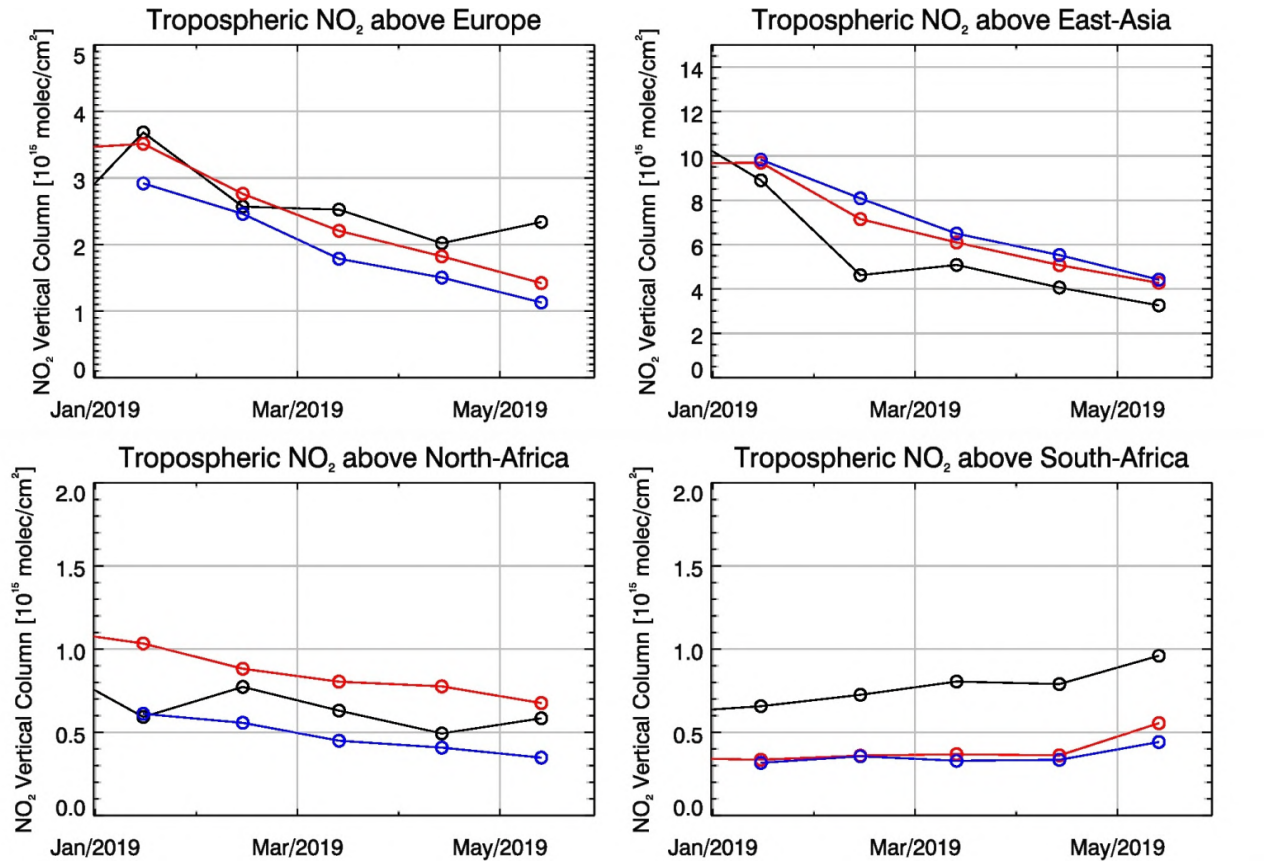

Figure 2.13.2: Same as Figure 2.13.1 but for the 2019 e-suite.

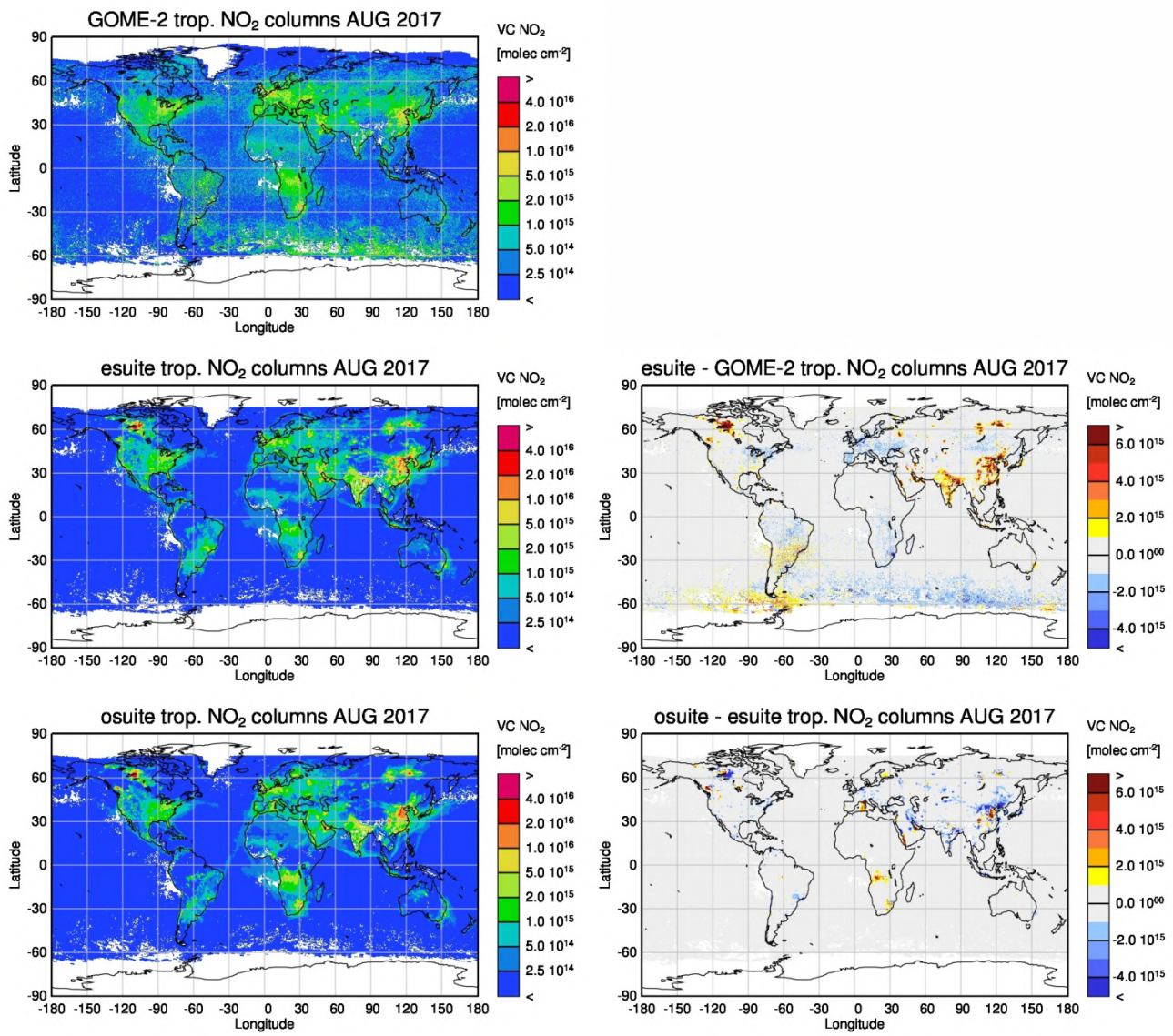

Figure 2.13.3: Monthly mean tropospheric NO_2 columns [molec cm-2] from GOME-2 compared to model runs for August 2017. GOME-2 is shown at the top. The middle row shows e-suite results on the left and the difference between pre-e-suite and GOME-2 on the right. The lower row shows o-suite results on the left and the difference between o-suite and e-suite on the right. GOME-2 and model data were gridded to 0.4 degree resolution. Model data were treated with the same reference sector subtraction approach as the satellite data. Emissions appear overestimated for boreal forest fires over Siberia and Northern America during summer which do not show up in the satellite observations for both e-suite and o-suite (the magnitude of the overestimation shows variability between both runs).

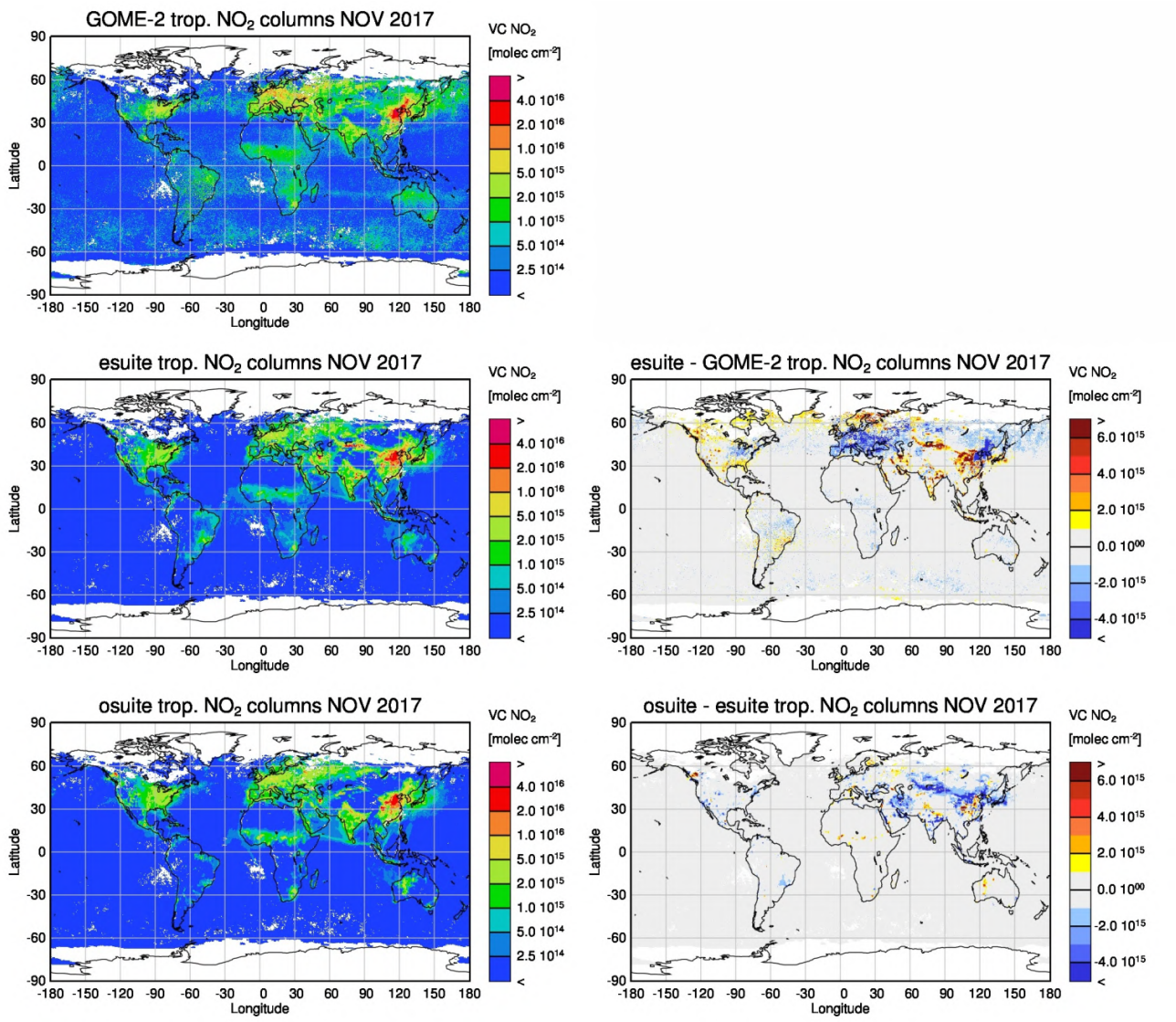

Figure 2.13.4: Same as Figure 2.13.3 but for November 2017. Values to the south of lake Balkhash in Kazakhstan are overestimated by the e-suite (in contrast to the o-suite), possibly related to changes in fire emissions.

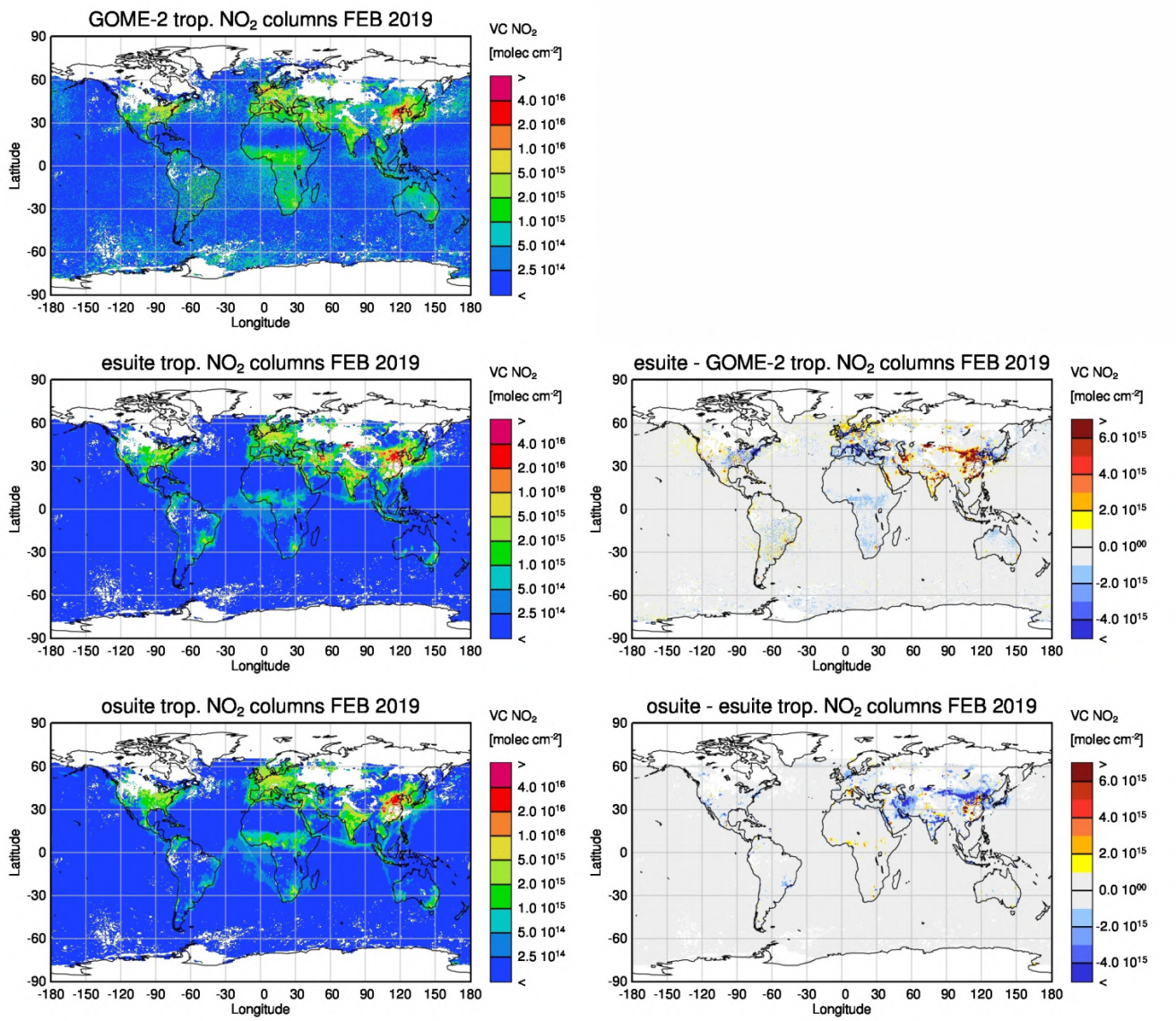

Figure 2.13.5: Same as Figure 2.13.4 but for February 2019 for the e-suite. Values to the south of lake Balkhash in Kazakhstan are overestimated by the e-suite (in contrast to the o-suite), possibly related to changes in fire emissions. This also applies to an area between China and Mongolia, possibly related to fire and/or anthropogenic emissions.

2.14 Tropospheric nitrogen dioxide comparisons with MAX-DOAS

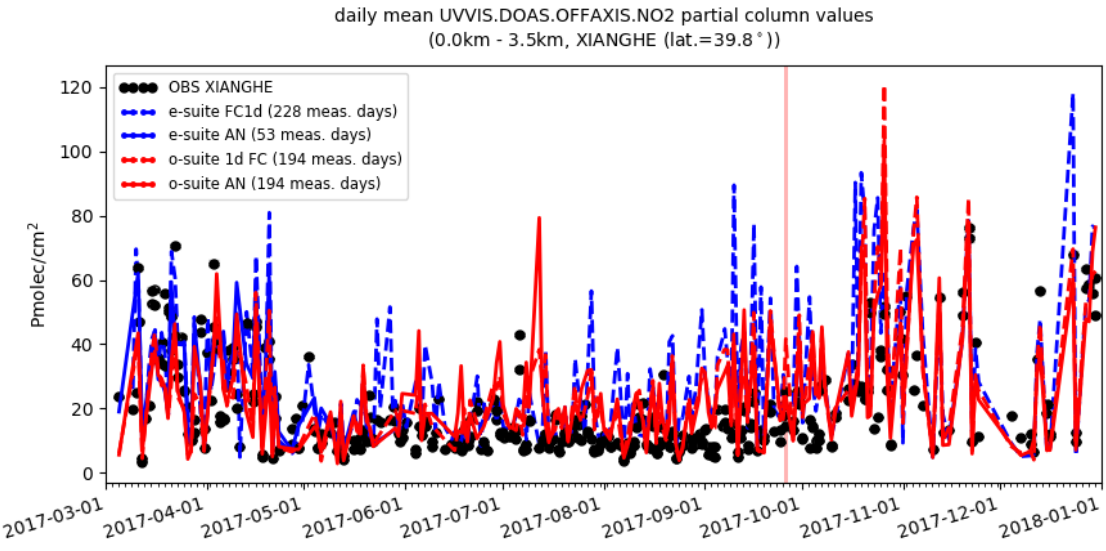

Fig. 2.14.1.: Comparison of daily mean bias between the 2017 pre-e-suite (blue) and o-suite (red) NO_2 partial column for the highly polluted Xianghe (Beijing) station. Both analysis and 1d forecast are shown. Little difference is observed: the pre-e-suite contains more high peaks which do not necessarily correspond to high peak events observed by the MAXDOAS instrument (the pre-e-suite analysis results are only partly available).

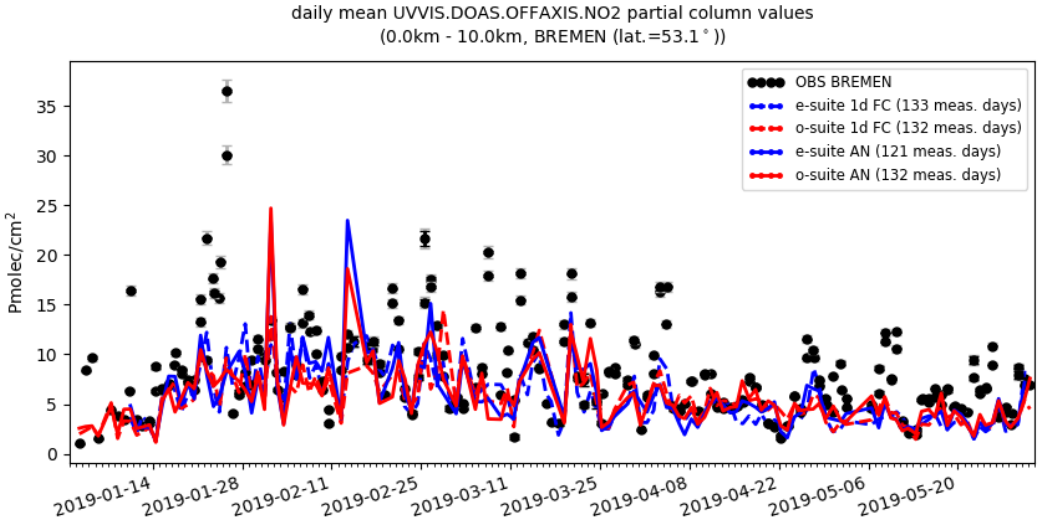

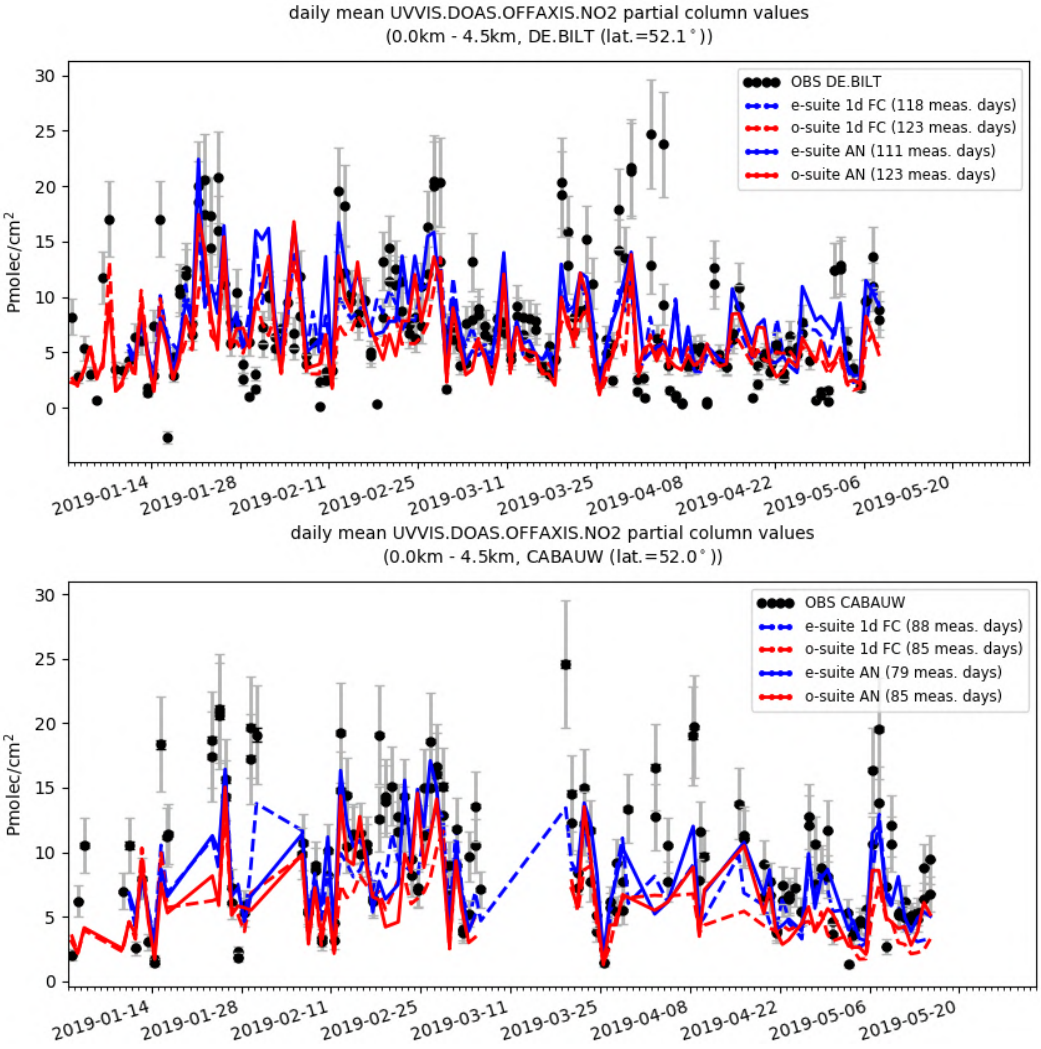
daily mean UVVIS.DOAS.OFFAXIS.NO2 partial column values
(0.0km - 4.5km, DE.BILT (lat.=52.1°))
OBS DE.BILT
e-suite 1d FC (118 meas. days)
o-suite 1d FC (123 meas. days)
e-suite AN (111 meas. days)
o-suite AN (123 meas. days)
Pmolec/cm²
daily mean UVVIS.DOAS.OFFAXIS.NO2 partial column values
(0.0km - 4.5km, CABAUW (lat.=52.0°))
OBS CABAUW
e-suite 1d FC (88 meas. days)
o-suite 1d FC (85 meas. days)
e-suite AN (79 meas. days)
o-suite AN (85 meas. days)
Pmolec/cm²

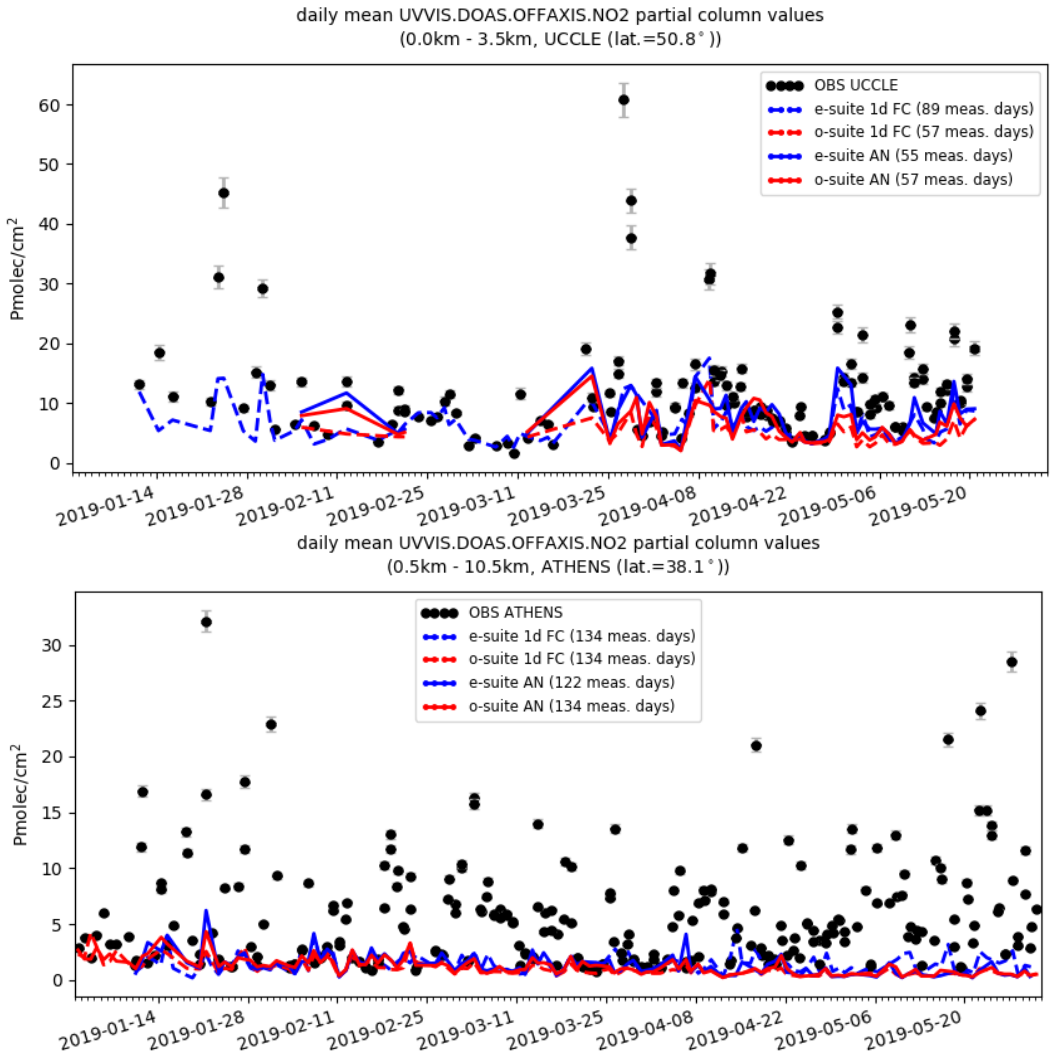

Fig. 2.14.2.: Comparison of daily mean bias between the e-suite (blue) and o-suite (red) NO_2 tropospheric partial column against the NO2 NDACC OFFAXIS measurements. From top to bottom: Bremen, De Bilt, Cabauw, Uccle, Athens. Both analysis and 1d forecast are shown. The overall e-suite columns are higher compared to the o-suite, and a bit closer to the observations. At Athens the high pollution events are not captured by the o-suite and e-suite.

2.15 Formaldehyde (HCHO)

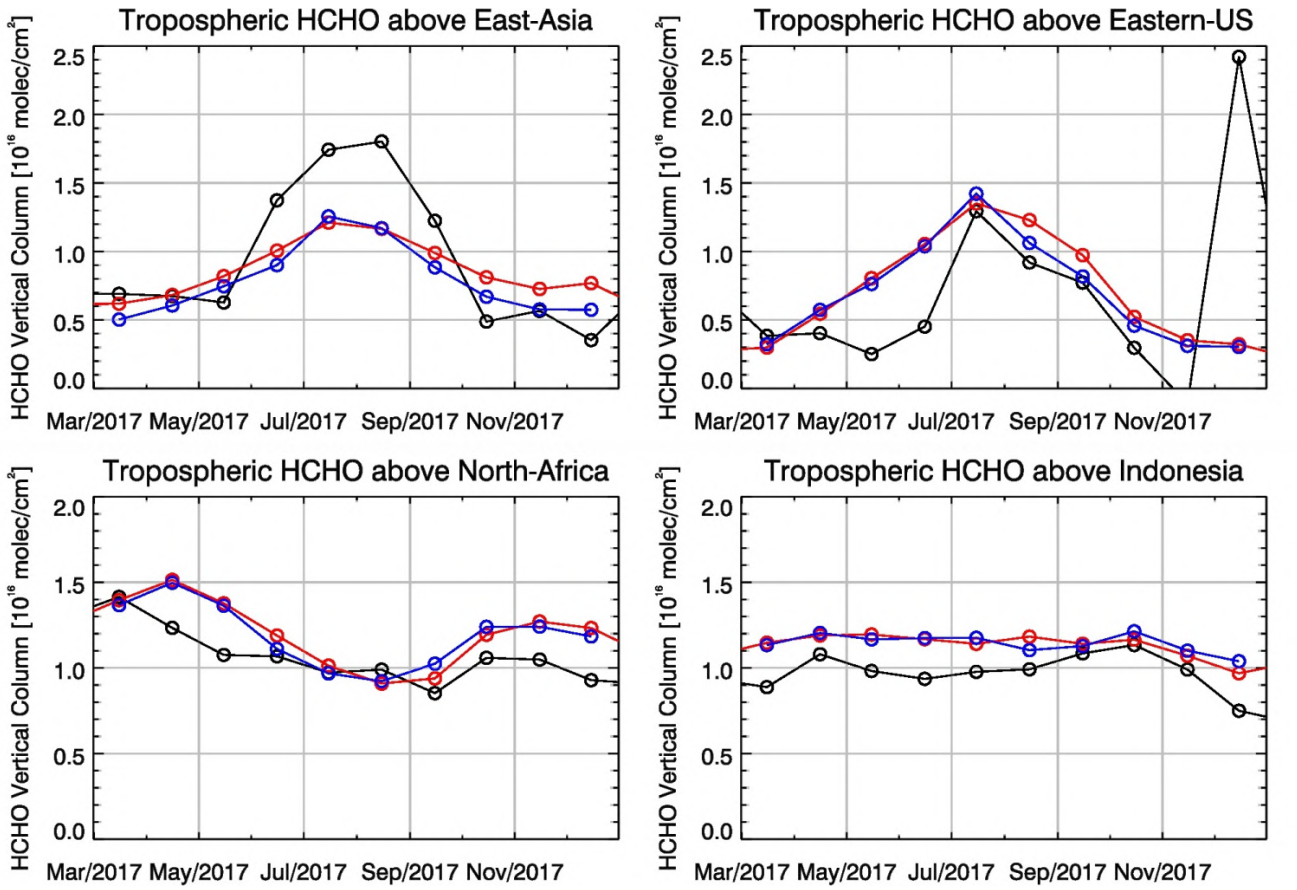

Figure 2.15.1: Time series of average tropospheric HCHO columns [10^{16} molec cm-2] from (black) GOME-2 compared to the (red) o-suite and (blue) pre-e-suite for different regions. Negative satellite retrieved values and large variability over Eastern US during Northern Hemisphere winter months are due to a lack of data (caused by instrument degradation) for this region.

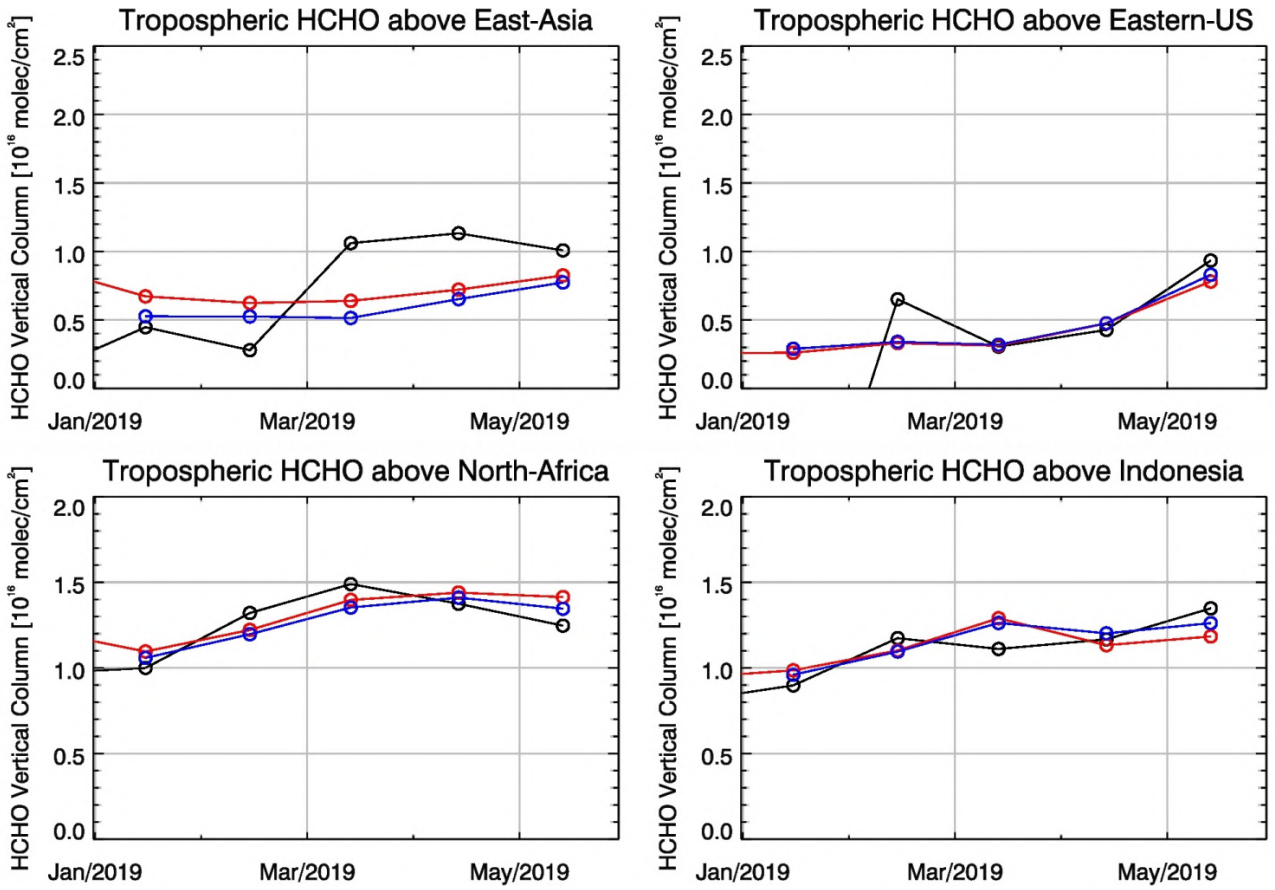

Figure 2.15.2: Same as Figure 2.15.1 but for the 2019 e-suite.

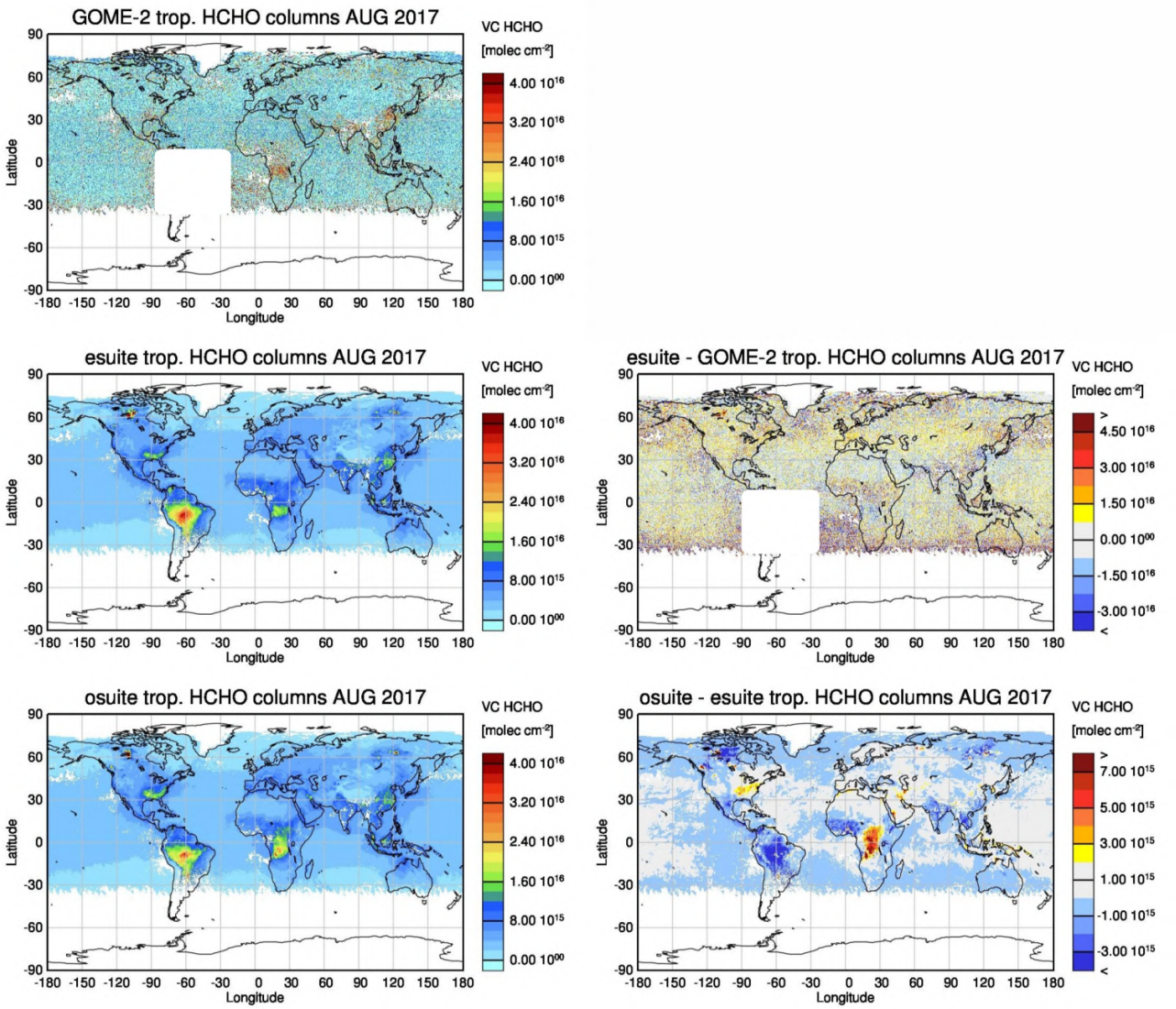

Figure 2.15.3: Monthly mean tropospheric HCHO columns [molec. cm^{-2}] from GOME-2 compared to model runs for August 2017. GOME-2 is shown at the top. The middle row shows e-suite results on the left and the difference between pre-e-suite and GOME-2 on the right. The lower row shows o-suite results on the left and the difference between o-suite and e-suite on the right. GOME-2 and model data were gridded to 0.4 degree resolution. Model data were treated with the same reference sector subtraction approach as the satellite data. Values in the region of the South Atlantic Anomaly are not valid and therefore masked out (white boxes in panels on the left). Values over Southern Africa are underestimated by the e-suite possibly related to fire emissions, the o-suite performed better in this case. Values decreased over Mecca and Teheran compared to the o-suite.

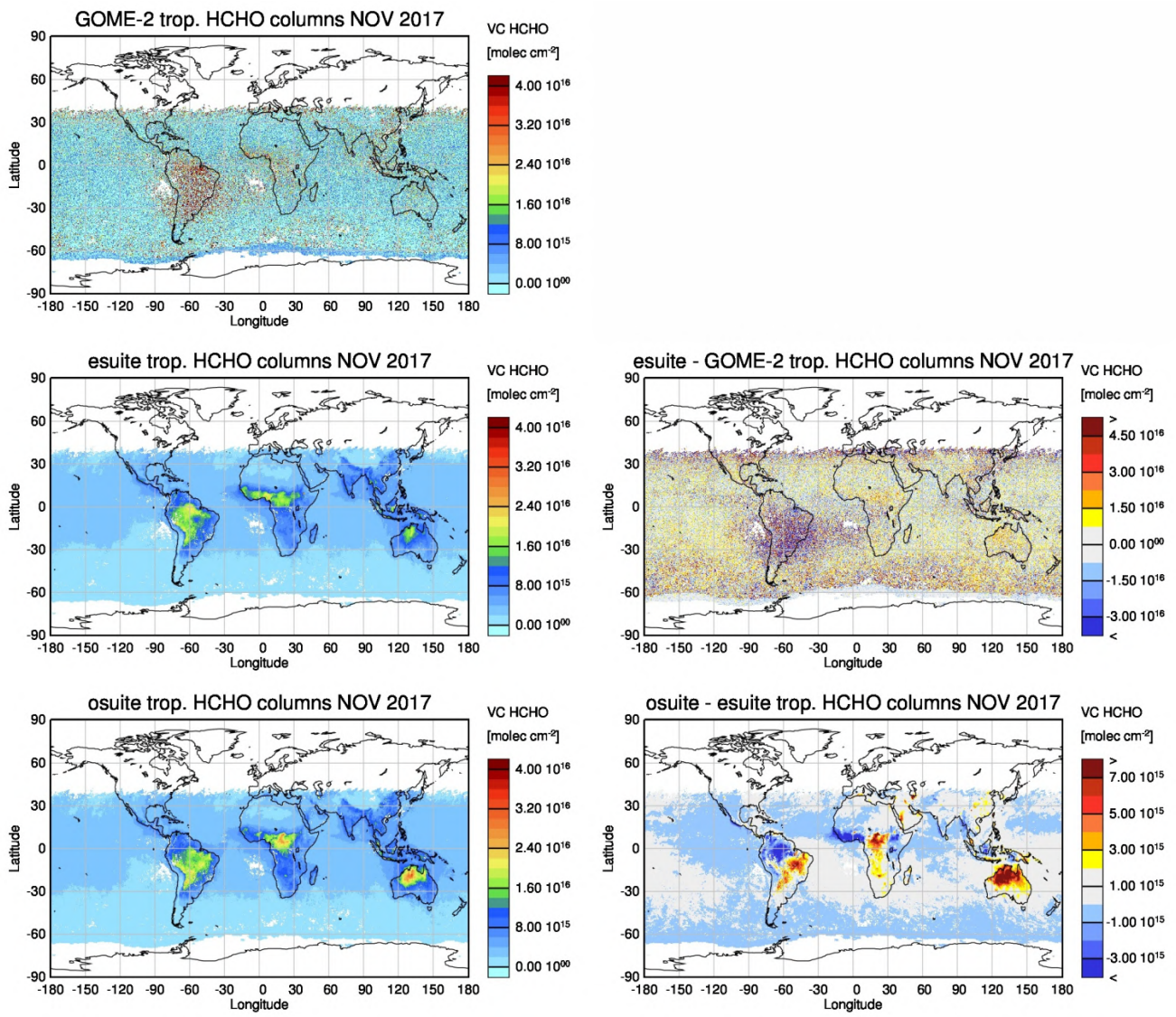

Figure 2.15.4: Same as Figure 2.15.3 but for November 2017. Values over Central Africa and Northern Australia are overestimated less by the e-suite than by the o-suite possibly related to changes in fire emissions. Values decreased over Mecca and Teheran compared to the o-suite.

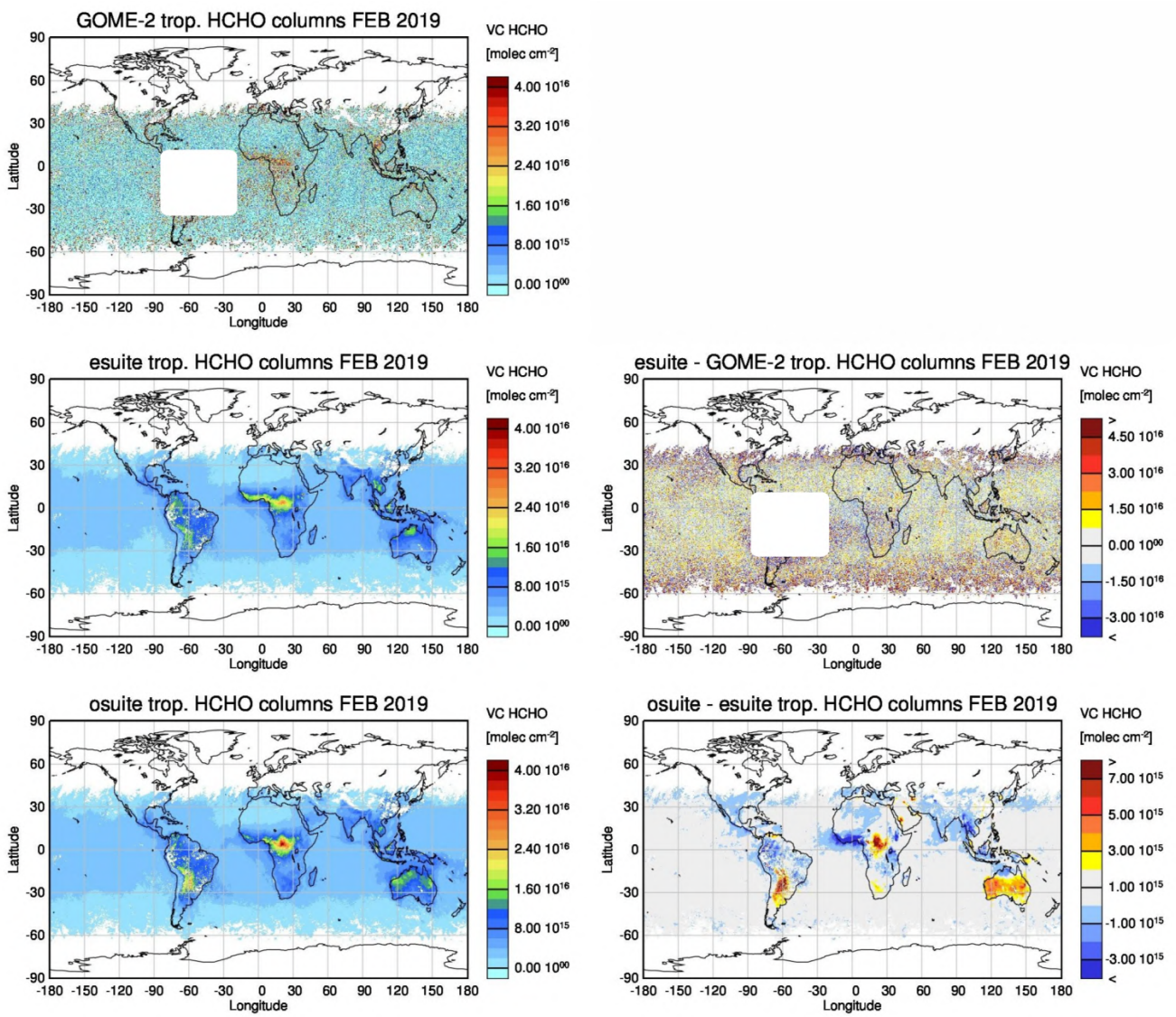

Figure 2.15.5: Same as Figure 8 but for February 2019 for the e-suite. Values over Central Africa are lower in the e-suite compared to the o-suite possibly related to changes in fire emissions, the o-suite performed better compared to GOME-2 in this case. Background values over Australia appear generally lower in the e-suite compared to the o-suite and are overall closer to the satellite observations in this region. Values decreased over Mecca and Teheran compared to the o-suite.

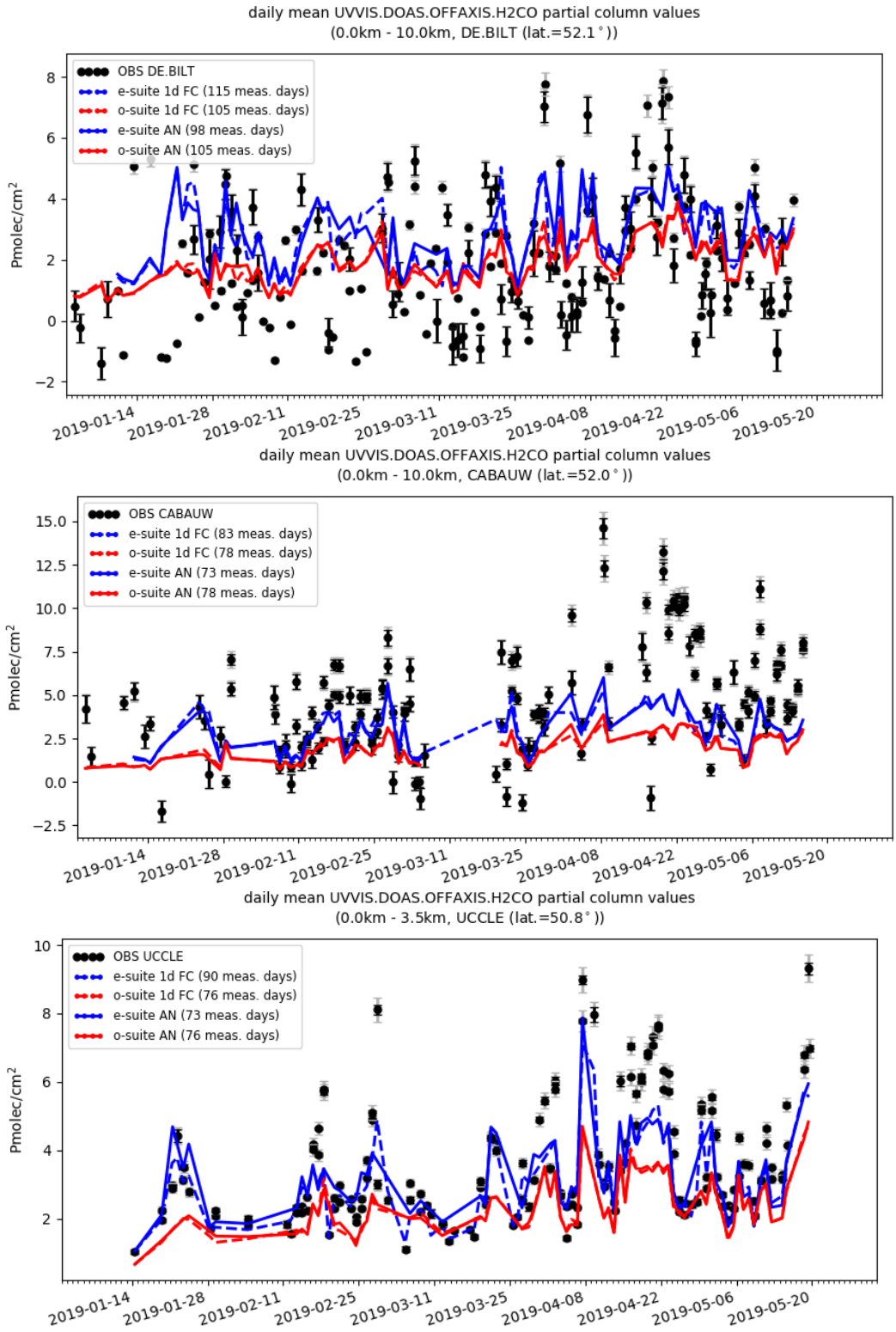

Figure 2.15.6. The 2019 e-suite (blue) and o-suite (red) compared to NDACC MAXDOAS observations (black). Analysis: solid lines; 1-day forecast: dashed lines. Stations included are De Bilt (top), Cabauw (middle) and Uccle (bottom). The comparisons show that the smoothed e-suite column values are higher compared to the o-suite, bringing the CAMS analysis closer to the observations. In particular the comparison at Uccle shows that the e-suite (AN and FC) captures more high pollution events.

2.16 Stratosphere: comparisons with ozone sondes

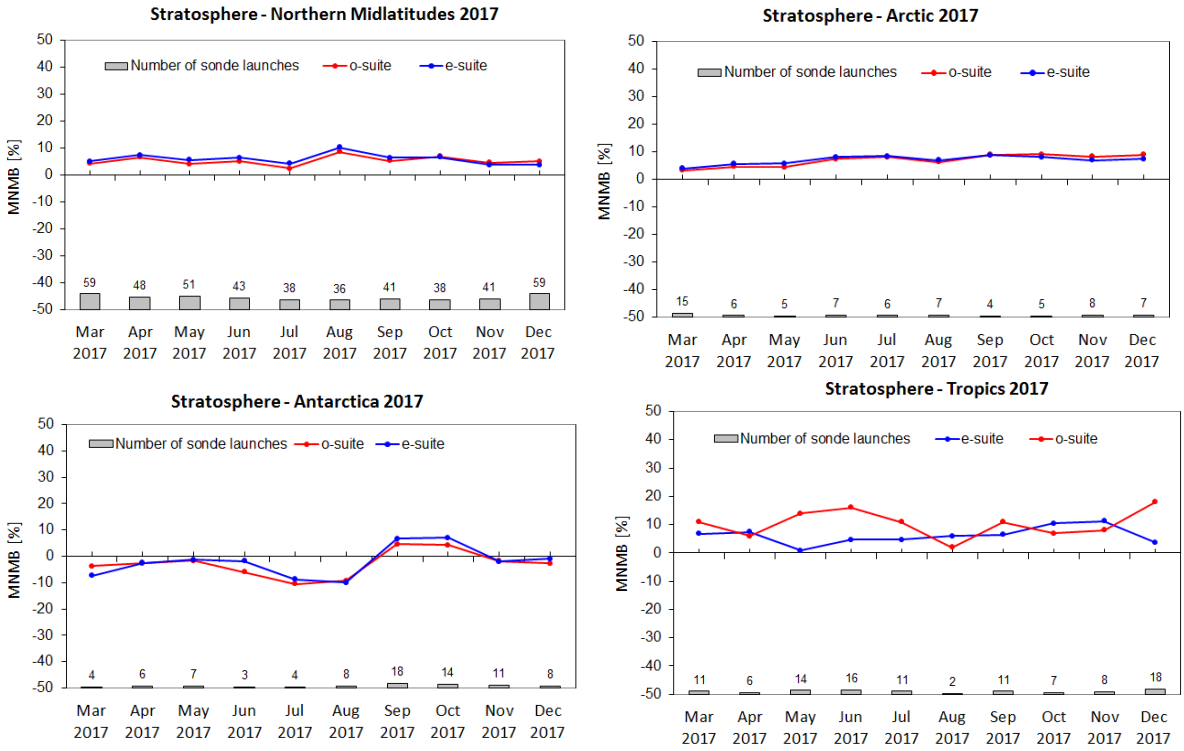

Fig 2.16.1: MNMBs for the o-suite (red) and pre-e-suite (blue) in 2017 integrated over the stratosphere (90-10 hPa; Tropics 60-10 hPa) of the Northern midlatitudes, Arctic, Antarctica and Tropics. For the Tropics, the 2017 pre-e-suite shows mostly lower MNMBs than the o-suite. We note that the biases reported in the next section at around 30 km do not show up clearly when integrating over this height range.

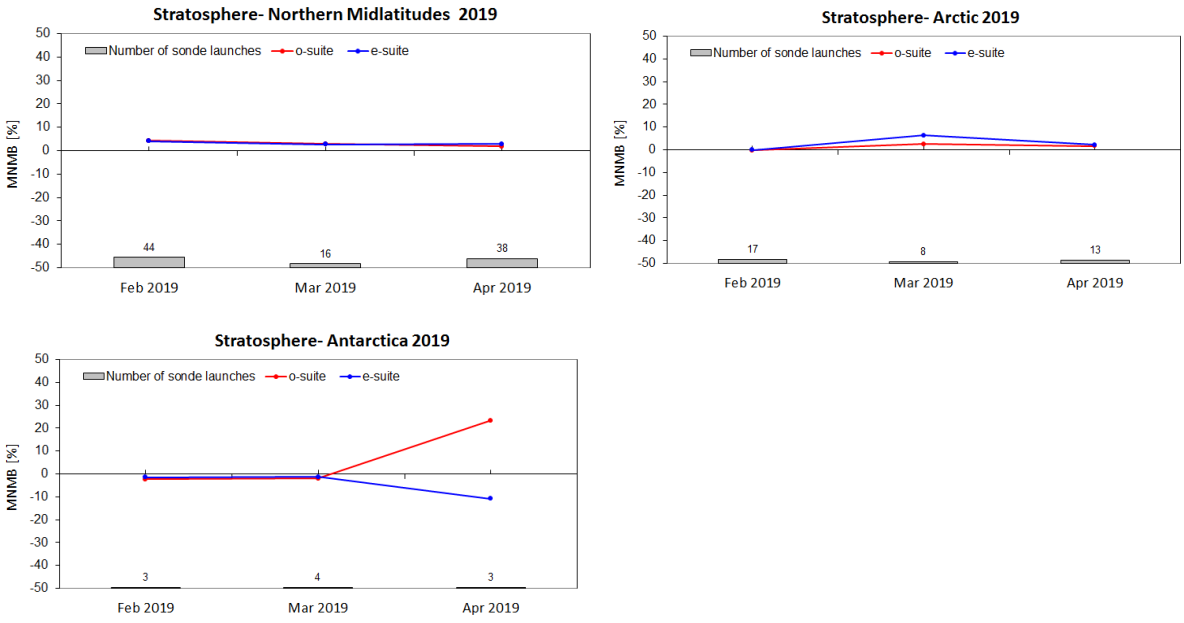

Fig. 2.16.2: MNMBs for the o-suite (red) and e-suite (blue) in 2019 over the stratosphere (90-10 hPa; Tropics 60-10 hPa)of the Northern midlatitudes, Arctic, and Antarctica. Observational data for the Tropics was not yet available.

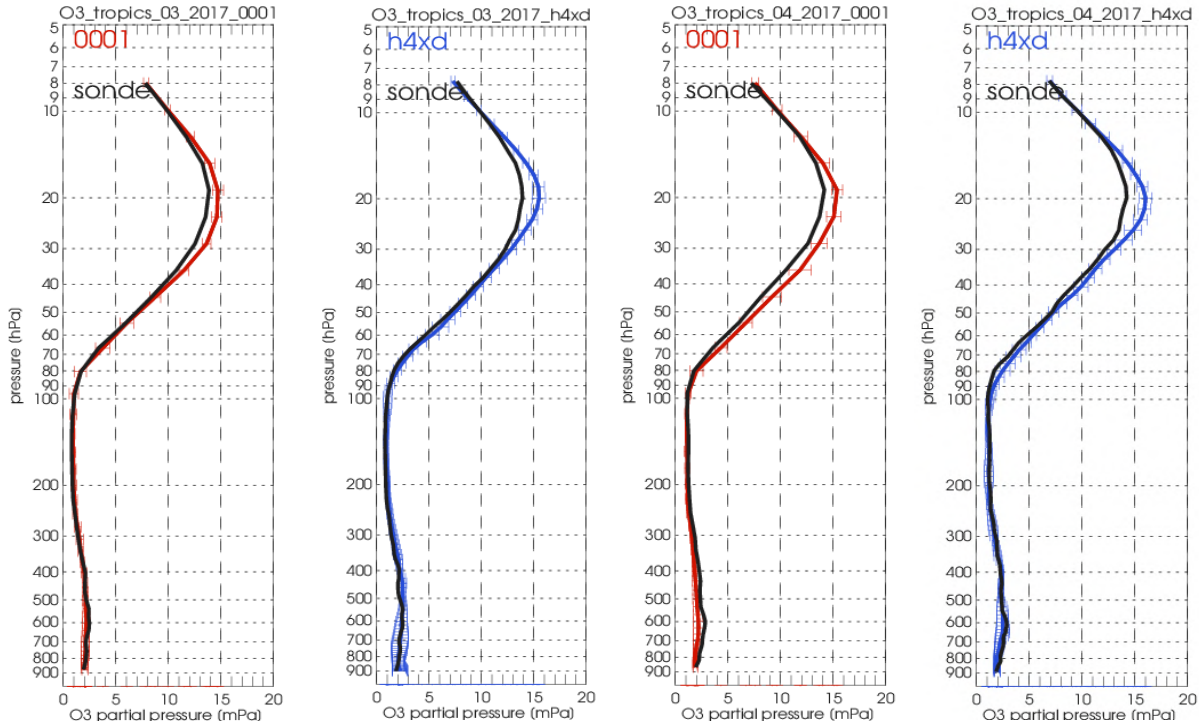

Fig. 2.16.3: Ozone sonde profiles for o-suite (red) and e-suite (blue) for March 2017 (left) and April 2017 (right) over the Tropics. An increased positive bias is observed at around 20 hPa.

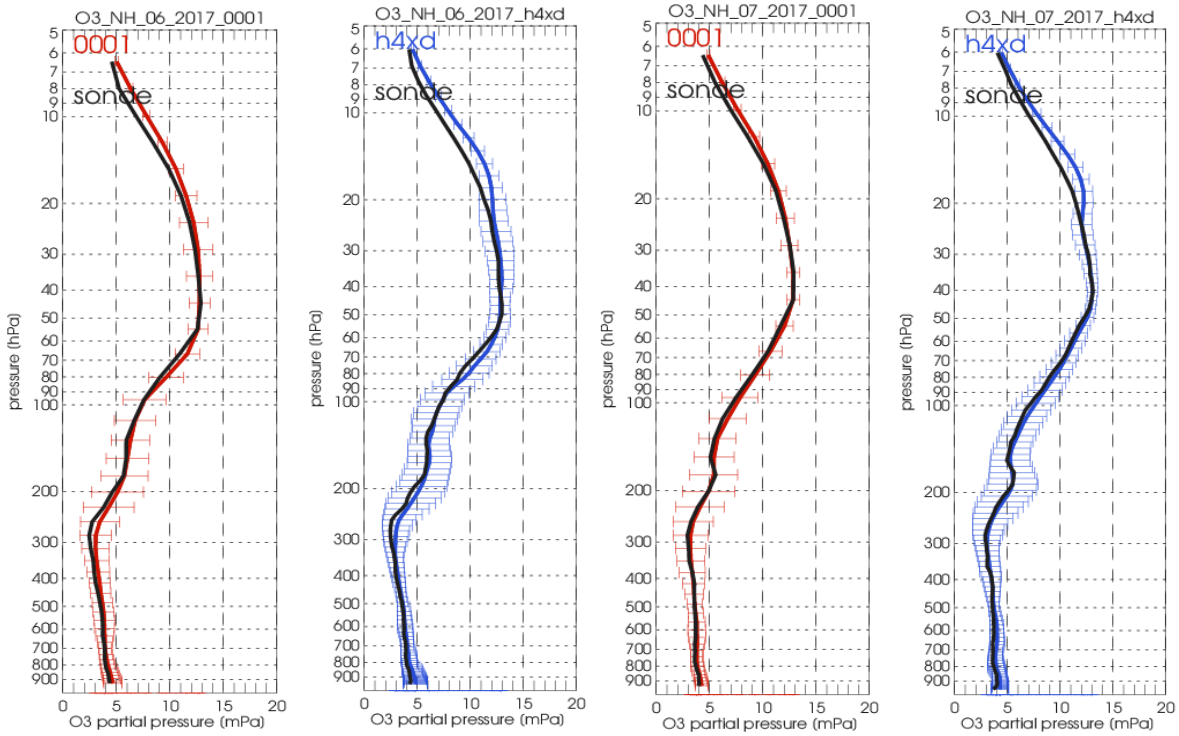

Fig. 2.16.4: Ozone sonde profiles for o-suite (red) and e-suite (blue) for June 2017 (left) and July 2017 (right) over the Northern Midlatitudes. An increased positive bias is observed at around 15 hPa.

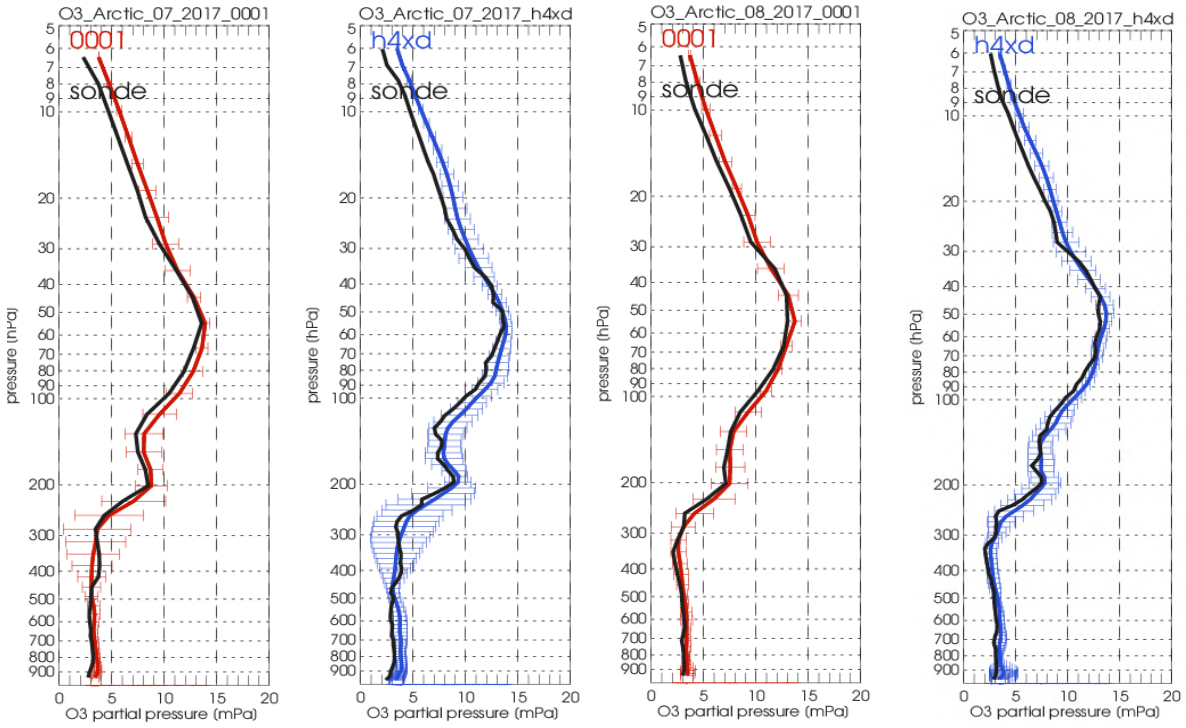

Fig. 2.16.5: Ozone sonde profiles for o-suite (red) and e-suite (blue) for July 2017 (left) and August 2017 (right) over the Arctic.

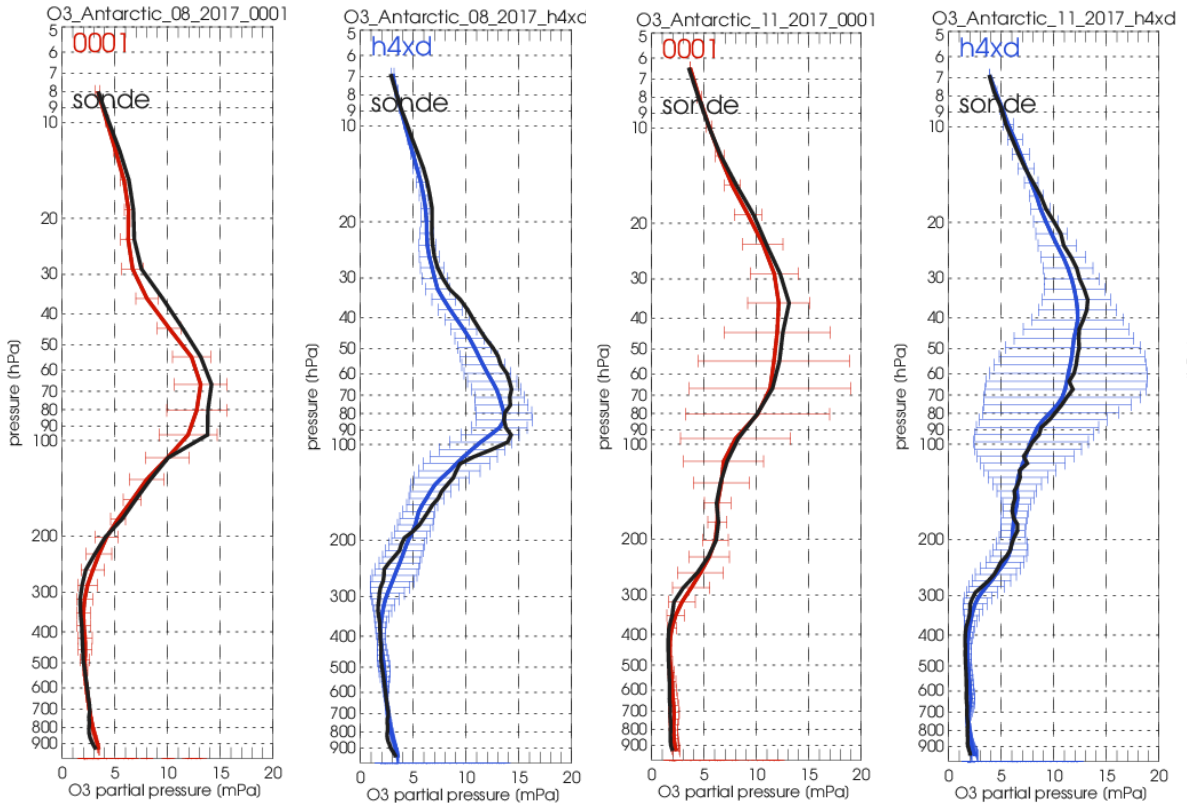

Fig. 2.16.6: Ozone sonde profiles for o-suite (red) and e-suite (blue) for August 2017 (left) and November 2017 (right) over the Antarctica.

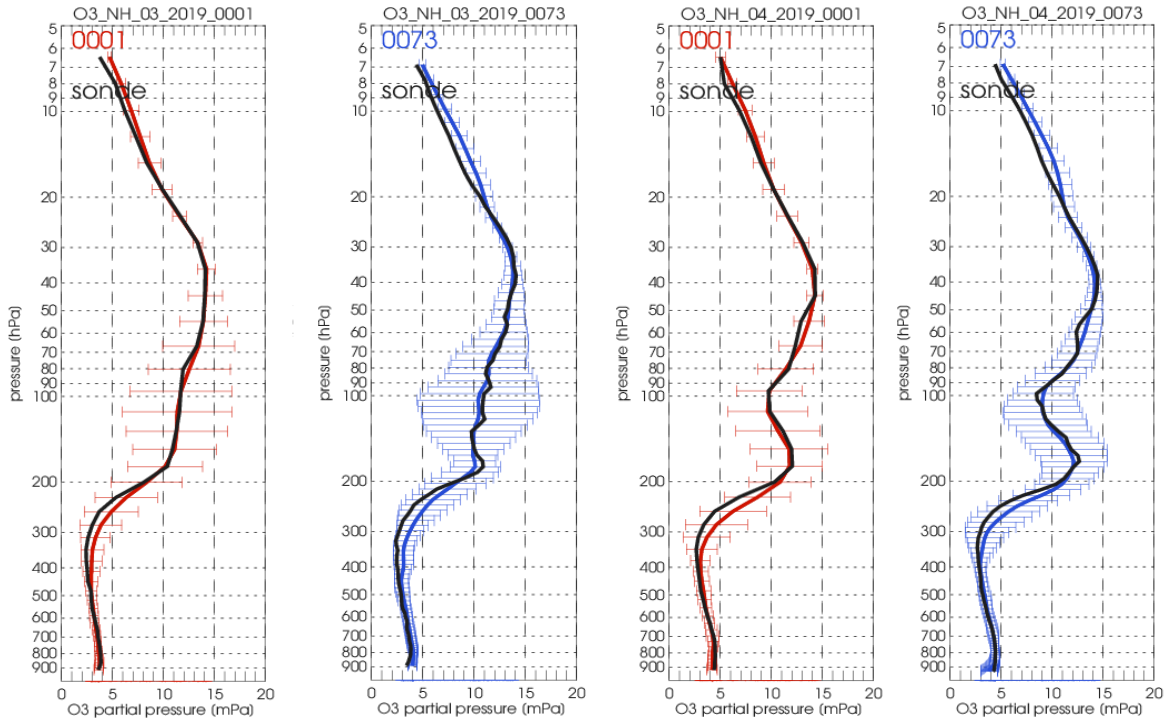

Fig. 2.16.7: sonde profiles for o-suite (red) and e-suite (blue) for March 2019 (left) and April 2019 (right) over the Northern Midlatitudes. An increased positive bias is observed at around 15 hPa.

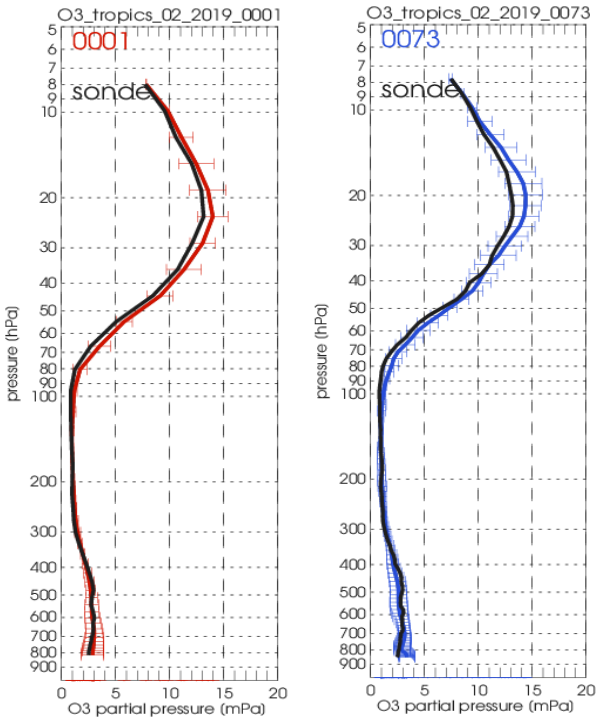

Fig.2.16.8: Ozone sonde profiles for o-suite (red) and e-suite (blue) for February 2019 (left) (right) over the Tropics. An increased positive bias is observed at around 20 hPa.

2.17 Stratospheric ozone: Comparison with satellite observations

The satellite observations of AURA MLS offline (version 4.2) and of ACE-FTS (version 3.6) are used.

All datasets are averaged over all longitudes and over the 5 usual latitude bands for stratospheric ozone: Antarctic (90°S-60°S), South mid-latitude (60°S-30°S), Tropics (30°S-30°N), North mid-latitude (30°N-60°N) and Arctic (60°N-90°N) and collocated with the observations.

The o-suite is represented in red, the e-suite (mc.0073) and pre-e-suite experiments (h4x1/h4xd) in blue and the experiment configured as the current o-suite (h30x) in magenta.

The comparisons include the analysis and the 4th day forecasts (96h to 120h) of stratospheric ozone. These forecasts are represented by dotted lines in the figures.

Pre-e-suite experiments (2017)

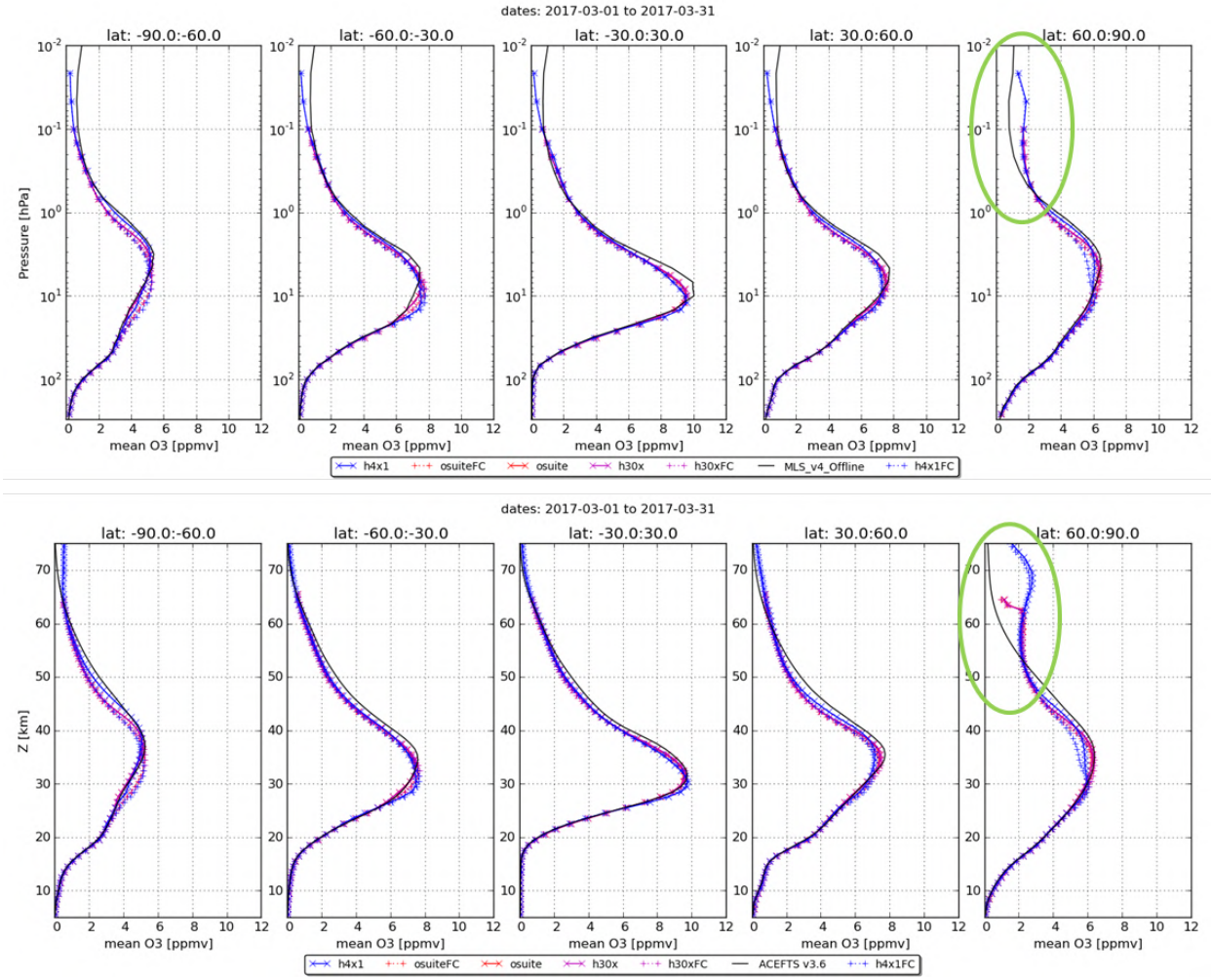

Figure 2.17.1: Monthly mean profiles for March 2017 using MLS (top) and ACEFTS (bottom) as reference. Blue curves: pre-e-suite; red curves: o-suite and experiment h30x; star: analysis; + symbol: 4-day forecast; black: observations. The differences between the model profiles are limited; the positive bias in the upper stratosphere, in the North polar region (typical for the spring season) persists for the supplementary highest model levels of the 137-level pre-e-suite compared to the 60-level o-suite.

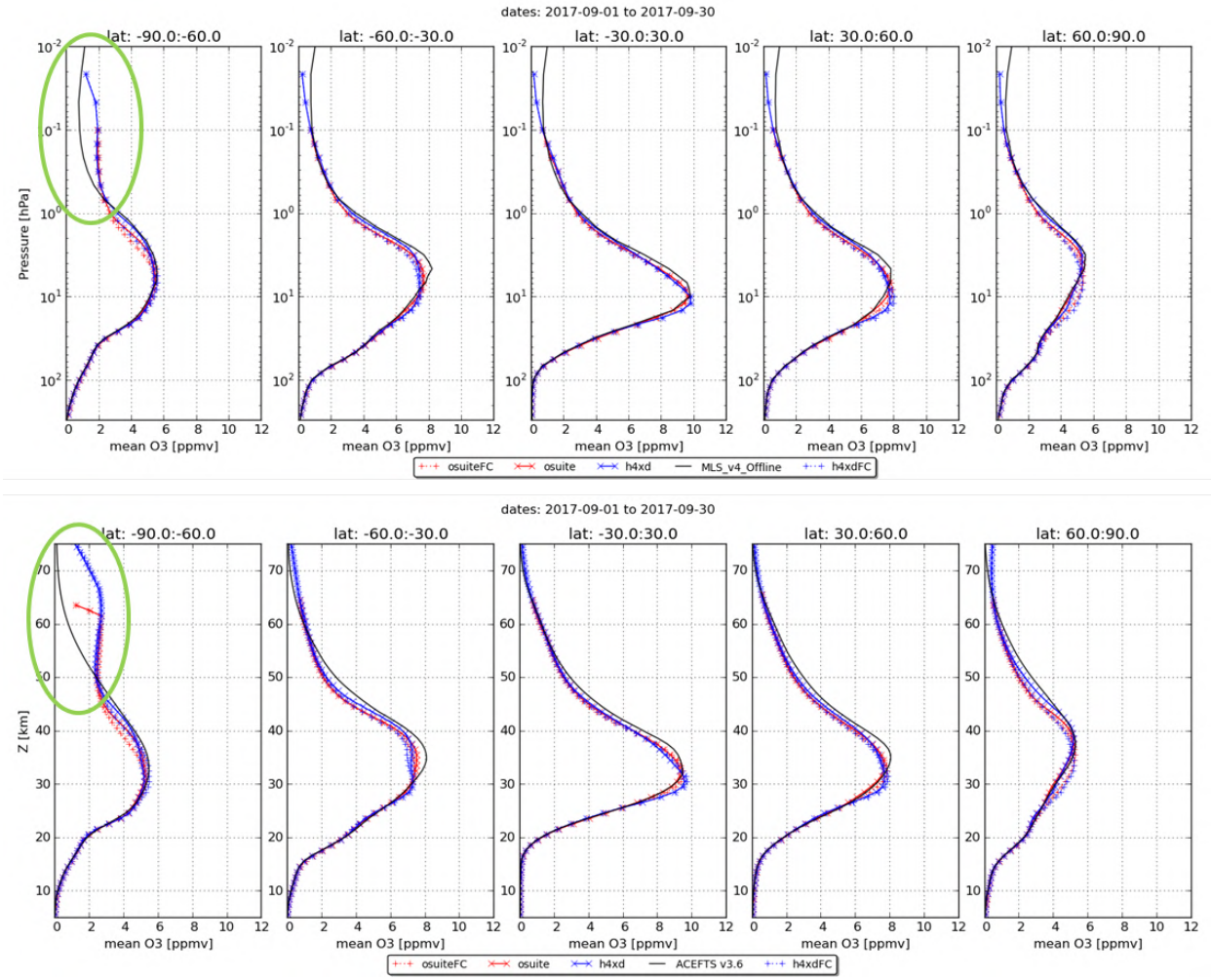

Figure 2.17.2: Monthly mean profiles for September 2017 using MLS (top) and ACEFTS (bottom) as reference. Blue curves: pre-e-suite; red curves: 2017 o-suite; stars: analysis; plus symbol: 4-day forecast; black: observations. As for March, the positive bias in the upper stratosphere in the South Polar region (typical for the winter and spring season) persists for the supplementary highest model levels.

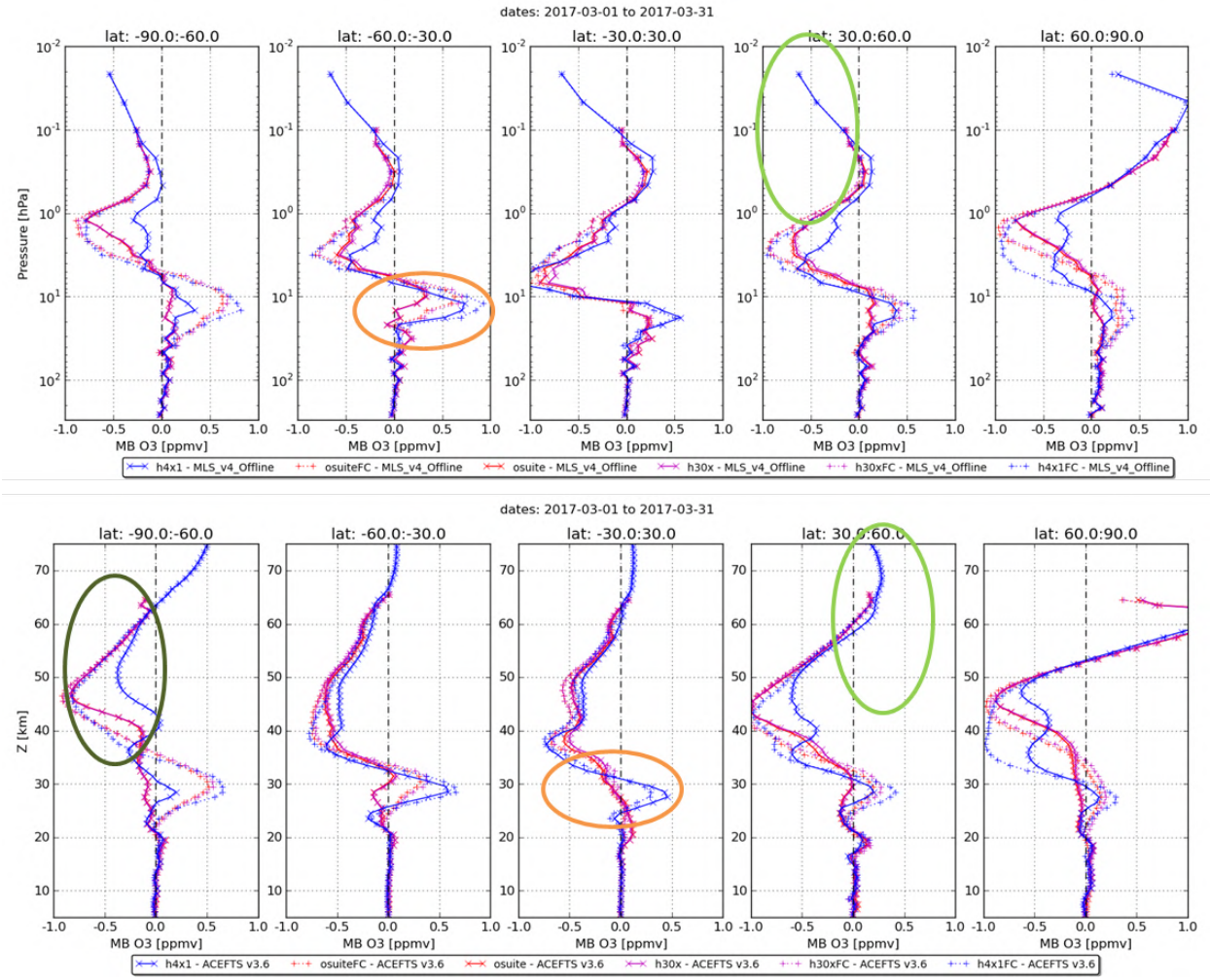

Figure 2.17.3: Monthly mean biases (in ppmv) for March 2017. Blue curves: pre-e-suite; red curves: o-suite and experiment h30x; star: analysis; + symbol: 4-day forecast; black: observations. Above ~40km/~5hPa the biases of analyses of the pre-e-suite are smaller than the o-suite (dark green circle), but the 4-day forecasts present similar (negative) biases. At ~30km/20hPa, the pre-e-suite has a more positive bias (orange circles): these characteristics are present at most latitude bands and months, with varying amplitude and vertical range. For the whole period (March 2017 to December 2017, except for the polar regions in winter/spring), the bias of the upper levels against ACE-FTS and MLS are of opposite sign; the monthly mean bias of the analysis for the pre-e-suite is always within ±1ppmV against MLS and ACE-FTS, while the o-suite has sometimes larger negative biases.

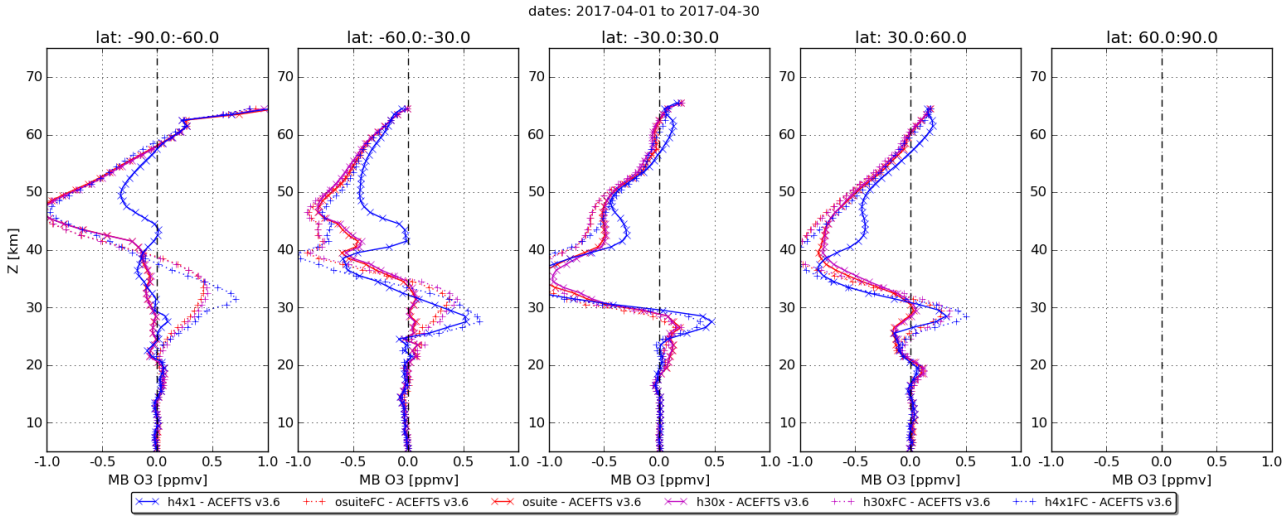
dates: 2017-04-01 to 2017-04-30
lat: -90.0:-60.0
lat: -60.0:-30.0
lat: -30.0:30.0
lat: 30.0:60.0
lat: 60.0:90.0
Z [km]
MB O3 [ppmv]
h4x1 - ACEFTS v3.6
osuiteFC - ACEFTS v3.6
osuite - ACEFTS v3.6
h30x - ACEFTS v3.6
h30xFC - ACEFTS v3.6
h4x1FC - ACEFTS v3.6

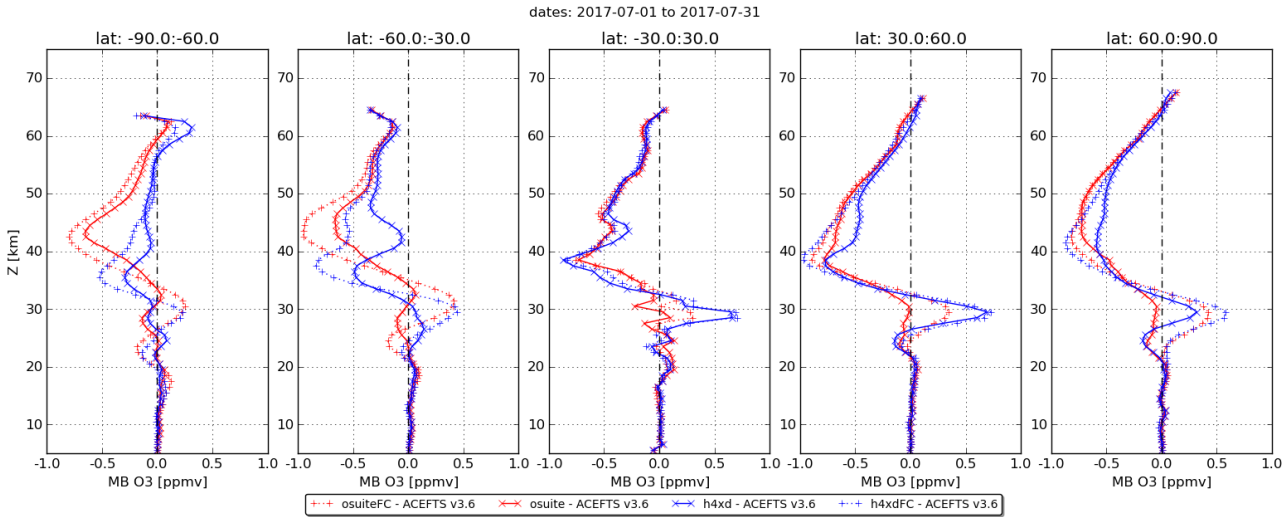
dates: 2017-07-01 to 2017-07-31
lat: -90.0:-60.0
lat: -60.0:-30.0
lat: -30.0:30.0
lat: 30.0:60.0
lat: 60.0:90.0
Z [km]
MB O3 [ppmv]
osuiteFC - ACEFTS v3.6
osuite - ACEFTS v3.6
h4xd - ACEFTS v3.6
h4xdFC - ACEFTS v3.6

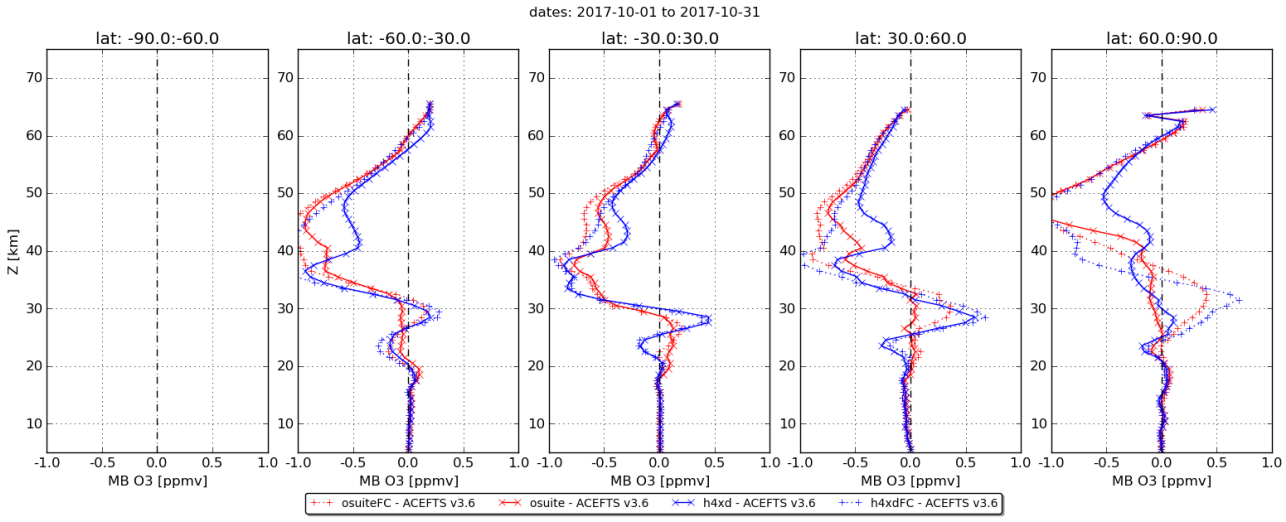
dates: 2017-10-01 to 2017-10-31
lat: -90.0:-60.0
lat: -60.0:-30.0
lat: -30.0:30.0
lat: 30.0:60.0
lat: 60.0:90.0
Z [km]
MB O3 [ppmv]
osuiteFC - ACEFTS v3.6
osuite - ACEFTS v3.6
h4xd - ACEFTS v3.6
h4xdFC - ACEFTS v3.6

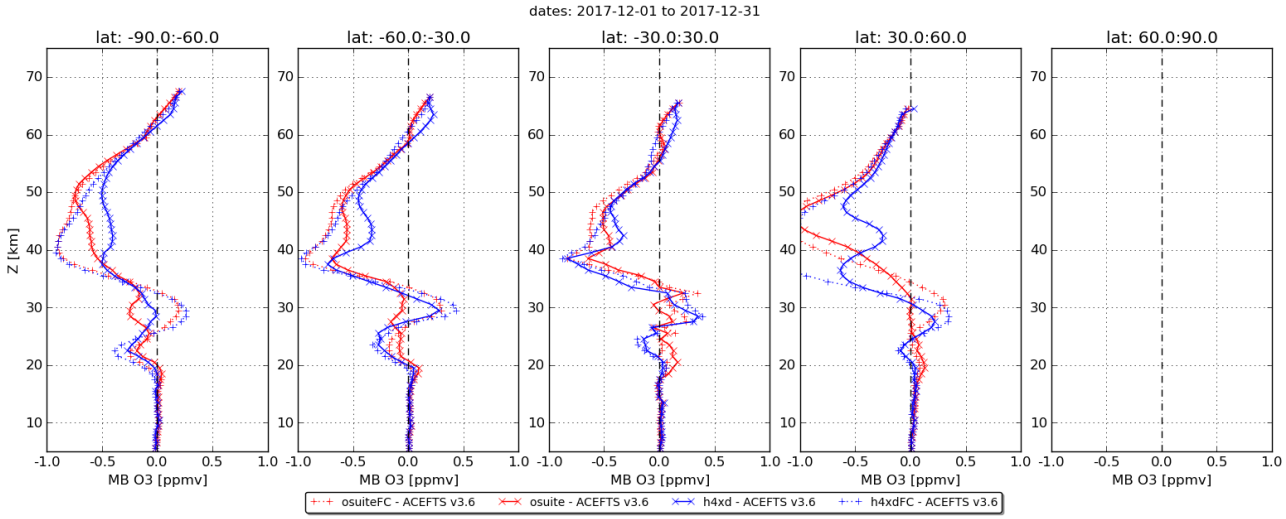

Figure 2.17.4: Monthly mean biases against ACE-FTS, for April, July, October and December 2017. Red: o-suite. Blue: pre-e-suite. Dotted lines: 4-day forecasts.

E-suite experiment (2019)

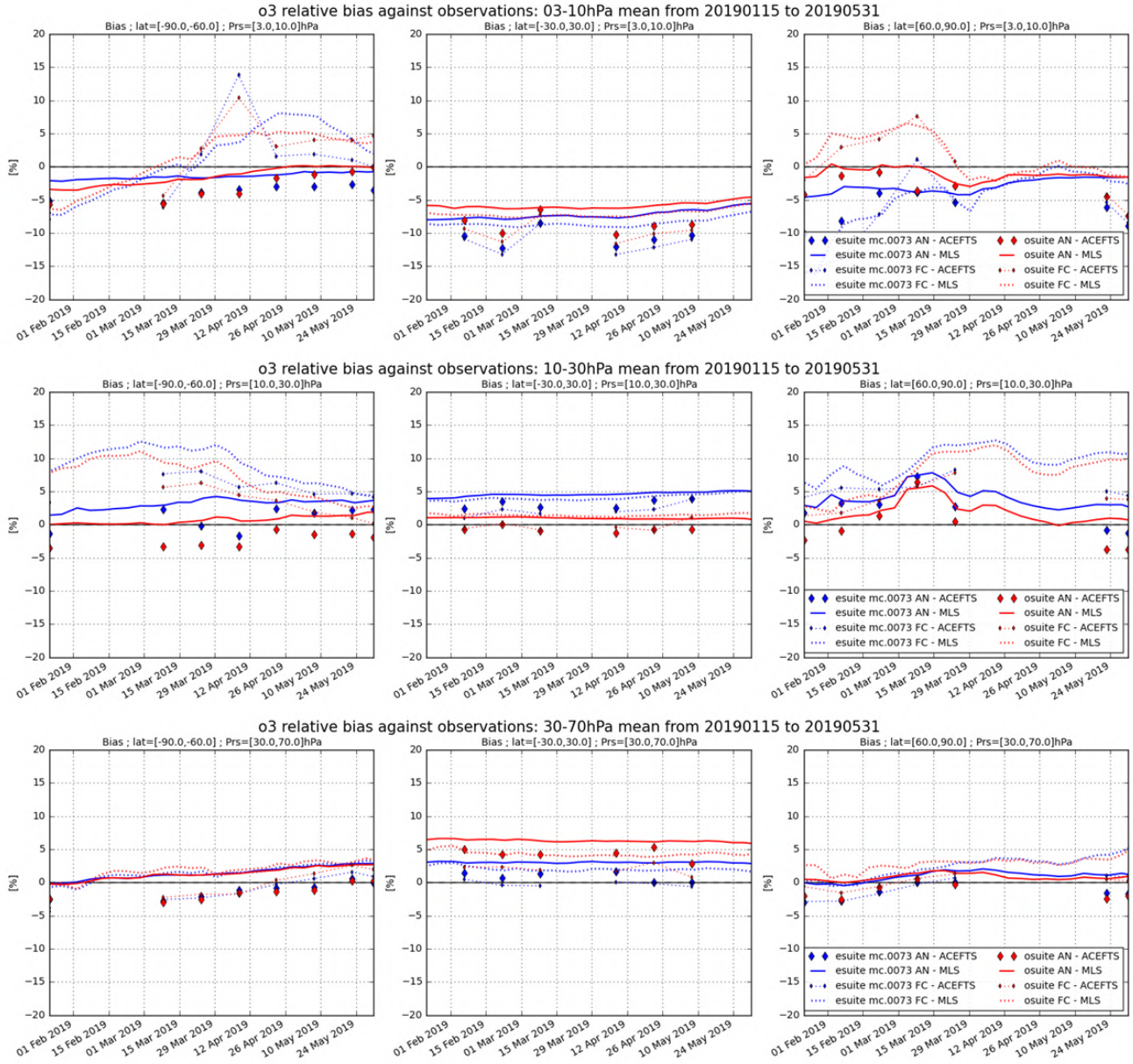

Figure 2.17.5: Timeseries of mean biases against ACE-FTS (diamonds) and MLS, for 2019-01-15 to 20190-05-31 (red: o-suite; blue: e-suite; dotted lines: 4-day forecasts). Top: 3-10hPa, biases in the analyses of e-suite are generally slightly more negative than for the o-suite (-3%). Middle: 10-30hPa, biases in the analyses of e-suite are generally slightly more positive than for the o-suite (+3%). Bottom: 30-70hPa: in the polar regions, biases in the e-suite and the o-suite are very similar to within ±5%; in the tropics, the e-suite performs better than the o-suite .

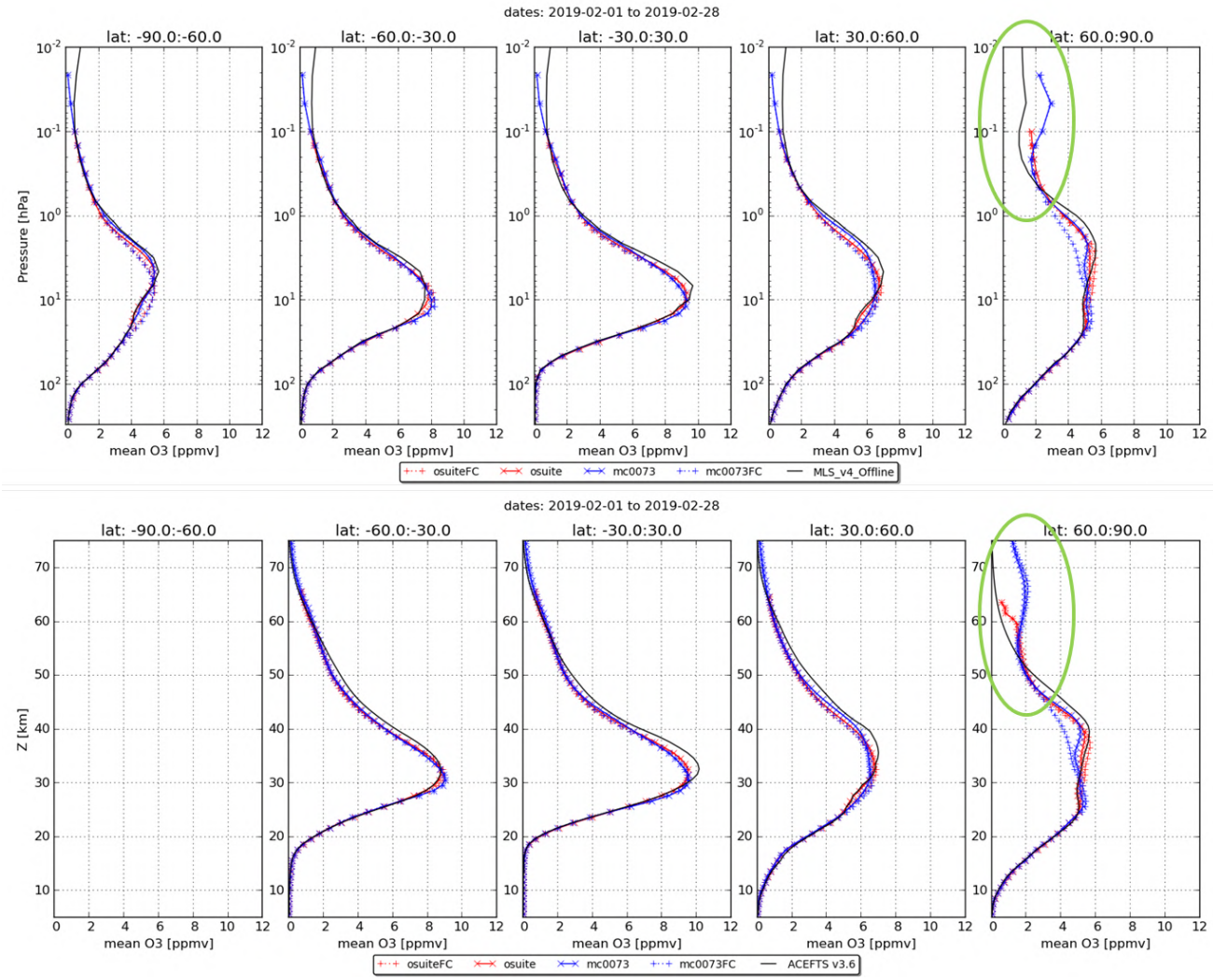

Figure 2.17.6: Monthly mean profiles for February 2019, using MLS (top) and ACEFTS (bottom) as reference (red: o-suite; blue: e-suite; dotted lines: 4-day forecasts). The differences between the model profiles are limited; the positive bias in the upper stratosphere, in the North polar region (typical for the spring season) persists for the supplementary highest model levels, comparable to the pre-e-suite findings.

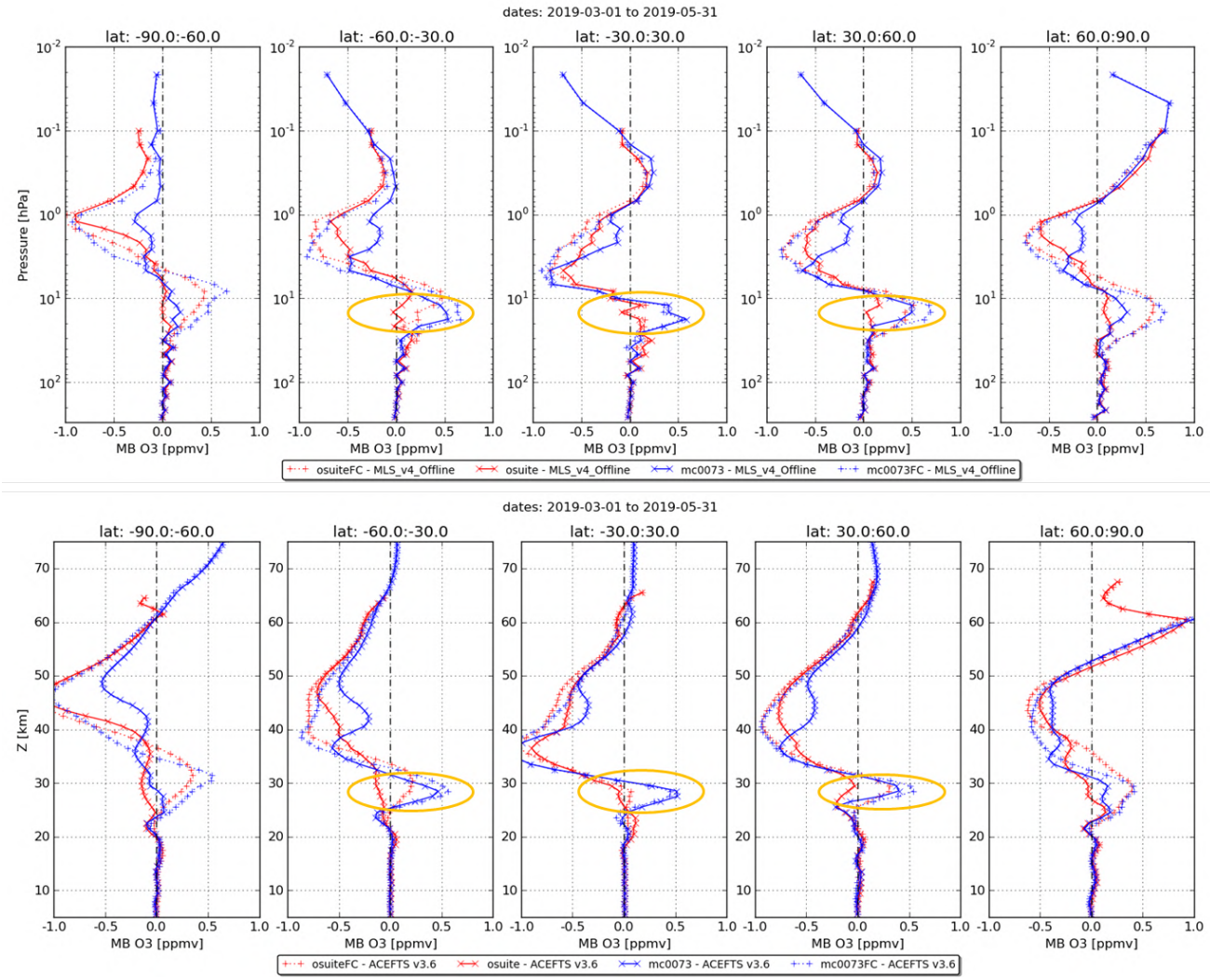

Figure 2.17.7: Monthly mean bias profiles for March to May 2019 using MLS (top) and ACEFTS (bottom) as reference (red: o-suite; blue: e-suite; dotted lines: 4-day forecasts). Above ~40km/~5hPa, the negative bias seen in the forecasts is better reproduced in the analyses of the e-suite than in the analyses of the o-suite. At around ~30km/20hPa, the profiles of the mean bias of the e-suite analyses are more distorted than the o-suite (higher negative values above; higher positive values below): these characteristics are particularly marked for the tropics and mid-latitudes (orange ellips).

2.18 Stratospheric ozone: Comparison with NDACC observations

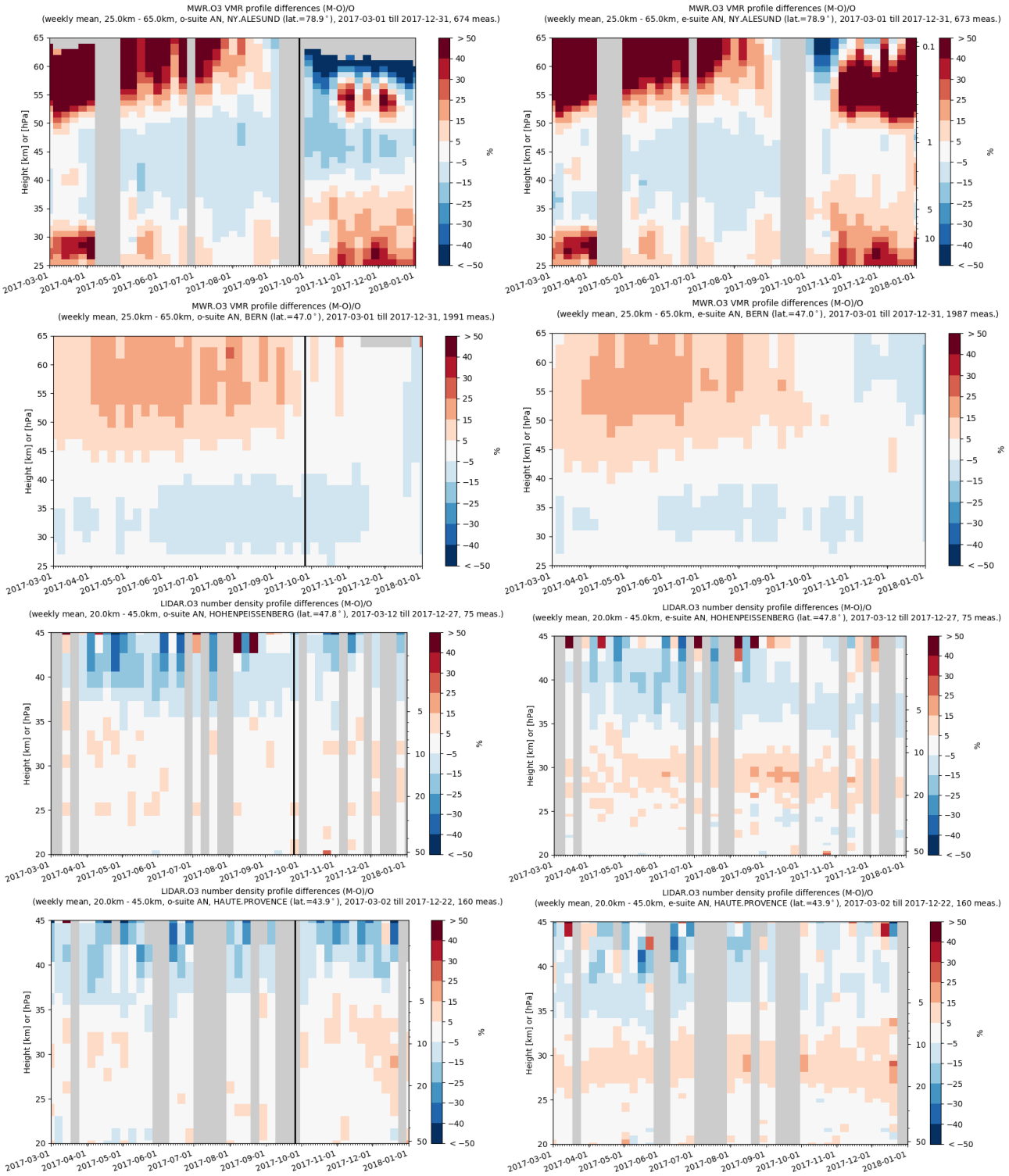

Fig. 2.18.1.: Comparison of weekly mean relative difference profiles between the o-suite (left column) and pre-e-suite (right column) O_3 concentration profile for the MWR NDACC stations at Ny Alesund and Bern (top 2 rows) and LIDAR NDACC stations at Hohenpeissenberg and OHP (bottom two rows). At Ny Alesund a significant increase in bias is observed above 50km. The 2 LIDAR stations see a positive bias (>5%) between 25km and 35km for the pre-e-suite, which agrees with the comparison against MLS and ACE-FTS.

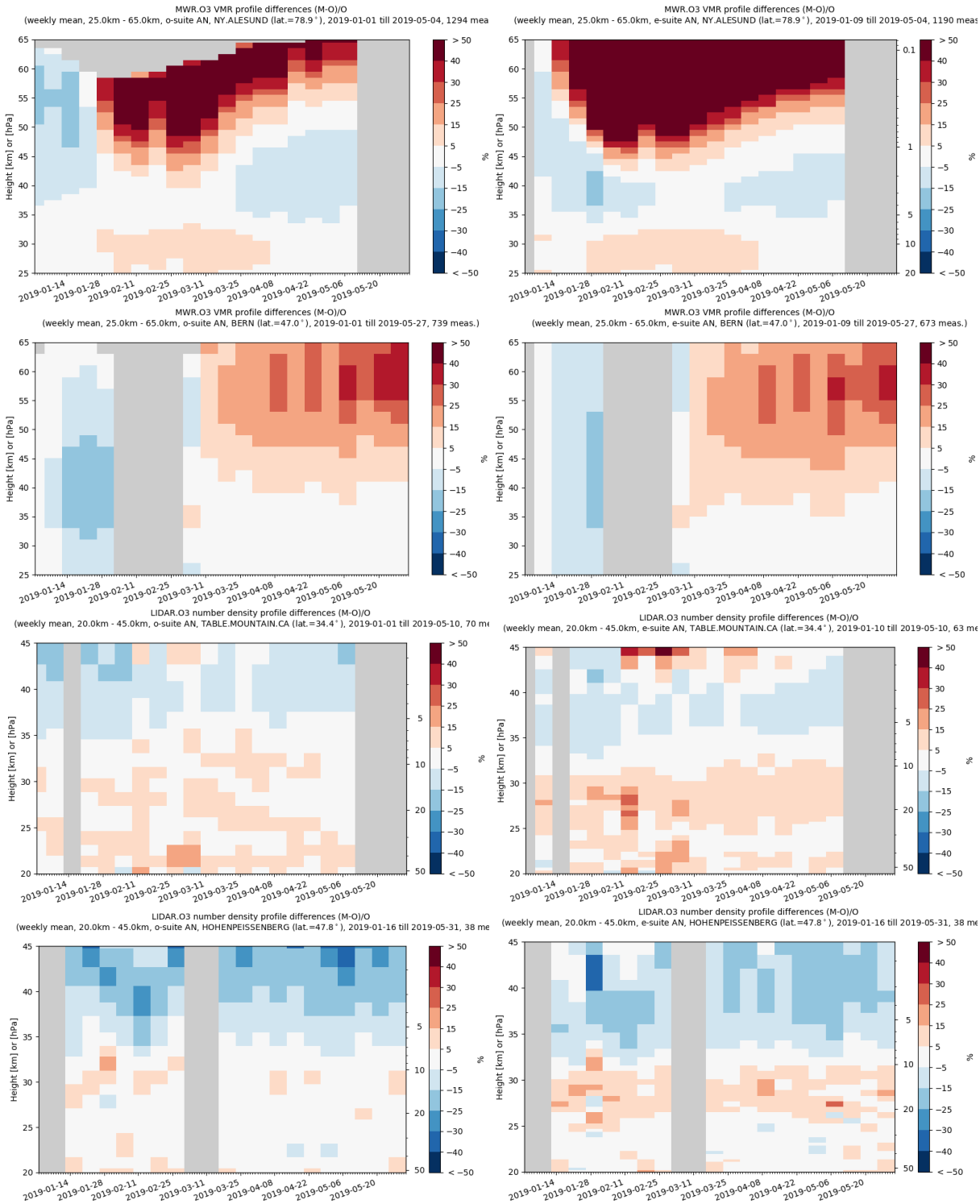

Fig. 2.18.2.: Comparison of weekly mean relative difference profiles between the 2019 o-suite analysis (left column) and e-suite analysis (right column) O_3 concentration profile for the MWR NDACC stations at Ny Alesund and Bern (top 2 rows) and LIDAR NDACC stations at Table Mountain (California) and Hohenpeissenberg (bottom two rows). At Ny Alesund a significant change in the profile shape is observed above 35km, in particular in January 2019. The 2 LIDAR stations see a positive bias (>5%) between 25km and 35km which agrees with the comparison against MLS and ACE-FTS and with the findings for the 2017 pre-e-suite.

2.19 Stratospheric NO2

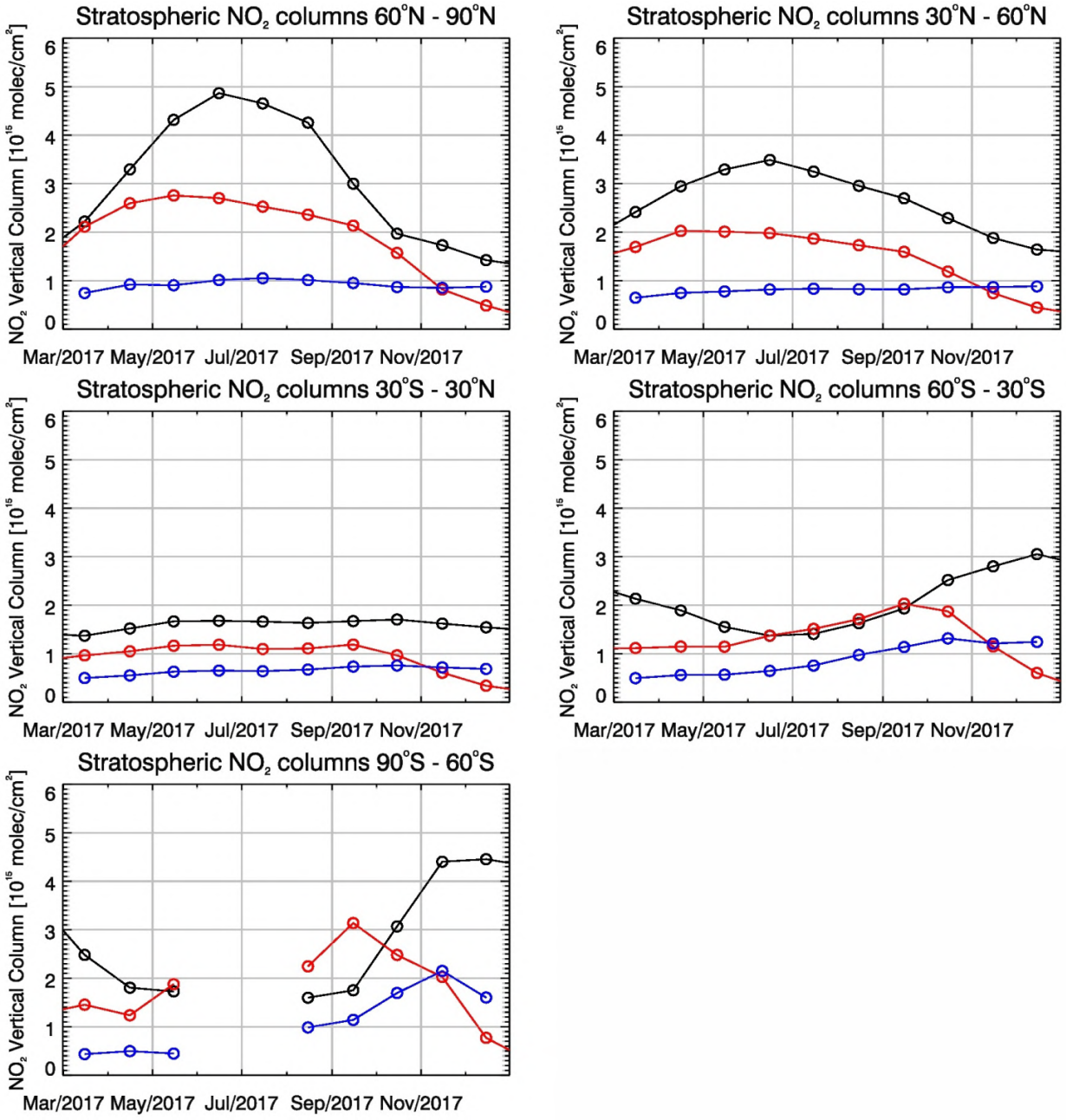

Figure 2.19.1: Time series of average stratospheric NO_2 columns [10^{15} molec cm-2] from (black) GOME-2 compared to the (red) o-suite and (blue) pre-e-suite for different latitude bands. The e-suites perform worse than the o-suite and shows a negative bias compared to GOME-2, a good agreement of model results and GOME-2 is not expected as stratospheric chemistry is not implemented in the runs.

3. References

Benedetti, A., J.-J. Morcrette, O. Boucher, A. Dethof, R. J. Engelen, M. Fisher, H. Flentjes, N. Huneeus, L. Jones, J. W. Kaiser, S. Kinne, A. Mangold, M. Razinger, A. J. Simmons, M. Suttie, and the GEMS-AER team: Aerosol analysis and forecast in the ECMWF Integrated Forecast System. Part II : Data assimilation, J. Geophys. Res., 114, D13205, doi:10.1029/2008JD011115, 2009.

Cariolle, D. and Teyssèdre, H.: A revised linear ozone photochemistry parameterization for use in transport and general circulation models: multi-annual simulations, Atmos. Chem. Phys., 7, 2183-2196, doi:10.5194/acp-7-2183-2007, 2007.

Dee, D. P. and S. Uppala, Variational bias correction of satellite radiance data in the ERA-Interim reanalysis. Quart. J. Roy. Meteor. Soc.,135, 1830-1841, 2009.

Eskes, H., Huijnen, V., Arola, A., Benedictow, A., Blechschmidt, A.-M., Botek, E., Boucher, O., Bouarar, I., Chabrillat, S., Cuevas, E., Engelen, R., Flentje, H., Gaudel, A., Griesfeller, J., Jones, L., Kapsomenakis, J., Katragkou, E., Kinne, S., Langerock, B., Razinger, M., Richter, A., Schultz, M., Schulz, M., Sudarchikova, N., Thouret, V., Vrekoussis, M., Wagner, A., and Zerefos, C.: Validation of reactive gases and aerosols in the MACC global analysis and forecast system, Geosci. Model Dev., 8, 3523-3543, doi:10.5194/gmd-8-3523-2015, 2015.

Eskes, H.J., S. Basart, A. Benedictow, Y. Bennouna, A.-M. Blechschmidt, S. Chabrillat, Y. Christophe, E. Cuevas, J. Douros, H. Flentje, K. M. Hansen, J. Kapsomenakis, B. Langerock, M. Ramonet, A. Richter, M. Schulz, N. Sudarchikova, A. Wagner, T. Warneke, C. Zerefos, Observations characterisation and validation methods document, Copernicus Atmosphere Monitoring Service (CAMS) report, CAMS84_2015SC3_D.84.8.1.1-2018_observations_v3.pdf, October 2018 (2018a). Available from: http://atmosphere.copernicus.eu/user-support/validation/verification-global-services

Eskes, H. J., S. Basart, A. Benedictow, Y. Bennouna, A.-M. Blechschmidt, S. Chabrillat, Y. Christophe, H. Clark, E. Cuevas, K. M. Hansen, U. Im, J. Kapsomenakis, B. Langerock, K. Petersen, M. Schulz, A. Wagner, C. Zerefos, Upgrade verification note for the CAMS near-real time global atmospheric composition service, Copernicus Atmosphere Monitoring Service (CAMS) report, CAMS84_2015SC3_D84.3.1.5_201802_esuite_v1.pdf, February 2018 (2018b)

Eskes et al., Upgrade verification note for the CAMS near-real time global atmospheric composition service, Addendum July 2018, CAMS84_2015SC3_D84.3.1.5_201802_esuite_v1.pdf (2018c).

Flemming, J., Huijnen, V., Arteta, J., Bechtold, P., Beljaars, A., Blechschmidt, A.-M., Diamantakis, M., Engelen, R. J., Gaudel, A., Inness, A., Jones, L., Josse, B., Katragkou, E., Marecal, V., Peuch, V.-H., Richter, A., Schultz, M. G., Stein, O., and Tsikerdekis, A.: Tropospheric chemistry in the Integrated Forecasting System of ECMWF, Geosci. Model Dev., 8, 975-1003, doi:10.5194/gmd-8-975-2015, 2015.

Flemming, J., Benedetti, A., Inness, A., Engelen, R. J., Jones, L., Huijnen, V., Remy, S., Parrington, M., Suttie, M., Bozzo, A., Peuch, V.-H., Akritidis, D., and Katragkou, E.: The CAMS interim Reanalysis of Carbon Monoxide, Ozone and Aerosol for 2003–2015, Atmos. Chem. Phys., 17, 1945-1983, doi:10.5194/acp-17-1945-2017, 2017.

Granier, C. et al.: Evolution of anthropogenic and biomass burning emissions of air pollutants at global and regional scales during the 1980–2010 period. Climatic Change (109), 2011

Huijnen, V., et al.: The global chemistry transport model TM5: description and evaluation of the tropospheric chemistry version 3.0, Geosci. Model Dev., 3, 445-473, doi:10.5194/gmd-3-445-2010, 2010.

Inness, A., Blechschmidt, A.-M., Bouarar, I., Chabrillat, S., Crepulja, M., Engelen, R. J., Eskes, H., Flemming, J., Gaudel, A., Hendrick, F., Huijnen, V., Jones, L., Kapsomenakis, J., Katragkou, E., Keppens, A., Langerock, B., de Mazière, M., Melas, D., Parrington, M., Peuch, V. H., Razinger, M., Richter, A., Schultz, M. G., Suttie, M., Thouret, V., Vrekoussis, M., Wagner, A., and Zerefos, C.: Data assimilation of satellite-retrieved ozone, carbon monoxide and nitrogen dioxide with ECMWF's Composition-IFS, Atmos. Chem. Phys., 15, 5275-5303, doi:10.5194/acp-15-5275-2015, 2015.

Kaiser, J. W., Heil, A., Andreae, M. O., Benedetti, A., Chubarova, N., Jones, L., Morcrette, J.-J., Razinger, M., Schultz, M. G., Suttie, M., and van der Werf, G. R.: Biomass burning emissions estimated with a global fire assimilation system based on observed fire radiative power, Biogeosciences, 9, 527-554, doi:10.5194/bg-9-527-2012, 2012.

Morcrette, J.-J., O. Boucher, L. Jones, D. Salmond, P. Bechtold, A. Beljaars, A. Benedetti, A. Bonet, J. W. Kaiser, M. Razinger, M. Schulz, S. Serrar, A. J. Simmons, M. Sofiev, M. Suttie, A. M. Tompkins, and A. Untch: Aerosol analysis and forecast in the ECMWF Integrated Forecast System. Part I: Forward modelling, J. Geophys. Res., 114, D06206, doi:10.1029/2008JD011235, 2009.

Schulz, M., Y. Christophe, M. Ramonet, Wagner, A., H.J. Eskes, S. Basart, A. Benedictow, Y. Bennouna, A.-M. Blechschmidt, S. Chabrillat, E. Cuevas, A. El- Yazidi, H. Flentje, K.M. Hansen, U. Im, J. Kapsomenakis, B. Langerock, A. Richter, N. Sudarchikova, V. Thouret, T. Warneke, C. Zerefos, Validation report of the CAMS near-real-time global atmospheric composition service: Period December 2018 -February 2019, Copernicus Atmosphere Monitoring Service (CAMS) report, CAMS84_2018SC1_D1.1.1_DJF2019_v1.pdf, doi:10.24380/7th6-tk72, June 2019.

Sindelarova, K., Granier, C., Bouarar, I., Guenther, A., Tilmes, S., Stavrakou, T., Müller, J.-F., Kuhn, U., Stefani, P., and Knorr, W.: Global data set of biogenic VOC emissions calculated by the MEGAN model over the last 30 years, Atmos. Chem. Phys., 14, 9317-9341, doi:10.5194/acp-14-9317-2014, 2014.

Williams, J. E., van Velthoven, P. F. J., and Brenninkmeijer, C. A. M.: Quantifying the uncertainty in simulating global tropo- spheric composition due to the variability in global emission es- timates of Biogenic Volatile Organic Compounds, Atmos. Chem. Phys., 13, 2857–2891, doi:10.5194/acp-13-2857-2013, 2013.

Annex 1: Acknowledgements for measurements used

We wish to acknowledge the provision of NRT GAW observational data by: Institute of Atmospheric Sciences and Climate (ISAC) of the Italian National Research Council (CNR), South African Weather Service, National Centre for Atmospheric Science (NCAS, Cape Verde), National Air Pollution Monitoring Network (NABEL) (Federal Office for the Environment FOEN and Swiss Federal Laboratories for Materials Testing and Research EMPA), Atmospheric Environment Division Global Environment and Marine Department Japan Meteorological Agency, Chinese Academy of Meteorological Sciences (CAMS), Alfred Wegener Institut, Umweltbundesamt (Austria), National Meteorological Service (Argentina), Umweltbundesamt (UBA, Germany)

We are grateful to the numerous operators of the Aeronet network and to the central data processing facility at NASA Goddard Space Flight Center for providing the NRT sun photometer data, especially Ilya Slutker and Brent Holben for sending the data.

The authors thank to all researchers, data providers and collaborators of the World Meteorological Organization's Sand and Dust Storm Warning Advisory and Assessment System (WMO SDS-WAS) for Northern Africa, Middle East and Europe (NAMEE) Regional Node. Also special thank to Canary Government as well as AERONET, MODIS, U.K. Met Office MSG, MSG Eumetsat and EOSDIS World Viewer principal investigators and scientists for establishing and maintaining data used in the activities of the WMO SDS-WAS NAMEE Regional Center (http://sds-was.aemet.es/).

We wish to acknowledge the provision of ozone sonde data by the World Ozone and Ultraviolet Radiation Data Centre established at EC in Toronto (http://woudc.org), by the Data Host Facility of the Network for the Detection of Atmospheric Composition Change established at NOAA (http://ndacc.org), by the Norwegian Institute for Air Research and by the National Aeronautics and Space Administration (NASA).

We wish to thank the NDACC investigators for the provision of observations at Ny Alesund, Bern, Jungfraujoch, Izaña, Xianghe, Harestua, Reunion Maido, Uccle, Hohenpeissen, Mauna Loa, Lauder and Haute Provence.

The authors acknowledge the NOAA Earth System Research Laboratory (ESRL) Global Monitoring Division (GMD) for the provision of ground-based ozone concentrations.

The MOPITT CO data were obtained from the NASA Langley Research Center ASDC. We acknowledge the LATMOS IASI group for providing IASI CO data.

SCIAMACHY lv1 radiances were provided to IUP-UB by ESA through DLR/DFD.

GOME-2 lv1 radiances were provided to IUP-UB by EUMETSAT.

The authors acknowledge Environment and Climate Change Canada for the provision of Alert ozone data and Sara Crepinsek – NOAA for the provision of Tiksi ozone data. Surface ozone data from the Zeppelin Mountain, Svalbard are from www.luftkvalitet.info. Surface ozone data from the Villum Research Station, Station Nord (VRS) were financially supported by "The Danish Environmental Protection Agency" with means from the MIKA/DANCEA funds for Environmental Support to the

Arctic Region. The Villum Foundation is acknowledged for the large grant making it possible to build VRS in North Greenland.

We acknowledge the National Aeronautics and Space Administration (NASA), USA for providing the OMPS limb sounder data (http://npp.gsfc.nasa.gov/omps.html) and the Aura-MLS offline data (http://mls.jpl.nasa.gov/index-eos-mls.php).

We thank the Canadian Space Agency and ACE science team for providing level 2 data retrieved from ACE-FTS on the Canadian satellite SCISAT-1.

The European Environment Information and Observation Network (Eionet) Air Quality portal provides details relevant for the reporting of air quality information from EU Member States and other EEA member and co-operating countries. This information is submitted according to Directives 2004/107/EC and 2008/50/EC of the European Parliament and of the Council.

We acknowledge the contribution of the ICOS Atmospheric Thematic Center (Lynn Hazan, Amara Abbaris, and Leonard Rivier) for the near real time data processing of surface CO_2 and CH_4 concentrations. The ICOS monitoring sites are maintained by the national networks: ICOS-Czech Rep. (Michal Marek, Katerina Komínková, Gabriela Vítková), ICOS-Finland (Olli Peltola, Janne Levula, Tuomas Laurila), ICOS-France (Michel Ramonet, Marc Delmotte, Sebastien Conil, Morgan Lopez, Victor Kazan, Aurélie Colomb, Jean Marc Pichon, Roxanne Jacob, Julie Helle, Olivier Laurent), ICOS-Germany (Matthias Lindauer, Dagmar Kubistin, Christian Plass-Duelmer, Dietmar Weyrauch, Marcus Schumacher), ICOS-Italy (Paolo Cristofanelli, Michela Maione, Francesco Apadula), ICOS-Norway (Cathrine Lund Myhre, Ove Hermansen), ICOS-Sweden (Jutta Holst, Michal Heliasz, Meelis Molder, Mikaell Ottosson Lofvenius, Anders Lindroth, Per Marklund), ICOS-Switzerland (Martin Steinbacher, Simon Wyss), European Commission, Joint Research Centre, Directorate for Energy, Transport and Climate (Peter Bergamaschi, Giovanni Manca).

The TCCON site at Orleans is operated by the University of Bremen and the RAMCES team at LSCE (Gif-sur-Yvette, France). The TCCON site at Bialystok is operated by the University of Bremen. Funding for the two sites was provided by the EU-project ICOS-INWIRE and the University of Bremen. The TCCON site at Réunion is operated by BIRA-IASB, in cooperation with UReunion and is funded by BELSPO in the framework of the Belgian ICOS program.

TCCON references:

Hazan, L., J. Tarniewicz, M. Ramonet, O. Laurent and A. Abbaris **(2016)**. *Automatic processing of atmospheric CO_2 and CH_4 mole fractions at the ICOS Atmosphere Thematic Centre*. Atmospheric Measurement Techniques 9(9): 4719-4736.

Blumenstock, T., F. Hase, M. Schneider, O. E. García, and E. Sepúlveda. 2017. "TCCON data from Izana (ES), Release GGG2014.R1." CaltechDATA. doi:10.14291/tccon.ggg2014.izana01.r1.

De Mazière, M., M. K. Sha, F. Desmet, C. Hermans, F. Scolas, N. Kumps, J.-M. Metzger, V. Duflot, and J.-P. Cammas. 2017. "TCCON data from Réunion Island (RE), Release GGG2014.R1." CaltechDATA. doi:10.14291/tccon.ggg2014.reunion01.r1.

Deutscher, N. M., J. Notholt, J. Messerschmidt, C. Weinzierl, T. Warneke, C. Petri, and P. Grupe. 2017. "TCCON data from Bialystok (PL), Release GGG2014.R1." CaltechDATA. doi:10.14291/tccon.ggg2014.bialystok01.r1/1183984.

Dubey, M. K., B. G. Henderson, D. Green, Z. T. Butterfield, G. Keppel-Aleks, N. T. Allen, J.-F. Blavier, C. M. Roehl, D. Wunch, and R. Lindenmaier. 2017. "TCCON data from Manaus (BR), Release GGG2014.R0." CaltechDATA. doi:10.14291/tccon.ggg2014.manaus01.r0/1149274.

Dubey, M. K., R. Lindenmaier, B. G. Henderson, D. Green, N. T. Allen, C. M. Roehl, J.-F. Blavier, et al. 2017. "TCCON data from Four Corners (US), Release GGG2014.R0." CaltechDATA. doi:10.14291/tccon.ggg2014.fourcorners01.r0/1149272.

Feist, D. G., S. G. Arnold, N. John, and M. C. Geibel. 2017. "TCCON data from Ascension Island (SH), Release GGG2014.R0." CaltechDATA. doi:10.14291/tccon.ggg2014.ascension01.r0/1149285.

Goo, T.-Y., Y.-S. Oh, and V. A. Velazco. 2017. "TCCON data from Anmeyondo (KR), Release GGG2014.R0." CaltechDATA. doi:10.14291/tccon.ggg2014.anmeyondo01.r0/1149284.

Griffith, D. W. T., N. M. Deutscher, V. A. Velazco, P. O. Wennberg, Y. Yavin, G. Keppel-Aleks, R. A. Washenfelder, et al. 2017. "TCCON data from Darwin (AU), Release GGG2014.R0." CaltechDATA. doi:10.14291/tccon.ggg2014.darwin01.r0/1149290.

Griffith, D. W. T., V. A. Velazco, N. M. Deutscher, C. Paton-Walsh, N. B. Jones, S. R. Wilson, R. C. Macatangay, G. C. Kettlewell, R. R. Buchholz, and M. O. Riggenbach. 2017. "TCCON data from Wollongong (AU), Release GGG2014.R0." CaltechDATA. doi:10.14291/tccon.ggg2014.wollongong01.r0/1149291.

Hase, F., T. Blumenstock, S. Dohe, J. Groß, and M.ä. Kiel. 2017. "TCCON data from Karlsruhe (DE), Release GGG2014.R1." CaltechDATA. doi:10.14291/tccon.ggg2014.karlsruhe01.r1/1182416.

Iraci, L. T., J. R. Podolske, P. W. Hillyard, C. Roehl, P. O. Wennberg, J.-F. Blavier, J. Landeros, et al. 2017. "TCCON data from Edwards (US), Release GGG2014.R1." CaltechDATA. doi:10.14291/tccon.ggg2014.edwards01.r1/1255068.

—. 2017. "TCCON data from Indianapolis (US), Release GGG2014.R1." CaltechDATA. doi:10.14291/tccon.ggg2014.indianapolis01.r1/1330094.

Kawakami, S., H. Ohyama, K. Arai, H. Okumura, C. Taura, T. Fukamachi, and M. Sakashita. 2017. "TCCON data from Saga (JP), Release GGG2014.R0." CaltechDATA. doi:10.14291/tccon.ggg2014.saga01.r0/1149283.

Kivi, R., P. Heikkinen, and E. Kyrö. 2017. "TCCON data from Sodankylä (FI), Release GGG2014.R0." CaltechDATA. doi:10.14291/tccon.ggg2014.sodankyla01.r0/1149280.

Liu, Cheng, Wei Wang, and Youwen Sun. 2018. "TCCON data from Hefei (PRC), Release GGG2014.R0." CaltechDATA. doi:10.14291/tccon.ggg2014.hefei01.r0.

Morino, I., N. Yokozeki, T. Matsuzaki, and M. Horikawa. 2017. "TCCON data from Rikubetsu (JP), Release GGG2014.R2." CaltechDATA. doi:10.14291/tccon.ggg2014.rikubetsu01.r2.

Morino, I., T. Matsuzaki, and M. Horikawa. 2017. "TCCON data from Tsukuba (JP), 125HR, Release GGG2014.R2." CaltechDATA. doi:10.14291/tccon.ggg2014.tsukuba02.r2.

Morino, Isamu, Voltaire A. Velazco, Akihiro Hori, Osamu Uchino, and David W. T. Griffith. 2018. "TCCON data from Burgos, Ilocos Norte (PH), Release GGG2014.R0." CaltechDATA. doi:10.14291/tccon.ggg2014.burgos01.r0.

Notholt, J., C. Petri, T. Warneke, N. M. Deutscher, M. Palm, M. Buschmann, C. Weinzierl, R. C. Macatangay, and P. Grupe. 2017. "TCCON data from Bremen (DE), Release GGG2014.R0." CaltechDATA. doi:10.14291/tccon.ggg2014.bremen01.r0/1149275.

Notholt, J., T. Warneke, C. Petri, N. M. Deutscher, C. Weinzierl, M. Palm, and M. Buschmann. 2017. "TCCON data from Ny Ålesund, Spitsbergen (NO), Release GGG2014.R0." CaltechDATA. doi:10.14291/tccon.ggg2014.nyalesund01.r0/1149278.

Pollard, David Frank, John Robinson, and Hisako Shiona. 2019. "TCCON data from Lauder (NZ), Release GGG2014.R0." CaltechDATA. doi:10.14291/tccon.ggg2014.lauder03.r0.

Sherlock, V., B. Connor, J. Robinson, H. Shiona, D. Smale, and D. F. Pollard. 2017. "TCCON data from Lauder (NZ), 120HR, Release GGG2014.R0." CaltechDATA. doi:10.14291/tccon.ggg2014.lauder01.r0/1149293.

—. 2017. "TCCON data from Lauder (NZ), 125HR, Release GGG2014.R0." CaltechDATA. doi:10.14291/tccon.ggg2014.lauder02.r0/1149298.

Strong, K., S. Roche, J. E. Franklin, J. Mendonca, E. Lutsch, D. Weaver, P. F. Fogal, J. R. Drummond, R. Batchelor, and R. Lindenmaier. 2018. "TCCON data from Eureka (CA), Release GGG2014.R3." CaltechDATA. doi:10.14291/tccon.ggg2014.eureka01.r3.

Sussmann, R., and M. Rettinger. 2017. "TCCON data from Garmisch (DE), Release GGG2014.R2." CaltechDATA. doi:10.14291/tccon.ggg2014.garmisch01.r2.

—. 2018. "TCCON data from Zugspitze (DE), Release GGG2014.R1." CaltechDATA. doi:10.14291/tccon.ggg2014.zugspitze01.r1.

Té, Y., P. Jeseck, and C. Janssen. 2017. "TCCON data from Paris (FR), Release GGG2014.R0." CaltechDATA. doi:10.14291/tccon.ggg2014.paris01.r0/1149279.

Warneke, T., J. Messerschmidt, J. Notholt, C. Weinzierl, N. M. Deutscher, C. Petri, and P. Grupe. 2017. "TCCON data from Orléans (FR), Release GGG2014.R0." CaltechDATA. doi:10.14291/tccon.ggg2014.orleans01.r0/1149276.

Wennberg, P. O., C. M. Roehl, D. Wunch, G. C. Toon, J.-F. Blavier, R. Washenfelder, G. Keppel-Aleks, N. T. Allen, and J. Ayers. 2017. "TCCON data from Park Falls (US), Release GGG2014.R1." CaltechDATA. doi:10.14291/tccon.ggg2014.parkfalls01.r1.

Wennberg, P. O., C. M. Roehl, J.-F. Blavier, D. Wunch, and N. T. Allen. 2017. "TCCON data from Jet Propulsion Laboratory (US), 2011, Release GGG2014.R1." CaltechDATA. doi:10.14291/tccon.ggg2014.jpl02.r1/1330096.

Wennberg, P. O., D. Wunch, C. M. Roehl, J.-F. Blavier, G. C. Toon, and N. T. Allen. 2017. "TCCON data from Caltech (US), Release GGG2014.R1." CaltechDATA. doi:10.14291/tccon.ggg2014.pasadena01.r1/1182415.

—. 2017. "TCCON data from Lamont (US), Release GGG2014.R1." CaltechDATA. doi:10.14291/tccon.ggg2014.lamont01.r1/1255070.

Wennberg, P. O., D. Wunch, Y. Yavin, G. C. Toon, J.-F. Blavier, N. T. Allen, and G. Keppel-Aleks. 2017. "TCCON data from Jet Propulsion Laboratory (US), 2007, Release GGG2014.R0." CaltechDATA. doi:10.14291/tccon.ggg2014.jpl01.r0/1149163.

Wunch, D., J. Mendonca, O. Colebatch, N. T. Allen, J.-F. Blavier, S. Roche, J. Hedelius, et al. 2017. "TCCON data from East Trout Lake, SK (CA), Release GGG2014.R1." CaltechDATA. doi:10.14291/tccon.ggg2014.easttroutlake01.r1.

Wunch, D., Toon, G. C., Sherlock, V., Deutscher, N. M., Liu, C., Feist, D. G., & Wennberg, P. O. (2015). The Total Carbon Column Observing Network's GGG2014 Data Version. Tech. rep., California Institute of Technology, Pasadena. doi:10.14291/tccon.ggg2014.documentation.R0/1221662

Copernicus Atmosphere Monitoring Service

ECMWF - Shinfield Park, Reading RG2 9AX, UK

Contact: info@copernicus-atmosphere.eu